

Net charge and protein-protein interactions of monoclonal antibodies: analytical assessment and application in protein formulation development

Dissertation

zur Erlangung des

Doktorgrades der Naturwissenschaften (Dr. rer. nat.)

der

Naturwissenschaftlichen Fakultät I – Biowissenschaften –

der Martin-Luther-Universität

Halle-Wittenberg,

vorgelegt

von Herrn Christian Lehermayr

geb. am 21.09.1984 in Steyr

Gutachter/in

1. Prof. Dr. K. Mäder

2. Prof. Dr. M. Pietzsch

3. PD Dr. H.-C. Mahler

Halle (Saale), 07.10.2013

Die Vorliegende Arbeit

***“Net charge and protein-protein interactions of monoclonal antibodies:
analytical assessment and application in protein formulation
development”***

wurde

an der Naturwissenschaftlichen Fakultät I – Biowissenschaften –

der Martin-Luther-Universität Halle-Wittenberg

unter Anleitung von Herrn Prof. Dr. Karsten Mäder

in Zusammenarbeit mit F.Hoffmann-La Roche Ltd.

unter Anleitung von Herrn Dr. Stefan Fischer

verfasst.

*“I have the solution!
But it only works for spherical chickens in vacuum.”*

From the Sitcom: The Big Bang Theory

ACKNOWLEDGEMENTS

Saying thank you or acknowledging someone should be one of the easiest things in the world but as the end of this thesis draws near one starts thinking; thinking about all the people that came into one's life but also about those who left. How one was changed how life changed. I had a great time including a lot of unforgettable moments and for that I'd like to thank many people.

First of all I'd like to thank my supervisors Dr. Hanns-Christian Mahler, Prof. Dr. Karsten Mäder and Dr. Stefan Fischer. Thank you Prof. Dr. Mäder and the Martin-Luther-University Halle-Wittenberg for the great supervision. Thanks Stefan for your big support, the constant discussions and brain picking that inspired me to find new ways of doing something and for saving me of too much digression. I'll never forget your constant calming me down and cheering me up with your typical "Alles wird gut!". Thinking of the famous "paper1" still causes me to smile. What a Christmas late night action that was. I couldn't have had a better supervisor! Hanns-Christian thanks for making all this possible. Your constant encouragement and your way of doing things will continue to inspire me. You are a beacon to a lot of people.

Apart from my supervisors there were a lot of great scientists I had the honor to work with. Dr. Arne Rufer and Dr. Francis Müller who supported me with AUC as well as their scientific advice; Dr. Alfred Ross who is an expert in asking the right questions and who supported me with the NMR measurements; Dr. Hendrik Metz with whom I had the opportunity to do the ESR measurements; Dr. Pierre Goldbach who was always the one knowing where to find rare material to do research on; Robert Müller who helped me a lot in getting started; Dr. Sonoko Kanai from whom I not only learned that some Japanese people think of chandeliers when they think of Austria but who is also an expert in polymer science and assisted me a lot especially in the development and application of light scattering methods; and Dr. Ulla Grauschopf for the cooperative work in the ammonium sulphate precipitation experiments and for asking questions by thinking out of the box.

Not to forget my 309 lab buddies Andrea Allmendinger, Dr. Kishore Ravuri and Dr. Sylvia Kiese. In our small research lab we could survive cold winter wind from "the crack", the jittering neon lights and the deafening sound of the CE laser ventilation by a good laugh every now and then. Of course having so much knowledge so tightly packed we did not lack scientific discussions. Kishore and Sylvia I owe you a lot. Thanks for helping me getting started and for always having a good advice whenever needed. There is only one thing to add "Alles wird besser mit Butter".

Furthermore, I would like to express my sincere thanks to F.Hoffmann-La Roche Ltd. and especially pRED including Dr. Michael Ausborn, Dr. Marcel Schmid and Dr. Günther Gross and the PRFN department under Dr. Oliver Stauch for funding my past three years of research. Not to forget the complete Biologics team that could be always counted on; including Florian Rossberg, Gerd Müller, Lucia De Lorzenzo, Michaela Grass, Severine Wittwer, and Thomas Steffen to only mention a few. Thanks Severine without you I would still be preparing the 600 formulations. So good teamwork not only when it comes to canoeing.

To my Love, Laurence thank you for your never ending positive energy and happiness or simply for being you. Thank you for your trust in me especially when it comes to Cro-Magnon or was it Grand Marnier? Pour toi, je peux marcher au plafond.

Finally I'd like to thank my mum and my dad. Without you this wouldn't have been possible. Thanks for all the support and for trying to understand what I was doing.

TABLE OF CONTENT

Acknowledgements.....	IV
Table of Content	VI
List of Tables	IX
List of Abbreviations/Lettercodes.....	X
1. Introduction.....	1
1.1. Determination of Charge Related Parameters.....	1
1.2. Determination of Protein-Protein Interactions	2
1.3. Protein-Protein Interactions and Implications for Protein Formulation	3
1.4. Scope of this Work	4
2. Materials and Methods	5
2.1. Sample Preparation.....	5
2.2. Storage of Samples for Stability Testing.....	8
2.3. Computed IEP/Charge Data based on Primary Amino Acid Sequence	9
2.4. Computed Relative Hydrophobicity based on Amino Acid Sequence.....	9
2.5. Isoelectric Focusing by Capillary Electrophoresis.....	9
2.6. Determination of Isoelectric Point by Measuring Electrophoretic Mobility and Mutual Diffusion Coefficient during pH Titration	10
2.7. Determination of Zetapotential and Net Charge	10
2.8. Determination of Second Virial coefficient (A_2) by Static Light Scattering...	13
2.9. Determination of Interaction Parameter k_D by Dynamic Light Scattering (DLS)	14
2.10. Determination of Self Diffusion Coefficient (D_s) by NMR	14
2.11. Determination of Hydrophobicity by Fluorescence	15
2.12. Determination of Hydrophobicity by ESR	15
2.13. Determination of Surface Activity by Drop Tensiometer	16
2.14. Determination of Ammonium Sulphate Precipitation Concentration	16
2.15. Analysis of Soluble Aggregates by Size Exclusion Chromatography	16
2.16. Turbidity and Subvisible and Visible Particle Analysis.....	17
2.17. Determination of Dynamic Viscosity by Plate-Cone Rheometer	17
2.18. Calculation of Propagation of Error.....	17
3. Results and Discussion	18
3.1. A_2 Method Development.....	18
3.1.1. Development of a Method for Determination of A_2 by SLS	18
3.1.2. Development of a Method for Determination of Protein-Protein-Interaction by DLS.....	21

3.1.3.	Method Development for Assessing A_2 by DLS	24
3.2.	Assessment of Isoelectric Point, Net Charge and Protein-Protein Interactions of Different mAbs.....	28
3.2.1.	Determination of IEP	28
3.2.2.	Zeta Potential and Net Charge.....	30
3.2.3.	Experimental confirmation of the concentration dependence of D_s	35
3.2.4.	Net Charge at Different pH Values	37
3.2.5.	Second Virial Coefficient A_2	38
3.2.6.	Second Virial Coefficient and Net Charge	39
3.2.7.	Evaluation of Non-Ionic Interactions.....	40
3.2.7.1.	Fluorescence Hydrophobicity Analysis.....	40
3.2.7.2.	Hydrophobic ESR Marker Binding.....	43
3.2.7.3.	Surface Tension Measurement	44
3.2.7.4.	Ammonium Sulphate Precipitation	47
3.2.7.5.	Calculated Hydrophobicity based on primary Amino Acid Sequence	49
3.3.	Structural Differences in mAb Subclasses (IgG1 vs. IgG4)	50
3.4.	Protein-Protein Interaction of mAbs in Different Pharmaceutically Relevant Buffer Systems.....	52
3.4.1.	Overview of the Formulation Screen	52
3.4.2.	Behavior of A_2 Varying Buffer and pH at Constant Ionic Strength	55
3.4.3.	Behavior of A_2 at Increasing Ionic Strength.....	57
3.4.4.	General Behavior of A_2 Comparing IgG1 to IgG4.....	61
3.4.5.	Diffusion Coefficients at Infinite Dilution (D_0) of the A_2 measurements in this chapter	65
3.5.	Applicability of A_2 for protein formulation development.....	66
3.5.1.	A_2 and Turbidity.....	66
3.5.2.	A_2 in Protein Stability	70
3.5.2.1.	mAbs Stability at 5 °C and Discussion of T=0 Results	71
3.5.2.2.	mAbs Stability at 25 °C	78
3.5.2.3.	mAbs Stability at 40 °C	83
3.5.2.4.	Shaking Stability.....	88
3.5.2.5.	Summary of the stability study	95
3.5.3.	Self-association of Antibodies	96
3.5.4.	A_2 and Dynamic Viscosity.....	98
3.6.	Assessment of D_m at High mAb Concentration.....	101
4.	Summary and Outlook.....	105
5.	Zusammenfassung und Ausblick (Übersetzung)	XII

Table of Contents

6.	References	XVIII
7.	Curriculum Vitae	XXV
8.	Eidesstattliche Erklärung	XXVII

LIST OF TABLES

Table 2.1.1. Overview on buffer systems which were used in sections 3.4 and 3.5.4. The table also includes the stock solutions used as well as the suppliers of the chemicals. The abbreviations of the buffers are shown in brackets. pK_a values are shown in the column "Buffer" ⁴²⁻⁴⁴	6
Table 2.1.2. Matrix of buffers used in sections 3.4 and 3.5.4; pH/buffer systems (buffer type, pH and ionic strength) are marked in blue.	7
Table 3.1.1. Comparison of time and material needed in A_2 determination by three different methods	26
Table 3.1.2. Additional test formulations T1-T6 analyzed by both SLS (by A_2) and DLS (by k_D). Parameters varied were buffer strength, buffer, pH and additional antibodies	26
Table 3.4.1. The conditions of D_0 values smaller than 3.9^{-11} m ² /s and the respective A_2 values from the 635 formulations tested. Data shown in increasing order of D_0	66

LIST OF ABBREVIATIONS/LETTERCODES

μ	electrophoretic mobility (m^2/Vs)
A_2	second virial coefficient (mol mL/g^2)
ANS	1-Anilino-8-Naphthalene Sulfonate
AU	absorbance unit
AUC	analytical ultra centrifugation
BSA	bovine serum albumin
CDR	complementarity determining region
D_0	diffusion coefficient at infinite dilution (m^2/s)
DLS	dynamic light scattering
D_m	mutual diffusion coefficient (m^2/s)
D_s	self diffusion coefficient (m^2/s)
ESR	electron spin resonance
FFR	fast field reversal
FTU	formazin turbidity unit
GFP	green fluorescent protein
His(NaCl)	20 mM His/His-HCl pH 6.0 + 150 mM NaCl
His(w/o)	20 mM His/His-HCl pH 6.0
HMW	high molecular weight
HPLC	high performance liquid chromatography
iCE	isoelectric focusing capillary electrophoresis
IEP	isoelectric point
IgG	immunoglobulin of the subclass G
LMW	low molecular weight
M	molecular mass (g/mol)
mAb	monoclonal antibody
MALS	multi angular light scattering
NMR	nuclear magnetic resonance
NPN	N-Phenyl-1-Naphthylamine
PC50	ammonium sulphate concentration 50% of protein is precipitated
rcf	relative centrifugal force
rh	relative humidity

List of Abbreviations

Rh	hydrodynamic radius (m)
SD	standard deviation
SEC	size exclusion chromatography
SIC	self-interaction chromatography
SLS	static light scattering
TFF	tangential flow filtration
UV	ultra violet
VEGF	vascular endothelial growth factor

1. INTRODUCTION

Therapeutic monoclonal antibodies (mAbs) are increasingly used in self-administration via the subcutaneous route. mAbs are typically dosed in the mg/kg range. However, the maximum volume for subcutaneous injection is limited (<1.5 mL)¹. Consequently, mAbs need to be administered in low volume which requires the development of highly concentrated mAb formulations (>100 mg/mL)¹. Typical challenges encountered for high-concentration protein formulations are protein aggregation and solution viscosity. Although being structurally highly conserved, mAbs may differ significantly in various aspects including their aggregation behavior and/or viscosity.²⁻⁶ Until now, it is not possible to predict the behavior of mAbs at high concentration. In this context, self-association and protein-protein interactions are believed to play a significant role governing both (non-covalent) aggregation and viscosity^{2-5,7-9}. It was thus the aim of this work to study both net charge and protein-protein interactions in a series of different monoclonal antibodies and also how protein-protein interaction affects stability and viscosity especially at high concentrations.

1.1. Determination of Charge Related Parameters

An inherent protein property of interest is its isoelectric point (IEP). The IEP is defined as the pH where net charge becomes zero¹⁰. It is a rule-of-thumb to define the formulation's pH not too close to IEP as this increases the risk of precipitation.¹¹ The IEP of proteins can be theoretically derived from the amino acid sequence¹² or determined experimentally using different methods, including isoelectric focusing (IEF) or isoelectric focusing capillary electrophoresis (iCE)¹³. These methods are typically used to determine charge heterogeneity. Apart from these methods, a more global approach is to assess the pH, where the electrophoretic mobility is zero, e.g. by laser Doppler velocimetry.¹⁰

Another important factor is the antibodies' net charge. On the protein design level, supercharging of green fluorescent protein (GFP) was described in literature as one approach to optimize proteins' stability behavior.⁹ Consequently, methodologies to reliably determine protein net charge are of special interest.

A theoretical approximation of total net charge can be based on primary amino acid sequence¹². It is assumed that at a given pH, every individual ionizable amino acid from the sequence is charged according to its pK_a value. For experimental net charge determination, various methods have been described¹⁴. Such methods are for example based on the Donnan Equilibrium. This approach requires experimental quantification of the unequal partitioning of diffusible ions¹⁵ across an ultramembrane during equilibrium dialysis of protein solutions. Net charge can also be derived from macro-ion mobility in an electric field if one compensates for the layer of counterions as described by Henry.^{16,17} This method employs either capillary electrophoresis or laser Doppler velocimetry for the assessment of electrophoretic mobility.^{10,17} Those methods usually assume a constant Stokes radius of proteins regardless of protein concentration or buffer conditions like pH and ionic strength.^{10,17,18} Durant et al. have demonstrated the validity of assessing the Stokes radius by dynamic light scattering. The study researched different protein charge

variants and refers to dilute solutions where the Stokes-Einstein relation can be assumed valid.¹⁹

1.2. Determination of Protein-Protein Interactions

An interesting surrogate parameter to study protein-protein interactions is the second osmotic virial coefficient (A_2). A_2 is from the virial expansion of the ideal gas law equation. It is used to describe non-ideal behavior of proteins in solution comprising all interaction forces between two protein molecules, including ionic, hard-sphere, Van der Waals, and other short-range interactions (e.g. hydrophobic interactions).^{15,20} However, higher order interactions are not included in this term. This adds an important limitation to A_2 , i.e. only two-body interactions are captured while using the underlying theories. Consequently, the situation where three-body and/or higher order interactions comes into play, may not necessarily be sufficiently described by A_2 . This limitation makes A_2 a dilute solution property.^{21,22}

A positive A_2 value defines protein molecules being repulsive, whereas negative values describe attractive behavior.^{8,20,23,24} This definition has been proposed and used in the context of protein crystallization, where experimental crystallization conditions were tailored to a window of negative A_2 in order to favor attractive protein interaction and eventually crystallization.²⁵ Factors like pH, temperature and ionic strength were shown to strongly influence A_2 .²⁵⁻²⁸ Several techniques can be used to measure A_2 , including static light scattering (SLS)²⁸⁻³⁰, analytical ultracentrifugation (AUC)^{3,31}, self-interaction chromatography (SIC)²⁶, membrane osmometry³² and – more recently – dynamic light scattering (DLS).^{5,29} As those different methods rely on different physical principles, they may not necessarily generate same quantitative results for A_2 .³¹

In SLS the change in light scattering intensity with protein concentration is analyzed. Depending on the nonlinear change in scattering intensity over concentration the degree of either attractive or repulsive particle-particle interaction (A_2) can be assessed. In AUC, similar to SLS, a non-linear concentration dependence is used to determine the degree of attractive or repulsive interaction. In contrast to SLS the change in sedimentation velocity is assessed rather than scattering intensity. In SIC the protein is first immobilized on a chromatography column. The same protein is then run through the modified column. In case of protein-protein self-interaction, retention times are increased, i.e. the protein of interest elutes later than in case of lower or no interaction. The readouts used are the UV signal and the retention time. In DLS the change in mutual diffusion coefficient (D_m) over concentration is recorded. Depending on the linear change of D_m over concentration protein interactions can be directly ranked. However up to now DLS only gives relative values. One can only determine which samples are more repulsive/less attractive as compared to others.²²

The quantitative A_2 methods described are time intense. Although attempts for SLS are described demonstrating a high throughput method combining SLS with a size exclusion column (SEC), it still takes about 15 minutes per single measurement.³³ SIC is also described being a high throughput method but it cannot be used to screen several different mAbs as it only works with the antibody immobilized on the column.²⁶ AUC is limited by the number of samples which can be analyzed simultaneously. Consequently, a quantitative

high throughput method for A_2 is highly desired. Such a method could be of special interest in larger screenings, such as formulation screening studies.

As outlined above A_2 gives the full picture of intermolecular forces, i.e. the sum of all forces in a two body interaction.^{15,20} The strongest forces among these intermolecular interactions are ionic interactions. As this type of interaction is highly dependent on other counter ions present, A_2 is usually strongly dependent on the buffer/formulation conditions.^{5,7} An analysis of shielded and non shielded conditions could therefore give a better picture of the non-ionic forces present. A non-ionic force of interest to protein-protein interaction is hydrophobic interaction that is thought to be very weak, i.e. the absence of interaction with the solvent. Due to this, the interaction with alike particles is favored in order to reduce the exposed hydrophobic surface to the surrounding solvent.²¹ Interestingly, especially those weak forces are described in literature to be main drivers for protein-protein interactions: the presence of hydrophobic patches or the presence of partially unfolded proteins are thought to be a possible route cause of attractive protein interactions, that may lead to aggregation. This should therefore be analyzed separately.^{8,34} Possible methods to assess protein hydrophobicity are theoretical calculation based on the amino acid composition^{34,35}, the binding of hydrophobic markers like fluorescence dyes (ANS, NPN)³⁶⁻³⁸, as well as precipitation assays using ammonium sulphate (salting out).^{15,21} As surface activity by surface tension measurement is described to define hydrophobicity of surfaces³⁹ with a known surface the hydrophobicity of the liquid can also be characterized.

1.3. Protein-Protein Interactions and Implications for Protein Formulation

Antibody formulation screens are very time intense and do consume a lot of material. As material usually is of limited availability especially in early stages of the development, efforts have been taken to develop predictive methods covering antibodies stability (aggregation behavior) and high concentration viscosity behavior.^{7,40} In this context protein interaction measurements are thought to be of importance.

Especially one of the most recent publications by Sajula et al.⁶ could demonstrate that stability of the one mAb tested was connected to A_2 in the respective formulation. The stability was assessed by either stressing the mAb by agitation or by temperature stress. Another publication also shows increased thermal stability at conditions where proteins more strongly repulse each other; Lawrence et al.⁹ could demonstrate that GFP mutants of higher charge had a reduced loss in their conformational stability as thermal stress was applied.

Attractive protein-interactions in highly concentrated protein formulations were shown to be the root cause of increased samples' viscosity. Liu et al.³ as well as Yadav et al.⁵ could show that viscosity increases in highly concentrated protein formulations at the isoelectric point, where repulsive protein interactions are lowest. This is in contrast to first experiments Tanford¹⁵ presented in 1956 where samples viscosity was found to be lowest at its isoelectric point. However this observation was made in solutions that were not that highly concentrated. An explanation might be that the more crowded solutions get the closer particles are forced together; this then promotes short-range attractive interactions

not predominant at more diluted conditions. It leads to the result that viscosity at very high protein concentrations is highest at samples IEP.

Another issue linked to protein-protein interaction is reversible self-association. Moore et al.⁴¹ could demonstrate that when ionic interactions are shielded the dimerization of the mAb investigated was enhanced. Importantly, this self-association was reversible and depending strongly on the buffer matrix (pH, ionic strength, counter ion). This reversible dimerization might lead to wrong conclusions when assessing storage stability and one should keep this possibility in mind. Self-association is therefore also an important factor not to forget in early formulation development.

Present literature did not cover any real time stability data as well as viscosity data that systematically compared more than one or two mAbs. The stability data are also mostly based on accelerated or stressed scenarios which might give a biased result compared to for example 2-8 °C storage as it done for most marketed liquid products due to increased chemical degradation.

1.4. Scope of this Work

How net charge and protein-protein interactions can be related to physical protein stability, self-association, and high concentration viscosity behavior was still elusive at the beginning of this work. Therefore this thesis first presents the assessment of physical properties namely the isoelectric point (IEP), net charge and zeta potential of different monoclonal antibodies (mAbs). Secondly protein-protein interactions (i.e. second virial coefficient) A_2 of various mAbs at low and high ionic strength conditions were measured and it was attempted to predict attractive protein-protein interaction behavior (attractive A_2) in the light of non-ionic protein interactions (e.g. the hydrophobicity). To do so techniques were applied to quantify the hydrophobicity of mAbs. The aim of the assessment of protein properties and protein-interactions was to apply and compare several different analytical approaches using different mAbs and to find possible correlations between these results. For A_2 determination it was important to establish and apply an analytical set-up which allows for miniaturization, i.e. consumes only few protein at reduced measurement. This is necessary in order to study pharmaceutical applicable buffer conditions and to deduce general mAb's A_2 behavior regarding ionic strength, pH and buffer ion valences. After this important goal (i.e. the development of a high throughput A_2 method) was accomplished the next aim was to apply this knowledge. The last part of this work was to understand how protein-protein interaction can be used as a predictive parameter, especially for applications in formulation development. The aim was to point out the importance of A_2 and how its modification (by using different pharmaceutically applied buffer conditions) can be used to predict various important formulation parameters. The relevant parameters for formulation development are formulation's turbidity, mAb's physical stability at stressed and unstressed storage conditions, including high concentrated solution as well as mAb's self-association behavior, and high concentration viscosity.

2. MATERIALS AND METHODS

2.1. Sample Preparation

Ten different monoclonal antibodies (mAbs) provided by F. Hoffmann-La Roche Ltd. (Basel, CH), purified using a series of chromatography and membrane separation steps were used. This included eight different IgG1 (mAb1-7, 10) and two IgG4 (mAb8 and mAb9).

All antibodies were formulated in 20 mM His/His-HCl (Ajinomoto, Louvain-la-Neuve, Belgium) buffer at pH 6.0 using tangential flow filtration (TFF) (Labscale Millipore TFF, Billerica, USA). The final formulation was prepared by addition of 20 mM His/His-HCl buffer pH 6.0 to a final protein concentration of 10 mg/mL. Respective formulation samples were used for second virial coefficient measurements by static and dynamic light scattering, isoelectric point determination by capillary electrophoresis, electrophoretic mobility measurements for assessing the zeta potential and net charge determination at pH 6.0. (sections 3.1 and 3.2)

For 20 mM His/His-HCl pH 6.0 formulations containing 150 mM NaCl (sections 3.13.2.7, 3.5.1, and 3.6), samples from the TFF process (as described above) were diluted to 10 mg/mL protein concentration adding His/His-HCl buffer and His/His-HCl buffer containing 3 M NaCl (Fluka, Buchs, CH) stock solution, respectively, to yield a final formulation of 20 mM His/His-HCl pH 6.0 containing 150 mM NaCl. These NaCl-containing formulations were used for second virial coefficient measurements by static and dynamic light scattering as well.

Samples for the stability study (sections 3.2.3 and 3.5.2) were prepared from stock solutions of the different mAbs in 20 mM His/His-HCl buffer pH 6.0. This was done by TFF as described above. The four different formulations (20 mM His/His-HCl buffer pH 6.0 \pm NaCl at 10 mg/mL and 100 mg/mL) for each of the five mAbs were prepared similarly to what was described above by subsequent dilution of buffer and 3 M NaCl stock solution.

For pH titration experiments (3.2.1 and 3.2.4), four selected mAbs (mAb 1, 3, 6, and 8) were used. Their formulation buffer was exchanged by ultrafiltration (Amicon Ultra 10kMWCO, Millipore, Billerica, USA) to 10 mM NaCl in water. The use of an unbuffered formulation for pH titration was intended to avoid the buffering during pH titration. Successful removal of Histidine during buffer exchange was demonstrated by HPLC-SEC-UV with a TSK G3000 SWXL, 7.8x300 mm column (Tosoh Bioscience, Stuttgart, Germany) and detection at 220 nm (data not shown).

For the Donnan experiment (3.2.2) the four mAbs (1, 3, 6 and 8) in 20 mM His/His-HCl pH 6.0 (prepared as above) were further concentrated using TFF to a protein concentration of ca. 150 mg/mL.

Samples prepared for section 3.4 and 3.5.1 (mAb1, mAb3, mAb4, mAb6, and mAb8) were formulated by exchange of buffer by TFF to water and subsequent addition of buffer stock solutions and water to yield the desired buffer and protein concentration.

Samples used in sections 3.4 and 3.5.4 (mAb4, mAb5, mAb6, mAb8, and mAb9) were prepared by dilution of protein present in water and subsequent addition of buffer components. First all antibodies' buffer was exchanged to H₂O by TFF (Labscale Millipore TFF, Billerica, USA) concentrating the samples to ca. 25 mg/mL or ca. 190 mg/mL for viscosity samples by ultrafiltration (Amicon Ultra 10 kMWCO, Millipore, Billerica, USA). The final formulations at different pH values within different buffers at defined ionic strengths 10-50 mM as well as the placebos were prepared by addition of different amounts/ratios of buffer's base and acid stock solutions and dilution by H₂O to yield a final 10 mg/mL or 150 mg/mL concentration at the target pH and target ionic strength. Successful formulation compounding was verified by measuring the pH value. The buffer stock solutions prepared as well as the set of formulations that were done for each of the five mAbs are shown in Table 2.1.1 and Table 2.1.2.

Table 2.1.1. Overview on buffer systems which were used in sections 3.4 and 3.5.4. The table also includes the stock solutions used as well as the suppliers of the chemicals. The abbreviations of the buffers are shown in brackets. pK_a values are shown in the column "Buffer"⁴²⁻⁴⁴.

Buffer	Base	Acid
Sodium Acetate (Na-Acet) pK_a 4.76	Na-Acetate 3H ₂ O ² (150 mM)	Acetic Acid ¹ (300 mM)
Histidine-HCl (His-HCl) pK_a 6.04	Histidine base ⁶ (250 mM)	His-HCl 1H ₂ O ⁶ (300 mM)
Histidine-Acetate (His-Acet) pK_a 4.76	Histidine base ⁶ (250 mM)	Acetic Acid ¹ (300 mM)
Sodium-Phosphate (Na-Phos) pK_a 7.2	Na ₂ HPO ₄ 1H ₂ O ⁷ (100 mM)	NaH ₂ PO ₄ ² (100 mM)
Sodium-Succinate (Na-Succ) pK_{a1} 4.21 pK_{a2} 5.64	Na ₂ -Succinate ⁵ (75 mM)	Succinic acid ² (175 mM)
Arginine-Succinate (Arg-Succ) pK_{a1} 4.21 pK_{a2} 5.64	Arginine base ⁶ (150 mM)	Succinic acid ² (175 mM)
Sodium Citrate (Na-Cit) pK_{a1} 3.13 pK_{a2} 4.76 pK_{a3} 6.4	Na-Citrate 2H ₂ O ⁴ (50 mM)	Citric Acid 1H ₂ O ³ (50 mM)

¹ Wacker Chemie, Munich, Germany, ² Merck, Darmstadt, Germany, ³ Univar AG, Zurich, Switzerland, ⁴ SA Citrique Belge, Tienen, Belgium, ⁵ Fluka, Buchs, Switzerland, ⁶ Ajinomoto, Louvain-la-Neuve, Belgium, ⁷ Budenheim, Budenheim, Germany

Table 2.1.2. Matrix of buffers used in sections 3.4 and 3.5.4; pH/buffer systems (buffer type, pH and ionic strength) are marked in blue.

	Na-Acet	His-HCl	His-Acet	Na-Phos	Na-Succ	Arg-Succ	Na-Cit	Ionic Strength
pH 5.0								10mM
								20mM
								30mM
								40mM
								50mM
pH 5.5								
pH 6.0								
pH 6.5								
pH 7.0								

Ionic strength is defined by Equation 1. So to generate a buffer of defined ionic strength the concentration and valence of the buffer ions present in solution must be determined.

$$I = 0.5 \sum_{i=1}^n C_i Z_i^2$$

Equation 1. Calculation of buffers ionic strength (mM) based on the sum of ions present in solution depending on the concentration C (mM) and the valence Z of the specific ion.⁴³

The concentration of ions present in solution is based on their dissociation in solution. The ratio of charged and uncharged ions is given by the Henderson-Hasselbalch equation, i.e. Equation 2.

$$pH = pK_a + \log \frac{[conjugate\ base]}{[acid]}$$

Equation 2. The Henderson-Hasselbalch equation describes how the ratio of conjugate base to acid, dependent on the buffers pK_a value, results in the solutions pH.⁴³

However this ratio is based on the dissociation parameter (pK_a). This parameter depends on different factors. So first, to be able to accurately calculate a buffer composition of defined ionic strength, one has to compensate for the temperature dependence of the thermodynamic pK_a . As described by Robert Beynon⁴⁵ thermodynamic pK_a values can be corrected by Equation 3.

$$pK_{a(corr)} = pK_a + \Delta pK_a / \Delta T (T - 25)$$

Equation 3. Is the equation that is used to correct the thermodynamic pK_a to the temperature at which the buffer is used, where $\Delta pK_a / \Delta T$ is the change of pK_a over temperature ($^{\circ}C$).⁴⁵

Especially for temperature sensitive buffers like Histidine ($\Delta pK_a/\Delta T$ of -0.022^{46}) the pK_a must be corrected. As the measurements were done at or close to $25\text{ }^\circ\text{C}$ no correction based on Equation 3 was necessary. Secondly pK_a is dependent on the ionic strength and the valence of the buffer ions as shown in Equation 4. Therefore the apparent pK_a value ($pK_{a(\text{apparent})}$) has to be used.

$$pK_{a(\text{apparent})} = pK_a + (2Z + 1)A \frac{\sqrt{I}}{1 + \sqrt{I}} - 0.1I$$

$$\text{with } A = 0.4918 + 0.0006614T + 0.000004975T^2$$

Equation 4. Is the equation used to calculate the apparent pK_a based on ionic strength I (mM), ion valence (Z) and the factor A , where T is the temperature ($^\circ\text{C}$).⁴⁵

Based on a target ionic strength and temperature (i.e. 25°C) the apparent pK_a values were calculated employing Equation 4. The next step was to calculate the ratios of ions present for the polyprotic buffer. The formulas for a diprotic buffer are shown below. However this can be easily expanded also to trivalent buffers⁴⁷. First the denominator (D) that represents 100% of all cations present is calculated, Equation 5.

$$D = [\text{H}^+]^2 + K_{a1(\text{apparent})}[\text{H}^+] + K_{a1(\text{apparent})}K_{a2(\text{apparent})}$$

Equation 5. Is the equation used to calculate 100% of all buffer species present (D), $[\text{H}^+]$ is the concentration of hydrogen ions based on pH and $K_{a(\text{apparent})}$ are the dissociation constants from the buffer species.⁴⁷

Then the ratios of the three different protonation stages of the buffer can be calculated. Equation 10 calculates the ratio of non-protonated buffer acid. Equation 7 calculates the ratio of single protonated buffer acid and Equation 8 represents the buffer base.

$$[\text{H}_2\text{A}] = \frac{[\text{H}^+]^2}{D}$$

Equation 6. Is the equation used to calculate the amount of nonprotonated acidic buffer species $[\text{H}_2\text{A}]$ present, $[\text{H}^+]$ is the concentration of hydrogen ions and D is given by Equation 5.⁴⁷

$$[\text{HA}^-] = \frac{[\text{H}^+] K_{a1(\text{apparent})}}{D}$$

Equation 7. Is the equation used to calculate the single protonated acidic buffer species $[\text{HA}^-]$ present, $[\text{H}^+]$ is the concentration of hydrogen ions, $K_{a1(\text{apparent})}$ is the dissociation constant for the first protonation and D is given by Equation 5.⁴⁷

$$[\text{A}^{2-}] = \frac{K_{a1(\text{apparent})}K_{a2(\text{apparent})}}{D}$$

Equation 8. Is the equation used to calculate the buffer base $[\text{A}^{2-}]$ present, $K_{a(\text{apparent})}$ are the dissociation constants for the first and the second protonation and D is given by Equation 5.⁴⁷

After the percentage of differently charged species in the solution is calculated one can apply Equation 1 with known ionic strength in order to calculate the buffer strength. The final recipe is the ratio of buffer acid (i.e. result of Equation 6 plus Equation 7) and buffer base (Equation 8) based on the calculated buffer strength.

2.2. Storage of Samples for Stability Testing

All formulations were filtered under aseptic conditions using a $0.22\text{ }\mu\text{m}$ MillexGV syringe filter (Millipore, Billerica, USA) and filled into 6 mL glass type 1 vials having a diameter of 20 mm. The vials were then sealed with a Teflon[®]-coated serum stoppers and crimped with aluminum caps. Samples were stored bottom-up at different conditions. $40\text{ }^\circ\text{C}$ stability

was assessed by storing the vials for 3 months at 40 °C (75%rh). 25 °C and 5 °C stability was tested by storing the vials for 11 months at either 25 °C (60%rh) or 5 °C. Shaking stability was tested by placing the vials horizontally on a shaker at 25 °C(60%rh) shaking at 200 amplitudes per minute.

2.3. Computed IEP/Charge Data based on Primary Amino Acid Sequence

Isoelectric point (IEP) and the total net charge based on the total amino acid sequence were calculated using the software EMBOSS IEP at a pH of 6.0. This software calculates total net charge based on the primary sequence of antibodies and based on the pK_a values of the different amino acids taking into account disulfide bonds, C- and N-termini.¹² The pK_a values used by the software are the following: N-Termini 8.6, C-Termini 3.6, Cysteine 8.5, Aspartic acid 3.9, Glutamic acid 4.1, Histidine 6.5, Lysine 10.8, Arginine 12.5 and Tyrosine 10.1. Besides total net charge, charge of different mAb domains has also been calculated using EMBOSS IEP. The calculation was done at pH values of 5.0, 6.0, and 7.0. As all Cysteins form disulfide bonds, this amino acid was neglected. mAbs were virtually cut into Fab and Fc part. The Fc part contained the hinge region.⁴⁸ Fab fragments were separated into variable heavy-, variable light-, constant heavy-, and constant light-chain.⁴⁹ Charge of the Fc part was assessed by calculating the charge of the two heavy chain parts (CH2+CH3). At the Fc terminals the negative charge from the carboxyl residue was added and at the Fab terminals a positive charge for the amino groups was added.

2.4. Computed Relative Hydrophobicity based on Amino Acid Sequence

The relative hydrophobicity of full mAbs was calculated by summing up the individual hydrophobicities of the different amino acids.³⁴ Finally the most hydrophobic mAb was set to 100% while the least hydrophobic was set to 0%. Hydrophobicities of each separate amino acid at pH 7.0 were taken from Monera et al.³⁴ As no value for Proline was available the value was taken from data published by Sereda et al.³⁵ The individual hydrophobicities used were as followed: Alanine 41, Arginine -14, Asparagine -28, Aspartic acid -55, Cysteine 49, Glutamine -10, Glutamic acid -31, Glycine 0, Histidine 8, Isoleucine 99, Leucine 97, Lysine -23, Methionine 74, Phenylalanine 100, Proline -46, Serine -5, Threonine 13, Tryptophan 97, Tyrosine 63, and Valine 76.

2.5. Isoelectric Focusing by Capillary Electrophoresis

10 mg/mL samples formulated in 20 mM His/His-HCl pH 6.0 were diluted in water to ca. 0.7 mg/mL and then 1:1 with sample buffer to yield a final solution containing ca. 0.35 mg/mL antibody, 0.7 %(v/v) methylcellulose (Convergent Bioscience, Toronto, Canada), 8 %(v/v) carrier ampholytes (85 % carrier ampholyte 8-10.5, and 15 % carrier ampholyte 3-10 (Sigma, St.Louis, USA)). For IEP determination, 1 μ l of each pH marker was added to 180 μ l of sample. pH markers used were pH 4.65 and pH 10.10 (Convergent Bioscience, Toronto, Canada). Determination of the isoelectric point (IEP) was carried out by isoelectric focusing capillary electrophoresis using an iCE280 FAST IEF Analyzer (Convergent Bioscience, Toronto, Canada) equipped with a CE System autosampler

(Prince Technologies, Emmen, Netherlands). By assuming a linear pH gradient between the two IEP markers, the antibodies' IEP was defined as the pH value of the main peak. Obviously, as a variety of charge variants are contained in the antibodies for various reasons more than one peak was seen in iCE280. Samples were measured in triplicates reporting the mean \pm SD.

2.6. Determination of Isoelectric Point by Measuring Electrophoretic Mobility and Mutual Diffusion Coefficient during pH Titration

Four mAbs (1, 3, 6 and 8) formulated in 10 mM NaCl/H₂O at 10 mg/mL protein concentration were titrated from pH 4 to pH 10. Titration was done using the MPT-2 Autotitrator (Malvern, Worcestershire, UK) with 1 M NaOH and 1 M HCl as titration solutions. The pH was initially adjusted to pH 4. Subsequently, pH was increased in steps of about 0.5 (\pm 0.2) pH units. At each 0.5 pH step, electrophoretic mobility together with mutual diffusion coefficient (D_m) were assessed using Zetasizer Nano Series (Malvern, Worcestershire, UK). 1 mL of a 10 mg/mL sample was filtered via a 0.2 μ m filter (Millipore, Billerica, USA) directly into a capillary cell (DTS1060, Malvern Worcestershire, UK) and sealed with corresponding plastic caps under laminar air flow. Electrophoretic mobility was determined by laser Doppler velocimetry by three independent measurements. Data analysis was done using Dispersion Technology Software V5.10 (Malvern, Worcestershire, UK). Per independent measurement, 40 cycles were run. The assessment was based on the fast field reversal (FFR) function to avoid extensive stress to the protein.

D_m was measured using dynamic light scattering by three independent measurements. Per independent measurement, D_m was assessed 12 times for 10 seconds duration.

IEP by electrophoretic mobility was defined as the pH where electrophoretic mobility crosses zero, assuming a straight line between the two data points enclosing the x-axis.¹⁰

IEP by D_m was chosen to be in the range of the lowest three data points measured (Figure 3.2.2).

Titration experiments were performed at least twice to show reproducibility. The figures show representative examples. Electrophoretic mobility and mutual diffusion coefficient are shown as the mean of three independent measurements \pm SD.

2.7. Determination of Zetapotential and Net Charge

Zetapotential ζ was determined using Zetasizer Nano Series (Malvern, Worcestershire, UK). ζ (V) is calculated based on Equation 9, where μ is the electrophoretic mobility measured by laser Doppler velocimetry (m^2/Vs), η is the solvent viscosity (water at 25 °C: 0.8872 mPa.s, Dispersion Technology Software V5.10, Malvern), ϵ ($\text{A}^2 \text{s}^4/\text{kg m}^3$) is absolute dielectric constant (derived from relative dielectric constant for water: 78.5, Dispersion Technology Software V5.10, Malvern) and $f(ka)$ is Henry's function using Huckel approximation (value=1, Dispersion Technology Software V5.10, Malvern). Zetapotential was assessed for all mAbs formulated in 20 mM His/His-HCl pH 6.0. Results are shown as mean of three independent samples \pm SD.

$$\zeta = \frac{\mu 3\eta}{2\epsilon f(ka)}$$

Equation 9. Determination of zeta potential, ζ is the zeta potential (V), μ is the electrophoretic mobility (m^2/Vs), η is the solvent viscosity (Pa.s), ϵ is absolute dielectric constant ($\text{A}^2 \text{s}^4/\text{kg m}^3$) and $f(ka)$ is Henry's function.¹⁰

Protein net charge was experimentally determined using 3 different approaches:

- a) employing electrophoretic mobility measurements combined with protein's self diffusion coefficient (D_s) based on Equation 10 for net charge determination; using a constant self diffusion ($D_{s \text{ const.}}$).
- b) employing electrophoretic mobility measurements combined with protein's self diffusion coefficient (D_s) based on Equation 10 for net charge determination; using a calculated self diffusion coefficient. (D_s)
- c) based on determination of Donnan equilibrium.

In case of a) and b) Equation 10 was used, where z is the net charge, μ the electrophoretic mobility measured by laser Doppler velocimetry (m^2/Vs), k_B the Boltzmann constant ($1.3807 \times 10^{-23} \text{ J/K}$), T the temperature (298 K), D_s the self diffusion coefficient (m^2/s), e the elementary charge ($1.6 \times 10^{-19} \text{ C}$).¹⁷

For both a) and b) the electrophoretic mobility was assessed using Zetasizer Nano Series (Malvern, Worcestershire, UK). 1 mL of a 10 mg/mL sample was filtered via a 0.2 μm filter (Millipore, Billerica, USA) directly into a capillary cell (DTS1060, Malvern Worcestershire, UK) and sealed with corresponding plastic caps under laminar air flow. Electrophoretic mobility was determined by laser Doppler velocimetry by three independent measurements. Data analysis was done using Dispersion Technology Software V5.10, Malvern. Per independent measurement, 40 cycles were run. In order to minimize protein stress, analysis was performed using the fast field reversal function (FFR).⁵

$$z = 3 \frac{\mu k_B T}{D_s e}$$

Equation 10. Determination of the net charge, z is the net charge (unitless), μ the electrophoretic mobility (m^2/Vs), k_B the Boltzmann constant ($1.3807 \times 10^{-23} \text{ J/K}$), T the temperature (K), D_s the self diffusion coefficient (m^2/s), e the elementary charge ($1.6 \times 10^{-19} \text{ C}$).¹⁷

As already mentioned above, two different approaches a) and b) have been applied for the calculation of the effective net charge based on Equation 10. For approach a), the self diffusion coefficient D_s was set constant to $4.37 \pm 0.13 \times 10^{-11} \text{ m}^2/\text{s}$. This value was determined experimentally as follows: it represents the mean intercepts from extrapolation to infinite dilution of D_m versus protein concentration for all eight antibodies measured in 20 mM His/His-HCl buffer \pm NaCl (data generated during k_D measurements, see Figure 3.1.6. The measured value is well comparable to what was recently published by Yadav et al. for a mAb measured at different conditions, i.e. $4.34 \pm 0.09 \times 10^{-11} \text{ m}^2/\text{s}$.⁵ This diffusion coefficient therefore will be referred to as $D_s \text{ const.}$

For approach b), D_s was determined based on a conversion from experimentally determined mutual diffusion coefficient D_m at 10 mg/mL. D_m is the primary measured variable in DLS (Zetasizer Nano Series, Malvern, Worcestershire, UK).

This approach is due to the fact, that D_s cannot be directly assessed by the methods described here.²² Efforts have been taken to convert the one into the other (i.e. D_m into D_s) as described elsewhere.⁵⁰⁻⁵² Le Bon et al. postulate an equation linking D_m and D_s (Equation 11) as described for β -Lactoclobulin⁵¹. This equation can be used to convert D_m to D_s which will be referred to as D_s conv. D_m is the mutual diffusion coefficient (m²/s), φ is the volume fraction (partial specific volume (= 0.739 mL/g for an IgG⁵³) times concentration (g/mL)), K is a constant (Equation 14), c is the protein concentration (g/mL), R_θ is the Rayleigh scattering intensity (1/cm), D_s is the self diffusion coefficient (m²/s) and M is the molecular mass of an antibody (150000 g/mol).

Having only D_m and the concentration c , it was possible to calculate A_2 by applying Equation 15 and 10, assuming D_0 ($4.37 \pm 0.13 \times 10^{-11}$ m²/s) and M (150000 g/mol) constant. Equation 13 then gave Kc/R which in combination with D_m can be used to calculate D_s by Equation 11. Equation 13 was proven to be linear up to 10 mg/mL (data not shown).

$$D_m = (1 - \varphi)^2 \frac{Kc}{R_\theta} D_s M$$

Equation 11. Conversion of self diffusion coefficient (D_s) from mutual diffusion coefficient (D_m) according to Le Bon et al., D_m is the mutual diffusion coefficient (m²/s), φ is the volume fraction (unitless), K is a constant (Equation 14), c is the protein concentration (g/mL), R_θ is the Rayleigh scattering intensity (1/cm), D_s is the self diffusion coefficient (m²/s) and M is the molecular mass of an antibody (150000g/mol).⁵¹

The net charges were determined for all mAbs formulated in 20 mM His/His-HCl pH 6.0. Results are reported as mean of three independent samples \pm SD. To show change of net charge upon pH variation, data from the pH titration experiment of mAb 1, 3, 6, and 8 was used. For experimental details please refer to 2.6.

Additionally, Donnan equilibrium (approach c)) was applied for net charge determination of four selected mAbs (1, 3, 6 and 8). The Donnan equilibrium was assessed by determining the inhomogeneous distribution of Histidine ions¹⁵ to the surrounding buffer after equilibrium dialysis using dialysis cassettes (Slide-A-Lyzer Cassette 10 kD MWCO, Thermo Scientific, Rockford, USA). 1 mL of protein formulated at 150 mg/mL protein concentration in 20 mM His/His-HCl buffer pH 6.0 was dialyzed against 20 mM His/His-HCl pH 6.0 buffer for two days at 2-8 °C. Afterwards, Histidine concentration, protein concentration and pH from permeate and retentate were measured. Density at the measured concentration of all mAbs was based on experimental data using a model mAb (data not shown). The total Histidine content (i.e. without discrimination between the positively charged His⁺ and the neutral free His base) was quantified using HPLC-SEC-UV with a TSK G3000 SWXL, 7.8x300 mm column (Tosoh Bioscience, Stuttgart, Germany) and a detection at 220 nm. Concentration of His⁺ was calculated from the measured total Histidine content (His⁺ and free His base) using measured pH and the Henderson Hasselbalch equation⁴⁴ (Histidine pK_a 6.04)⁴⁴. For the calculation of charge, Equation 12 was used. Z is the resulting net charge (unitless), C_{3+} is the concentration of His⁺ ions (mol/mL) in the retentate. C_{3+}' represents the His⁺ ion concentration in the permeate (mol/mL), ρ is density of the retentate (g/cm³), ρ' the density permeate (g/cm³), c_2 is the protein concentration in the retentate (g/mL) and M is molecular mass of the antibody (150000 g/mol). The mean of two independent samples \pm absolute deviation is shown.

$$Z = \frac{-C_{3+}^2 + \left(\frac{C_{3+}'}{\rho'} \left(\rho - \frac{c_2}{1000} \right) \right)^2}{\frac{c_2}{M_2} C_{3+}}$$

Equation 12. Calculation of protein net charge based on Donnan Equilibrium, Z is the resulting net charge (unitless), C_{3+} is the concentration of His⁺ ions in the retentate (mol/mL), C_{3+}' represents the His⁺ ion concentration in the permeate (mol/mL), ρ is density of the retentate (g/cm³), ρ' the density permeate (g/cm³), c_2 is the protein concentration in the retentate (g/mL) and M is molecular mass of the antibody (150000 g/mol).⁵⁴

2.8. Determination of Second Virial coefficient (A_2) by Static Light Scattering

Second virial coefficients (A_2) of mAbs were analyzed by static light scattering (SLS). A_2 is derived from Debye plots^{25,28} (Equation 13 and Equation 14). A series of different mAb concentrations (5x1 mL serial dilutions from 1 mg/mL to 5 mg/mL) was injected into a three angle SLS detector coupled to RI detection (miniDawn Treos and rEX, Wyatt, Santa Barbara, USA) in batch mode starting from lowest protein concentration. A 0.1 μ m filter (Whatman, Maidstone, UK) was attached to the inlet in order to on-line filter every sample prior analysis. The RI detector was used for online-quantification of the protein concentration per plateau ($dn/dc = 0.185$ mL/g for proteins^{55,56}). The software used was ASTRA Software 5.3.4.10, Wyatt, Santa Barbara, USA. After each sample injection and measurement, protein-free formulation buffer was injected until Rayleigh scattering reached baseline levels.

The excess Rayleigh scattering of the 90° angle was used to generate a Debye plot (y-axis: Kc/R_θ , x-axis: protein concentration) based on Equation 13 where K is a system constant (Equation 14), n_0 is the refractive index of the solvent (water at 658 nm, 25°C: 1.331, from Astra Software, Wyatt, Santa Barbara), dn/dc the refractive index increment of the antibody (0.185 mL/g for proteins^{55,56}), N_A is Avogadro's number (6.022×10^{23} mol⁻¹) and λ the laser wavelength (6.58×10^{-5} cm), c is the concentration of antibody (g/mL) determined by RI detector, R_θ is the recorded Rayleigh scattering intensity of the 90° angle (1/cm), M is the molecular mass (g/mol) of the protein (inverse intercept of y-axis) and A_2 is the second virial coefficient (slope divided by two) (mol mL/g²). The measured MW for the 8 mAbs (ranging from 151.6 – 163.2 kDa) were in the range of the actual MW (i.e. theoretical M_w incl. glycopattern, 147.7 – 153.0 kDa, for details see Figure 3.1.4). For every monoclonal antibody, two formulations were tested, i.e. 20 mM His/His-HCl pH 6.0 in absence or presence of 150 mM NaCl. Results are presented as mean \pm absolute deviation of two independent measurements.

$$\frac{Kc}{R_\theta} = \frac{1}{M} + 2A_2c$$

Equation 13. Debye plot used to determine second virial coefficient, K is a system constant (Equation 14), c is the concentration of antibody (g/mL), R_θ is the recorded Rayleigh scattering intensity of the 90° angle (1/cm), M is the molecular mass (g/mol) of the protein and A_2 is the second virial coefficient (mol mL/g²)^{25,28}

$$K = 4\pi^2 \left(\frac{dn}{dc} \right)^2 n_0^2 N_A^{-1} \lambda_0^{-4}$$

Equation 14. System constant K from Equation 13 where n_0 is the refractive index of the solvent (unitless), dn/dc the refractive index increment of the antibody (mL/g), N_A is Avogadro's number ($6.022 \times 10^{23} \text{ mol}^{-1}$) and λ the laser wavelength (cm)^{25,28}

2.9. Determination of Interaction Parameter k_D by Dynamic Light Scattering (DLS)

Assessment of the interaction parameter k_D ^{5,22,29} (Equation 15 and Equation 16) was performed via dynamic light scattering (DLS) using a DynaPro plate reader (Wyatt, Santa Barbara, USA) with a 384 well Sensoplate, black and glass bottom (Greiner Bio-One, Kremsmünster, Austria). The software used was Dynamics V6, Version: 6.11.1.3, Wyatt, Santa Barbara, USA. Sample preparation was done by filtering samples using a 0.2 μm filter (Millipore, Billerica, USA). 10 measurements à 2 seconds per well were performed. Serial dilutions (10 mg/mL to 3 mg/mL) in 20 mM His/His-HCl buffer with and without 150 mM NaCl were prepared. D_m was plotted versus protein concentration c (g/mL) to get k_D . More precisely, k_D is calculated from the slope divided by the intercept which is D_0 (Equation 15).

The relation between k_D and A_2 is shown in Equation 16. D_m is the mutual diffusion coefficient as measured in DLS (m^2/s), D_0 the diffusion coefficient at infinite solute dilution (m^2/s), A_2 the second virial coefficient (mol mL/g^2), M the molecular mass of the protein (g/mol), ζ_1 is from the virial expansion of the concentration dependent friction coefficient (mL/g) and v_{sp} the partial specific volume of protein. Results are presented as mean \pm absolute deviation of two independent measurements.

$$D_m = D_0(1 + k_D c + \dots)$$

Equation 15. Dependency of D_m from D_0 , the interaction parameter k_D and solute concentration, D_m is the mutual diffusion coefficient (m^2/s), D_0 the diffusion coefficient at infinite solute dilution (m^2/s), c the antibody concentration (g/mL)^{22,40}

$$k_D = 2A_2M - \zeta_1 - v_{sp}$$

Equation 16. Relation between the interaction parameter k_D and the second virial coefficient A_2 (mol mL/g^2), M is the molecular mass of the protein (g/mol), ζ_1 is from the virial expansion of the concentration dependent friction coefficient (mL/g) and v_{sp} is the partial specific volume of protein (mL/g)^{22,40}

What is also recorded when measuring D_m is the sample's scattering intensity. This is important for comparison to samples turbidity under 3.5.1.

2.10. Determination of Self Diffusion Coefficient (D_s) by NMR

All NMR spectra were taken on a Bruker 600 MHz Avance II spectrometer (Bruker Biospin GmbH, Ettlingen, Germany) equipped with a cryogenic QCI probehead at a temperature of 300 K. Spectrometer operation and data processing were done on Topspin 2.1 (Bruker BioSpin GmbH). Samples were spiked with 5 % NMR-grade D_2O . Short disposable 5 mm NMR tubes (Bruker) were used. 1D ^1H (zero-go with presaturation) and diffusion edited 1D DOSY-presat (Diffusion Ordered Spectroscopy) with a gradient strength of 5, 20, 67.3 and 95 % of the current strength, of the Bruker GAB gradient unit (uncalibrated) of PGSE type, spectra were acquired. Integrals were extracted by use of Amix Software (Bruker,

Rheinstetten). The acquisition parameters were as follows: name of pulse sequence of Bruker library was ledbpgppr2s1d; number of repetitions for different gradients 32 (5 %), 64, 128, 256 (95 %) to compensate for reduction of signal to noise; interscan relaxation delay for thermal equilibration 1.5 s; diffusion time 300 ms; number of datapoints acquired 32k; gradient shape SMSQ10.100. For processing an exponential line-broadening window function with lb 2 was used with 64k datapoints of processed spectra.

The self diffusion coefficient was determined based on the Stejskal Tanner formalism (Equation 17).⁵⁷ To do so the system constant needs to be determined.

To determine the system constant Histidine in a 20 mM His/His-HCl pH 6.0 buffer was measured. Assuming that the Histidine is freely diffusing in the placebo formulation and that the hydrodynamic radius of Histidine is equal to the hydrodynamic radius measured at similar conditions by Germann et al.,⁵⁸ based on Stokes-Einstein, equation the self diffusion coefficient of Histidine was calculated.²² Knowing the self diffusion coefficient (D_s) and the gradient G^2 (slope) the system constant (K_{nmr}) could be calculated based on the signal intensity (I) using Equation 17. K was found to be -2.08×10^6 s/T².

$$I = I_0 \exp(-K_{nmr} D_s G^2)$$

Equation 17. System constant (K_{nmr}) was calculated by dividing the slope by the self diffusion coefficient D_s .⁵⁷

2.11. Determination of Hydrophobicity by Fluorescence

Hydrophobicity by fluorescence was assessed using a Varian Cary Eclipse System (Varian, Palo Alto, US) with a 1 mL quartz cuvette 10.00 mm (Hellma, Müllheim, Germany). The software used was Cary Eclipse Scan Application V1.1(132) (Varian, Palo Alto, US). 10 μ l mAb or BSA at (10 mg/mL) was diluted with 1.5 mL of respective buffer and 2 μ l of a 10 mM solution of NPN marker (N-Phenyl-1-naphthylamin) (dissolved in Ethanol) was added. The set up for the measurement was as follows: Excitation at 265 nm, Emission scan from 270 nm to 650 nm, Excitation Slit 2.5 nm, Emission Slit 5 nm, Smoothing 19, Manual Voltage gain 1000, and Emission filter Auto. The emission signal of the protein excites the marker. Proximity to the protein (binding) and immobilization of marker causes a blue shift and a strong signal increase.³⁸

2.12. Determination of Hydrophobicity by ESR

Non-invasive ESR measures the interaction of paramagnetic molecules with their molecular environment. Using nitroxides as spin probes, it is possible to assess binding of hydrophobic markers to the protein. Binding influences the tumbling behavior of the nitroxyl radicals which is characterized by the rotational correlation time τ_c . ESR spectra were recorded (first derivation) using a Magnettech X-Band (9.4 GHz) spectrometer. ESR parameters were set as follows: field centre 335.3 mT, scan range 4.81 mT, scan time 600 s, modulation amplitude 78 μ T, dampening 6 dB. The spin probe 5-Doxyl (2-(3-Carboxypropyl)-4,4-dimethyl-2-tridecyl-3-oxazolidinyloxy) was solved in Acetone, aliquoted, and solvent was evaporated. Then the spin probe was re-dissolved with 10 mg/mL antibody solution in 20 mM His/His-HCl pH 6.0 \pm 150 mM NaCl to yield a spin probe concentration of 0.5 μ M. Finally the ESR spectra were compared.

2.13. Determination of Surface Activity by Drop Tensiometer

Surface activity was assessed by a Krüss Easy Drop Tensiometer (Krüss, Hamburg, Germany) using a 1 mL Inject-F syringe (B. Braun, Melsungen, Germany) containing the sample, equipped with a 1.8 mm diameter needle (Krüss, Hamburg, Germany). The drop was generated within a quartz cuvette sealed by a plastic cap having an opening for the syringe needle. To protect the drop from evaporation the bottom of the cuvette was filled with water. The drop volume did not change over time; therefore no evaporation took place (data not shown). The drop shape was analyzed by the software Drop Shape Analysis (DSA) V1.92.1.1 (Krüss, Hamburg, Germany). The theory how surface tension can be determined by pendant drop volume and radius of curvature at the apex is described in literature.⁵⁹ Measurement was done by recording a 30 minutes video with 450 frames. To calculate the surface tension the density of the solution was considered. Since two different formulations and two different protein concentrations were tested the densities used were as follows: 10 mg/mL solutions and placebo in 20 mM His/His-HCl pH 6.0 had a density of 1.0028 g/mL. 10 mg/mL solutions and placebo in 20 mM His/His-HCl pH 6.0 + 150 mM NaCl had a density of 1.0076 g/mL. 100 mg/mL solutions in 20 mM His/His-HCl pH 6.0 had a density of 1.0287 g/mL. 100 mg/mL solutions in 20 mM His/His-HCl pH 6.0 + 150 mM NaCl had a density of 1.0335 g/mL.

2.14. Determination of Ammonium Sulphate Precipitation Concentration

Different mAbs were diluted with ammonium sulphate solutions to yield a dilution series of 1 mg/mL mAb solutions containing 0-2 M ammonium sulphate. The formulation buffer was 20 mM His/His-HCl pH 6.0. After centrifugation (60 s at 16 rcf) the supernatant was collected and remaining protein concentration was determined by UV. Afterwards the ammonium sulphate concentration at which 50 % of protein are precipitated (PC50) was determined by a sigmoidal fit in Origin 7SR1 v 7.0300(B300). The error shown is the deviation from the predicted (fitted) value and is represented as χ^2 divided by the degrees of freedom.

2.15. Analysis of Soluble Aggregates by Size Exclusion Chromatography

Size Exclusion High Performance Liquid Chromatography (SE-HPLC) was done on an Alliance 2795 combined with a 2487-UV detector (Waters Corporation, Milford, MA). The column used was a TSK G3000 SWXL, 7.8x300 mm column (Tosoh Bioscience, Stuttgart, Germany). The separation was performed using a mobile phase of 200 mM potassium phosphate buffer pH 7.0 including 250 mM KCl. A flow rate of 0.5 mL/min at a constant temperature of 25 °C was used. Samples were injected at 10 mg/mL and a total loading amount of 200 µg. Detection was performed at a wavelength of 280 nm. To analyze irreversible aggregate levels of mAb6 and not the reversible dimers samples were prepared according to a special HPLC-SEC method for mAb6 (provided by Hoffmann-La Roche Ltd.). mAb6 was diluted to 0.5 mg/mL and stored for at least 24 h at 30°C prior to injection of 100µL of sample. The total soluble high molecular mass products (peak areas of dimers and higher soluble oligomers) relative to the total peak area was calculated

using the Empower 2 Chromatography Data System software (Waters Corporation) and reported as “%HMW”.⁶⁰

2.16. Turbidity and Subvisible and Visible Particle Analysis

For turbidity assessment 1.5 mL of sample was filled under particle free conditions into clean 11 mm glass tubes (HACH Lange GmbH, Düsseldorf, Germany) and analyzed in a HACH 2100AN turbidimeter (HACH Company, Loveland, CO). As the samples turbidity is compared to reference suspensions of Formazin standards the result is given in Formazin turbidity units (FTU).⁶¹

Visible particle analysis was performed on a V90-T (SEIDENADER, Markt Schwaben, Germany). Samples were spun and moving particles were classified after spinning stopped. Different scores were assigned to the amount of particles in the vial (0 particles = 2; 1 particle = 4, 2-10 particles = 6; >10 particles = 8). As two vials were always analyzed the final score was the sum of both (scores) divided by two.

After that the amount of subvisible particles present was counted by light obscuration technique using a HIAC ROYCO 3000A particle counter (HACH Lange, Düsseldorf, Germany).⁶¹ Data is presented as cumulative counts per mL.

2.17. Determination of Dynamic Viscosity by Plate-Cone Rheometer

Samples' viscosity was assessed by a MCR300 rheometer (Anton Paar GmbH, Graz, Austria) using a plate-cone measurement system (Cone: CP50-0.5 Anton Paar GmbH, Graz, Austria). Measurement was done at 20 °C. 380µl of Sample was equilibrated for one minute at a shear rate of 10⁻⁸, then shear rate was increased from 100-2000⁻⁸ within one minute. Finally - during a holding step at a shear rate of 2000⁻⁸ - dynamic viscosity was recorded six times over 15 seconds. The averaged value was the result of a single measurement. Measurements were done as duplicates reporting the mean ± absolute deviation.

2.18. Calculation of Propagation of Error

When the mean values are a combination of several experimentally determined variables (i.e. in a linear function), the propagation of error (= propagation of uncertainty) has to be considered.⁶² Equation 18 shows how error propagation was calculated, s_z being the standard deviation of the result z calculated from the variables x and y having a standard deviation of s_x and s_y .

$$\left(\frac{s_z}{z}\right)^2 = \left(\frac{s_x}{x}\right)^2 + \left(\frac{s_y}{y}\right)^2$$

Equation 18. Error propagation calculation for x times y or x divided by y ⁶²

3. RESULTS AND DISCUSSION

3.1. A_2 Method Development

3.1.1. Development of a Method for Determination of A_2 by SLS

To successfully establish an A_2 determination method by means of static light scattering (SLS) some prerequisites were necessary. As SLS is performed in batch mode, a stable light scattering signal, i.e. a stable plateau, is needed for each concentration level analyzed. In addition successful removal of protein from the sample cell is required prior to the next measurement. This can be controlled by reaching the baseline level after each sample measured. An example of Rayleigh scattering recorded for different protein concentrations can be seen in Figure 3.1.1. It shows that by injecting the samples via syringe pump and using an in-line filter (0.1 μm , Whatman, Maidstone, UK) stable plateaus could be generated and also successful removal of sample (stable baseline) was demonstrated.

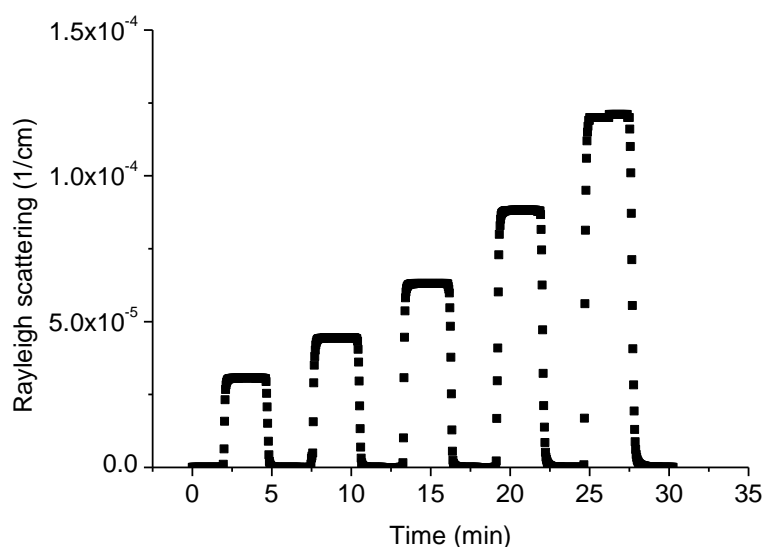


Figure 3.1.1. Rayleigh scattering at 90°-angle upon injecting different mAb concentrations (up to 5 mg/mL) into MALS detector (batch mode). After each sample injection, the measurement cell was flushed with placebo until baseline was reached

On increasing protein concentration the Rayleigh scattering increases depending on the second virial coefficient (A_2) (see Equation 13). It is known from literature that mAbs differ in their A_2 behavior especially within different formulation conditions.^{5,7} A_2 for example can reflect charge-charge interactions that are dependent on the protein studied as well as the amount of buffer ions surrounding it.^{6,8} So the next step was to demonstrate that the method is sensitive enough to show that different antibodies show different Rayleigh scattering within the same formulation. Two formulation conditions were chosen namely 20 mM His/His-HCl (pH 6.0) with and without 150mM NaCl. Especially in the Histidine formulation without NaCl differences between the mAbs could be seen. How a valid measurement is defined is described further down this section. The Rayleigh scattering of eight mAbs over concentration is shown in Figure 3.1.2.

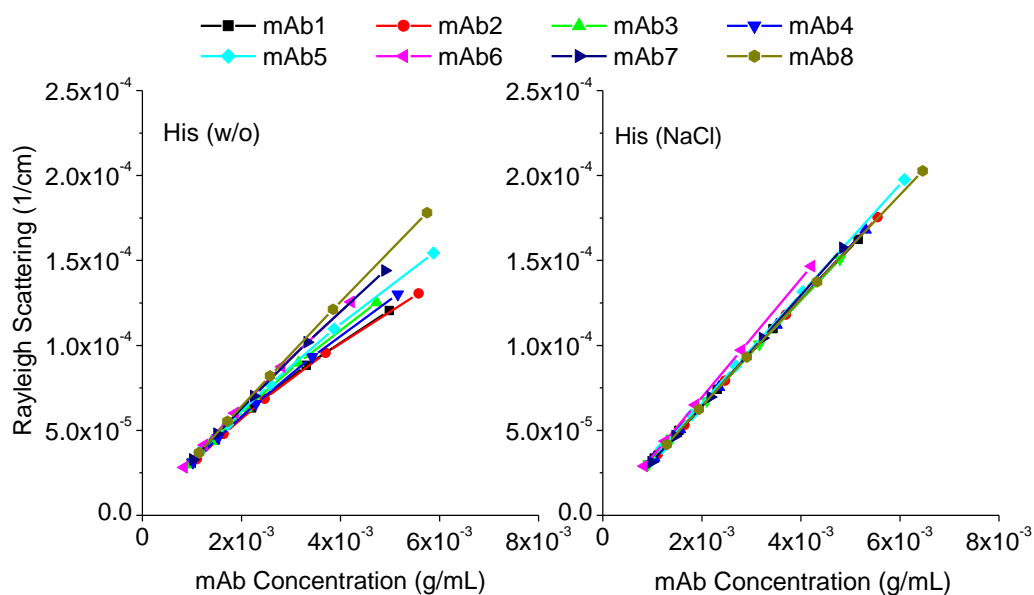


Figure 3.1.2. The 90° Rayleigh scattering at increasing protein concentration of eight mAbs at two different formulations (left: 20 mM His/His-HCl (pH 6.0), right: 20 mM His/His-HCl (pH 6.0) + 150 mM NaCl). Data are shown as one representative example of $n=2$.

The more attractive particles are, the smaller their statistical separation distance and the bigger the particles appear (i.e. density fluctuations).²² The scattered light intensity is dependent on particle size. So attractive particles will show stronger Rayleigh scattering.²² The prerequisite for analysis based on Rayleigh scattering is that the particles are small compared to excitation light wavelength. It should be smaller than 1/20 of the wavelength.⁶³ In this case (as the laser wavelength was 658 nm) not bigger than ca. 33 nm. As a mAb has a radius of about 5.1 nm this condition is given.¹⁷ Recording the difference in scattering intensity of multiple mAbs at increasing protein concentration is essential for the measurement of A_2 by SLS because the difference in Rayleigh scattering (scattering intensity) with concentration is necessary to be able to apply Equation 13 (p.13) (i.e. Debye plot), and determine A_2 .

The analysis of A_2 by using Debye plot requires two criteria to be met. First, the generated slope in the Debye plot needs to be linear. This is indicated by Equation 13 (p.13). A nonlinear slope would deviate from this underlying model. A non-linearity can be caused by higher order interactions. Examples of high concentration Rayleigh signals and the link to higher order interactions were for example observed and published by Scherer et al.⁶⁴ For assessing A_2 in the final method, the protein concentration has to be within the linear range of the Debye plot.

The Debye plots are shown in Figure 3.1.3. It nicely demonstrates that the resulting Debye plots of the Rayleigh scattering are linear at the defined protein concentration range. A negative slope represents an attractive two particle interaction (negative A_2) and a positive slope a repulsive two particle interaction (positive A_2).⁸ Within the His(w/o) condition the mAbs are repulsive (positive slopes) whereas in the His(NaCl) condition these repulsions are shielded by counter ions resulting in slopes that are at or close to zero attraction/repulsion. These results were expected and will be explained later.

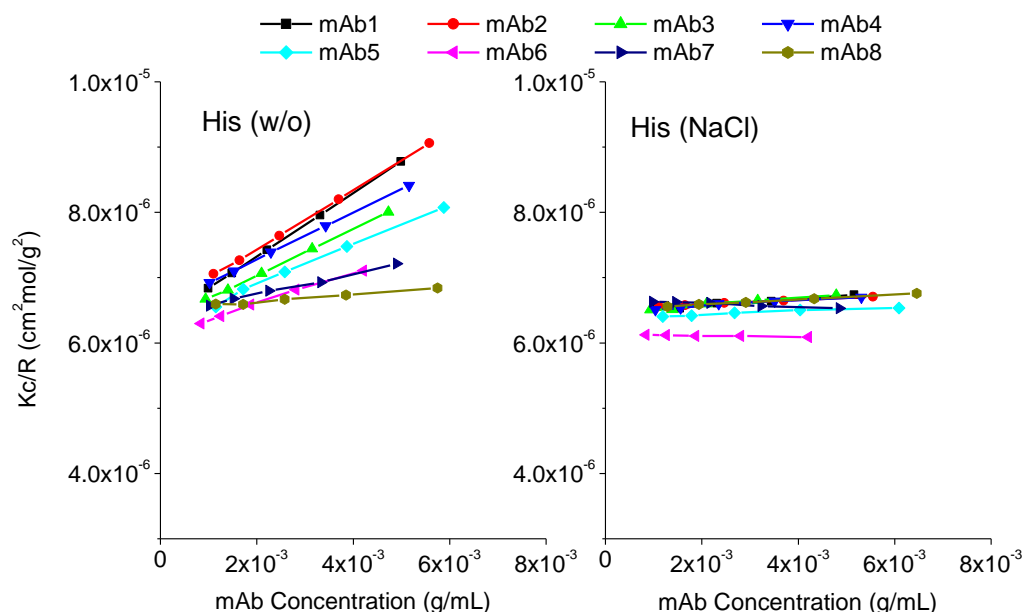


Figure 3.1.3. Debye plots of eight different mAbs at two different formulations (left: 20 mM His/His-HCl (pH 6.0), right: 20 mM His/His-HCl (pH 6.0) + 150 mM NaCl). Data are shown as one representative example of $n=2$.

The second prerequisite for a successful and accurate A_2 determination by Debye plot is the molecular mass control. As given by Equation 13 (p.13) the intercept of the Debye plot is the inverse molecular mass (g/mol). If the measured molecular mass is wrong either the sample is aggregated/fractionated or other variables were not set/determined correctly, like for example the protein concentration. Therefore monitoring the detected molecular mass serves as a good means to control each SLS experiment. This can be seen in Figure 3.1.4. Expected molecular mass data was based on primary amino acid sequence and the glycopattern. All determined molecular mass values were within the expected range. Deviations are due to the fact that via SLS only an averaged value is measured.⁸ If dimers/multimers/fractions of mAbs are present the molecular mass can vary from expected values.

It was possible to successfully establish a method that allowed measurement of A_2 using the 90° Rayleigh scattering. As this is the method development part, further discussion of the A_2 results for the different mAbs within different formulation conditions can be found under 3.2.5 and onwards.

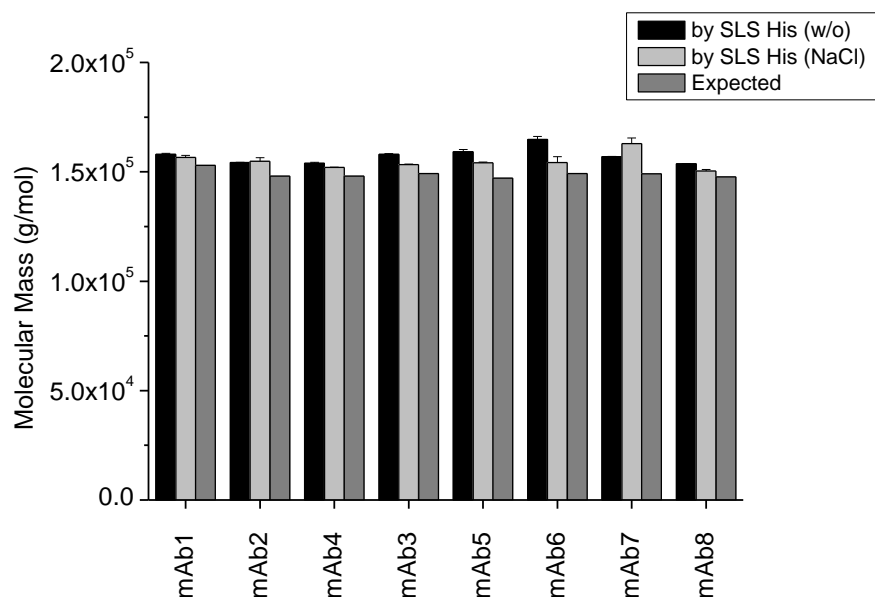


Figure 3.1.4. Comparison of measured average molecular mass (g/mol) of eight different antibodies within two formulations (His (w/o): 20 mM His/His-HCl (pH 6.0), His (NaCl): 20 mM His/His-HCl (pH 6.0) + 150 mM NaCl) to the expected molecular mass based on primary amino acid sequence and main glycosylation pattern. Data are shown as mean of $n=2 \pm$ absolute deviation.

3.1.2. Development of a Method for Determination of Protein-Protein-Interaction by DLS

Assessment of protein-protein interaction by means of dynamic light scattering (DLS) can be done by measuring the fluctuation of the scattered light. This is different to SLS since in SLS the average scattering intensity is assessed. The frequency of this fluctuation is dependent on the diffusion speed that two particles have relative to each other. Therefore DLS measures the so-called mutual diffusion coefficient (D_m). As the diffusion of two particles relative to each other is dependent on their interaction, a change of D_m over concentration can be used to derive the interaction parameter k_D which is related to A_2 .^{5,22,65}

Similar to SLS measurements and determination of A_2 , k_D determination by DLS has two prerequisites. Based on Equation 15 (p.14) k_D can be determined by dividing the slope of D_m over protein concentration c by the intercept. In order to apply Equation 15 the slope needs to be linear for concentration ranges tested. This could be demonstrated for eight different mAbs within two different formulations (20 mM His/His-HCl (pH 6.0) \pm 150 mM NaCl) and is shown in Figure 3.1.5. For the chosen concentration range (3-10 mg/mL) slope linearity could be successfully demonstrated. The nonlinear concentration range in DLS is covered in chapter 3.6.

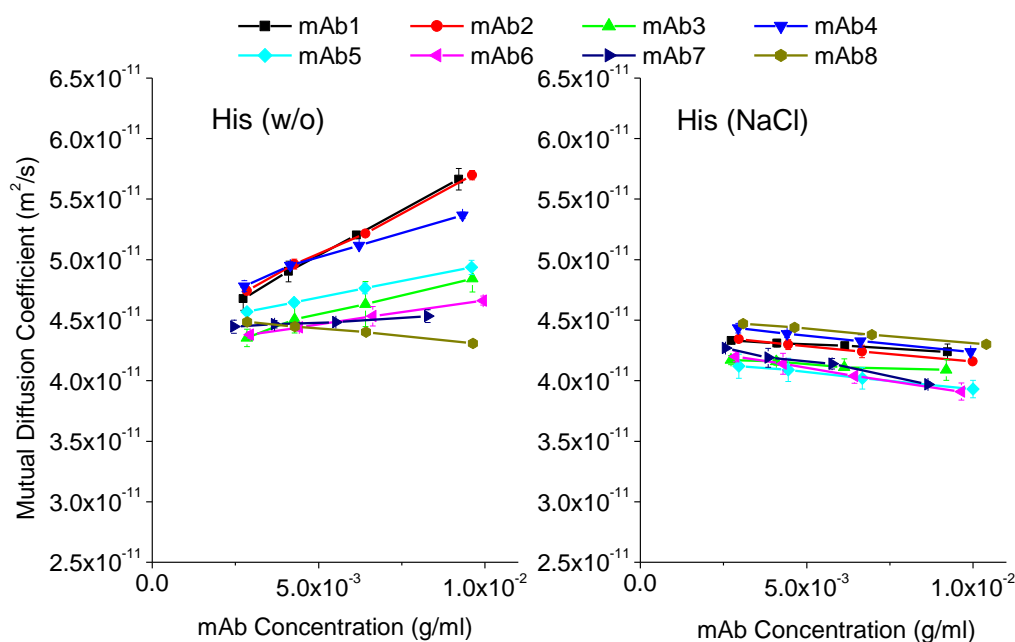


Figure 3.1.5. Mutual diffusion coefficient (D_m) (m^2/s) was recorded at different mAb concentrations for eight mAbs within two formulation conditions (left: 20 mM His/His-HCl (pH 6.0), right: 20 mM His/His-HCl (pH 6.0) + 150 mM NaCl). Data are shown as mean of $n=2 \pm$ absolute deviation.

The second prerequisite for a successful k_D determination is the D_0 control, i.e. the diffusion coefficient at infinite dilution. Similar to SLS where molecular mass is determined as a control, the intercept in DLS as shown by Equation 15 (p.14) gives D_0 . This diffusion coefficient at infinite dilution is by definition directly related to the hydrodynamic radius of the protein, based on Stokes-Einstein equation (Equation 20, p.31). As mAbs have a similar molecular mass they also share a common hydrodynamic radius (i.e. D_0)⁵. If the hydrodynamic radius is outside the expected range either the sample is aggregated/fractionated or a measurement parameter wasn't determined correctly (e.g. mAb concentration).

Figure 3.1.6 demonstrates that the measured D_0 for all mAbs are in a similar range. The averaged value over the eight mAbs is $4.37 \pm 0.13 \times 10^{-11} m^2/s$ and is well comparable to what was recently published by Yadav et al.⁵ (i.e. $4.34 \pm 0.09 \times 10^{-11} m^2/s$, measured for a single mAb at 6 different pH values at low and high ionic strength).

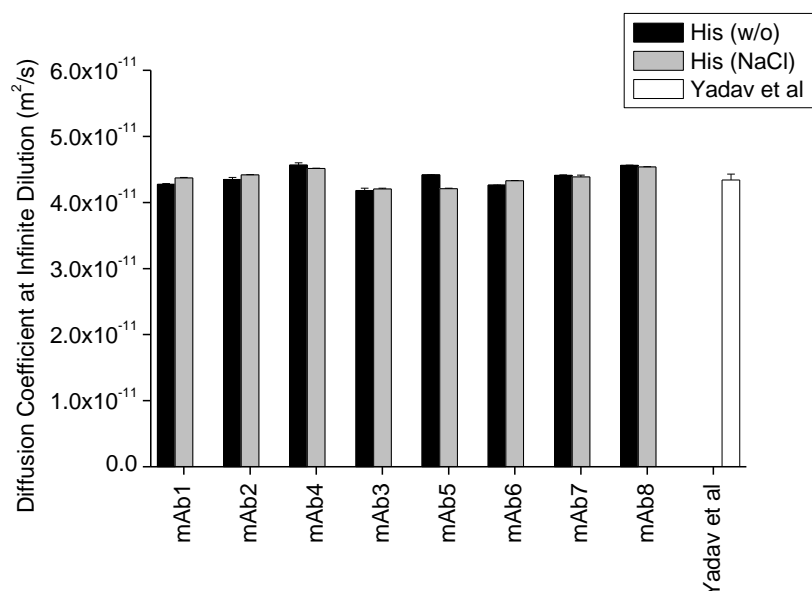


Figure 3.1.6. Diffusion coefficient at infinite solute dilution (i.e. D_0 , m²/s) for eight different antibodies at two different formulation conditions compared to the value reported by Yadav et al⁵. Data are shown as intercepts of the linear fit \pm fit error ($n=2$).

So far the DLS A_2 method development could demonstrate that valid measurements correctly determine the interaction parameter k_D . In a next step it is shown that k_D by DLS and A_2 by (SLS) are related as indicated by Equation 16 (p.14). Since data were obtained for A_2 (SLS) and k_D (DLS) for the same samples (same mAbs and formulation buffers) a direct comparison of both was possible. This is illustrated in Figure 3.1.7.

Figure 3.1.7 shows the mAbs in descending order of their A_2 value. With only two exceptions, namely mAb2 in His(w/o) and mAb4 in His(NaCl), the values gained for k_D (DLS) have the same rank order as the ones for A_2 (SLS). From this it was concluded that DLS and SLS are complementary methods for the screening of protein-protein interactions.

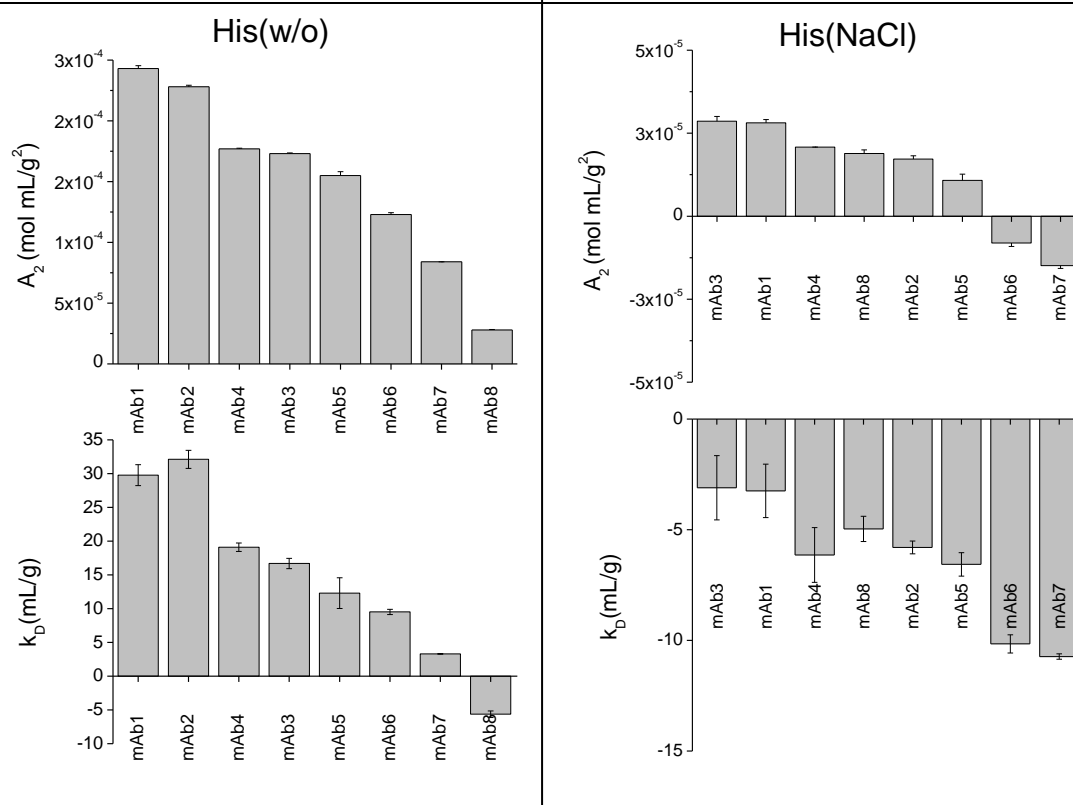


Figure 3.1.7. Comparison of A_2 (mol mL/g²) values and k_D (mL/g) values for eight different mAbs at two different formulation conditions (left: 20 mM His/His-HCl (pH 6.0), right: 20 mM His/His-HCl (pH 6.0) + 150 mM NaCl). mAbs are sorted in descending A_2 order at the respective buffer. Data are shown as mean of $n=2 \pm$ absolute deviation.

Although the results of the two methods provide comparable ranking the read-out should be further discussed. SLS data revealed that in the His(NaCl) two mAbs (mAb6 and mAb7) were attractive. They had a negative slope = negative A_2 . On the other hand in DLS all mAbs do show negative slopes (negative k_D). Consequently, assessing k_D by DLS alone would not provide the information on attraction or repulsion but will help to rank order different repulsive/attractive conditions. The reason is that at $2A_2M < \zeta_{1+V_{sp}}^{22}$ all k_D values are negative even if A_2 is positive.

In summary, the assessment of k_D provided the same qualitative information on relative protein-protein interaction as the SLS method. However, the magnitude and direction of protein-protein interaction (i.e. attraction or repulsion) could not be easily determined or read-out.

3.1.3. Method Development for Assessing A_2 by DLS

As mentioned before (3.1.2) the mAbs' k_D ranking was found to follow the same trend as A_2 by SLS (Figure 3.1.7). However assessing k_D by DLS alone would not have provided the information on attraction or repulsion, i.e. by positive versus negative values. This is a major drawback of the DLS method. One was able to overcome this limitation by a simple shortcut, i.e. by plotting A_2 values (SLS) versus k_D (DLS) values (Figure 3.1.8). The plot encompasses data for both low and high ionic strength conditions and provided a linear relation (Equation 19) which enables to translate k_D from DLS into A_2 values and therefore to judge on attractive (negative A_2 values) or repulsive forces (positive A_2 values). A challenge that was encountered shall be briefly described: The empirical Equation 19 is $k_D = 1.06A_2M - 8.9$. Based on Equation 16 ($k_D = 2A_2M - \zeta_{1+V_{sp}}$), one would expect a factor of 2

for the thermodynamic term. Applying Yamakawa theory⁶⁶, Frost and Caroline⁶⁷ report that ζ_1 can be described as $\zeta_1 = \lambda A_2 M + v_h$. Consequently, Equation 16 can be expressed as $k_D = (2 - \lambda) A_2 M - v_h - v_{sp}$, where v_h is the hydrodynamic volume and λ is a term related to molecular dimensions.⁶⁶ Various different λ values have been reported in polymer-related literature⁶⁶ suggesting that deviations from a factor 2 are not anomalous and rather reflect a shape factor.

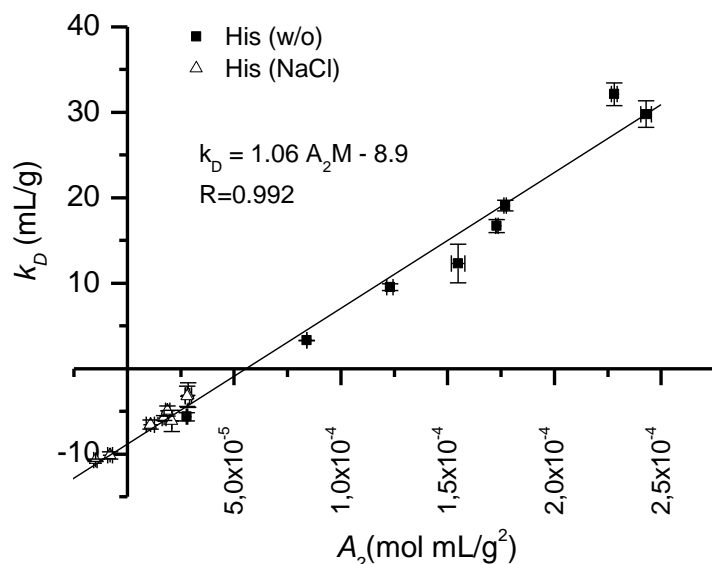


Figure 3.1.8. Interaction parameter (k_D , mL/g by DLS) as a function of second virial coefficient (A_2 , mol mL/g² by SLS) of eight different mAbs formulated in 20 mM His/His-HCl (pH 6.0) \pm 150 mM NaCl. Data are shown as mean of $n=2 \pm$ absolute deviation.

$$k_D = 1.06 A_2 M - 8.9$$

Equation 19. Empirical equation to link the interaction parameter (k_D , DLS) and second virial coefficient (A_2 , SLS) derived from Figure 3.1.8. The equation bases on data from 8 different mAbs both in low ionic and high ionic strength conditions (20 mM His/His-HCl pH 6.0 \pm 150 mM NaCl).

This simple shortcut using an empirical equation (Equation 19) presented a huge step forward in fast and easy everyday A_2 assessment. It greatly reduces the time but also the material necessary and even offers the opportunity for automation. As hydrodynamic radius for antibodies is constant (shown by Figure 3.1.5) the method could even be further miniaturized/accelerated. In essence, assuming a constant D_0 would allow for a single measurement to derive D_m , extrapolation to the expected D_0 and calculate k_D , and A_2 . This offers the possibility to assess A_2 even if material is very limited (e.g. in a very early development phase). However one has to bear in mind that an important control (verification of D_0) is then skipped and results should be taken with precaution. The comparison of the different methods is given in Table 3.1.1. It can be possible to even further miniaturize the method by going to 1536 well plates but this was not a focus in this thesis.

Table 3.1.1. Comparison of time and material needed in A_2 determination by three different methods

Method	Static Light Scattering (SLS)	Dynamic Light Scattering (384 well) Standard Method	Dynamic Light Scattering (384 well) Short Method
principle	Debye Plot	k_D determination and conversion to A_2	k_D determination and conversion to A_2 (assuming D_0 constant)
concentration series?	Yes	Yes	No
volume/measurement (initial samples)	5000 μ l at 5 mg/mL	150 μ l at 10 mg/mL	50 μ l at 10 mg/mL
protein mass/per measurement	25 mg	1.5 mg (4 wells)	0.5 mg (1 well)
replica (n=?)	2	3 (12 wells)	3 (3 wells)
total protein mass	50 mg	4.5 mg	1.5 mg
measurement time	half a day (n=2)	15 min (n=3)	3 min (n=3)
automation	No	Yes	Yes

Overall, the DLS approach described is a powerful methodology to analyze the second virial coefficient A_2 with low protein consumption and in a faster manner than e.g. batch mode injections into SLS detectors. Importantly, one could run this assay on a well plate (384 well plates were used throughout the study) which may pave the way to routine assessment of A_2 and even automation.

To further increase the confidence in the DLS A_2 method (empirical Equation 19) additional antibodies and formulations were tested to see whether they fit the empirical equation (Equation 19). As shown in Figure 3.1.9 the six additional test conditions (illustrated in red) described in Table 3.1.2 are fitting in quite well. Hence the equation was assumed to be universal for mAbs formulated in pharmaceutically applied buffer systems.

Table 3.1.2. Additional test formulations T1-T6 analyzed by both SLS (by A_2) and DLS (by k_D). Parameters varied were buffer strength, buffer, pH and additional antibodies

Data point	Antibody	Condition
T1	mAb2	10 mM Sodium-Citrate (pH 4.5)
T2	mAb1	10 mM Potassium-Phosphate (pH 6.0)
T3	mAb9	20 mM His/His-HCl (pH 6.0)
T4	mAb9	20 mM His/His-HCl (pH 6.0) + 150 mM NaCl
T5	mAb10	20 mM His/His-HCl (pH 6.0)
T6	mAb10	20 mM His/His-HCl (pH 6.0) + 150 mM NaCl

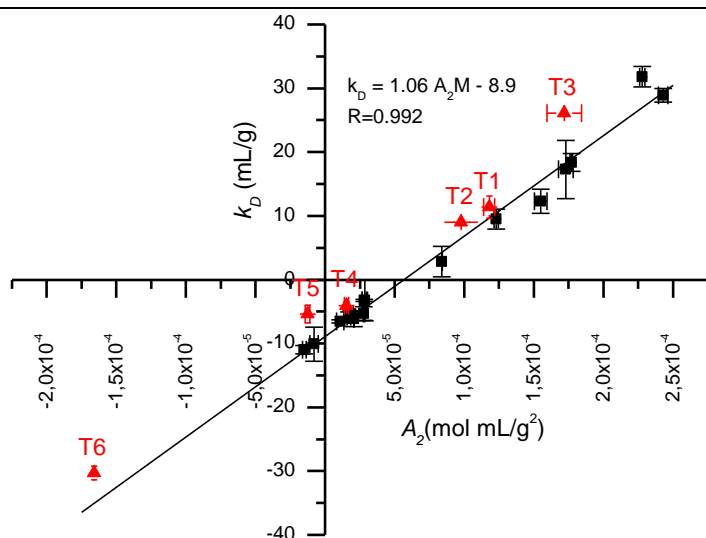


Figure 3.1.9. Interaction parameter (k_D , mL/g by DLS) as a function of second virial coefficient (A_2 , mol mL/g² by SLS) of eight different mAbs formulated in 20 mM His/His-HCl (pH 6.0) \pm 150 mM NaCl. In addition six test formulations (T1-6) were added. Data are shown as mean of $n=2 \pm$ absolute deviation, T6 A_2 $n=1$.

Even greater confidence about the universal applicability of the empirical antibody DLS equation (Equation 19) was gathered when the results were compared to published results by Saluja et al.⁶ The direct comparison is given in Figure 3.1.10. The published values on A_2 and k_D are based on a mAb of a different subclass as used in this thesis (i.e. IgG2) formulated in conditions that were not tested during method development. The authors also used a different experimental set up to determine A_2 . They employed DLS to determine k_D as described in this thesis, but used AUC to determine ζ_1 (k_s) which allowed calculation of A_2 based on Equation 16 (p.14). Importantly, this direct comparison of thesis data to published data further supports the universal applicability of Equation 19 and even strengthens the deviation of the factor 2 as already discussed. In addition Connolly et al.⁶⁸ compared the k_D values of eight different mAbs to A_2 values determined by sedimentation velocity. They came to the conclusion that they found a similar relation of k_D and A_2 for for their mAbs studied even though a different technique was applied (AUC instead of SLS). The relation was $k_D = 1.33 A_2 M - 8.2$ which is in good agreement with the results obtained within this thesis work ($k_D = 1.06 A_2 M - 8.9$).⁶⁸

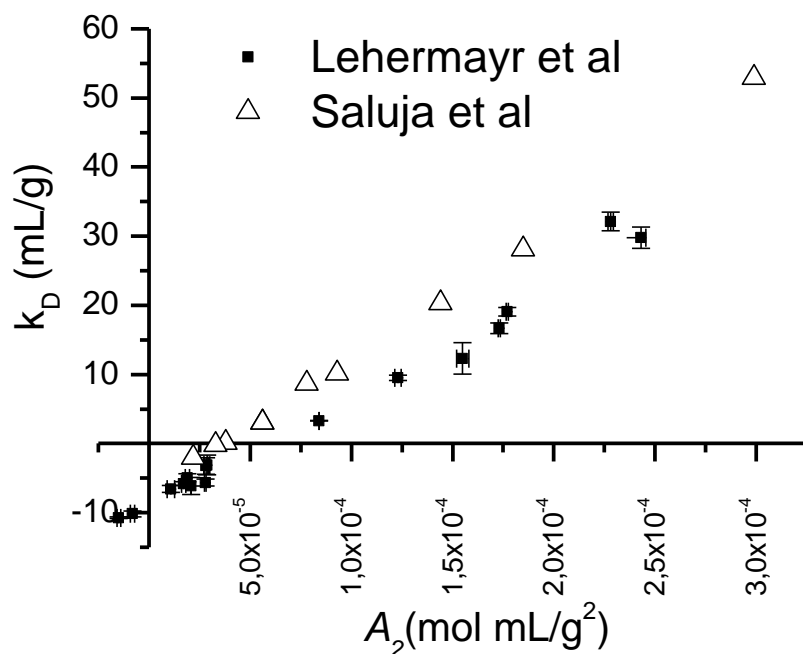


Figure 3.1.10. Interaction parameter (k_D , mL/g by DLS) as a function of second virial coefficient (A_2 , mol mL/g² by SLS) of eight different mAbs (7xIgG1 and 1xIgG4) formulated in 20 mM His/His-HCl (pH 6.0) \pm 150 mM NaCl as published by Lehermayr et al.⁶⁵ (mean of $n=2 \pm$ absolute deviation) compared to second virial coefficient (A_2 , DLS/AUC) as a function of interaction parameter (k_D , DLS) of one mAb (IgG2) at different formulation conditions (mAb in 10 mM acetate buffer + 0, 10, 20, 50, 100 mM NaCl and mAb in 10 mM acetate buffer + 50 mM salt (NaOAc, NaI, or NaSCN)) as published by Saluja et al⁶. (raw data provided by authors).

3.2. Assessment of Isoelectric Point, Net Charge and Protein-Protein Interactions of Different mAbs

This chapter aims to assess and compare inherent protein characteristics of different mAbs, i.e. isoelectric point, net charge, as well as resulting biophysical properties such as zeta potential and protein-protein interactions (second virial coefficient). Moreover experiments to quantify protein hydrophobicity/surface activity.

3.2.1. Determination of IEP

The isoelectric point of the antibodies was determined using four different methods. The four methods to determine IEP were: a) calculation based on the primary amino acid sequence, b) measurement by iCE, c) determination of the pH of zero electrophoretic mobility, and d) determination of the pH of minimum mutual diffusion coefficient. Results are summarized in Figure 3.2.1.

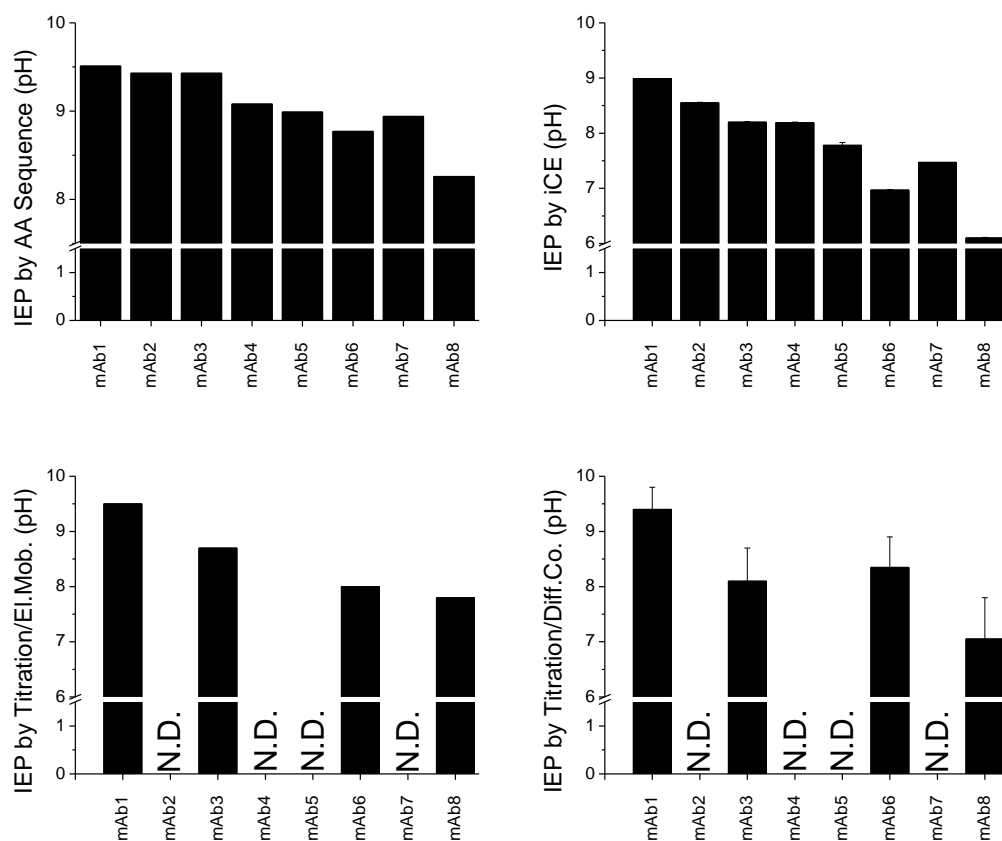


Figure 3.2.1. Isoelectric point of eight mAbs determined by calculation based on AA sequence, measurement via iCE (mean of $n=3\pm SD$), electrophoretic mobility μ by Doppler velocimetry (one representative result of $n=2$), or via mutual diffusion coefficient D_m as assessed by DLS (one representative result of $n=2$). N.D., not determined. mAbs ordered in descending order by their net charge.

The IEPs calculated based on AA sequence were in the range of approximately 8.3 to 9.5 (Figure 3.2.1). The measured IEPs in iCE follow the same rank order, but provided in general lower IEP values than theoretical calculation. Electrophoretic mobility measurements for selected mAbs (mAb 1, 3, 6, and 8) during pH titrations provided the same rank order. During pH titration, D_m reached a minimum at IEP as assessed by other methods (Figure 3.2.2). IEP determination by D_m could only give a range for IEP because one was not able to determine the minimum between the three lowest data points measured.

The ranking of mAbs was found consistent for all methods suggesting that all methods can be used as a tool to assess relative IEPs (Figure 3.2.1). The rank order found was mAb1>mAb2>mAb3>mAb4>mAb5>mAb7>mAb6>mAb8. Absolute IEP differed between different approaches. The theoretical calculation of the IEP was only based on the primary amino acid sequence, not taking into account charge of buried amino acids or glycosylation patterns that might have an influence.^{14,69} The IEP assessment by iCE provided in general lower IEPs compared to the other methods. iCE differs in two main aspects from Doppler velocimetry and the measurement of diffusion coefficient: firstly, iCE provides individual IEPs for all charge species resolved in the electropherogram while the proteins' IEP was defined as the IEP of the main species. Consequently, one did not assess an average IEP over all charge species which is different from Doppler velocimetry (electrophoretic mobility) and DLS (D_m) where one assesses IEP globally in "batch mode"

without separating different species. Secondly, iCE requires measurement in a matrix of ampholytes whereas Doppler velocimetry and assessment of D_m as a function of pH was performed in a low ionic strength matrix (10 mM NaCl/H₂O). The change in D_m over pH reaching a minimum at antibodies' IEP (Figure 3.2.2) is similar to what was described in a recent publication by Yadav et al.⁵ Since D_m reflects interaction^{5,22,29}, repulsive interaction and therefore D_m is lowest when antibodies' net charge becomes zero, i.e. at their IEP.

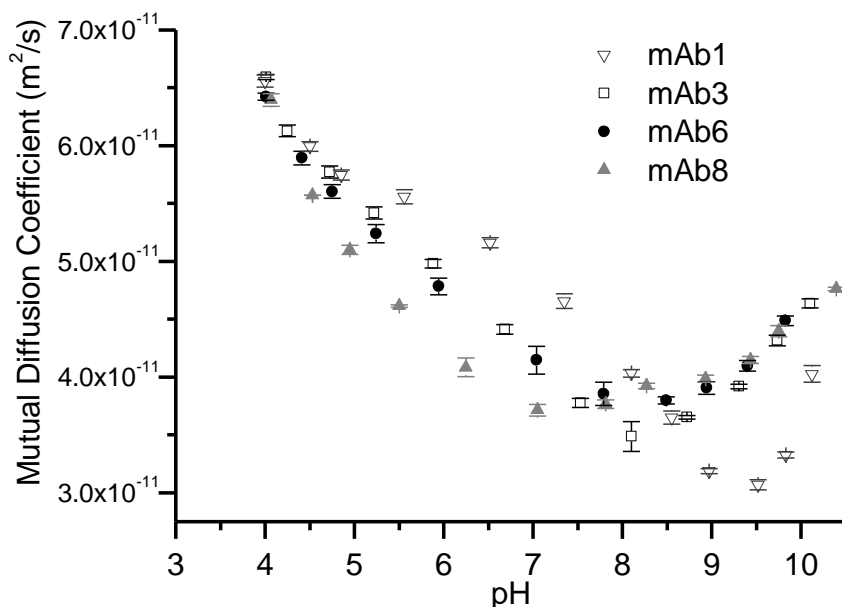


Figure 3.2.2. Mutual diffusion coefficient (D_m , m²/s) of four mAbs (mAb 1, 3, 6, and 8) obtained from dynamic light scattering measurements (DLS) in 10 mM NaCl/H₂O as a function of pH (4-10), mean of $n=3\pm SD$.

3.2.2. Zeta Potential and Net Charge

In this section the charge properties of the different mAbs were determined. Therefore zeta potential and net charge was measured.

The mAbs' net charge at pH 6.0 was (i) calculated using the primary amino acid sequence and the software tool EMBOSS, and (ii) net charge was also determined experimentally by three different approaches:

Both a) and b) are based on Equation 10 (p.11) which requires electrophoretic mobility f and the diffusion coefficient D_s . In the simplified approach a) D_s was considered to be constant and using a diffusion coefficient which was experimentally determined for my mAbs at dilute solution (i.e. by extrapolation to infinite dilution) (D_s const.), i.e. $4.37\pm 0.13\times 10^{-11}$ m²/s. In approach b) one included D_s values which were converted from experimentally determined D_m at 10 mg/mL, thereafter referred to as D_s conv.

Approach c) was using the Donnan equilibrium. The data obtained from those approaches are summarized in Figure 3.2.3.

As already mentioned in the experimental net charge determination by a) and b), one had to face a challenge with Equation 10 (p.11) which shall be discussed as follows. Equation 10 requires knowledge on the self diffusion coefficient (D_s). In a simplified model, Chase et al.¹⁷ and others^{10,18} considered D_s constant ($D_s = D_0$), i.e. D_s at infinite protein dilution,

where the Stokes-Einstein-relation is valid. With increasing concentration however, inner friction will increase and D_s will decrease.^{22,50-52,70,71} Piaggio et al.⁷² highlight the importance of including these considerations into net charge determination rather than calculating with the constant diffusion coefficient at infinite dilution.

The necessity of using D_s instead of D_0 shall be explained using the example of Chase et al.¹⁷ This should not imply that the author's assumption was wrong; it should only clarify why for the method used in this thesis one cannot assume D_s to be constant. The authors determined the hydrodynamic radius by AUC. Afterwards the diffusion coefficient is calculated based on the Stokes-Einstein equation (Equation 20).

$$D_0 = \frac{k_B T}{6\pi\eta R_h}$$

Equation 20. The Stokes-Einstein equation relating the diffusion coefficient at infinite dilution to Boltzmann's constant (k_B), temperature (T), solvent's viscosity (η), and hydrodynamic radius (R_h)

Contrary to D_0 , self diffusion coefficient as defined by Equation 21 is friction dependent.

$$D_s = \frac{k_B T}{f}$$

Equation 21. The self diffusion coefficient (D_s) as a function of Boltzmann's constant (k_B), temperature (T), and inner friction (f) as described by Nernst-Einstein.²²

Albert Einstein already showed that as the solute concentration increases the inner friction has to increase too.⁷¹ The reason for this is, that other particles in solution interfere with the free movement of a single particle. In other words the self diffusion D_s (Equation 21) is impaired. An equation that gives the concentration dependence of friction is shown by Equation 22.

$$f = f_0(1 + f_1 c + \dots)$$

Equation 22. The friction coefficient (f) as a function of concentration, virial expansion.²²

Chase et al. however, due to their very dilute conditions (0.33 mg/mL)¹⁷, defined D_s to be constant ($D_s = D_0$). This allows direct substitution of the friction coefficient in Equation 23 by Equation 21. Equation 23 shows the dependence of particle mobility in an electric field based on charge.

$$\mu = \frac{z^* e}{f}$$

Equation 23. Description of the mobility of an ion in the electric field in dependence of apparent net charge (z^*), elementary charge (e) and the friction coefficient (f).¹⁷

This then leads to the formula published by Chase et al.¹⁷ This equation was used for net charge determination (Equation 24).

$$z^* = \frac{\mu k_B T}{D_s e}$$

Equation 24. Apparent net charge (z^*) based on the mobility of an ion in the electric field (μ), the self diffusion coefficient (D_s), the Boltzmann's constant (k_B), and elementary charge (e).¹⁷

This approximation can be done for very dilute sample concentrations. However this is not the case for the experimental set up used within this thesis.

The measurement conditions in this thesis required a mAb concentration of 10 mg/mL. This is about 30 times the concentration used for example by Chase et al.¹⁷ Therefore it was decided to additionally compensate for the increased particle friction and compare it to the non-friction compensated approach ($D_s=D_0$).

Because friction is increasing with concentration, D_s is decreasing to values $<D_0$. This means that based on Equation 24, using a correct D_s value will always result in a higher net charge than by choosing $D_s=D_0$. In other words if friction is neglected the resulting net charge is underestimated.

A challenge is that D_s is not easy to be determined analytically.²² Described possible experimental approaches are NMR²² and methods based on tracer diffusion²². As D_m data was at hand one could use an approach suggested by Le Bon et al.⁵¹ (Equation 11, p.12). This was done to convert D_m into D_s (referred to as $D_s\ conv.$). This approach was based on a diverging pattern (the higher D_m , the lower D_s , see also Figure 3.2.4). Figure 3.2.4 illustrates the situation at a given condition, i.e. a given protein concentration (10 mg/mL) and a defined pH/buffer system (20 mM His/His-HCl, (pH 6.0)). More precisely, Figure 3.2.4 shows the situation for several mAbs in one single condition. However, it is important to emphasize that this diverging pattern between D_m and D_s is reported especially for one single macromolecule with varying conditions, e.g. with increasing concentration as described for polymers.²² Consequently, $D_s\ conv.$ at 10 mg/mL is different (lower) from $D_s\ const. = D_0$ as it will decrease with increasing concentration. This will result in different (higher/lower) experimentally determined charge values (Equation 24).

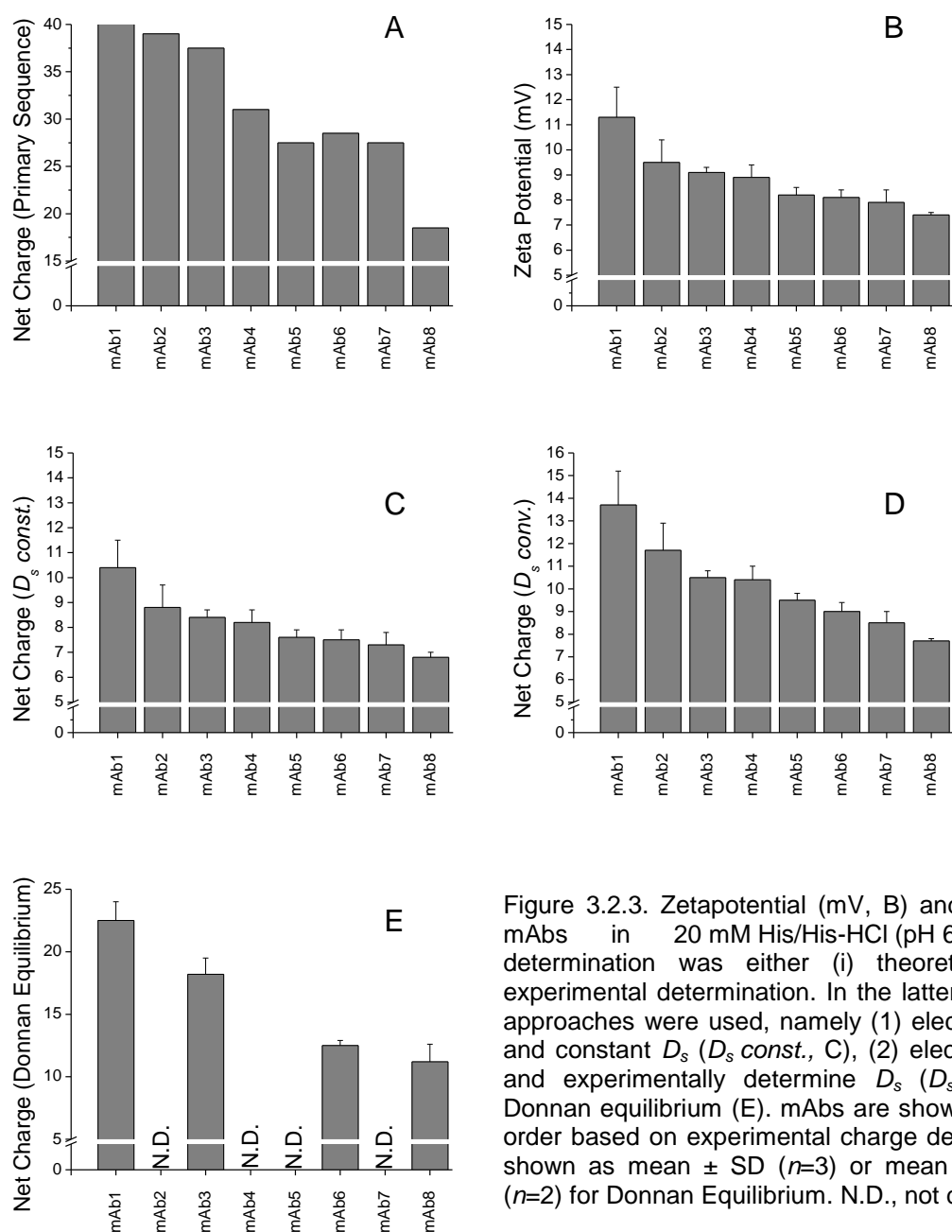


Figure 3.2.3. Zetapotential (mV, B) and net charge of eight mAbs in 20 mM His/His-HCl (pH 6.0). Net charge determination was either (i) theoretical (A) or by (ii) experimental determination. In the latter case, three different approaches were used, namely (1) electrophoretic mobility μ and constant D_s (D_s const., C), (2) electrophoretic mobility μ and experimentally determine D_s (D_s conv., D), and (3) Donnan equilibrium (E). mAbs are shown in descending rank order based on experimental charge determination. Data are shown as mean \pm SD ($n=3$) or mean \pm absolute deviation ($n=2$) for Donnan Equilibrium. N.D., not determined.

As seen in Figure 3.2.3, the antibodies differed prominently in their net charge at the given buffer condition. Though, numerical values differed significantly between theoretical and experimental methods, the ranking of the antibodies' net charge was found to be consistent between the experimental methods. The zeta potential and experimentally determined net charge follow a similar rank order as the IEP (Figure 3.2.1). The theoretical net charge provided a rank order well matching the experimentally determined values with one exception: mAb6 was slightly higher calculated. Determination of net charge by Equation 10 (p.11) using D_s conv. provided higher charge values than using the same equation assuming constant D_s (D_s const.). The reason for this was that, due to particle-particle friction, diffusion is reduced (D_s conv.) and not constant.

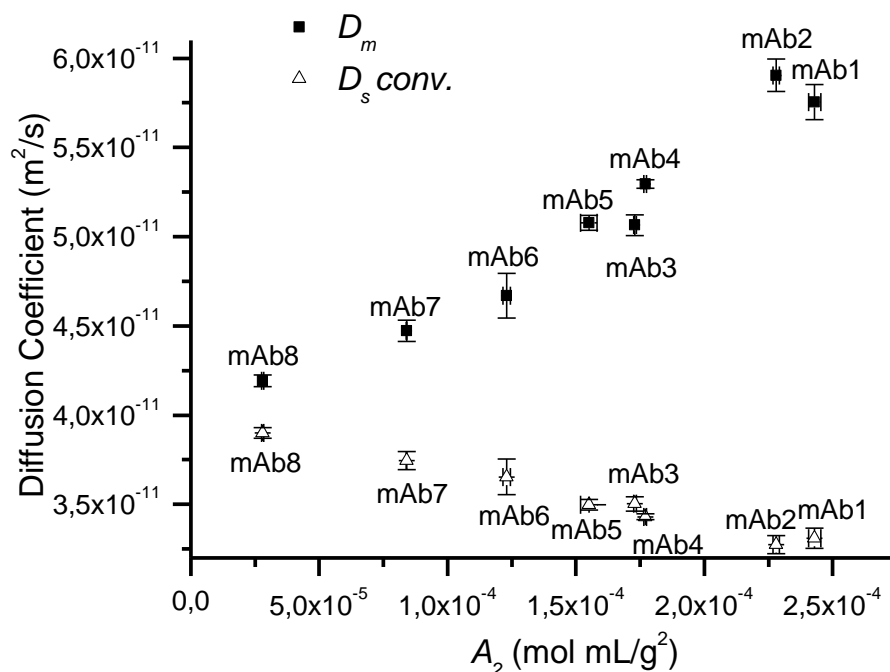


Figure 3.2.4. Experimentally determined D_m (m^2/s) and the resulting $D_s \text{ conv.}$ (m^2/s) (based on Equation 11, 10 mg/mL, mean of $n=3 \pm \text{SD}$) and second virial coefficient A_2 (mol mL/g^2 , mean of $n=2 \pm \text{SD}$) for eight mAbs in 20 mM His/His-HCl (pH 6.0). Note that the figure illustrates the situation at the given condition only (buffer and protein concentration), since the diffusion coefficient as well as A_2 varies with conditions.

The theoretical net charge was in general assessed higher than the experimental data revealed. Potential reasons for this deviation are manifold. Calculations based on primary sequence do not account for the three-dimensional structure where amino acids may be exposed or buried. In addition, pK values of the ionizable groups in folded proteins are influenced by charge-charge interactions, charge-dipole interactions (hydrogen bonding) and the Born effect (dehydration), as discussed by Grimsley et al.⁷³ These effects are highly protein-dependent and cannot be easily considered in net charge calculation based on primary sequence. Moreover, effects from the glycopattern (e.g. via sialic acid)⁶⁹ and charge variants in the molecule are not considered in theoretical calculations. Finally, counter ion binding is also not considered in theoretical calculations.

For selected mAbs, the Donnan equilibrium was used to analyze net charge. The data based on Donnan fits well the overall mAb rank order. Absolute differences in charge obtained from different methodologies can be expected due to the different underlying principles. Challenges associated with net charge determination via Donnan equilibrium may be non-specific interactions of solutes directly with the protein through a variety of electrostatic and non-electrostatic interactions. More precisely, the issue is that Histidine interaction with the mAb may not just be through charge. Those phenomena may affect the net charge derived from the Donnan experiment.^{14,54}

Overall, the net charge determination is consistent over the different methodologies and provided a similar rank order for the different mAbs (Figure 3.2.3). The net charge and zeta potential ranking follows the IEP ranking of mAbs with the only exception of mAb6. Consequently, the simple assessment of IEP via calculation may provide useful information to the formulation scientist regarding differences of several mAbs. However, this assessment may be misleading for choosing an appropriate buffer condition for a

formulation, as for all methodologies, the experimentally determined IEP was found to be lower than calculated. In addition, the IEP in respective formulation condition may also strongly vary based on counter ion binding.

3.2.3. Experimental confirmation of the concentration dependence of D_s

The importance of using D_s in net charge determination instead of the D_0 was discussed and demonstrated under 3.2.2. To recap, Figure 3.2.5 shows that D_m increases whereas D_s decreases ($D_s < D_0$) with concentration (for the studied mAbs). So the approach in this work was based on a mathematical conversion from D_m to D_s as suggested by Le Bon et al.⁵¹ However a confirmation that D_s is generally lower than D_0 as well as the inverse relationship of D_m and D_s (the higher D_m the lower D_s) still lacked experimental confirmation. It was therefore the next logical step to determine D_s experimentally.

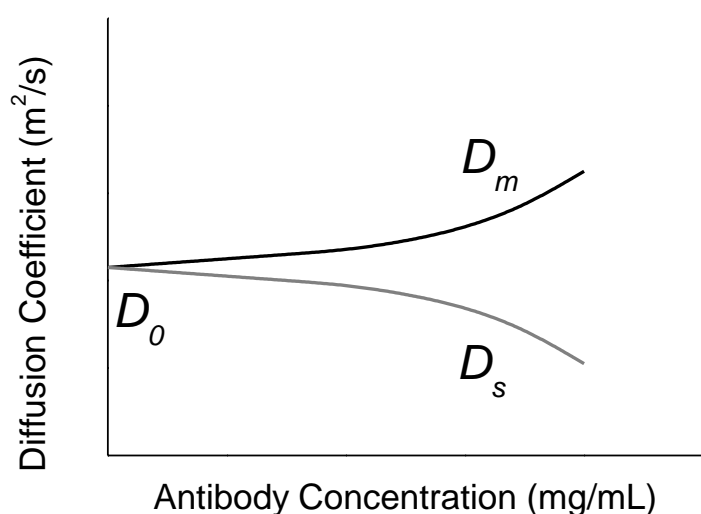


Figure 3.2.5. Diffusion coefficient with increasing antibody concentration. At infinite dilution the diffusion coefficient is called D_0 (m^2/s). Mutual diffusion coefficient (D_m , m^2/s) usually increases whereas self diffusion coefficient (D_s), always decreases. Figure adapted for mAbs^{22,71}.

The chosen experimental approach was based on field gradient NMR. The details are given in the method description 2.10. The analyzed samples were five different mAbs at 10 mg/mL and 100 mg/mL formulated in 20 mM His/His-HCl pH 6.0 ± 150 mM NaCl.

What needed to be confirmed first was, that as concentration is increased, D_m usually is higher whereas D_s is lower than D_0 . Or, as based on Figure 3.2.5, D_m is always larger than D_s . The results are shown in Figure 3.2.6. They nicely confirm the theory since D_m was always found to be larger than D_s . mAb8 is a special case for which D_m decreases with concentration. Nevertheless its D_s was also lower than its D_m , what was expected based on the theoretical calculation (Equation 11).

At 100mg/mL the trend is even stronger. As concentration increases single particles diffuse even slower. It was therefore demonstrated that the importance of using D_s instead of D_0 in net charge determination increases with the samples concentration.

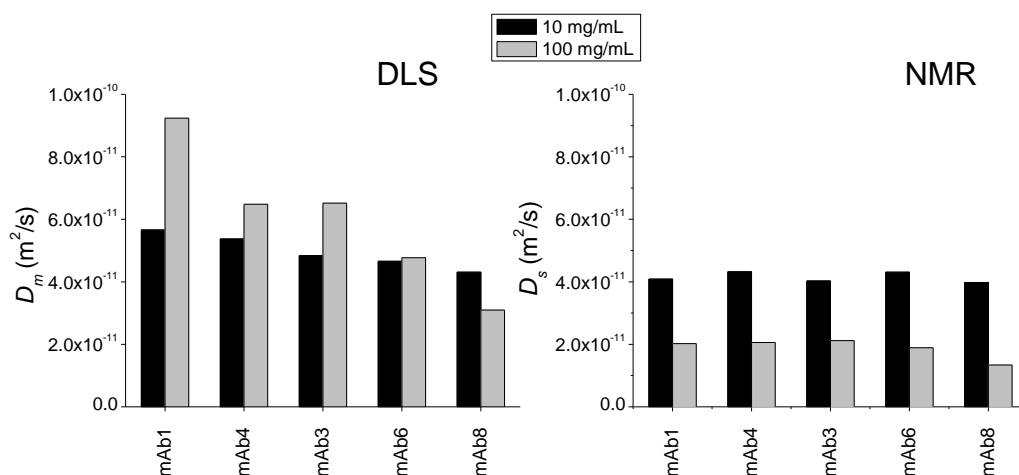


Figure 3.2.6. D_m (m²/s by DLS) and D_s (m²/s by NMR) at two different protein concentrations (namely 10 and 100 mg/mL) in 20 mM His/His-HCl (pH 6.0) for five mAbs.

The next step is the comparison of the mathematically converted D_s conv. to the experimentally determined D_s values. This is shown by Figure 3.2.7. A strong experimental confirmation of the theory was not given. All determined D_s values were larger than D_s conv. and in addition there is no clear inverse relation that the higher D_m the lower D_s . What is however still a promising result is, that all measured D_s values were below D_0 . This stresses out the importance of using D_s instead of D_0 in net charge determination especially at non dilute protein concentrations (e.g. 10 mg/mL). Therefore this strengthens the approach chosen in this work for a D_s dependent net charge determination.

The results generated by NMR are promising and further confirming/comparing work is advised. A good starting point would be doing measurements at different concentrations similar to DLS experiments (3.1.2). The extrapolation of D_s to infinite diluted protein concentration (D_0) would verify the correct calibration of the NMR system. This would also give clarification if D_s like D_m changes linear with concentrations up 10 mg/mL. It would also give the information how much a 5% sample dilution by D₂O (necessary in sample prep) is influencing the result.

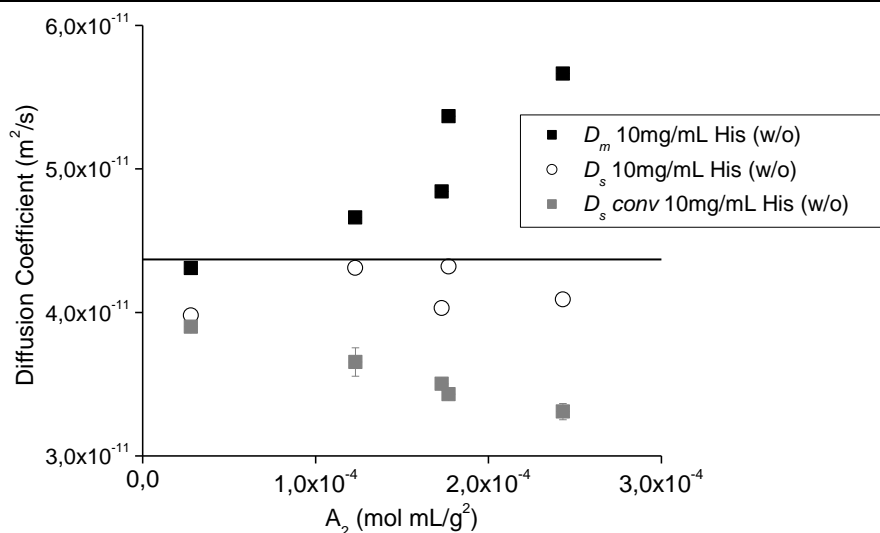


Figure 3.2.7. Mutual diffusion coefficient (D_m , m²/s by DLS) and self diffusion coefficient (D_s , m²/s by NMR) of five mAbs in 20 mM His/His-HCl (pH 6.0) at 10 mg/mL, and comparison to converted self diffusion (from D_m , i.e. $D_s\ conv.$, m²/s). The line marks D_0 being 4.37×10^{-11} m²/s. D_m and $D_s\ conv.$ values are showing the mean of $n=3 \pm SD$

3.2.4. Net Charge at Different pH Values

Net charge of selected antibodies was determined at different pH values. This was based on net charge determination by method a) and b) employing Equation 10. See 2.7. Figure 3.2.8 shows the results obtained for mAb1, 3, 6, and 8 respectively.

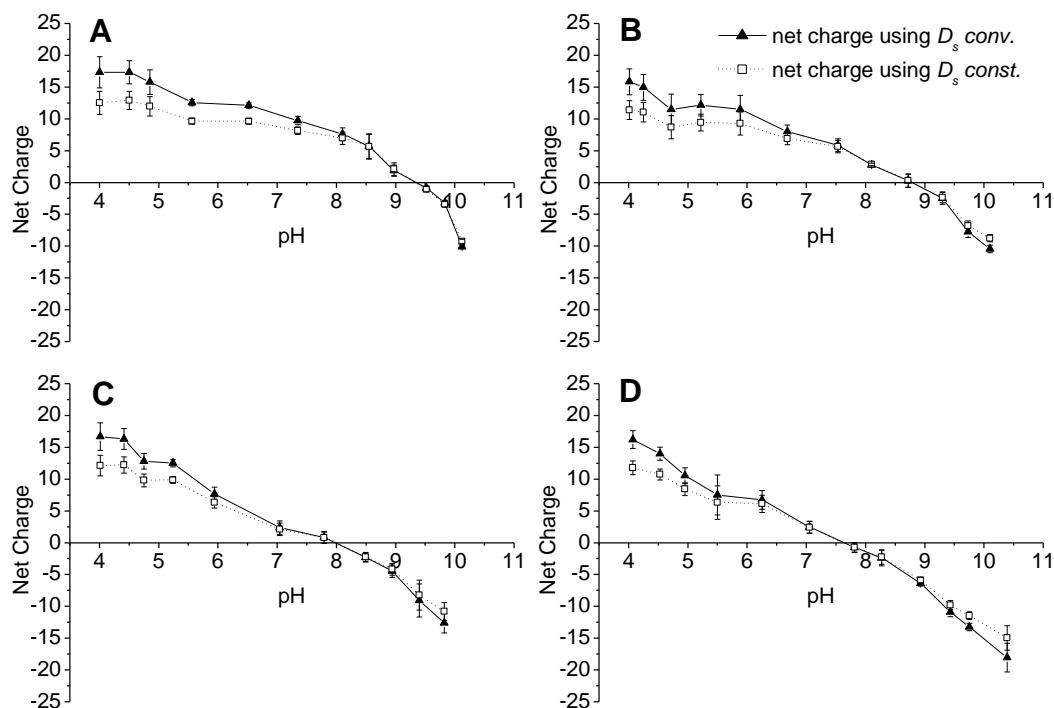


Figure 3.2.8. Net charge of mAb1 (A), 3 (B), 6 (C), and 8 (D) in 10 mM NaCl/H₂O as a function of pH (pH 4 to 10), according to Equation 10 based on electrophoretic mobility μ and either constant D_s ($D_s\ const.$) or D_s upon conversion from D_m ($D_s\ conv.$), $n=3 \pm SD$

As expected, all antibodies carry a net positive charge at pH values below the IEP and a net negative charge at pH values above the IEP. The net charge variations over pH are different for the different antibodies, i.e. the charge profiles differ. In the example of mAb6 (Figure 3.2.8C) the charge profile around IEP runs relatively flat, whereas for mAb1 (Figure 3.2.8A), net charge increases more strongly with pH change, especially around IEP. Therefore it should be stressed out that net charge ranking at a chosen pH must not fully relate to the IEP. This is shown Figure 3.2.9 where one can see that at pH 6.0 the net charge of mAb7 is the second lowest whereas counting from the lowest IEP it is on the third place. The data also shows that assuming constant diffusion coefficient ($D_s \text{ const.}$) yields lower net charges at low pH values in contrast to the use of $D_s \text{ conv.}$ whereas around the IEP this difference vanishes.

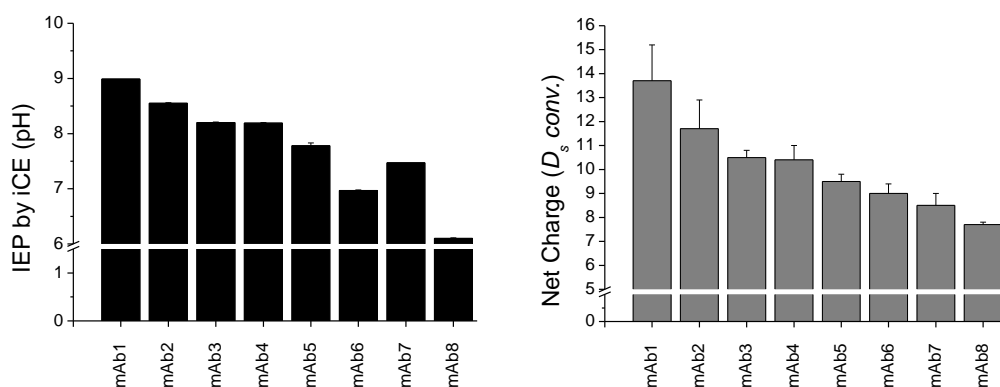


Figure 3.2.9. Comparison of isoelectric point, IEP (by iCE, mean of $n=3 \pm \text{SD}$) and net charge based on electrophoretic mobility and $D_s \text{ conv.}$ (mean of $n=3 \pm \text{SD}$) of eight mAbs in 20 mM His/His-HCl (pH 6.0)

3.2.5. Second Virial Coefficient A_2

It is an important question to assess how those inherent parameters (IEP, charge) translate into biophysical behavior, e.g. protein-protein interactions. In this context the second virial coefficient (A_2) was assessed for all mAbs. The A_2 comprises all interaction forces between two protein molecules, including ionic, hard-sphere, Van der Waals, and other short-range interactions (e.g. hydrophobic interactions).^{20,21} The ionic interaction is the strongest force since the potential energy and range is by far the highest.²¹ Consequently, two extreme conditions have been chosen, namely a low ionic strength condition (20 mM His/His-HCl pH 6.0) and high ionic strength condition (20 mM His/His-HCl pH 6.0 \pm 150 mM NaCl). The latter serves to shield the proteins' charge and to elaborate on interactions different from charge-charge interactions.

Second virial coefficients (A_2) have been assessed using static light scattering (SLS) with multi angular light scattering (MALS) detector. The results were already presented in the method development part (see 3.1, Figure 3.1.7, p.24). A_2 of monoclonal antibodies at low ionic strength conditions (20 mM His/His-HCl buffer, pH 6.0) as determined by SLS were all positive, suggesting repulsive behavior. This repulsive behavior changed at high ionic strength conditions (20 mM His/His-HCl (pH 6.0) + 150 mM NaCl) as A_2 reduced significantly for all mAbs tested, however to a different extent. The A_2 values in high ionic strength provided a completely new mAb rank order. mAb8, e.g. remained almost

unchanged with respect to A_2 , whereas others changed dramatically and finally became attractive (mAb6 and mAb7).

The analysis of A_2 in low ionic strength condition by means of SLS provided a similar rank order as the zeta potential and net charge determination ranking (see Figure 3.2.3, p.33). The data suggests that at low ionic strength condition the protein charge is predominant and causes repulsion. This observation is consistent with literature on different types of protein-protein interaction, e.g. by Chari et al.⁴⁰ The interesting observation was made after addition of 150 mM NaCl because the rank order changed completely. It was assumed that ion shielding reduces long-range charge-charge interactions and favors mid and short range interactions such as hydrophobic interactions.⁴⁰ Experimental means to measure these nonionic interactions are presented in the next section. The magnitude of A_2 change differs for the mAbs tested regardless of their inherent protein charge. The drawback of measuring A_2 is that one cannot conclude what the main driver for the interaction, i.e. the type of interaction, is. The observations in high ionic strength emphasize the importance of choosing appropriate formulation conditions⁷⁴ and show again that mAbs' behavior cannot be generalized. Therefore, prediction of mAb behavior is very difficult. On the other hand, tailoring formulation conditions to favor a high effective net charge may be a suitable means to favor repulsion. Tailoring formulations was studied in detail in chapter 3.4. How this translates into protein stability, e.g. their aggregation behavior and possibly into viscosity behavior is elucidated in chapter 3.5.

3.2.6. Second Virial Coefficient and Net Charge

Figure 3.2.10 shows A_2 (SLS) and the net charge of eight different mAbs at a given buffer condition and protein concentration, namely in 20 mM His/His-HCl pH 6.0 at a protein concentration of 10 mg/mL. Net charge has been determined by using Equation 10 (p.11) based on electrophoretic mobility and either a) D_s *const.* or b) D_s *conv.* At the given low ionic strength buffer condition, the mAbs with the highest net charge showed the highest A_2 (i.e. the highest degree of repulsion). Note that using D_s *conv.* results in higher net charges than using D_s *const.* (the theory behind has been discussed in Chapter 3.2.2).

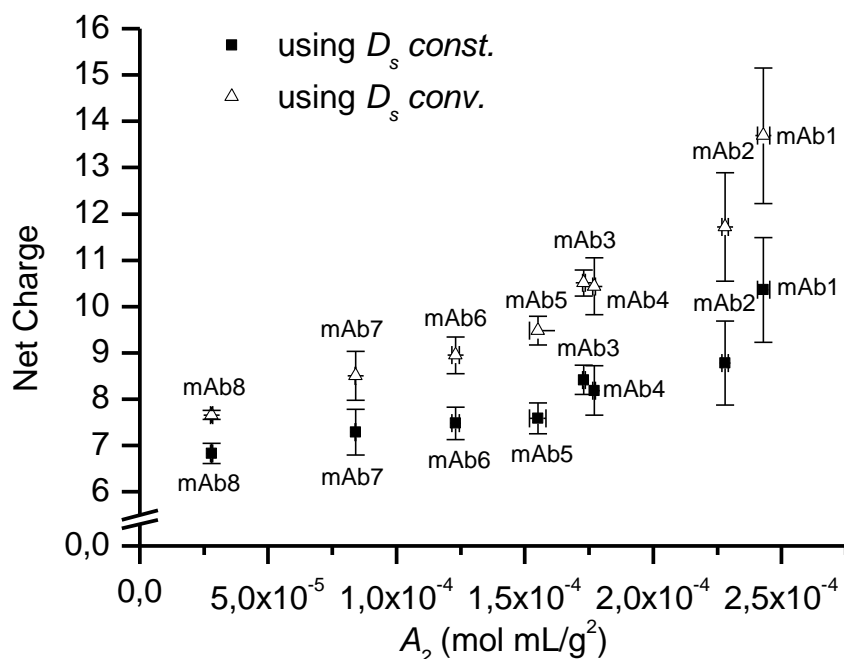


Figure 3.2.10. Net charge ($n=3$) based on Equation 10 using either a) D_s const. or b) D_s conv. as a function of second virial coefficient A_2 (SLS, $n=2$). The graph illustrates eight different mAbs at a given low ionic strength condition, i.e. 20 mM His/His-HCl (pH 6.0) and at a mAb concentration of 10 mg/mL. Data are shown as mean \pm SD ($n=3$) or mean \pm absolute deviation ($n=2$).

3.2.7. Evaluation of Non-Ionic Interactions

Assuming that attractive non-ionic interactions are caused by hydrophobic interactions, different methods to determine mAbs' hydrophobicity were tested. The aim was to possibly explain mAbs' different A_2 behavior at different formulation conditions as discussed under 3.2.5. Several techniques were applied: binding of a hydrophobic fluorescence dye, a hydrophobic ESR probe, measuring surface activity, ammonium sulphate precipitation, and calculation of hydrophobicity based on primary amino acid sequence.

3.2.7.1. Fluorescence Hydrophobicity Analysis

First the mAbs' hydrophobicity was determined by analysis of binding of a hydrophobic fluorescence marker called NPN (N-Phenyl-1-naphthylamin). In literature also ANS (1,8-anilino-1-naphthol sulfonic acid) is commonly used. However when using ANS it cannot be excluded that the molecule interacts with its charged moiety (i.e. sulfo-group) instead of its hydrophobic part and was therefore excluded.^{38,75} NPN is not charged. NPN binding causes a peak shift from 460 nm emission to 420 nm as well as an intensity increase.^{37,38,75} The excitation peak is at 350 nm.⁷⁵ This is within the emission spectrum of protein (Figure 3.2.11), a fluorescence resonance energy transfer approach was chosen based on work published by Togashi et al. to additionally screen for a proximity effect of the fluorescence dye.³⁶ To cause an emission spectrum in the range of 350 nm the proteins were excited at 265 nm. This is demonstrated for BSA as model compound; only binding of marker to the protein resulted in a peak shift and intensity increase of the NPN emission (Figure 3.2.11). The emission spectrum of BSA strongly excites NPN resulting in

a strong signal increase if it is bound to the protein. The resonance energy transfer from BSA to NPN is shown as the emission peak of BSA decreases.

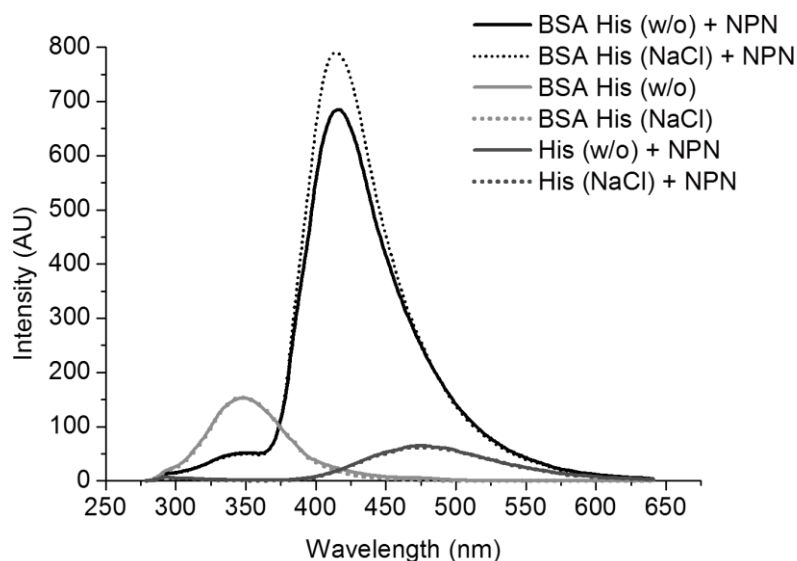


Figure 3.2.11. Fluorescence intensity at different emission wavelength (nm). Placebos containing the fluorescence marker (His (w/o) and His (NaCl) + NPN), BSA two formulations (His (w/o) and His (NaCl)), and BSA in (His (w/o) and His (NaCl) + NPN). Data are shown as the mean of $n=2$.

Interestingly, the signal gets stronger at high ionic strength (BSA His (NaCl) + NPN) as compared to low ionic strength (BSA His (w/o) + NPN) which might be a hint that non-ionic interactions (i.e. hydrophobic interactions) are favored if charges are shielded by counter ions. Figure 3.2.12 shows the BSA signals with baseline subtracted. Baseline was the placebo formulation containing NPN only.

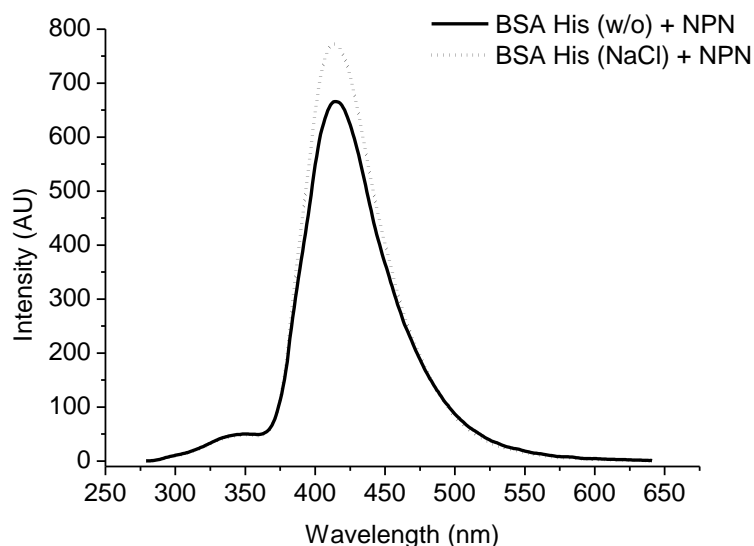


Figure 3.2.12. Emission scans of BSA shown in two formulations (His (w/o) and His (NaCl) + NPN) with baseline subtracted (baseline being the respective placebo + NPN). Data are shown as the mean of $n=2$.

For this study the same eight antibodies as measured for A_2 determination were tested within the same formulation conditions. The following two figures (Figure 3.2.13 and Figure 3.2.14) show the recorded results for the 8 mAbs tested in 20 mM His/His-HCl (pH 6.0) \pm 150 mM NaCl.

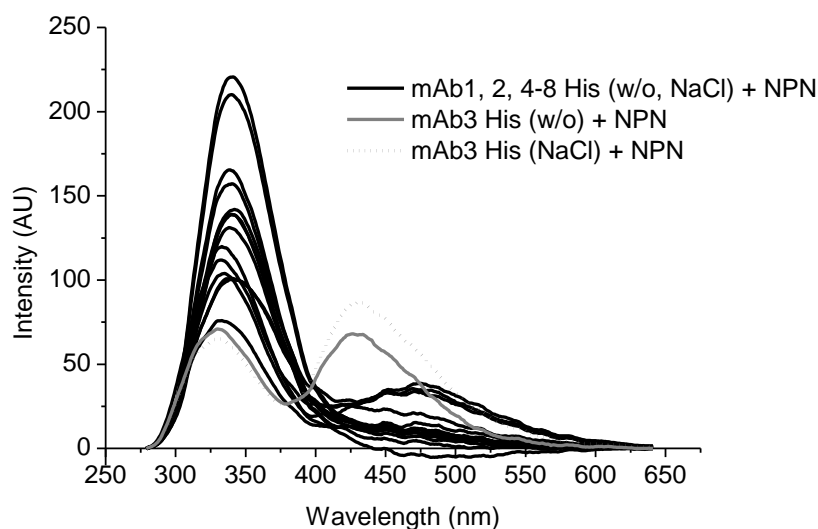


Figure 3.2.13. Emission scans of all non-marker binding mAbs and mAb3 + NPN measured at the same protein concentration. Data are shown as the mean of $n=2$.

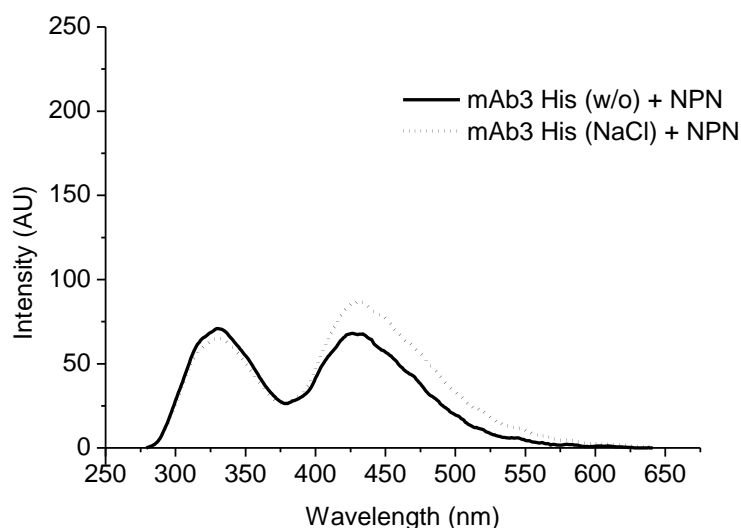


Figure 3.2.14. Emission scans of mAb3 + NPN in two formulations (His (w/o) and His (NaCl)). Data are shown as the mean of $n=2$.

Only mAb3 did show the NPN peak shift and signal increase indicating NPN binding that was higher if NaCl was present (Figure 3.2.14). This again could be a hint that non-ionic interactions (i.e. hydrophobic interactions) are favored if charges are shielded by counter ions.

Note that the mAbs differ in their emission spectrum (350 nm). This happens when emission energy is transferred to bound NPN like it was shown for BSA (Figure 3.2.11). But this also happened because of differences in the proteins amino acid sequence. It was expected that due to the numbers of Phenylalanine, Tyrosine and Tryptophan the emission peaks have different intensities.⁷⁶

The final result was that only mAb3 was positive for NPN binding which was further enhanced as NaCl was added. This could not be connected to any A_2 behavior because mAb3 as compared to for example mAb6 was still among the most repulsive mAbs, speaking against the theory that A_2 is capable of showing hydrophobic interactions. Maybe mAb3 has a specific interaction site for the hydrophobic NPN dye not connected to protein-interaction. What strengthens this assumption is that mAb3 targets an aggregate protein. As aggregates by themselves are more hydrophobic (loss of ordered structure) an aggregate specific mAb has to have a more hydrophobic CDR to be able to bind.⁷⁷ A small hydrophobic marker is likely to enter this binding site.

To rule out possible mAb specific marker interactions like the presence/absence of specific binding pockets, it was decided to test these mAbs additionally by a hydrophobic ESR marker. For this an ESR marker was used which – in contrast to aromatic rings present in NPN bears a long alky chain

3.2.7.2. Hydrophobic ESR Marker Binding

Similar to the approach by fluorescence, a hydrophobic ESR marker having a long alkyl chain (i.e. 5-Doxyl) was tested. Binding of the marker caused a change in signal that can be seen when comparing the marker within placebo Figure 3.2.15 versus the marker in the presence BSA which binds the marker well (Figure 3.2.16).

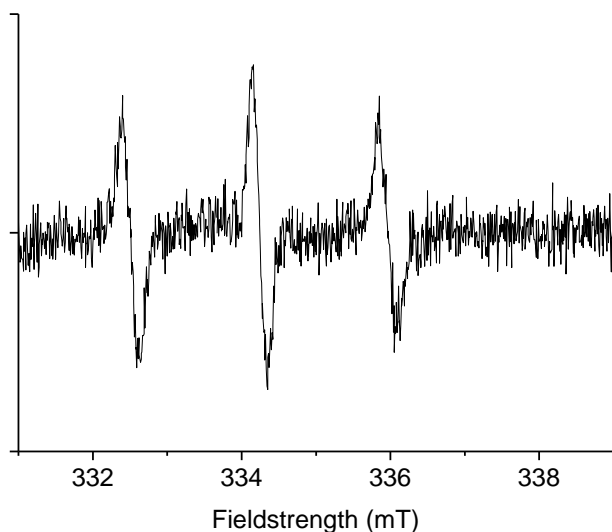


Figure 3.2.15. Resonance spectrum of placebo (His (w/o)) containing the spin probe 5-Doxyl.

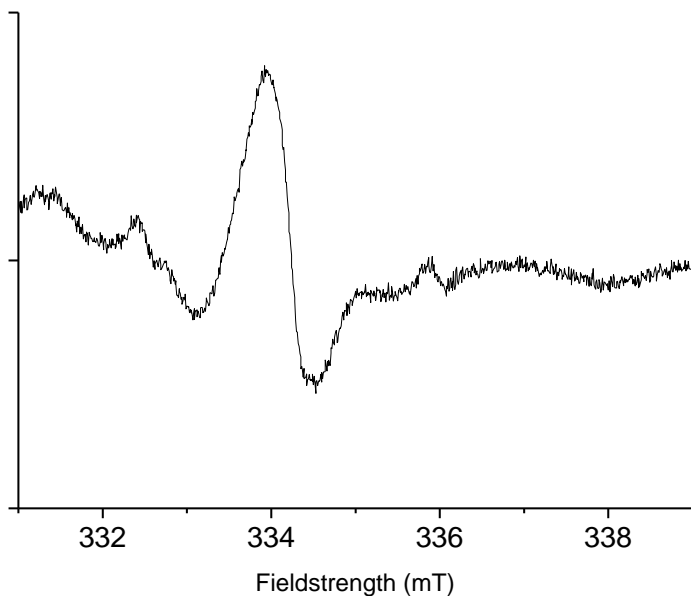


Figure 3.2.16. Resonance spectrum of BSA in His (w/o) containing the spin probe 5-Doxyl.

When testing the eight mAbs one was able to repeat the results gained by fluorescence marker binding. Again mAb3 was the only mAb showing a positive result for hydrophobic marker binding (Figure 3.2.17). In ESR no difference between salt and no salt added to the formulation could be found.

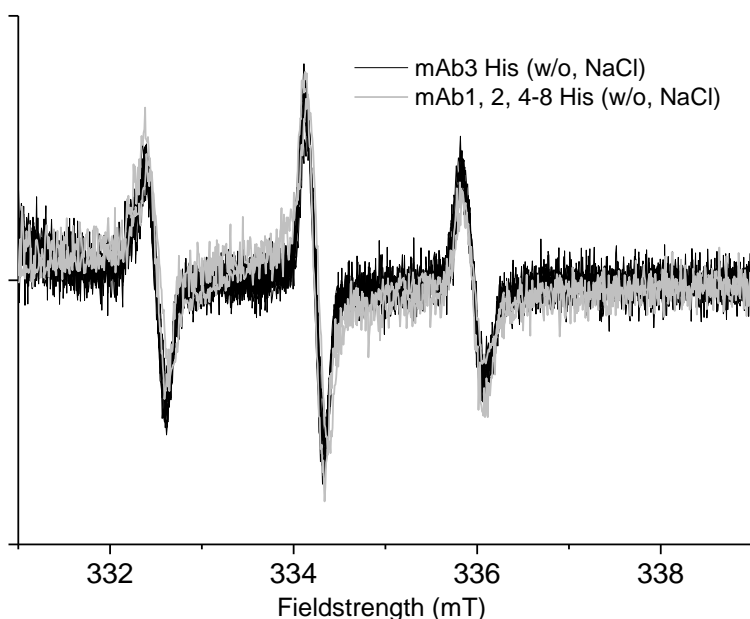


Figure 3.2.17. Overlay of ESR spectra of all mAbs tested in His (w/o) and His (NaCl) containing the spin probe 5-Doxyl. Black representing the non-binding mAbs (1, 2, 4-8) and gray represents the only mAb interacting with the marker (binding) that is mAb3.

3.2.7.3. Surface Tension Measurement

Surface tension of five selected mAbs was tested by pending drop method at 10 and 100 mg/mL in 20 mM His/His-HCl (pH 6.0) \pm 150 mM NaCl. The working hypothesis was

that as hydrophobic substances will try to avoid the water environment they will more strongly move to the liquid-air interface (surface) therefore reducing the surface tension.²¹ Consequently, surface tension measurement is a means to discriminate proteins based on their lipophilicity. In contrast to the fluorescence and ESR method (see 2.11 and 2.12), the surface tension method is label free and does not depend on any specific marker binding. As can be seen in Figure 3.2.18 the surface tension decreased over 30 minutes for all mAbs whereas the placebo's surface tension stayed constant. This is valid for all mAbs at all conditions regardless of their protein concentration (10 mg/mL versus 100 mg/mL). It can be concluded that the mAbs are surface-active. This is a known phenomenon for proteins and has been previously also described for mAbs.⁷⁸ An interesting observation was made while comparing the different mAbs in 10 mg/mL. At 10 mg/mL in low ionic strength the the surface tension after 30 min related to the mAbs net charge (Figure 3.2.3) and A_2 with the exception of mAb3 (mAb1=mAb4<mAb6<mAb8<mAb3, see Figure 3.2.20). However, it's likely too simple just to rank based on net charge. It should be mentioned that mAb3 was the only mAb where ESR and fluorescence showed evidence for lipophilicity (see section 3.2.7.1, 3.2.7.2). So one concluded mAb3 had the highest lipophilicity. In the low ionic strength condition at 10 mg/mL, mAb3 was found to decrease the surface tension strongest, i.e. it has lowest affinity to the hydrophilic liquid compartment. The other mAbs followed the net charge ranking in low ionic strength which is likely a surrogate for their hydrophilicity. The more charged a molecule, the more hydrophilic, the more it tries to stay within the hydrophilic liquid solution.¹⁵ In addition the increase of the buffer's ionic-strength accelerated the drop in surface tension. The conclusion is that shielding net charge by counterions make the mAbs more lipophilic and more prone to the liquid-air interface (Figure 3.2.18 A and B). When ionic strength was increased the drop in surface tension at 10 mg/mL is stronger and also the ranking after 30 minutes is different. Obviously as charge effects are shielded by counter ions the hydrophobicity is increased (salting out effect). At 10 mg/mL after NaCl addition the mAbs (with the exception of mAb3) followed the A_2 ranking (+NaCl) (see Figure 3.2.20). mAb1 and 4 are the most repulsive and also least surface active ones whereas the antibody which was attractive (negative A_2), mAb6, showed the highest surface activity. What is also worth to point out is that mAb8 like within the A_2 measurements did hardly change its behavior at low or high ionic strength. mAb3 again was an outlier as it was also shown within the other hydrophobicity assays. Again the reason probably is that this mAb does not interact with itself (positive A_2) but with (hydrophobic) aggregates (its target). If a small molecule like the marker fits into this hydrophobic pocket a positive result is generated. Namely that A_2 at high ionic strength should give a picture of non-ionic protein interactions like hydrophobic ones. One can see that at 10 mg/mL even after 30 minutes there was still no equilibrium at the interface established as surface tension was still declining. It seems that the process slows down when approaching equilibrium. In literature one example was found where it is described that even for surfactants – i.e. highly surface-active compounds - equilibrium was not reached within seconds.⁷⁹ When increasing the concentration of mAbs by a factor of 10 the drop in surface tension is stronger, i.e. is happening more quickly and with lower resulting surface tension. As more protein is present the saturation at the interface may likely increase faster. Also the differences between low and high salt are no longer that predominant. Therefore it seems that as a

maximum occupancy of mAb in the interface is reached, surface tension is no longer reduced.

By doing surface tension measurements one was able to distinguish/rank the mAbs for their surface activity and hence hydrophobicity. mAb3 had the highest surface activity/hydrophobicity which is in accordance with the results from fluorescence and ESR. Except for mAb3 surface activity was related to A_2 at respective formulations, which is a very promising result as it proofs that A_2 can also be used for information on mAbs hydrophobicity.

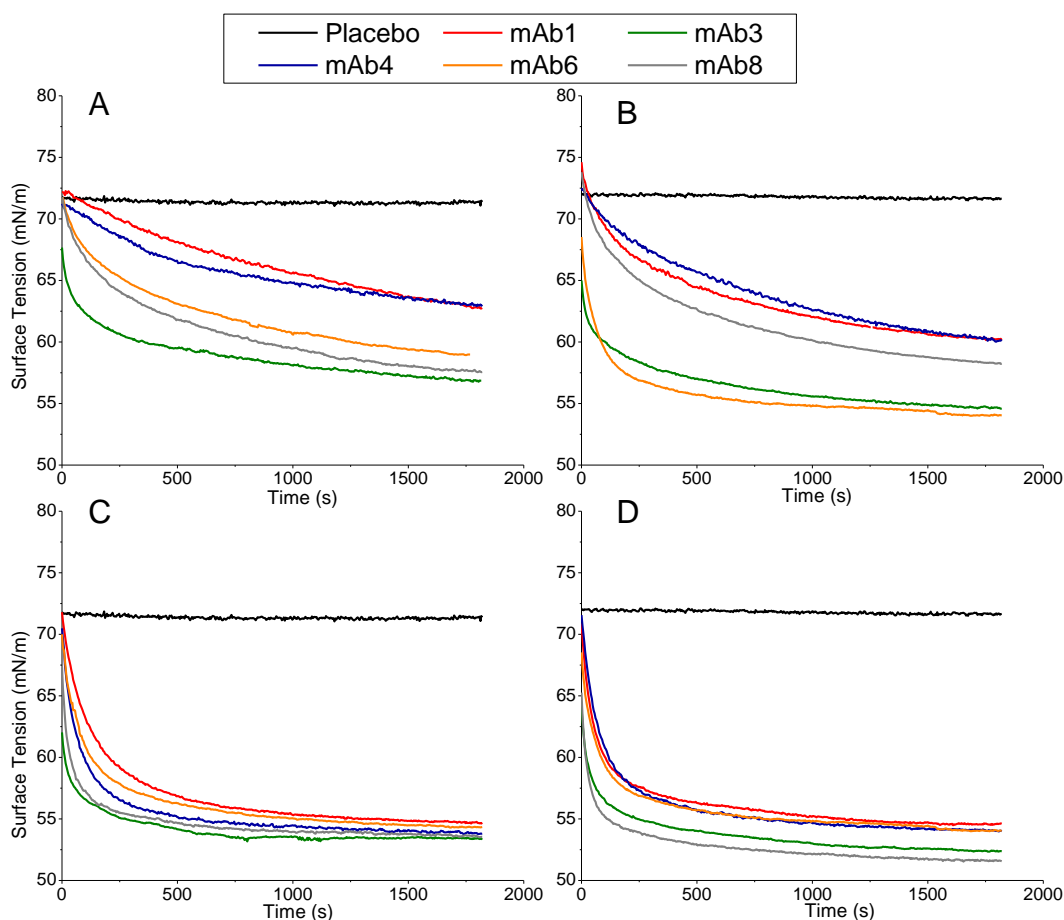


Figure 3.2.18. Change of surface tension over time of five mAbs at two formulation conditions His (w/o), quartiles A, C and His (NaCl) quartiles B, C measured at two different mAb concentrations namely 10 mg/mL (A, B) and 100 mg/mL (C, D). Data are shown as the mean of $n=3$, with SD being below 3%.

To better visualize the discussed results a comparison of measured surface tension after 30 minutes of measurement is shown in Figure 3.2.19. Differences are caused by the different kinetics of surface tension drops over time. Results were not biased by the evaporation of the recorded drop as the volume of the drop did not change significantly over 30 minutes (data not shown). Surface tension measurement was found to be the most distinctive method when it comes to rank mAbs based on hydrophobicity.

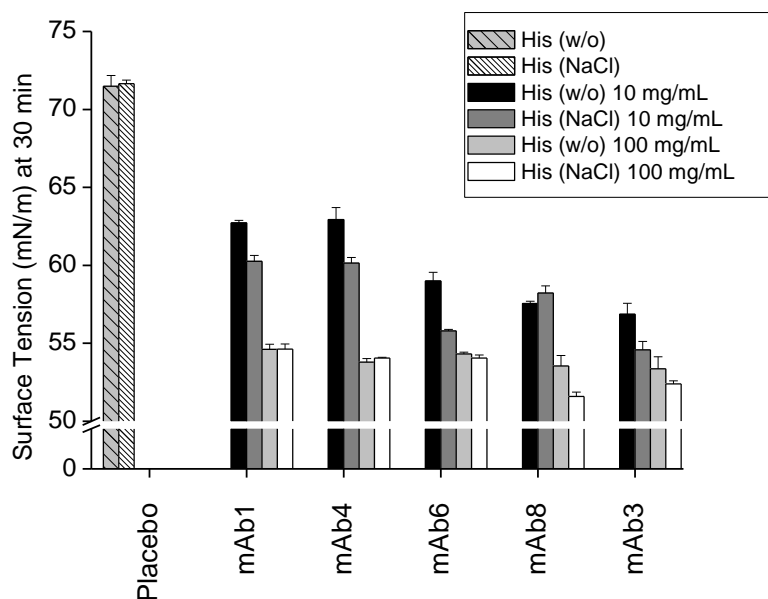


Figure 3.2.19. Surface tension after 30 minutes of five mAbs at two formulation conditions (His (w/o) and His (NaCl)) measured at two different mAb concentrations namely 10 and 100 mg/mL. Data are shown as mean of $n=3 \pm$ SD.

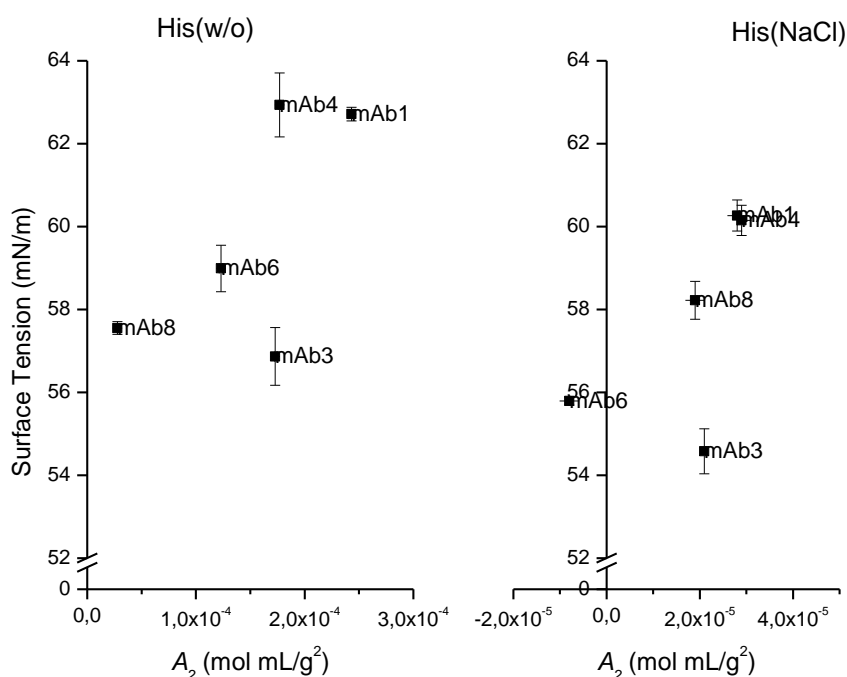


Figure 3.2.20. Surface tension after 30 minutes of five mAbs at two formulation conditions (His (w/o) and His (NaCl)) measured at a mAb concentration of 10 mg/mL and the respective A_2 values. Data are shown as mean \pm SD ($n=3$, Surface tension) and mean \pm absolute deviation ($n=2$, A_2).

3.2.7.4. Ammonium Sulphate Precipitation

This assay was chosen in order to shield any ionic interactions by the presence of high salt and to make non-ionic interactions predominant. An increase in counter ions causes the mAbs to attract each other based on non-ionic interactions (shown for mAb6 in A_2 determination, Figure 3.1.7). The question was: Is this also reflected in the mAbs

precipitation behavior using ammonium sulphate? The aim was to see if protein-protein interactions upon charge shielding do correlate with the amount of ammonium sulphate needed for precipitation. The ammonium sulphate concentration necessary to precipitate 50% of protein (PC50) was determined for eight mAbs. Figure 3.2.21 shows mAb7 at increasing ammonium sulphate concentration and how the inflection point was determined (PC50). The higher PC50 the more ammonium sulphate is necessary to precipitate the proteins. In Figure 3.2.22 the mAbs are ranked by their PC50 in descending order. Ranking (mAb3 > mAb1 > mAb8 > mAb4 > mAb2 > mAb7 > mAb6 > mAb5) as compared to the A_2 ranking (+NaCl) is different (mAb4 > mAb1 > mAb3 > mAb8 > mAb2 > mAb5 > mAb6 > mAb7). Probably ammonium sulphate precipitation results indicate a mixture of ionic and non-ionic interactions. The best example is mAb3. It was shown to be the most hydrophobic antibody but it has the highest PC50. This is probably due to the fact that mAb3 has also a high charge. It was therefore concluded that not only hydrophobic interactions are important in PC50 but also the proteins' charge.^{15,20}

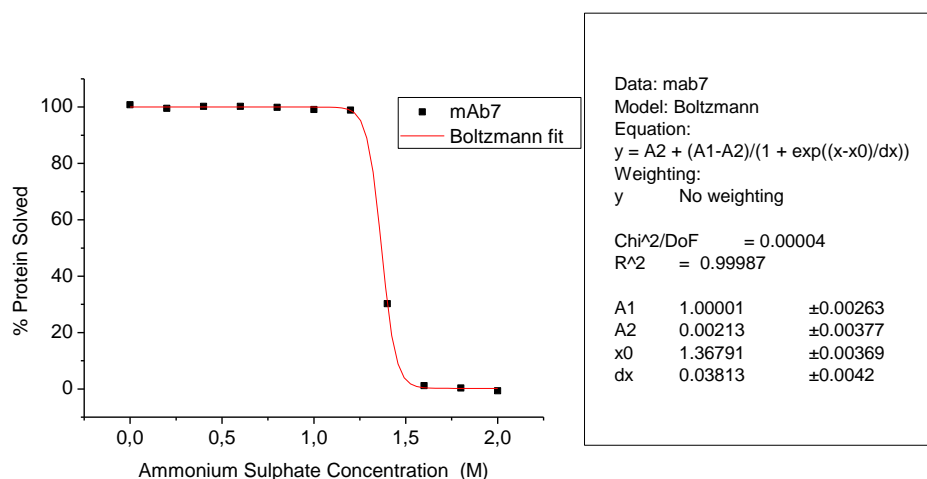


Figure 3.2.21. Fit equation to determine the ammonium sulphate concentration where 50% protein is precipitated (PC50) on the example of mAb7.

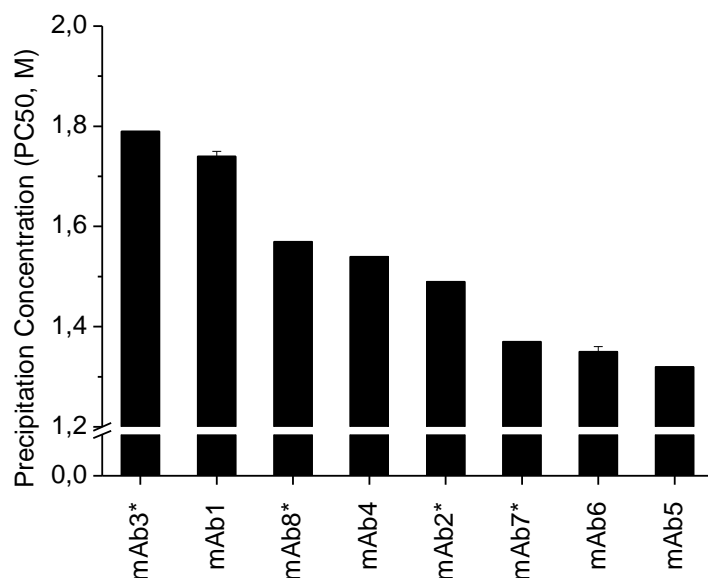


Figure 3.2.22. mAbs sorted by the ammonium sulphate concentration necessary to precipitate 50% of protein (PC50). Results are shown as the inflection point \pm error of the fit. (*)Data provided by Dr. Ulla Grauschopf.

3.2.7.5. Calculated Hydrophobicity based on primary Amino Acid Sequence

Based on an individual hydrophobicity index of amino acids at pH 7.0 published by Monera et al.³⁴ the relative hydrophobicity was calculated based on the amino acid sequence of the full mAb. One can see that mAb3 which is also the mAb having the highest positive results for hydrophobic interactions in ESR, fluorescence and surface tension shows the highest relative hydrophobicity (Figure 3.2.23). Further comparison to surface tension (Figure 3.2.18) indicates a similar ranking. In low ionic strength at 10 mg/mL the ranking was mAb1<mAb4<mAb6<mAb8<mAb3 as compared to calculated hydrophobicity that lead to mAb4<mAb1<mAb8<mAb6<mAb3. It was concluded that that already a calculated relative hydrophobicity can give a first hint on antibody's measured hydrophobicity. This is unexpected as it was thought that hydrophobic amino acids are facing to the proteins core. These amino acids should therefore not contribute to mAbs' hydrophobicity in its native 3D structure.

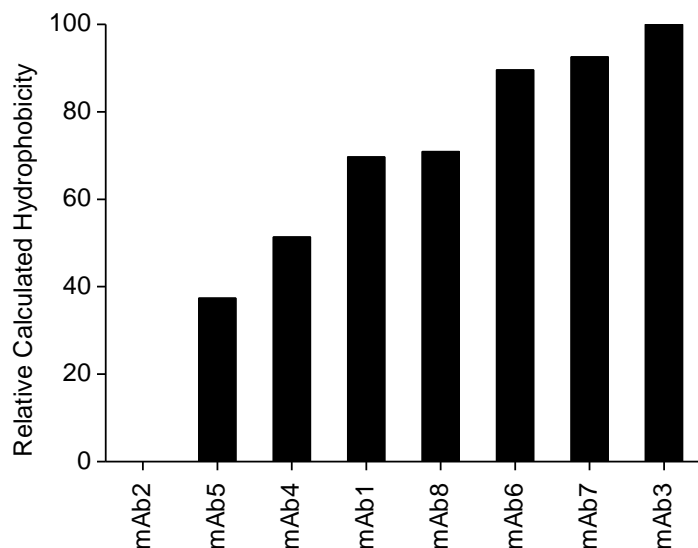


Figure 3.2.23. mAbs ranked by their relative hydrophobicity based on the primary amino acid sequence summing up the products of amino acids times individual hydrophobicity based on Monera et al. and Sereda et al.^{34,35}

3.3. Structural Differences in mAb Subclasses (IgG1 vs. IgG4)

This section shall elaborate on structural differences between the IgG1 and IgG4 molecules tested in the subsequent section 3.4. It is known from literature, that one of the main differences between IgG1 and IgG4 is the position of the disulfide-bonds.^{80,81} However as disulfide-bonds are not contributing to the overall charge of mAbs, the position of the disulfide bonds has probably no influence on ionic interaction. A more important difference regarding protein-interaction is the difference in the Fc region. The Fc domain of IgG4 antibodies bears no effector function.⁸² The reason for that is that IgG4 mAbs as compared to IgG1 mAbs have a Lysine (L235E) exchanged by a Phenylalae. So by definition Fc parts of IgG4 antibodies do lack a positive charge resulting in a less charged, i.e. more negatively charged Fc region.^{83,84}

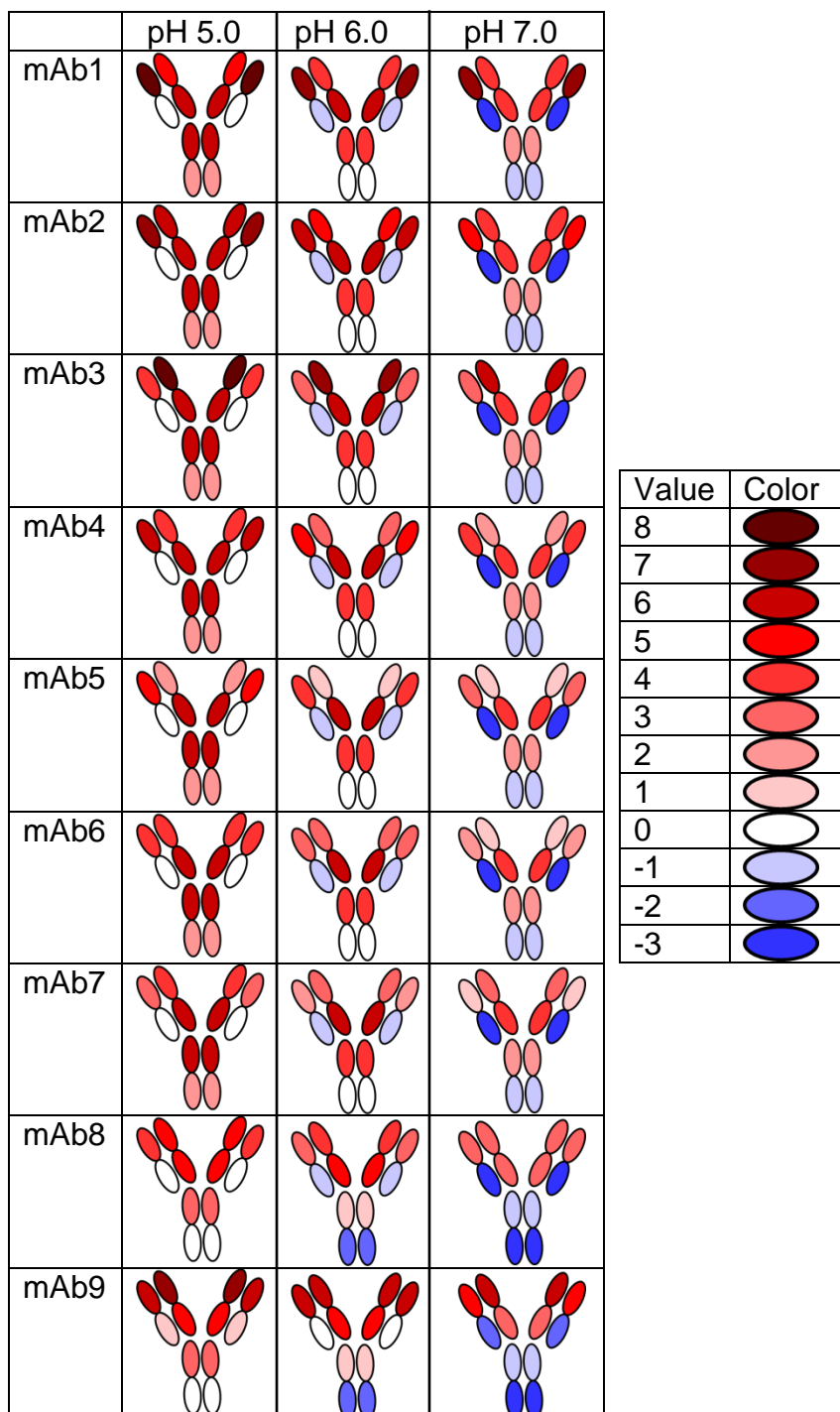


Figure 3.3.1. Calculated net charge of different subunits of mAbs as a function of pH. Blue representing negative and red/black positive charges.

Based on primary sequence information only theoretical net charge determination was conducted as described already in 2.3, however net charge was not assessed for the whole mAb, but for partial mAb structures. More precisely net charge was calculated within Fab fragments (namely for VH, VL, CH, CL) and Fc fragment (i.e. CH2 and CH3). Then the net charge of each unit was calculated at three different pH values. The result is shown in Figure 3.3.1. The more reddish/blackish the color is the higher (more positive) the charge and the more bluish the lower (more negative) the charge is. The figure demonstrates what is expected. As pH increases from 5.0 to 7.0 the mAbs positive net

charge is reduced. Comparison of the IgG1 mAbs (1-7) also shows that the color code is following the determined net charge ranking at pH 6.0 (equals numbering of mAbs 1-7). This is consistent over all pH values. However what was very interesting was the resulting charge map of the two IgG4 antibodies (mAbs 8-9). Although net charge of mAb8 and mAb9 is lower at pH 6.0 as compared to mAb1-7 the charge distribution is varies. Obviously the Fc domain is different as compared to IgG1 mAbs. At pH 6.0 and even more pronounced at pH 7.0 the Fab domains are positively charged whereas the Fc domain is negatively charged (pH 6.0: CH₂+CH₃=-1, pH 7.0 CH₂+CH₃=-4). Compared to IgG1 antibodies at pH 6.0 the Fc part is still positively charged (CH₂+CH₃=4) whereas at pH 7.0 the Fc domain is overall uncharged (CH₂+CH₃=0). This observation, that IgG4 mAbs have a more negative at pH 6.0 and pH 7.0, might rise the possibility of having a molecule with a higher dipole momentum.⁸⁵

The importance of this observation will be discussed in the next chapter 3.4. This finding offers a very plausible explanation for attractive protein-protein interaction (A_2) seen at low ionic strength, i.e. conditions where long range ionic-interactions are favored. This was found to be specific for the two IgG4 mAbs analyzed.

3.4. Protein-Protein Interaction of mAbs in Different Pharmaceutically Relevant Buffer Systems

Employing the high throughput method developed under 3.1.3 five mAbs were screened for their A_2 in different pharmaceutically applied buffer systems varying pH, buffer ions and ionic strength. This assessment of A_2 in the relevant buffer systems should enable a better understanding in behavior and eventually modeling of A_2 at different formulation conditions. In the following, five mAbs were screened under the conditions described in Table 2.1.2 on p.7, varying ionic buffer strength from 10 to 50 mM, the pH from 5.0 to 7.0 and the valence (charge) of buffer anions from 1 to 3.

3.4.1. Overview of the Formulation Screen

The following overviews should give the big picture before the results are shown and discussed in detail. A first overview of the screen done for three IgG1 mAbs can be seen in Figure 3.4.1. It shows that within the formulations the second virial coefficient A_2 was very different. Highest differences are seen at low ionic strength (10 mM). As the ionic strength is increased the repulsion is in general reduced as expected. It indicates that the high repulsive behavior is based on ionic interactions that are decreased by the presence of counter ions. Please note that the rather busy figure is shown by intention to illustrate that the decrease of repulsiveness with increasing ionic strength is a common theme for all IgG1 mAbs within the various formulation conditions tested.

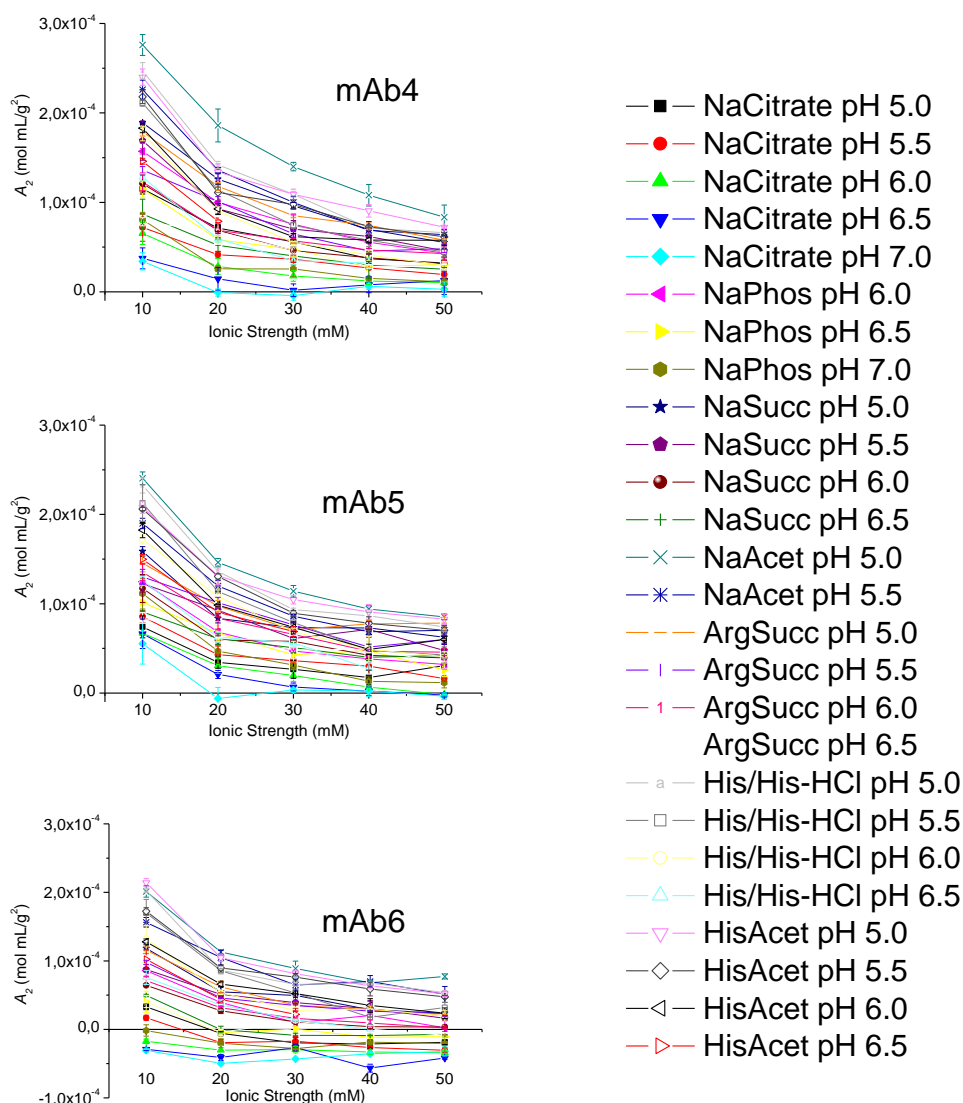


Figure 3.4.1. Overview of formulation screens of three different IgG1 mAbs. Each color represents the second virial coefficient A_2 at different ionic strengths of one tested formulation. Data are shown as mean of $n=3 \pm$ error of the linear regression.

A first overview of the two IgG4 mAbs (Figure 3.4.2) shows that especially at low ionic strength the second virial coefficient is very different in the formulations tested as compared to the examples shown for the three IgG1 molecules. Compared to the IgG1 mAbs these antibodies showed also attractive behavior which was found highest at lowest ionic strength. The most interesting observation was that with increasing ionic strength this attraction was reduced. Moreover, the repulsive formulations showed similar behavior as the IgG1 formulations, i.e. their repulsiveness got reduced with increasing ionic strength. The high attractiveness for some of the IgG4 formulations was unexpected and contrasts the data obtained for the IgG1 molecules (see Figure 3.4.1). More surprisingly, the attractiveness got diminished with increasing ionic strength. This finding may indicate that the repulsive as well as the attractive behavior at low ionic strength must be related to long range ionic interactions. The difference to the data shown earlier on (see 3.2.6) is that attraction for the IgG4 molecules happened at a condition where one would assume primarily charge-charge interactions, namely low-ionic strength condition. So far – for the mAbs described in this thesis – attraction occurred only under ion-shielding conditions, i.e.

high ionic strength, where no charge-charge interaction is assumed. A possible explanation for this IgG4 behavior is found in chapter 3.3 where it is shown that IgG4 mAbs are likely to show ionic attractive interactions due to their unequal charge distribution (positive Fab- and net negative Fc-part). This is – so far – only a hypothesis. Assuming this hypothesis holds true it becomes clear that global net charge alone may not be a means to predict repulsiveness or attractiveness at low ionic strength condition. In fact local charges and local charge-charge interactions may change the protein behavior. Similar examples are already given in literature. For example Kanai et al² could show that a site specific self-interaction of mAbs in solution might be the cause for increased viscosity. This can be decreased by the addition of salts.

The data emphasizes that ionic strength has a significant influence on A_2 . Consequently, the experimental set-up, i.e. fixing ionic strength levels, was chosen by intention. Often, e.g. in formulation screenings, buffers of equal molar concentration are compared. The following figure shall illustrate how different the resulting ionic strength is depending on the buffer system used (Figure 3.4.3).^{20,86} It shows that buffers of equal molar buffer concentration have a very different ionic strength that is also pH dependent.

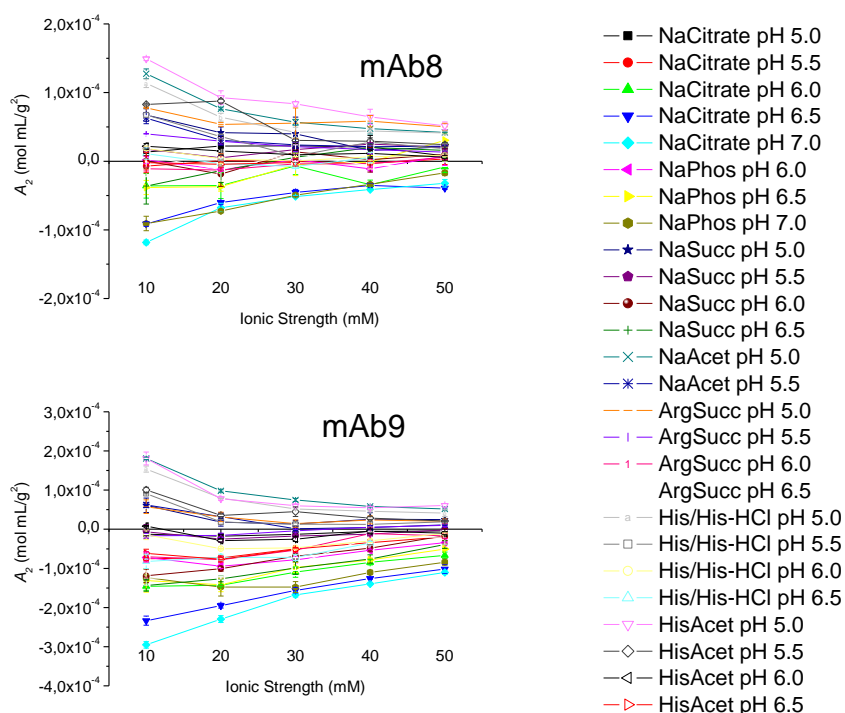


Figure 3.4.2. Overview of formulation screens of two different IgG4 mAbs. Each color represents the second virial coefficient A_2 at different ionic strengths of one formulation tested. Data are shown as mean of $n=3 \pm$ error of the linear regression.

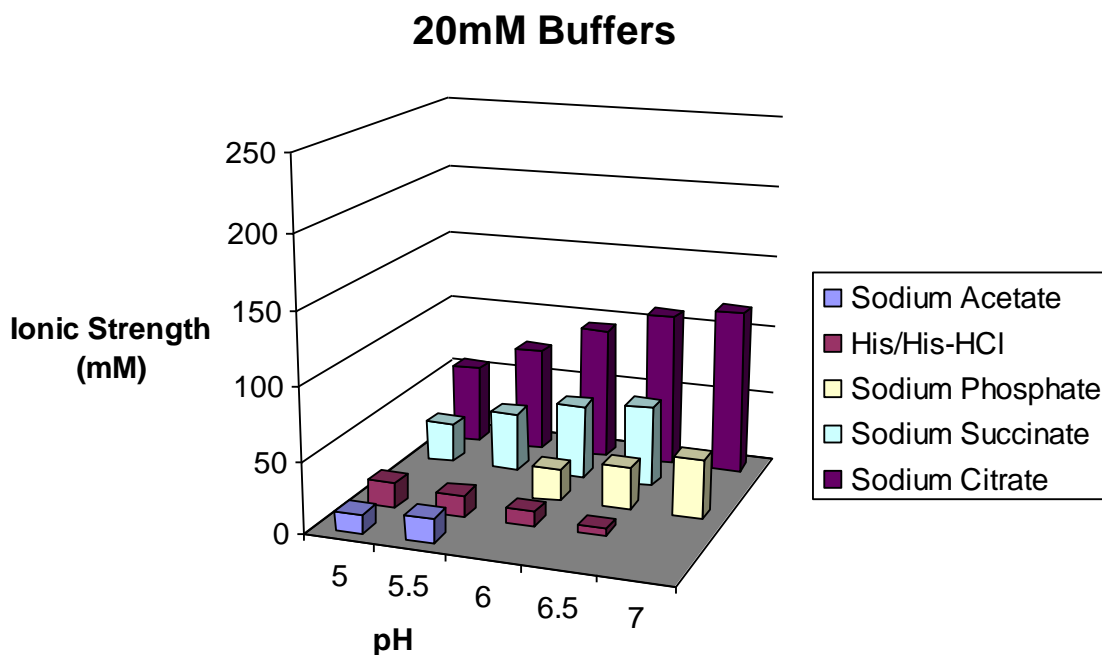


Figure 3.4.3. Differences in ionic strength of different buffers at constant molar buffer concentration (20 mM) over pH. Data shown represents a theoretical calculation based on equations described in chapter 2.1.

The preparation of buffers at constant ionic strength at several pH values is cumbersome and shall briefly be discussed. As outlined in Figure 3.4.3 buffers pH, ion valence, and also buffer ion distribution is based on the buffers pK_a . pK_a values are not only dependent on temperature but also on buffer's ionic strength.^{45,87} An example is given by Figure 3.4.4. It shows how the distribution of ions and therefore the necessary buffer composition changes with an increase in ionic strength in order to keep the pH constant. In other words dilution of buffers can cause a pH shift due to the very same effect. Therefore one should be careful when formulating by dilution using stock solutions.^{45,87} All these effects had to be and were considered when preparing the formulations.

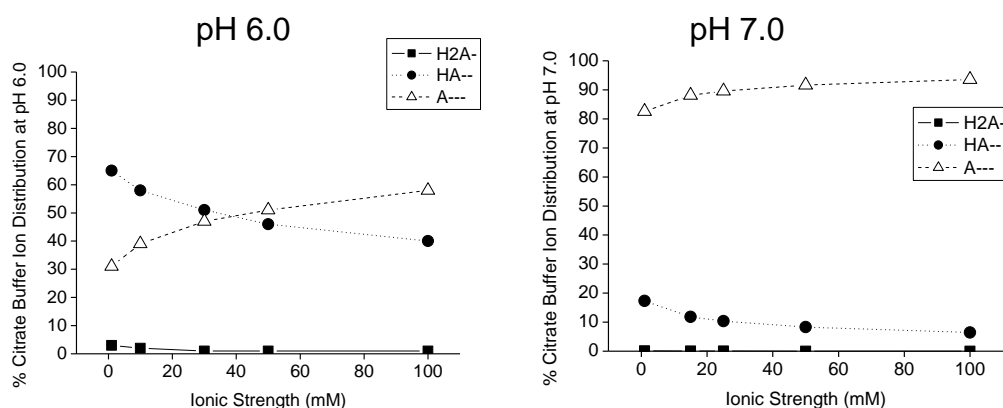


Figure 3.4.4. Change of ion composition on ionic strength increase at constant buffer's pH based on the theoretical calculations.^{45,87} Calculated for citrate buffer at two pH values based on equations found in chapter 2.1.

3.4.2. Behavior of A_2 Varying Buffer and pH at Constant Ionic Strength

After having shown the overall difference in IgG1 and IgG4 behavior, a more detailed analysis of results shall be discussed in this section. The experimental set-up has been

chosen that way that constant ionic strength conditions could be compared. The following section shall especially elaborate on the role of buffer ion, i.e. counterion in protein-protein interaction. As the differences at constant ionic strength were most predominant at low ionic strength the results at 10 mM ionic strength are shown and discussed by intention. The behavior of A_2 for an IgG1 antibody (mAb4) in the 10 mM ionic strength conditions can be seen in Figure 3.4.5. As expected it shows that with increasing pH the repulsion is reduced. This can be seen for every individual buffer system. As already discussed earlier on, this is likely due to the fact that overall positive net charge is lowered as mAbs are formulated closer to the IEP. The data showed in addition, that – despite the normalization of ionic strength, which is mainly governed by buffer ion valence – subsets of counter-ion valences could be elaborated. With an increase in buffer valence the repulsion is reduced – despite equal ionic strength. From this result one could conclude that it is not only a matter of ionic strength when modifying protein interactions but that also the valence of the counter ion has to be taken into account. This is important information to the formulation scientist, as this might govern the decision on appropriate buffer system, e.g. driven by the need to increase repulsiveness of a system. According to literature a possible explanation could be that multivalent ions have the likelihood to crosslink mAbs, which could lead to a stronger reduction in repulsive protein-protein interaction.⁸⁸ However, this was mainly described for the area of highly concentrated formulations and may not easily be transferred to the low concentration condition. That these buffer valence effects were not caused by other buffer properties, like buffer concentration or overall ion concentration, is discussed in the next section.

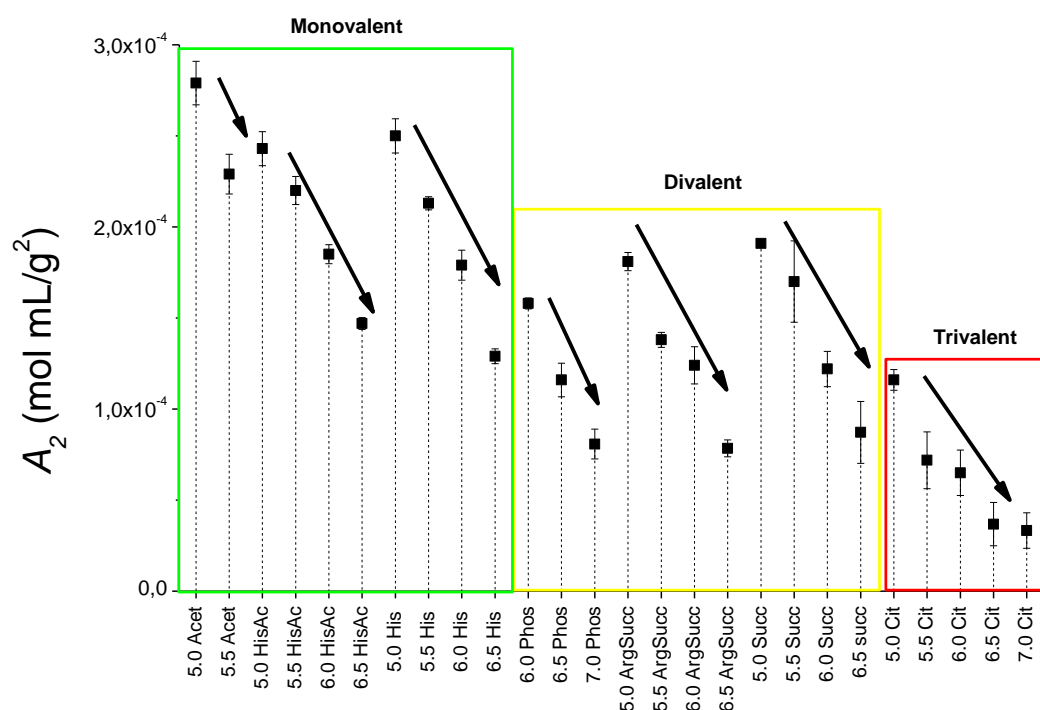


Figure 3.4.5. Snapshot of the formulation screen of mAb4 looking at A_2 values in different buffers measured at 10 mM ionic strength. Data are shown as mean of $n=3 \pm$ error of the linear regression.

A snapshot for an IgG4 antibody (mAb9) at the 10 mM formulation condition can be seen in Figure 3.4.6. The behavior is similar to what was shown for an IgG1 (Figure 3.4.5). The difference here is, that values are not shifted from repulsive to non-interacting (zero A_2) but from repulsive to attractive. One can see that with increasing pH the repulsion is reduced

and attraction is increased. Again the data showed in addition, that – despite the normalization of ionic strength, which is mainly governed by buffer ion valency – subsets of counter-ion valences could be elaborated. With an increase in buffer valence the repulsion is reduced and attraction is increased.

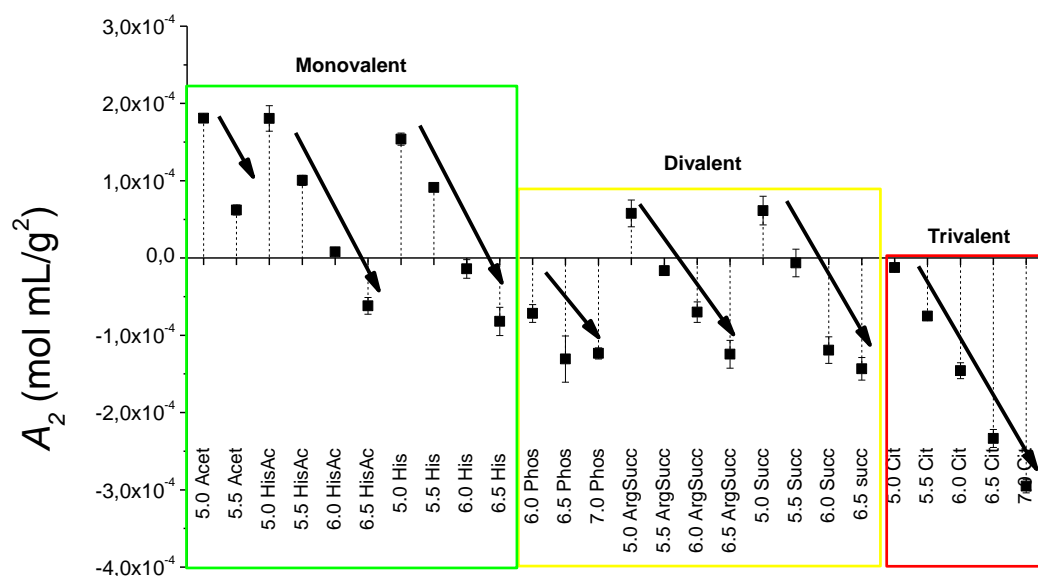


Figure 3.4.6. Snapshot of the formulation screen of mAb9 looking at A_2 values in different buffers measured at 10 mM ionic strength. Data are shown as mean of $n=3 \pm$ error of the linear regression.

3.4.3. Behavior of A_2 at Increasing Ionic Strength

In a next step two representative results for an IgG1 (i.e. mAb4) and an IgG4 (i.e. mAb9) were compared in detail focusing at different pH values, the behavior at different ionic strengths and buffer species. Comparisons are shown in the following figures (pH 5.0: Figure 3.4.7, pH 6.0: Figure 3.4.9 and pH 7.0: Figure 3.4.11). At pH 5.0 and low ionic strength one can see that both mAbs are mainly repulsive. As ionic strength increases the repulsion for both is reduced. As already stressed out under 3.4.2 the unexpected observation made, was, that although ionic strength was kept constant buffer valence has an influence on protein-protein interaction. All the mono-valent buffers were found to be most repulsive (NaAcetate, HisAcetate, His/His-HCl), the tri-valent buffer (NaCitrate) was found to be least repulsive and the di-valent species (NaSuccinate, ArgSuccinate, and NaPhosphate) are found in-between.

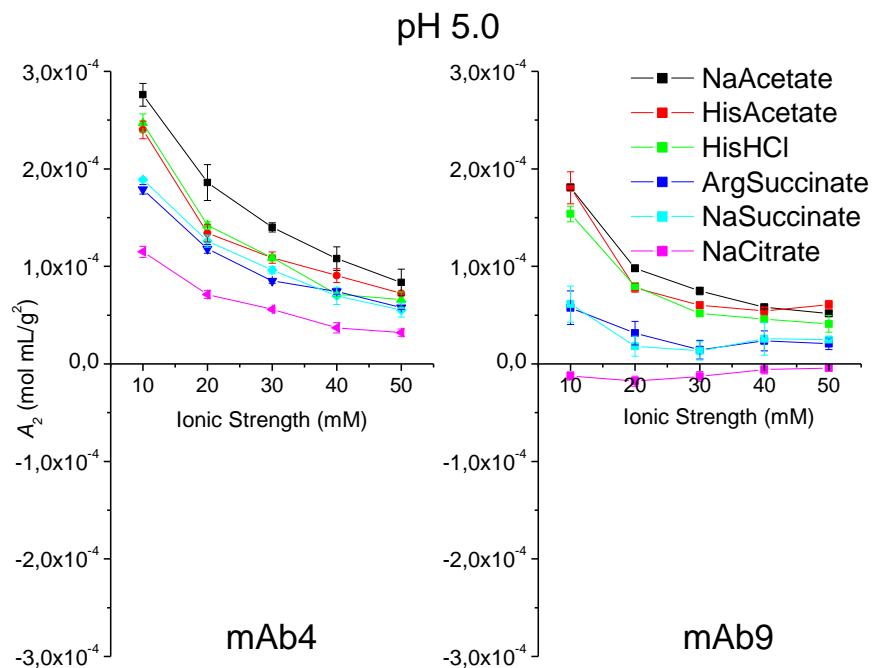


Figure 3.4.7. Comparison of A_2 values of mAb4 and mAb9 for all pH 5.0 formulations. Data are shown as mean of $n=3 \pm$ error of the linear regression.

The next figure (Figure 3.4.8) shows that a difference in buffer concentration (mM) or buffer's ion concentration (i.e. the concentration of ions independently of their valences summed up in mM) is not the reason for a difference in A_2 . If differences would have been caused by a different ion concentration or the buffer concentration, then the differences between the buffer's A_2 behavior would have vanished. This was not the case. It was therefore concluded that it is in fact the buffers ion valence that does cause different behaviors in A_2 .

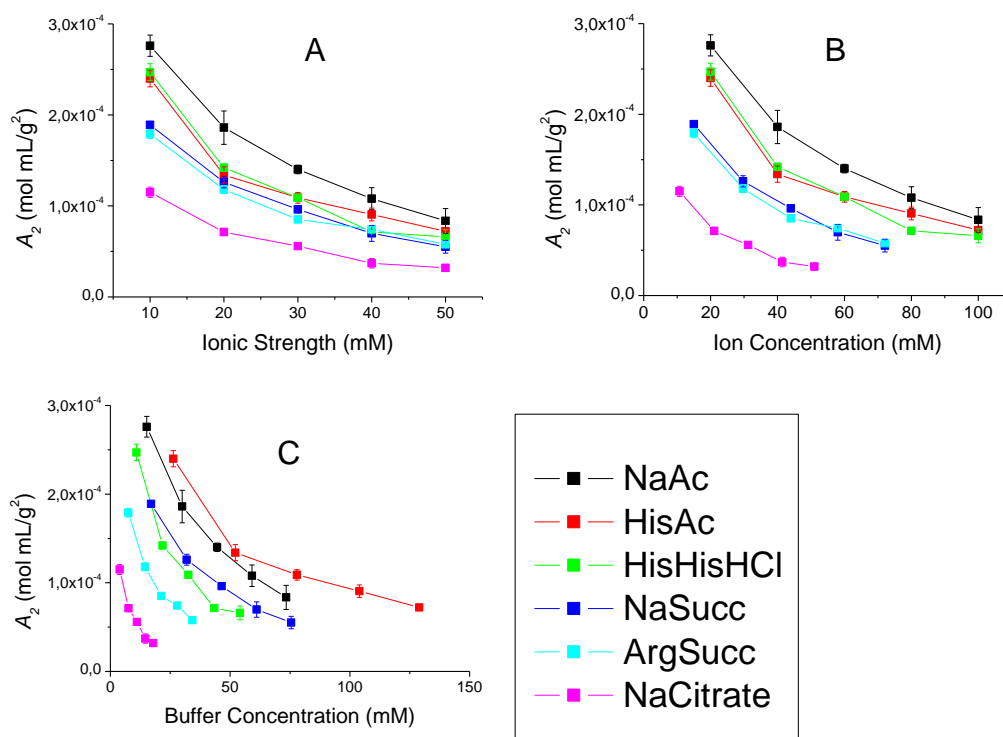


Figure 3.4.8. A_2 values of mAb4 for all pH 5.0 formulations as a function of Ionic Strength (mM, A), Ion Concentration (mM, B), and Buffer Concentration (mM, C). Data are shown as mean of $n=3 \pm$ error of the linear regression.

At pH 6.0 (Figure 3.4.9) the two mAbs (mAb4 and mAb9) start to show an even stronger subclass specific (different) behavior (IgG1 vs IgG4). Whereas mAb4 was still mainly repulsive at low ionic strength mAb9 gave the opposite result. At low ionic strength mAb9 is mainly attractive. This can be explained by the different charge distributions of IgG1 and IgG4 as discussed under 3.3. It is not related to the IEP of the mAbs as both mAbs have a relatively high and also similar IEPs (computed IEPs: mAb4: 9.08 and mAb9 9.20). As the IgG4 molecule has a positively charged F(ab) and a negatively charged Fc it is likely that the opposite charged parts attract each other. This leads to attractive protein-protein interaction. As counter ion concentration in the buffer is increased this ionic self-interaction is reduced.

Again the data showed, that – despite the normalization of ionic strength, which is mainly governed by buffer ion valence – subsets of counter-ion valences could be elaborated. This is similar to what was already discussed for the pH 5.0 data. Surprisingly the phosphate buffer containing mAb4 was behaving like a monovalent buffer. The reason for this was probably that at pH 6.0 phosphate buffer is indeed mainly monovalent (Figure 3.4.10). On the other hand citrate buffer does form di- and trivalent species at this pH and ionic strength (Figure 3.4.4). It was therefore concluded that multivalent buffers are not necessarily always causing a less repulsive mAb behavior than monovalent ones. This information can be very valuable to a formulation scientist.

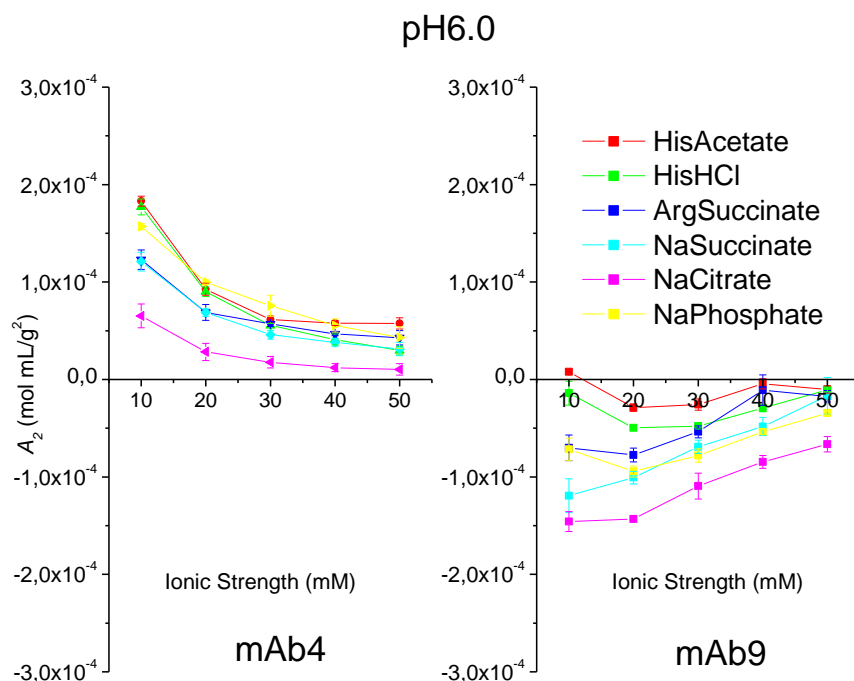


Figure 3.4.9. Comparison of A_2 values of mAb4 and mAb9 for all pH 6.0 formulations. Data are shown as mean of $n=3 \pm$ error of the linear regression.

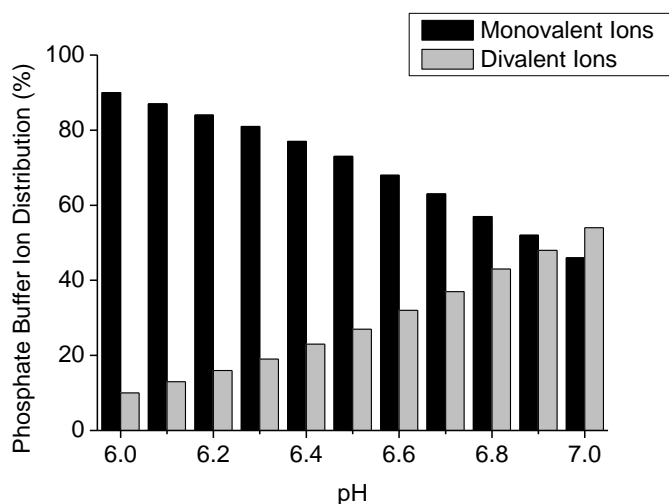


Figure 3.4.10. Phosphate buffer's ion distribution as a function of pH. It represents a theoretical calculation based on equations found in chapter 2.1

At pH 7.0 the already described discrepancy between IgG1 (mAb4) and an IgG4 (mAb9) is even more pronounced (Figure 3.4.11). According to Figure 3.3.2 mAb9 as compared to mAb4 has a very distinct unequal charge distribution (positive Fab, negative Fc). That's why it was expected that especially at low ionic strength mAb9 was even more attractive than at pH 6.0 whereas mAb4 was getting less repulsive. Apart from this also at pH 7.0 a trivalent buffer (citrate) reduces repulsion /increases attraction stronger than a divalent buffer (phosphate). This observation was found to be independent of the antibody subclass, the net charge or the charge distribution on the subdomains (Figure 3.3.2).

At pH 7.0 phosphate buffer is mainly present in its divalent form (Figure 3.4.10) and citrate buffer acts mainly as a trivalent one (Figure 3.4.4).

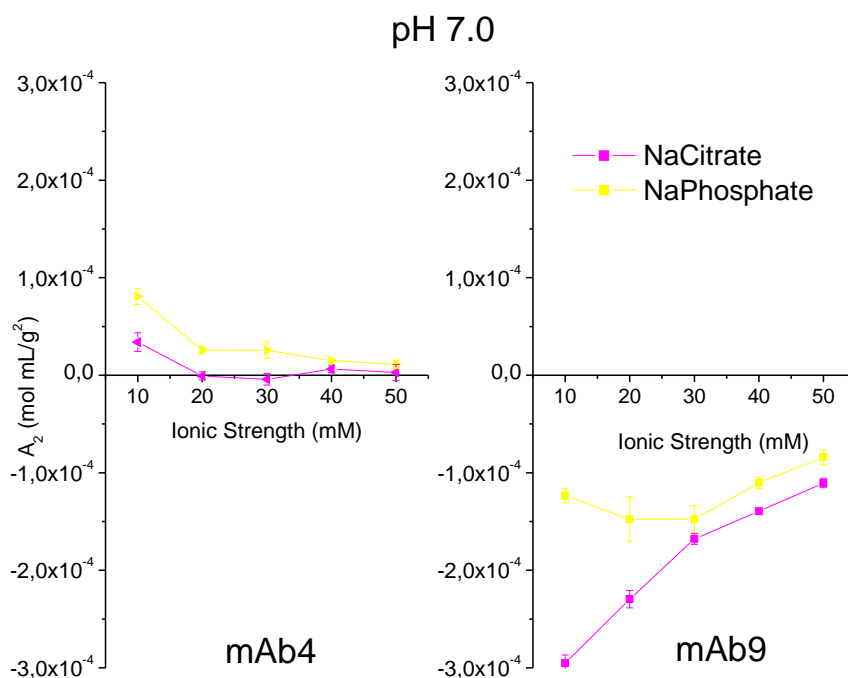


Figure 3.4.11. Comparison of A_2 values of mAb4 and mAb9 for all pH 7.0 formulations. Data are shown as mean of $n=3 \pm$ error of the linear regression.

3.4.4. General Behavior of A_2 Comparing IgG1 to IgG4

Figure 3.4.1 and Figure 3.4.2 indicate that IgG1 and IgG4 mAbs have a similar pattern in the different formulation conditions regarding their A_2 . This section aims to elaborate on how similar they behave over all formulation conditions tested. A direct comparison of the three IgG1 and the two IgG4 tested is shown in the following figures. First, IgG1 formulations shall be compared. Figure 3.4.12 shows A_2 data obtained in all the buffer conditions outlined earlier on (for an overview see Table 2.1.2 and Figure 3.4.1) and compares the three IgG1 molecules, namely mAb5 to mAb6 and mAb6 to mAb4. As one can see the overall behavior of the three different mAbs at the conditions tested was similar. That is why plotting the respective A_2 values of two mAbs, within the different formulations, results not in a data point cloud but rather in a straight line. The mAbs only differ in their absolute A_2 values. This is probably related to net charge. mAb4 having the highest net charge also has the highest A_2 values. mAb5 has the second highest A_2 maximum and mAb6 the lowest of the three mAbs tested. Note that mAb6 also gets attractive. Overall the relative values are comparable; conditions more repulsive/less attractive for one mAb are also more repulsive/less attractive for another mAb. Differences will be discussed later (Figure 3.4.15).

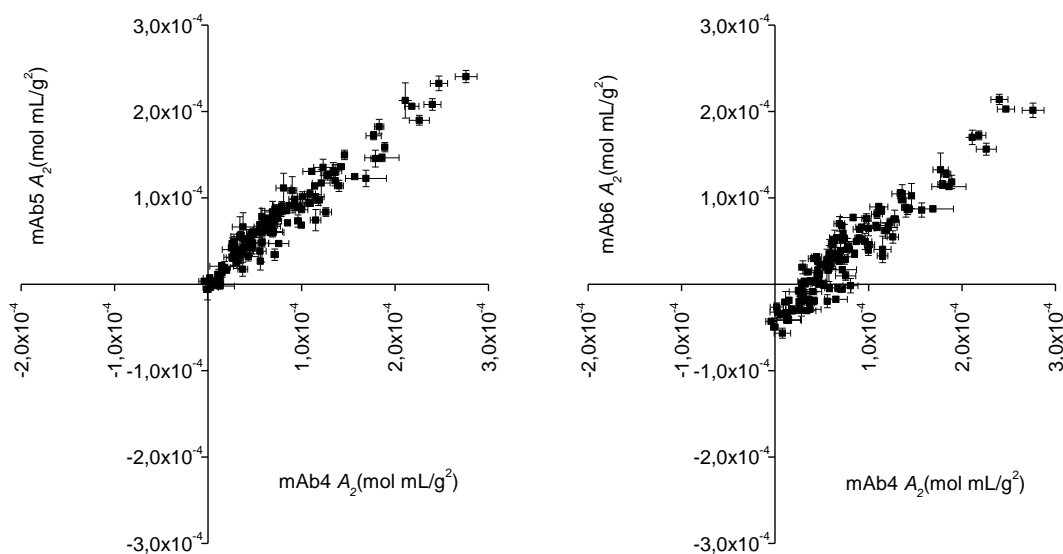


Figure 3.4.12. Comparison of A_2 values of different IgG1 mAbs (mAb4-6) at the same buffer conditions (see Table 2.1.2). Data are shown as mean of $n=3 \pm$ error of the linear regression.

The behavior of an IgG1 molecule and an IgG4 molecule is different. This can be seen when comparing A_2 values within the formulations tested. The following figure (Figure 3.4.13) compares mAb4 to two IgG4 mAbs. This time a data point cloud is formed which is indicating that IgG1 and IgG4 mAbs are behaving different within the same formulations. The reason for that was already shown in Figure 3.4.1 and Figure 3.4.2. Especially at low ionic strength IgG4 mAbs close to or at pH 7.0 are highly attractive (negative A_2). This attractive behavior is reduced as ionic strength increases. IgG1 mAbs on the other hand tend to be more repulsive at low ionic strength what is reduced by the increase of ionic strength.

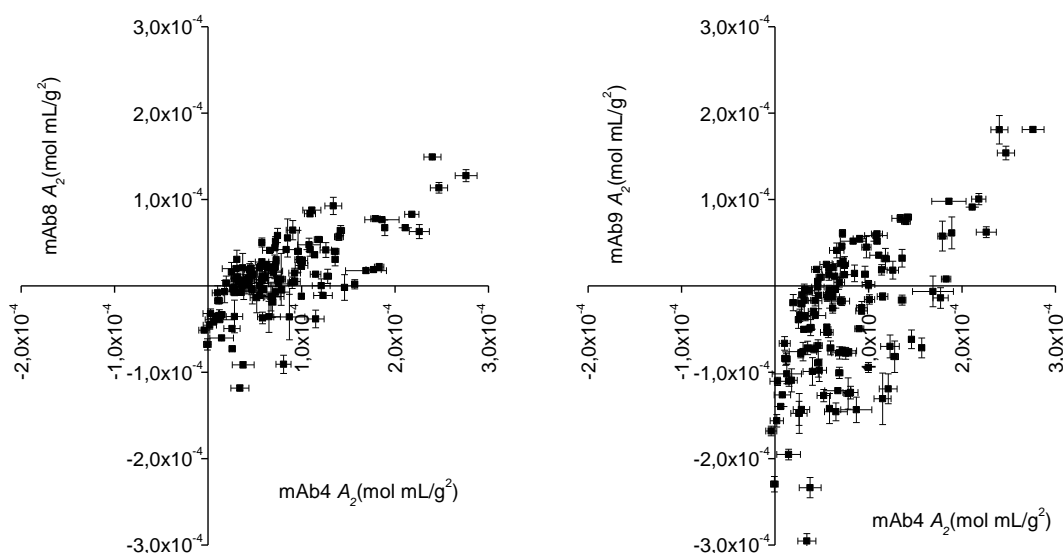


Figure 3.4.13. Comparison of A_2 values of an IgG1 (mAb4) versus two IgG4 antibodies (mAb8 and mAb9) at the same buffer conditions (see Table 2.1.2). Data are shown as mean of $n=3 \pm$ error of the linear regression.

In a next step the two IgG4 mAbs analyzed were compared. The result is shown in Figure 3.4.14. Clearly the two IgG4 antibodies behaved similar regarding their A_2 value within the

different formulations. That is why this direct comparison results in a straight line rather than a data point cloud. This strengthens the result that the two IgG subclasses (IgG1 and IgG4) behave similar to their environment (formulation) within their groups in respect to A_2 . However the behavior between the two IgG subgroups cannot be compared.

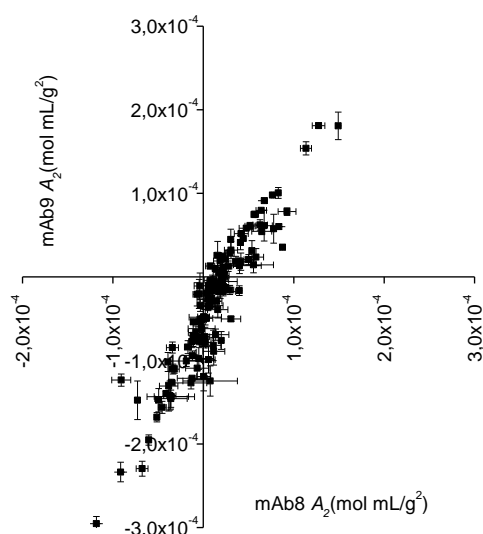


Figure 3.4.14. Comparison of A_2 values of two different IgG4 mAbs (mAb8 and mAb9) at the same buffer conditions (see Table 2.1.2). Data are shown as mean of $n=3 \pm$ error of the linear regression.

So the relative A_2 values among IgG subclasses (IgG1 or IgG4) are comparable; conditions more repulsive/less attractive for one mAb are also more repulsive/less attractive for another mAb. A possible reason for the absolute differences found might be net charge. Figure 3.4.15 shows a comparison of measured net charge at pH 6.0 of three IgG1 mAbs to their overall range of all A_2 values measured per mAb's formulation screen. As one can see, as net charge decreases the values measured for A_2 are shifted to the left. So as net charge is reduced mAbs get less repulsive/more attractive.

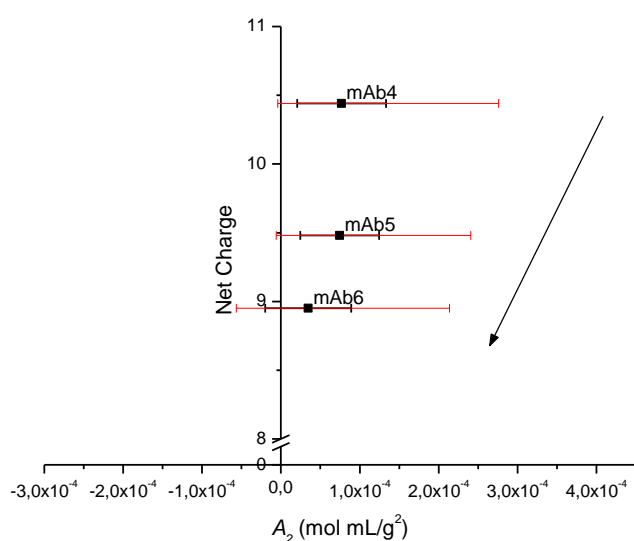


Figure 3.4.15. Three IgG1 mAbs (4-6) and their A_2 values measured in the formulation screen (see Table 2.1.2) compared to effective net charge (based on μ and D_s conv., measured at pH 6.0). The dots and the black error bars represent the mean \pm standard deviation. The red bars represent the min/max value of measured A_2 range.

Next the A_2 values of the IgG4 mAbs are compared to their calculated net charge. The calculated net charge had to be used as no measured net charge data for mAb9 was available. Figure 3.2.16 shows that as net charge is reduced the range of maximum and minimum measured A_2 values is reduced. Both are moving closer to zero.

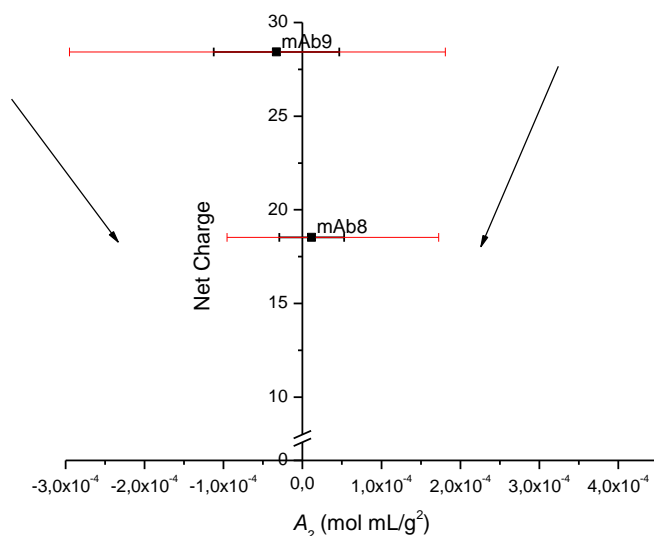


Figure 3.4.16. Distribution of all A_2 values measured in the formulation screen (see Table 2.1.2) for two IgG4 mAbs (mAb8 and mAb9) compared to calculated net charge (at pH 6.0). The dots together with the black error bars represent the mean \pm standard deviation. The red bars represent the min/max value of measured A_2 .

Earlier A_2 at low and high ionic strength (3.2.5 and 3.2.6) was analyzed and data was interpreted that way that A_2 at low ionic strength followed net charge but a high ionic strength behavior could not be predicted. With the present knowledge from this chapter the data was reanalyzed. The result is shown in Figure 3.4.17. Similar to what was found in this chapter the IgG1 mAbs follow the net charge ranking with respect to A_2 . As charge decreases the repulsion (A_2) is reduced. This was independent of low or high ionic strength. On the other hand the only IgG4 mAb analyzed did not follow this trend. The ionic strength hardly influenced its A_2 behavior. At high ionic strength the A_2 values for the IgG1 antibodies do not directly follow the net charge ranking although there seems to be an overall trend (to more attractive the lower the net charge). A reason for this is that at high ionic strength mid and short range interactions are more pronounced as long range ionic-interactions (charge-charge) are shielded by counterions. This has been already discussed in 3.2.7.

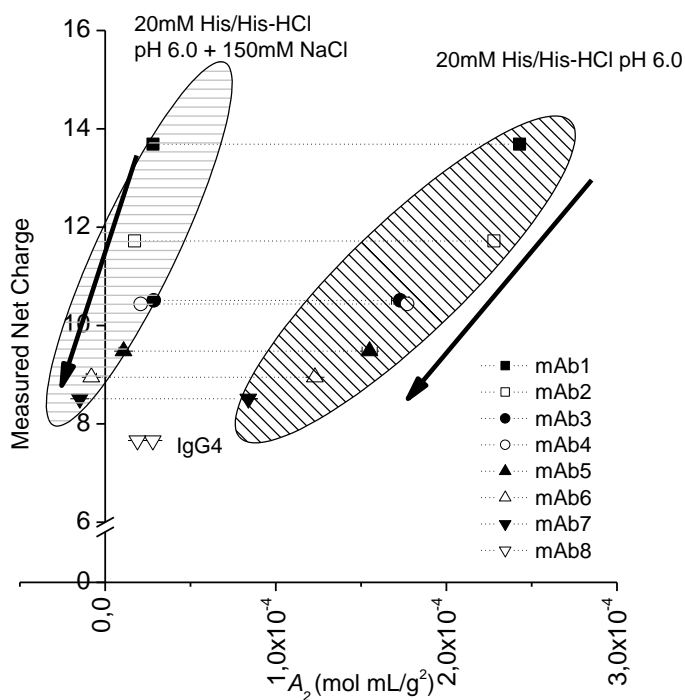


Figure 3.4.17. A_2 values measured at low and high ionic strength compared to effective net charge (based on μ and D_s conv., at pH 6.0) of eight different mAbs. A_2 data are shown as mean of $n=3 \pm$ error of the linear regression.

3.4.5. Diffusion Coefficients at Infinite Dilution (D_0) of the A_2 measurements in this chapter

As D_0 was found to be constant for mAbs (3.1.2) this section compares the D_0 for all mAbs measured in the various conditions as outlined in Table 2.1.2. The D_0 intercepts are shown in Figure 3.4.18. All 635 formulations tested are plotted.

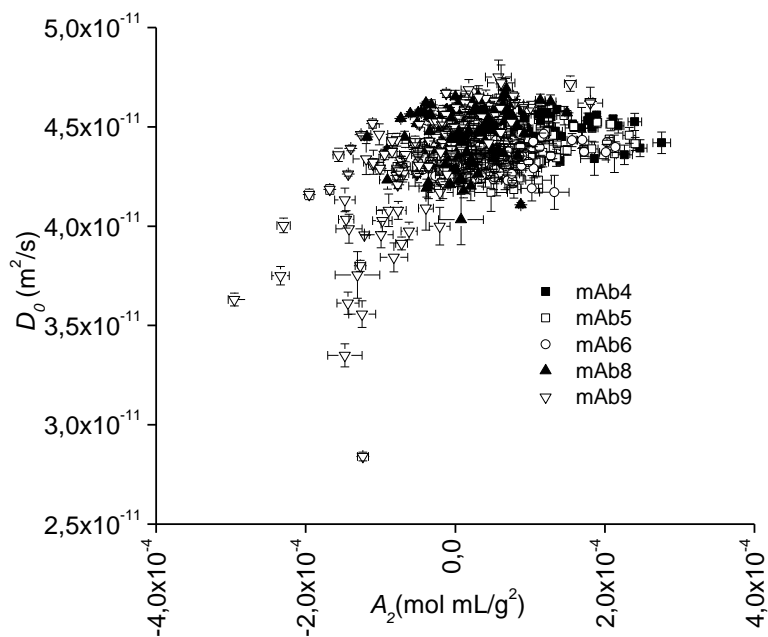


Figure 3.4.18. Comparison of all D_0 values from the formulation screen (see Table 2.1.2). D_0 and A_2 data are shown as mean of $n=3 \pm$ error of the linear regression.

Most D_0 values are in the expected range which is around $4.37 \pm 0.13 \times 10^{-11}$ m²/s. Connolly et al.⁶⁸ reported a range of 3.9 to 4.8×10^{-11} m²/s for 29 different mAbs tested. In the data set presented here, only nine data points out of 635 were out of this expected range. This is only 1.4% of all measurements and points out the reliability of the A_2 method developed in this thesis. It could be applied for a broad range of mAbs and conditions.

What is interesting about the outliers, is, that they are not randomly distributed. All the outliers are from a single antibody, namely mAb9. The conditions where D_0 was not within the expected limits and the respective A_2 are given in Table 3.4.1.

Table 3.4.1. The conditions of D_0 values smaller than 3.9×10^{-11} m²/s and the respective A_2 values from the 635 formulations tested. Data shown in increasing order of D_0 .

pH	Ionic Strength (mM)	Buffer	mAb	$D_0 \times 10^{-11}$ (m ² /s)	$A_2 \times 10^{-04}$ (mol mL/ g ²)
7.0	10	NaPhosphate	mAb9	2.84±0.02	-1,23±0,07
7.0	20	NaPhosphate	mAb9	3.35±0.06	-1,48±0,23
6.5	10	ArgSucc	mAb9	3.56±0.07	-1,25±0,18
6.5	10	NaSuccinate	mAb9	3.61±0.06	-1,43±0,15
7.0	10	NaCitrate	mAb9	3.63±0.03	-2,95±0,08
6.5	10	NaCitrate	mAb9	3.75±0.05	-2,34±0,12
6.5	10	NaPhosphate	mAb9	3.75±0.01	-1,31±0,30
6.5	20	NaSuccinate	mAb9	3.80±0.03	-1,27±0,07
6.5	10	NaCitrate	mAb9	3.84±0.07	-0,82±0,18

It is obvious that the D_0 values had become smaller only at very attractive A_2 conditions which are high pH and low ionic strength in multivalent buffer systems. A reduced diffusion (lower D_0) means that the average hydrodynamic radius of mAb9 had become larger.⁷¹ As it is known from the previous chapter (3.3) mAb9 at these conditions has the most unequal charge distribution of all the mAbs tested. It has a highly charged Fab fragment (more than mAb8) and negatively charged Fc part. Because at low ionic strength ionic interactions are strong it was concluded that this could have led to a formation of mAb9 agglomerates that were then detected by a reduced D_0 (= increased hydrodynamic radius).

3.5. Applicability of A_2 for protein formulation development

This chapter elaborates on possible applications of the second virial coefficient how it might be used to predict turbidity and how it impacts stability as well as its influence on HPLC-SEC aggregate levels for mAbs having self-association issues. Finally A_2 is assessed in respect to formulations dynamic viscosity.

3.5.1. A_2 and Turbidity

A_2 by static light scattering (SLS) is assessed by recording the light scattering intensity based on Equation 13 (p.13). Turbidity is usually also measured by determining the intensity of scattered light (either at 180° or 90°).⁸⁹ Therefore also turbidity measurements and A_2 values should be related. If no large particles (scatterer) are present in the formulation, one should be able to calculate turbidity based on the A_2 value. That at

constant protein concentration A_2 values and turbidity are related can be seen in Figure 3.5.1. To make sure that no large particles were present, all samples were filtered by an $0.22\ \mu\text{m}$ filter before analysis. The figure shows a formulation screen of about 600 A_2 /FTU measurements including five different mAbs. The conditions tested can be seen in Table 2.1.1 on page 6. As A_2 decreases the turbidity increases as expected (Equation 13, p.13). All samples in the plot are compared at a constant protein concentration (i.e. 10 mg/mL).

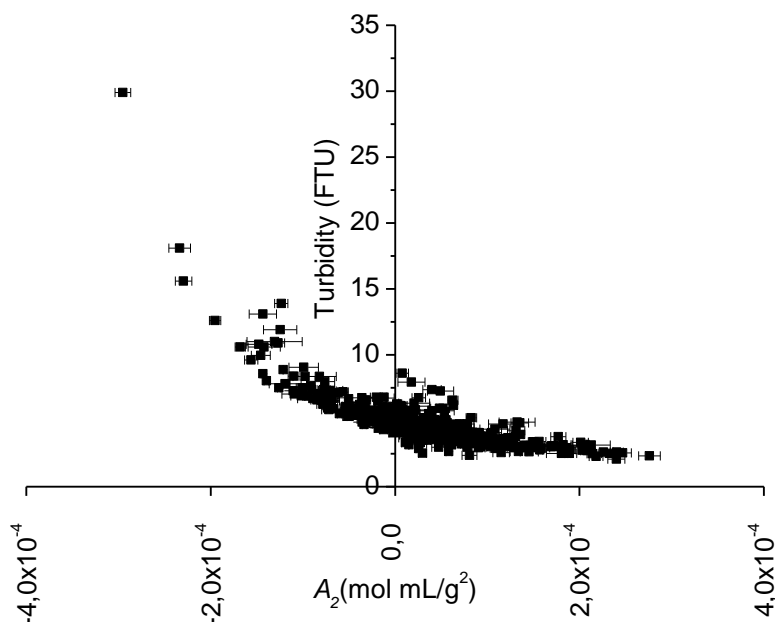


Figure 3.5.1 A_2 as a function of samples' turbidity of 5 mAbs tested in the formulations indicated under 3.4 Antibodies Formulation Screen (see Table 2.1.2). A_2 data are shown as mean of $n=3 \pm$ error of the linear regression.

Turbidity is usually assessed by a turbidimeter which records the light scattering intensity at 90° that is then, based on a calibration curve by Formazin, converted to Formazin turbidity units (FTU). In a simplified model, Turbidity (FTU) was set equal to Rayleigh light scattering intensity R_θ (1/cm). This simplification assumes that the turbidity measured by the turbidimeter is caused by Rayleigh scattering events only. This easy alteration of Equation 13 (p.13) leads to the following equation for turbidity assessment (Equation 25).

$$\frac{Kc}{Turb} = \frac{1}{M} + 2A_2c$$

Equation 25. Altered Equation 13 (p.13) that can be used to determine a samples turbidity (FTU). K is a system constant, c is the concentration of antibody (g/mL), $Turb$ is the turbidity (FTU), M is the molecular mass (g/mol) of the protein and A_2 is the second virial coefficient (mol mL/g²)^{25,28}

Now, Equation 25 can be applied to turbidimeter measurements. However, a prerequisite is to determine the system constant K for the turbidimeter. This has been conducted as follows. Based on a formulation screen of 600 samples at a given protein concentration, given molecular weight, determined A_2 values (from the 600 samples), and turbidity measurements (FTU, from the 600 samples), the system constant could be calculated employing Equation 25. Figure 3.5.2 shows the calculated system constant for each measurement as well as the average value (black line) and the standard deviation (red lines). Outliers can be found within all five mAb screens and are not systematically found at one specific condition (e.g. buffer, pH or ionic strength). Outliers are probably due to the

fact that turbidity was only measured as a single measurement and deviations due to small scratches, air bubbles, or maybe dust could not always be excluded.

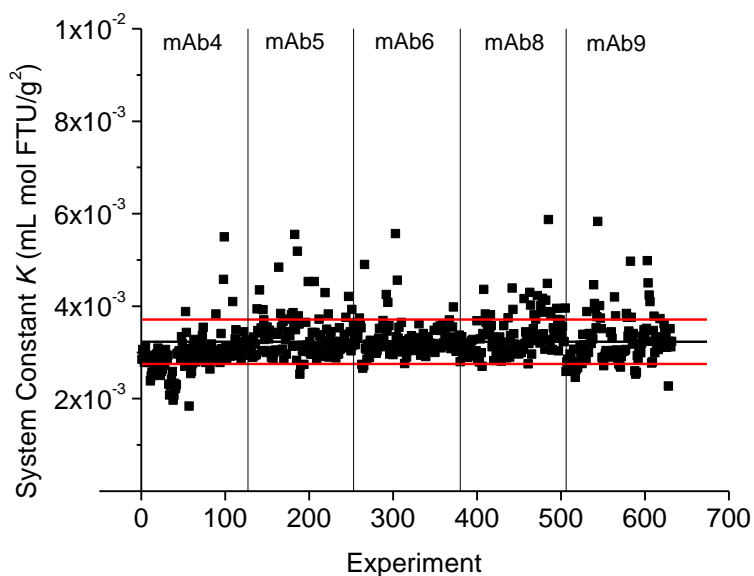


Figure 3.5.2. Based on turbidity and the A_2 values shown in Figure 3.5.1 the system constant K was calculated. Black line is indicating the average value and the red lines are showing the standard deviation. The conditions tested for each mAb are shown in Table 2.1.2.

The system constant K for this particular system (i.e. the turbidimeter) was $3.23 \times 10^{-3} \text{ mL mol FTU/g}^2$. To test the applicability of this model, another data set has been studied. More precisely, five mAbs were analyzed for their A_2 value in two different formulations namely $20 \text{ mM His/His-HCl (pH 6.0)} \pm 150 \text{ mM NaCl}$ at two different protein concentrations 10 and 100 mg/mL . Based on the A_2 value and the mAb concentration one could calculate the expected turbidity using Equation 25. Figure 3.5.3 shows the predicted versus the actually measured turbidity. It shows that there is a good connection between calculated and predicted turbidity even if concentrations up to 100 mg/mL were used. The outlier for predicted turbidity at 40 FTU (measured turbidity) can be explained by its error range due to high error in A_2 determination that followed in a big propagation of the error. The result nicely demonstrates that with a known A_2 value, measured at 10 mg/mL , the turbidity can be predicted even for higher protein concentration. However, it should be considered that A_2 may not necessarily be applicable to very high protein concentrations as it represents a dilute solution property. In addition, optical phenomena are likely to occur (multi scattering).⁶⁴ Importantly, all the formulations were filtered via $0.22 \mu\text{m}$ and are free of subvisible or visible particles. Although additional experiments are needed to see what the limits in respect to protein concentration and maximum turbidity are, this approach might be used to get an estimate in what range the turbidity at any chosen protein concentration will be once the A_2 for this condition is known. Importantly, this first assessment can again be based on low volume method using DLS Plate Reader. The turbidity/opalescence of a formulation is of importance as the compendial monograph for monoclonal antibodies only allows liquids to be slightly opalescent.⁹⁰

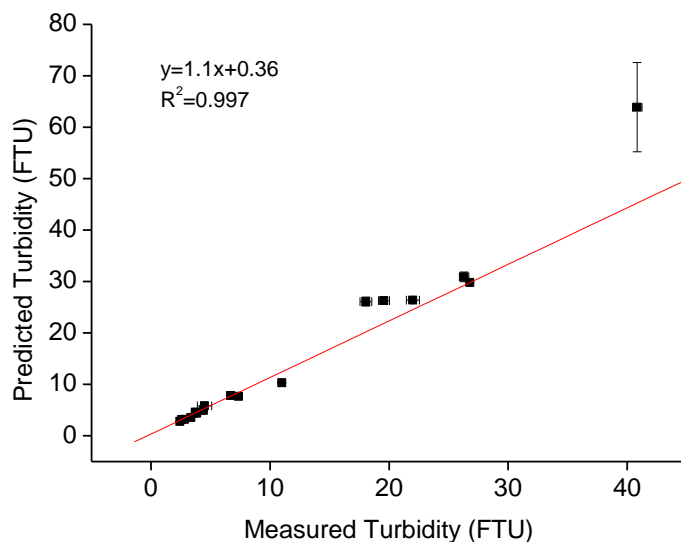


Figure 3.5.3. Predicted turbidity (based on system constant K and A_2) as a function of measured turbidity of 5 mAbs at 10 and 100 mg/mL in two formulations namely 20 mM His/His-HCl (pH 6.0) \pm 150 mM NaCl. Data are shown as mean of $n=3 \pm$ error in the linear regression (in A_2 determination used for turbidity prediction) and the mean of $n=2 \pm$ absolute deviation for measured turbidity.

Another option to assess turbidity values and spare protein material shall be briefly discussed in the following paragraph. As published by Yadav et al.⁹¹ DLS also records a parameter similar to the light scattering intensity in SLS. This parameter is called normalized intensity. As described scattering intensity and turbidity are linear related therefore it was only logical to also plot the recorded normalized intensities from DLS to the measured FTU values to see how those two parameters correlate. As shown in Figure 3.5.4 there is a linear relation of normalized intensity and measured turbidity for the 600 samples from the formulation screen as well as for the samples used to test the turbidity prediction (Figure 3.5.3). So recording “normalized intensity” in a 384 well plate format might be a good alternative to measurement in a 2 mL vial. This miniaturized turbidity measurement can be very useful in formulation development as material especially in early stage is rare. However the method’s limitations should be kept in mind. Figure 3.5.3 shows that samples that had about the same normalized intensity varied in their measured FTU values. Between a normalized intensity of 2.5×10^7 counts/s the measured FTU values ranged from about 2-8 FTU. The method is therefore not capable to give defined FTU values. It rather shows in which range the FTU values will approximately be. This miniaturized turbidity measurement is not related to turbidity prediction based on A_2 which means that the A_2 value is not necessary in this context.

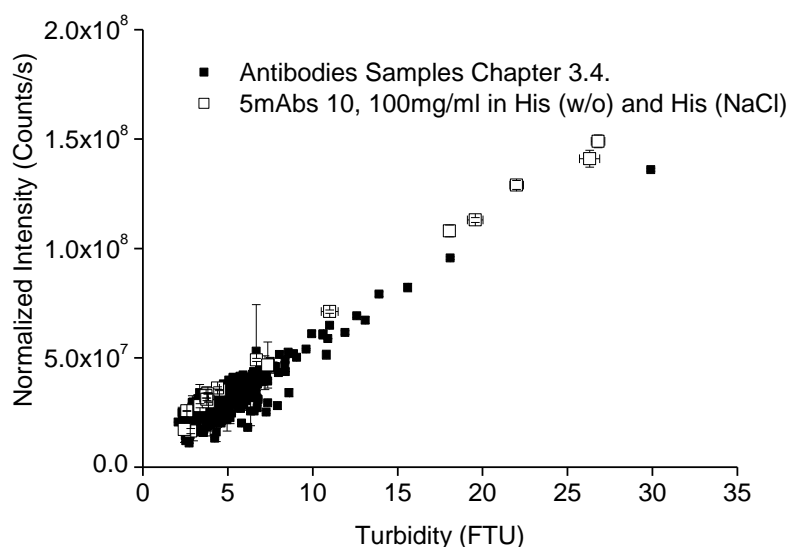


Figure 3.5.4. Alternative method for turbidity estimation in 384 well plate format showing the recorded normalized intensity (by DLS platereader) as a function of turbidity of the about 600 formulations chapter 3.4 and of five mAbs at 10 and 100 mg/mL in two formulations namely 20 mM His/His-HCl (pH 6.0) \pm 150 mM NaCl. Data are shown as the mean of $n=2 \pm$ absolute deviation for turbidity and as the mean of $n=3 \pm$ SD for normalized intensity.

3.5.2. A_2 in Protein Stability

There are hints in literature that protein-protein interaction is related to proteins aggregation/precipitation stability.⁷⁻⁹ Lawrence et al.⁹ could demonstrate that supercharged molecules (highly repulsive molecules) are more stable to temperature stress. On the other hand highly attractive A_2 is linked to protein precipitation/crystallization.²⁵ If protein-protein interaction relates also to long term stability is still controversially discussed.⁸

To find out if protein-protein interaction can be related to mAb's stability, a stability study was set up using selected mAbs which have been biophysically characterized in this thesis. The most important question to be answered was: is A_2 linked to protein stability? Protein stability in this case focused on physical stability (i.e. aggregation/precipitation propensity). The working hypothesis was that the more attractive mAb molecules are, the higher the likelihood that they touch, the less stable they are. The study comprised 5 mAbs (mAb1, 3, 4, 6, and 8) within two formulations (20 mM His/His-HCl (pH 6.0) \pm 150 mM NaCl) whereof the biophysical characterization has been already described in chapter 3.2. The respective A_2 values can be seen in Figure 3.1.7 p.24. At low ionic strength [His(w/o)] all mAbs are repulsive. At this condition electrostatic repulsion is favored and so the degree of repulsion is related to their net charge (chapter 3.2). At high ionic strength these long range electrostatic interactions are shielded by counter ions favoring short range interactions. For example mAb6 got attractive which was thought to be unfavorable when it comes to aggregation/precipitation stability. The set-up of the stability study also included two different mAb concentrations 10 mg/mL and 100 mg/mL. This was intended in order to find out the importance of A_2 (which is assessed at dilute solution conditions) in more crowded solutions. Given the current product developments⁶⁸, concentrations much higher than 10 mg/mL are in focus (e.g. for developing prefilled syringes that can be conveniently applied by the patient himself).

During formulation development, stability studies are usually run at real-time (5°C) and accelerated conditions (25°C and 40°C). Accelerated conditions are employed to get the read-out earlier as compared to real-time. A potential risk associated is that higher stress temperatures might favor different degradation pathways. Consequently, the accelerated studies may not represent pathways relevant to real-time conditions.⁹² The conditions tested here were 5 °C (real-time storage), 25 and 40°C (accelerated temperature) as well as shaking stress (interfacial stress). The working hypothesis was that at 5 °C, 25 °C, and 40 °C the aggregation/precipitation propensity is related to A_2 . Interfacial stress (by means shaking stability) was included in order to find out if A_2 can also be related to this stress.

The parameters assessed were soluble aggregate levels by HPLC-SEC, turbidity by turbidimeter, subvisible particle counts by light obscuration and visible particles by visual inspection.

3.5.2.1. mAbs Stability at 5 °C and Discussion of T=0 Results

Liquid mAb solutions are usually stored/shipped at 5 °C. This temperature is therefore referred to as the intended storage temperature or real-time condition, where mAbs are (in the proper formulation) stable for ca. 2 years. Looking at the initial %HMW levels of the mAbs (Figure 3.5.5) one immediately sees that already at T=0 the aggregate levels are different. This was expected because the initial amount of soluble aggregates present depends on inherent properties of specific mAbs and also depends on purification process and bulk storage time, i.e. age. It is therefore difficult to get drug substance material of different mAbs with exactly the same soluble aggregate level. In order to keep this difference visible, the HPLC-SEC data was not normalized by its initial value. The level of soluble aggregates was initially elevated for mAb3 and mAb6 (about 3.5 %). This is still low because more than 95 % of mAb was present as monomer. It was known that mAb6 has the possibility to form reversible dimers (section 3.5.3). To be able to exclude these effects in SEC data, and to only monitor aggregates, a slightly different SEC method was applied for this mAb only (dilution/incubation of sample before injection, see methods).

Figure 3.5.5 shows that at intended storage (5 °C) at 10 mg/mL, aggregate levels for up to 11 months did not change. Independently of the initial aggregate levels (elevated for mAb3 and mAb6) and the formulation conditions His (w/o) or His (NaCl), the aggregate levels after 11 months stayed constant. Even for the slightly attractive condition of mAb6, i.e. His (NaCl), no change could be observed up to 11 months. This lead to the conclusion that the mAbs tested are very stable when stored at 5 °C at 10 mg/mL. Next the impact of an increased concentration (100 mg/mL) shall be discussed.

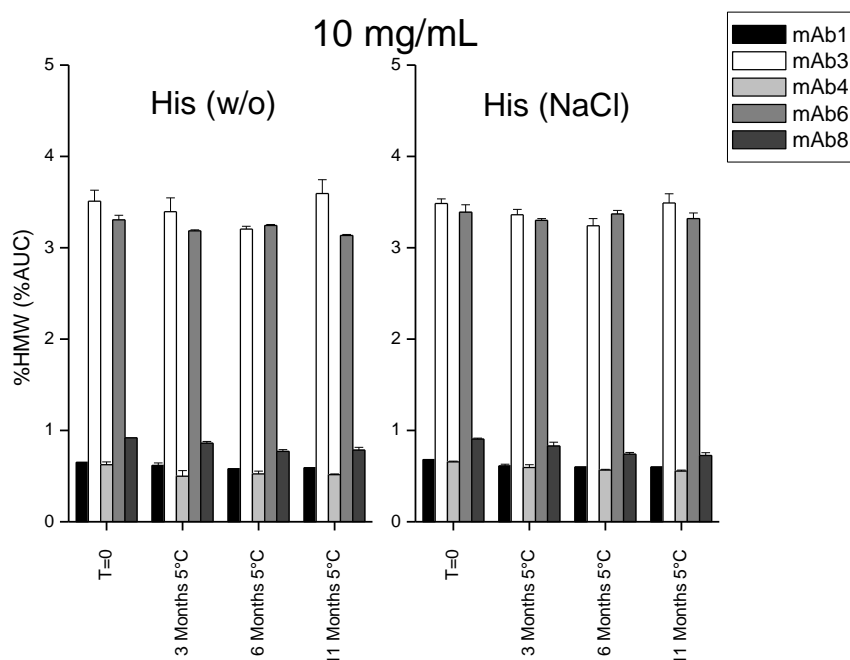


Figure 3.5.5. Soluble aggregate levels (%HMW) of five different mAbs at 10 mg/mL stored at 5 °C for up to 11 months. mAbs were formulated in 20 mM His/His-HCl (pH 6.0) \pm 150 mM NaCl. Data are shown as mean of $n=2 \pm$ absolute deviation.

When increasing the concentration from 10 mg/mL to 100 mg/mL (Figure 3.5.6) the initial aggregate levels stayed at the same level. However after 11 months at 100 mg/mL there seemed to be a slight trend. The aggregate levels of mAb3 and mAb6 had slightly increased but the change was very minor (<0.4 %HMW increase). This was observed independently of the ionic strength so could not be related to A_2 . Because no significant change was observed at 5 °C storage this nicely demonstrates the need for accelerated stability data (storage at >5 °C) to discriminate formulations with respect to their stability performance.

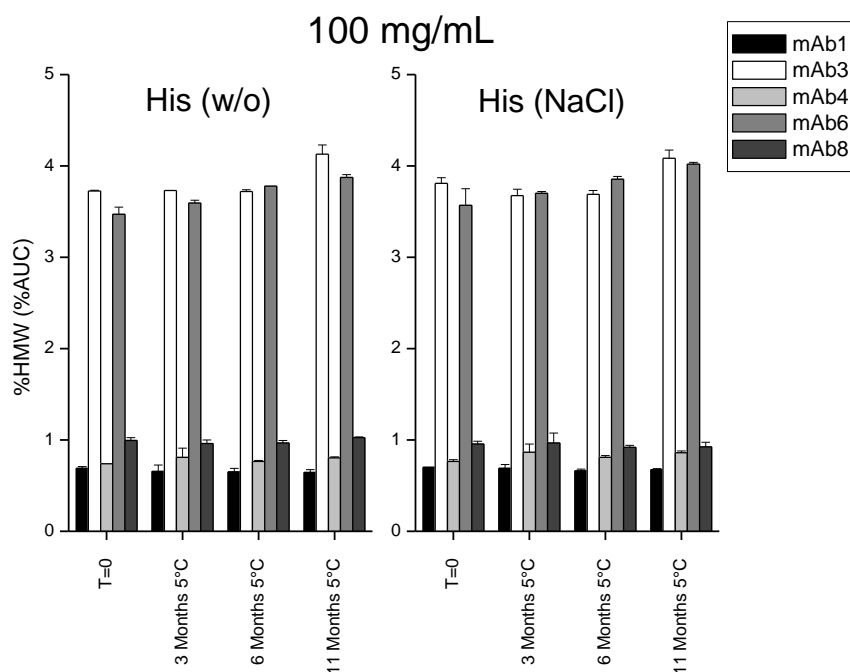


Figure 3.5.6. Soluble aggregate levels (%HMW) of five different mAbs at 100 mg/mL stored at 5 °C for up to 11 months. mAbs were formulated in 20 mM His/His-HCl (pH 6.0) \pm 150 mM NaCl. Data are shown as mean of $n=2 \pm$ absolute deviation.

Next the turbidity results are discussed. The results at T=0 are related to the A_2 . This was expected and extensively discussed in chapter 3.5.1. Therefore the A_2 values fit the turbidity ranking at T=0 (Figure 3.5.7). The more repulsive a mAb is the lower its measured turbidity. Since A_2 is lower at His (NaCl) as compared to His (w/o), the turbidity is higher. It is also not surprising that the turbidity is concentration dependent. That is why the turbidity is higher at 100 mg/mL (Figure 3.5.8) than at 10 mg/mL (Figure 3.5.7). What is interesting is the change of turbidity during storage. As bigger particles do scatter more light, the appearance of larger aggregates must be reflected in samples' turbidity.²² At 10 mg/mL the turbidity hardly changed after 11 months storage (Figure 3.5.7). There was a slight increase for mAb8 and mAb4 in both formulations but the changes were very minor and no trends could be seen. Also at 100 mg/mL the change in turbidity over time could be neglected.

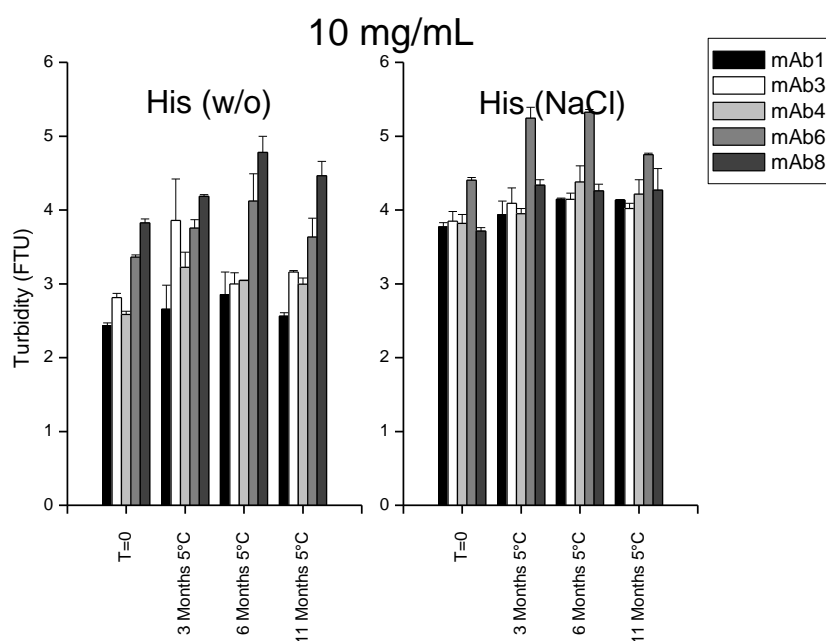


Figure 3.5.7. Turbidity of five different mAbs at 10 mg/mL stored at 5 °C for up to 11 months. mAbs were formulated in 20 mM His/His-HCl (pH 6.0) ± 150 mM NaCl. Data are shown as mean of n=2 ± absolute deviation.

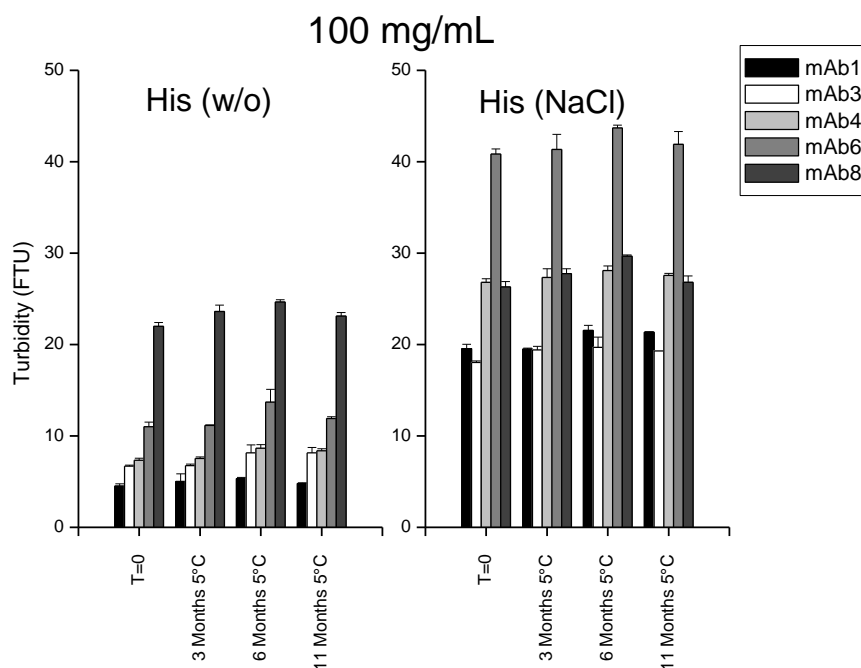


Figure 3.5.8. Turbidity of five different mAbs at 100 mg/mL stored at 5 °C for up to 11 months. mAbs were formulated in 20 mM His/His-HCl (pH 6.0) ± 150 mM NaCl. Data are shown as mean of $n=2 \pm$ absolute deviation.

Next the particle counts are discussed. The two size-classes that were reported are particles $>2 \mu\text{m}$ and $>10 \mu\text{m}$. These two are chosen by intention. Particle concentrations $>10 \mu\text{m}$ have strict requirements by the pharmacopeias because particles $>8 \mu\text{m}$ are a safety concern when it comes to clogging of capillaries in the lung.^{92,93} But also the $>2 \mu\text{m}$ give valuable information to the formulation scientist. This additional information helps to predict upcoming issues up with the $>10 \mu\text{m}$ particles.⁹³ If for example no $>10 \mu\text{m}$ particles but a lot of $>2 \mu\text{m}$ particles are seen within a formulation, the likelihood that at the next stability time point $>10 \mu\text{m}$ particles will pop up are high. The reason is that small aggregates proceed further to form bigger particles over time that then precipitate.⁹³

First of all at both concentrations (10 mg/mL or 100 mg/mL) at the respective buffer (His (w/o) or His (NaCl)), the two different particle populations ($>2 \mu\text{m}$ and $>10 \mu\text{m}$) were comparable. The 10 mg/mL data for the different mAbs/formulations can be seen in Figure 3.5.9 and Figure 3.5.10. The 100 mg/mL mAbs/formulations data can be compared using Figure 3.5.11 and Figure 3.5.12. Generally the $>10 \mu\text{m}$ particle counts are lower than the $>2 \mu\text{m}$ but that's expected as the counting method used is cumulative. What was interesting was that $>2 \mu\text{m}$ data followed the same trend as $>10 \mu\text{m}$ data regarding increase in particle concentration over stability. What was most surprising was that within all formulations subvisible particle counts were already elevated at T=0. Before filling, the samples were filtered by 0.22 μm filter. All particles must therefore have been formed after filtration. Since the formulations contained no additional stabilizers particles can have evolved within two days between filtration and subvisible analysis. Furthermore all vials were visually inspected after filling. This visual inspection included swirling (agitation) of the samples. As no surfactant was present, that would have protected the samples⁹⁴, this could have led to an increase in subvisible particle concentration. At 10 mg/mL mAb6 had

strongly elevated particle counts in the His (w/o) formulation and even more at high ionic strength, His (NaCl). At 100 mg/mL not only mAb6 had highly elevated counts at low ionic strength but also mAb8. At high ionic strength all subvisible particle counts strongly increased. If this theory holds true and if really interfacial stress during visual inspection caused the appearance of these particles then the levels of initial particles should fit the trend of subvisible particle increase during shaking. Comparison and discussion of T=0 particles and mAbs stability on interfacial stress (shaking) is shown in the section 3.5.2.4. There the overall conclusion was that, yes mAbs most sensitive to shaking stress also had increased particle concentrations already at T=0. This could only be judged on turbidity measurements as particle counts most of the time exceeded the upper count limit.

Furthermore it was observed that for some mAbs (e.g. mAb6) particle counts slightly increased reaching a maximum at 3 or 6 months but then decreased again below T=0 levels. This effect was not so clearly seen at 10 mg/mL but was obvious at 100 mg/mL. Especially mAb6 and mAb8 showed this phenomenon. A similar observation was made by visual inspection (Figure 3.5.13). That subvisible particles decreased below T=0 after 11 months of static storage can possibly be explained by results published by Kiese et al.⁹⁵ There it was shown that particles generated by interfacial stress are reversible when spiked into non-aggregated samples. Why subvisible particles increased between 3-6 months could not be explained. Even in visible particle inspection (Figure 3.5.13) this decrease was observed so particles could not have progressed further to form larger aggregates.

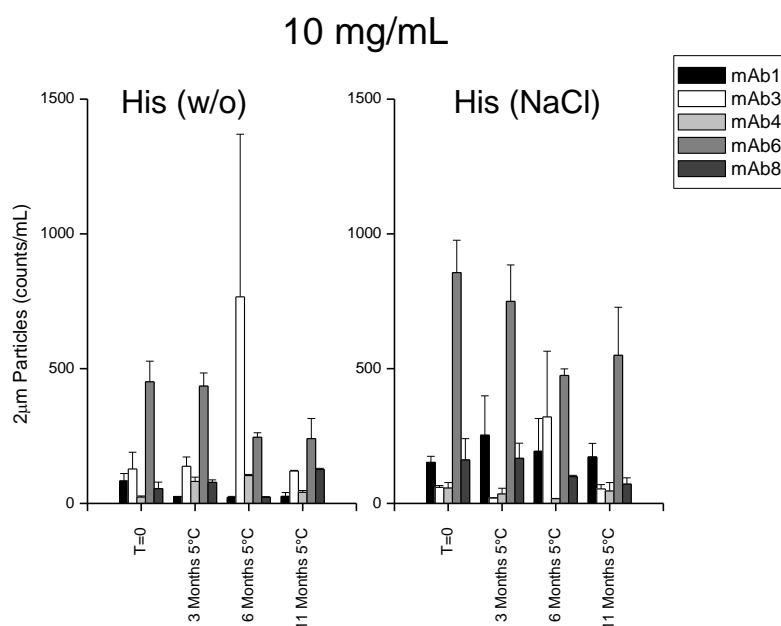


Figure 3.5.9. Cumulative subvisible particle counts >2 µm of five different mAbs at 10 mg/mL stored at 5 °C for up to 11 months. mAbs were formulated in 20 mM His/His-HCl (pH 6.0) ± 150 mM NaCl. Data are shown as mean of n=2 ± absolute deviation.

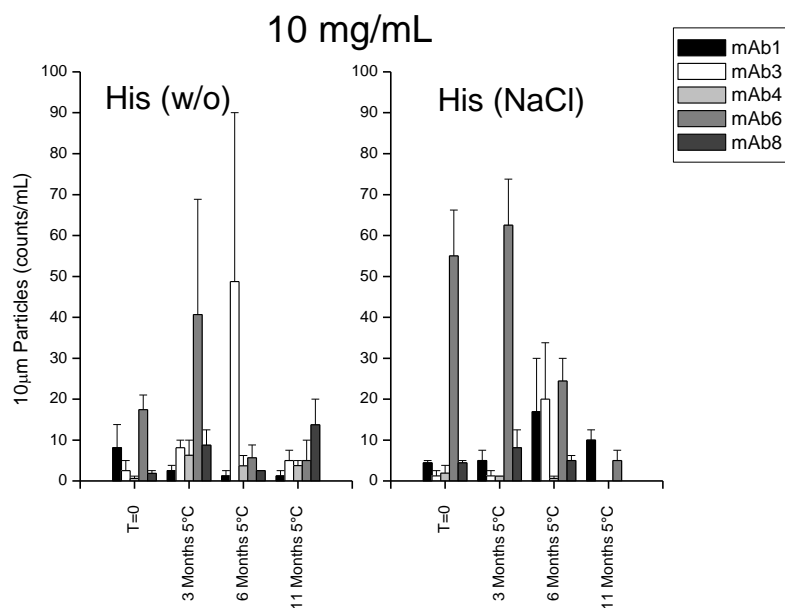


Figure 3.5.10. Cumulative Subvisible Particle counts >10 µm of five different mAbs at 10 mg/mL stored at 5 °C for up to 11 months. mAbs were formulated in 20 mM His/His-HCl (pH 6.0) ± 150 mM NaCl. Data are shown as mean of n=2 ± absolute deviation.

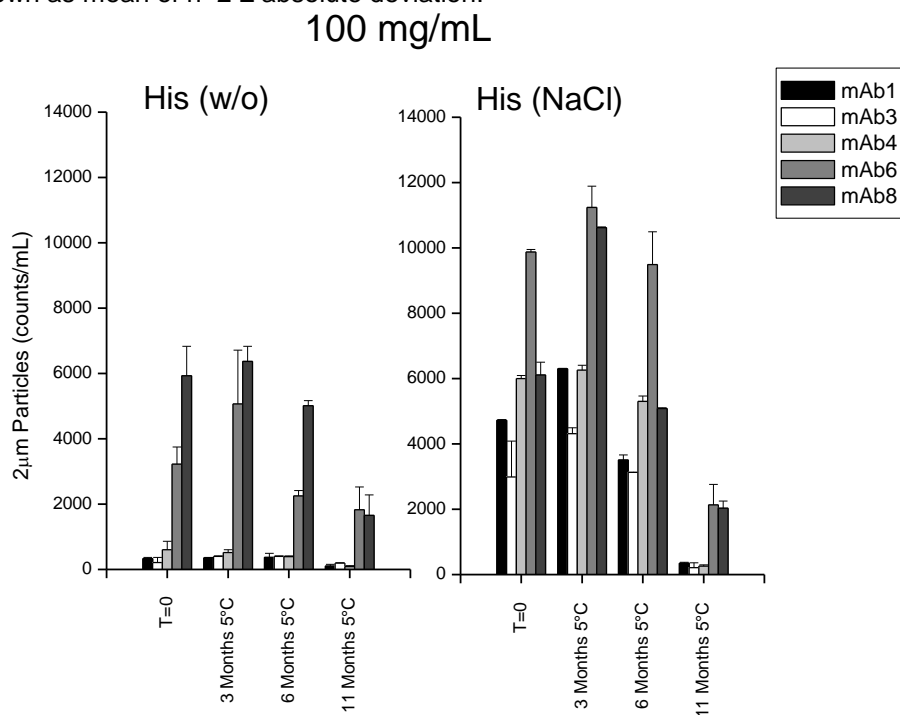


Figure 3.5.11. Cumulative Subvisible Particle counts >2 µm of five different mAbs at 100 mg/mL stored at 5 °C for up to 11 months. mAbs were formulated in 20 mM His/His-HCl (pH 6.0) ± 150 mM NaCl. Data are shown as mean of n=2 ± absolute deviation.

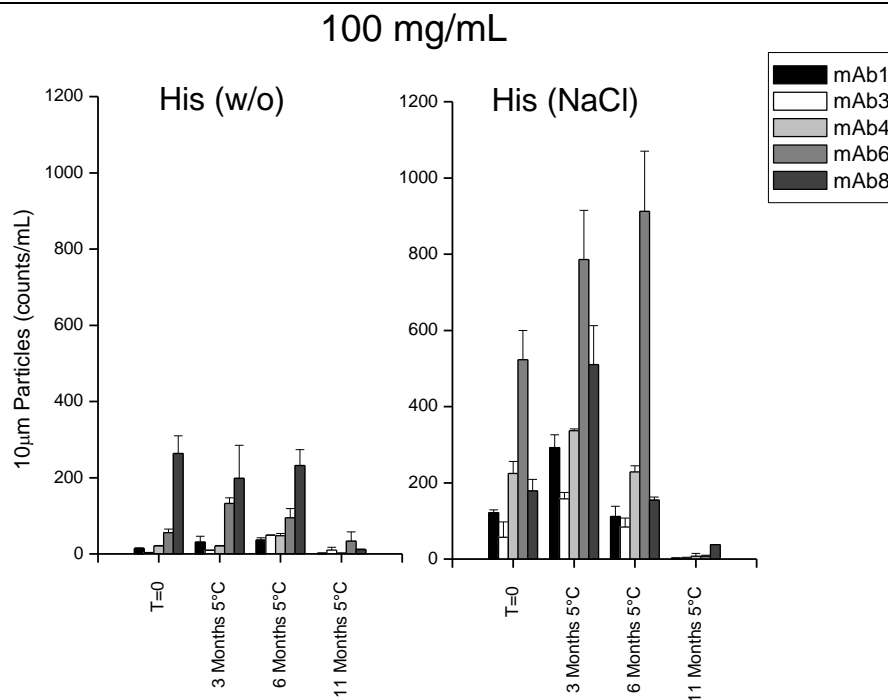


Figure 3.5.12. Cumulative Subvisible Particle counts >10 µm of five different mAbs at 100 mg/mL stored at 5 °C for up to 11 months. mAbs were formulated in 20 mM His/His-HCl (pH 6.0) ± 150 mM NaCl. Data are shown as mean of n=2 ± absolute deviation.

Presence of visible particles at T=0, increase at 3 months and reduction after 11 months was also seen in visual inspection of vials, especially for mAb6 similar to subvisible particle analysis. As 100 mg/mL samples are more turbid, these vials are more difficult to inspect and particles are more easily overlooked. Visual inspection also is very susceptible to human errors as well as the possibility that particles may stick somewhere and are not seen. The visible particle data should therefore be taken with caution and only be used to support the big picture (Figure 3.5.13).

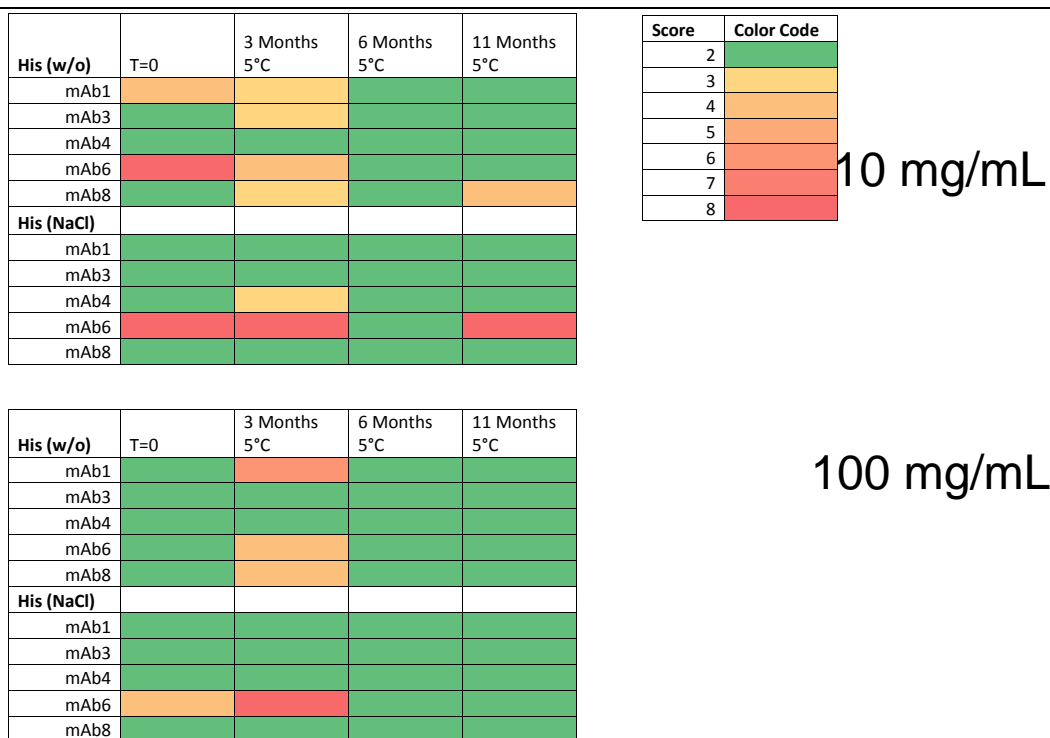


Figure 3.5.13. Visual inspection scores of five different mAbs at 10 mg/mL and 100 mg/mL stored at 5°C for up to 11 months. mAbs were formulated in 20 mM His/His-HCl (pH 6.0) \pm 150 mM NaCl. Data are shown as mean of $n=2 \pm$ absolute deviation. The higher the score the more particles were observed.

3.5.2.2. mAbs Stability at 25 °C

An increase of temperature from 5 °C to 25 °C is expected to decrease the samples stability. It is known that higher temperature increases hydrophobic interactions because the probability of the appearance of partially unfolded states in the mAbs' structure is higher. This can then more easily lead to aggregation.^{92,96}

The %HMW (soluble aggregate) levels of the different mAbs are shown in Figure 3.5.14. The mAbs behavior was found to be independent of their formulation condition (high vs. low ionic strength) and did not change except for one of them. mAb3 %HMW levels reduced continuously over time. This was unexpected and the present data only gives very limited hints to explain this phenomenon. At 5°C no decrease in %HMW (Figure 3.5.5) was seen and neither turbidity (Figure 3.5.16) nor particle counts (Figure 3.5.18) decreased over. At 40 °C (Figure 3.5.21) this decrease was also seen after one month but increased after three. What happened to mAb3 cannot be explained. One possible explanation is that this might be caused by dissociation of reversible aggregates that only dissociated at low concentrations (10 mg/mL) and at elevated temperatures (25 °C and 40 °C) independently of the formulation condition (high/low ionic strength).

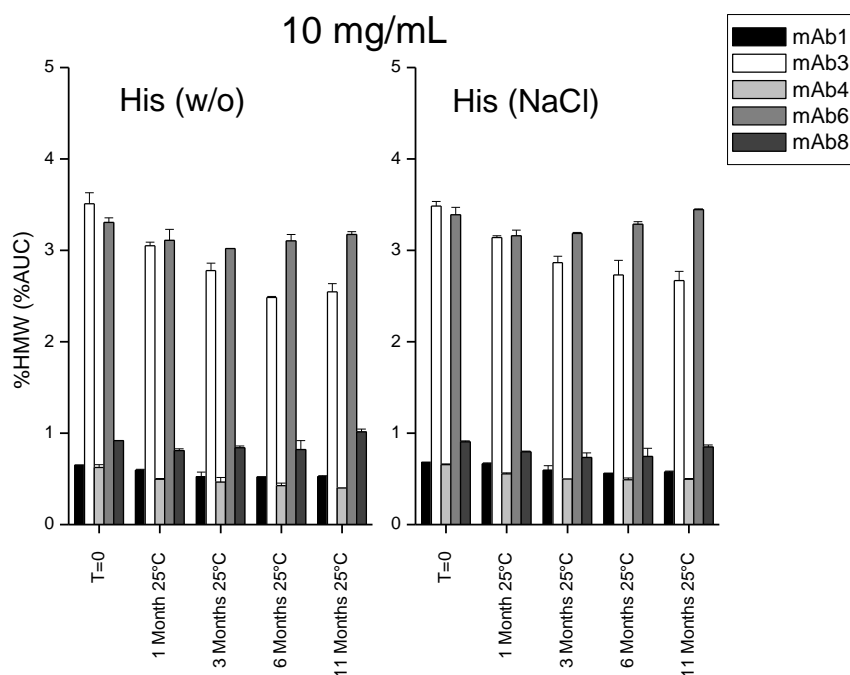


Figure 3.5.14. Soluble aggregate levels (%HMW) of five different mAbs at 10 mg/mL stored at 25 °C for up to 11 months. mAbs were formulated in 20 mM His/His-HCl (pH 6.0) \pm 150 mM NaCl. Data are shown as mean of $n=2 \pm$ absolute deviation.

When the concentration was set to 100 mg/mL, 25 °C storage for 11 months started to show differences (increase) in aggregate levels (Figure 3.5.15). There was no longer a decrease of aggregates observed for mAb3 given the error bars. There was also no strong increase of aggregates over time in the His (w/o) formulation (<0.2 %). Independently of formulation (high or low ionic strength) the increase of aggregate levels for all mAbs after 11 months was only minor (<0.5 %) for mAb1, mAb3, and mAb4. The two mAbs for which aggregates increased were mAb6 and mAb8. In the His (w/o) formulation mAb6 increased by about 2 %HMW whereas mAb8 increased by 1 %HMW. In the His (NaCl) formulation mAb6 increased by 2.2 %HMW and mAb8 by 0.55 %HMW. After NaCl addition the increase in aggregate levels for mAb6 is higher whereas for mAb8 it is reduced. This fits to what is expected based on protein interaction analysis (A_2 , see chapter 3.4). mAb8 and mAb6 are the two least repulsive mAbs and therefore have increased aggregation in the His (w/o) formulation. On NaCl addition mAb6 gets attractive causing higher aggregation rates whereas mAb8 got more stable. That aggregation rate for mAb8 on NaCl addition decreased was interesting because it was found out previously that NaCl addition to IgG4 mAbs can reduce mAb interactions (chapter 3.4). Maybe this is what also happened here.

In the His (w/o) formulation mAb6 and mAb8 increased in aggregation (mAb6 stronger than mAb8). These two had the lowest A_2 at this condition. On the other hand in the NaCl containing formulation only mAb6 increased in aggregate levels whereas mAb8 had lower aggregate levels as compared to the His (w/o) formulation. At 25 °C after 3 months the changes measured by SEC are very small and will be further discussed with the 40 °C data. At 25 °C temperature stress the increase in aggregates over time was stronger at 100 mg/mL than at 10 mg/mL. This was expected because the presence of more molecules increases the probability of interaction/aggregation.

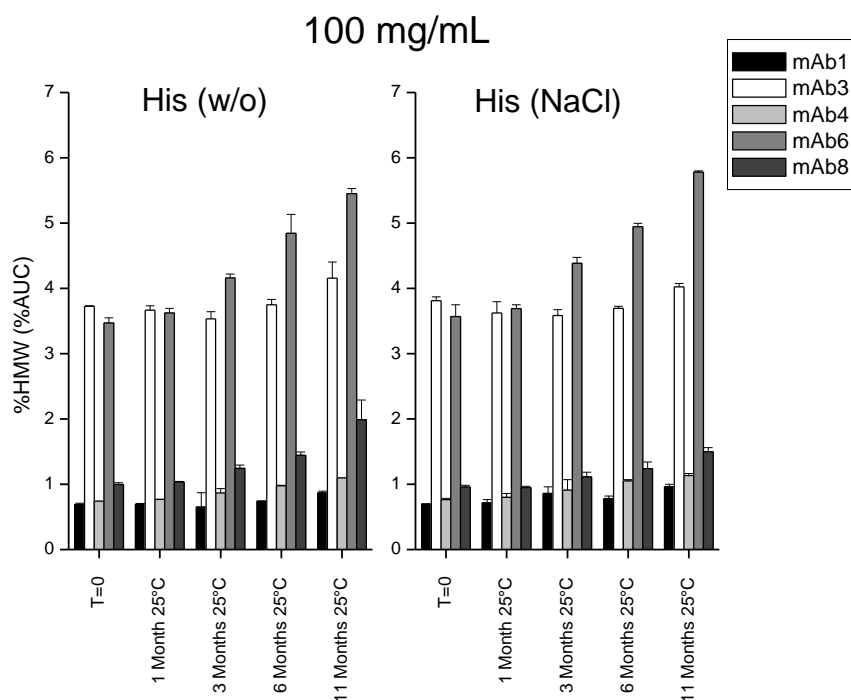


Figure 3.5.15. Soluble aggregate levels (%HMW) of five different mAbs at 100 mg/mL stored at 25 °C for up to 11 months. mAbs were formulated in 20 mM His/His-HCl (pH 6.0) ± 150 mM NaCl. Data are shown as mean of n=2 ± absolute deviation.

Turbidity analysis at 25 °C as compared to 5 °C showed an increase for mAb8 and mAb6 (Figure 3.5.16 and Figure 3.5.17) which is in consent with the SEC-HPLC data at 100 mg/mL. No reduction in turbidity was observed like within the 5 °C formulation. As the turbidity increase was also seen at 10 mg/mL and not only at 100 mg/mL like with SEC it was concluded that in this case turbidity measurements were more sensitive to change than SEC.

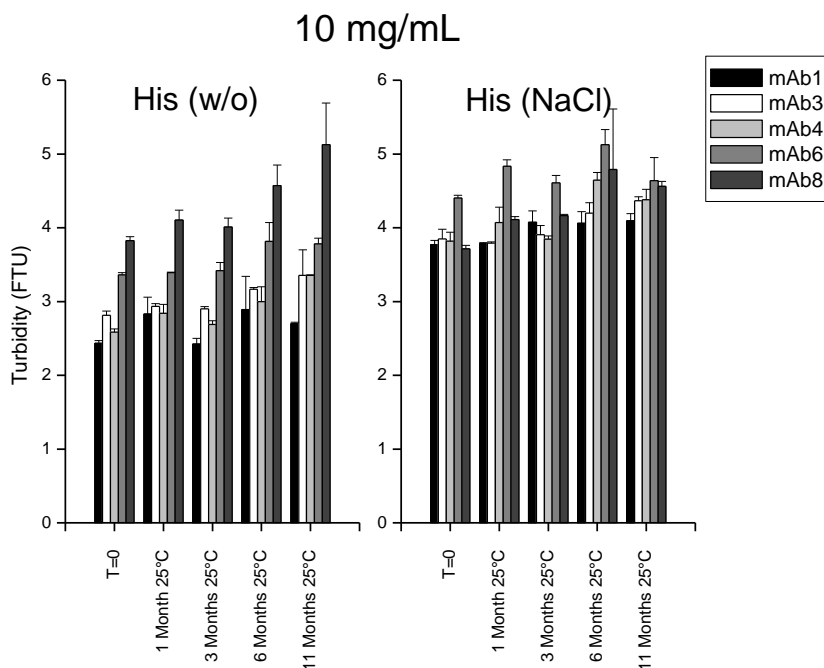


Figure 3.5.16. Turbidity of five different mAbs at 10 mg/mL at 25 °C stored for up to 11 months. mAbs were formulated in 20 mM His/His-HCl (pH 6.0) ± 150 mM NaCl. Data are shown as mean of n=2 ± absolute deviation.

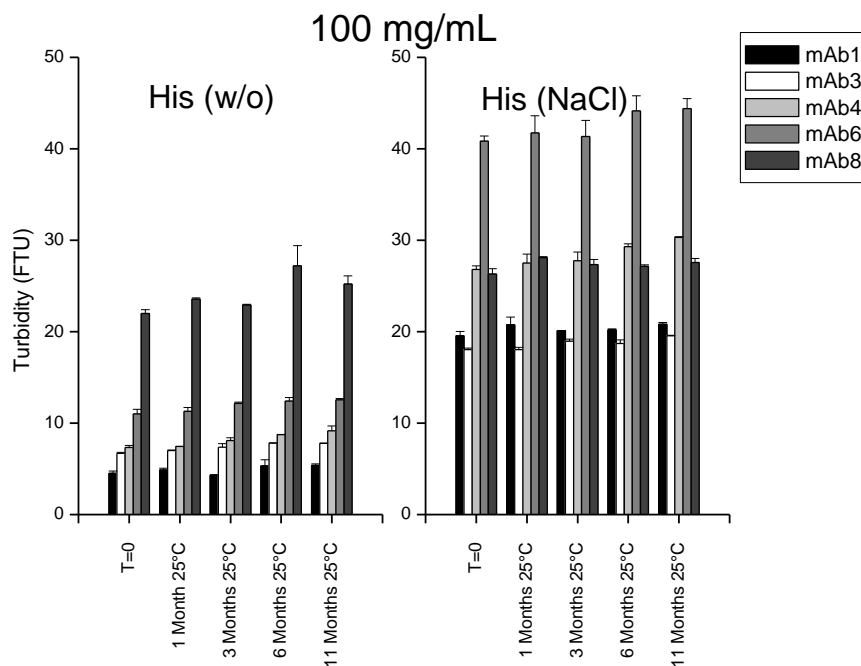


Figure 3.5.17. Turbidity of five different mAbs at 100 mg/mL at 25°C stored for up to 11 months. mAbs were formulated in 20 mM His/His-HCl (pH 6.0) ± 150 mM NaCl. Data are shown as mean of n=2 ± absolute deviation.

The cumulative subvisible particle counts for 25 °C storage are shown in Figure 3.5.18 and Figure 3.5.19. At 25 °C like at 5 °C particle counts stayed constant or increased at 3 or 6 months and then tended to decrease after 11 months.

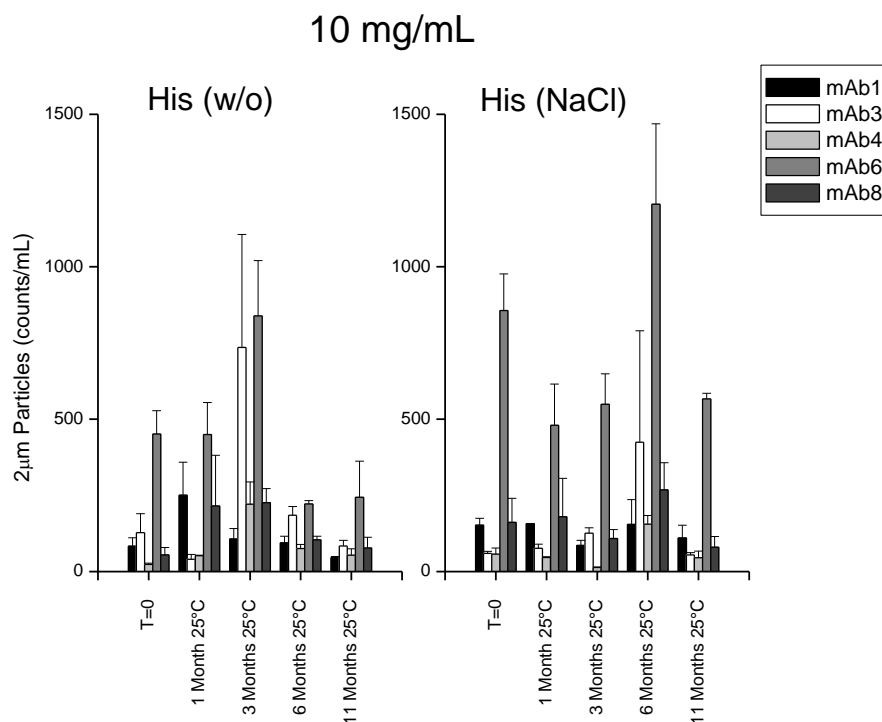


Figure 3.5.18. Cumulative subvisible particle counts >2 µm of five different mAbs at 10 mg/mL at 25 °C stored for up to 11 months. mAbs formulated in 20 mM His/His-HCl (pH 6.0) ± 150 mM NaCl. Data are shown as mean of n=2 ± absolute deviation.

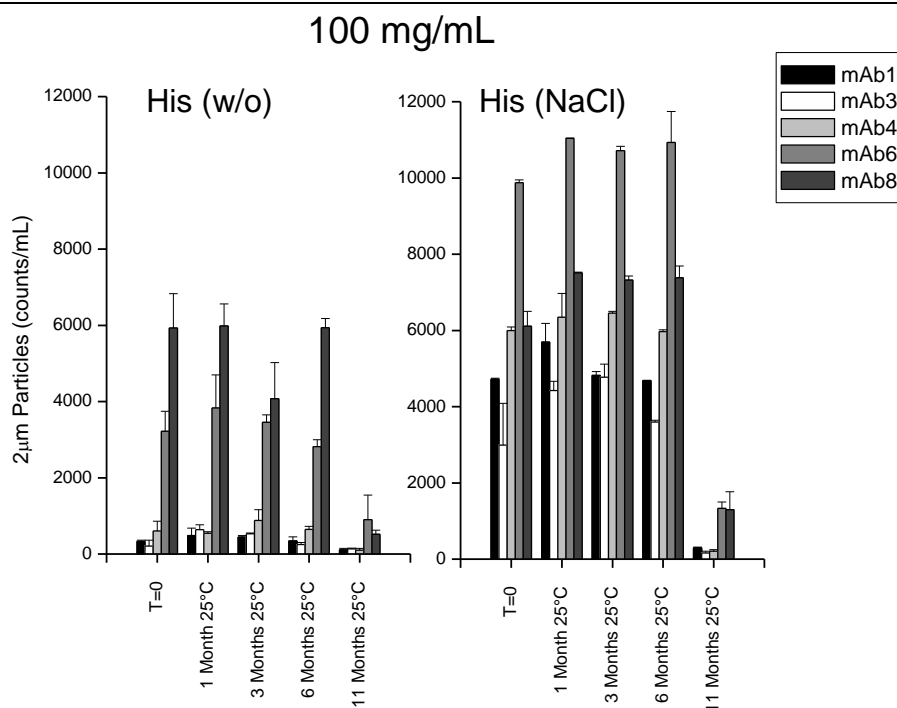


Figure 3.5.19. Cumulative subvisible particle counts >2 μm of five different mAbs at 100 mg/mL at 25 °C stored for up to 11 months. mAbs formulated in 20 mM His/His-HCl (pH 6.0) ± 150 mM NaCl. Data are shown as mean of n=2 ± absolute deviation.

The visual inspection (Figure 3.5.20) was able to verify what was also measured for the subvisible particles. Particle counts tended to be the lowest at 11 months with a peak at 3-6 months.

His (w/o)	T=0	1 Month 25°C	3 Months 25°C	6 Months 25°C	11 Months 25°C
mAb1	Green	Green	Green	Green	Green
mAb3	Green	Green	Green	Green	Green
mAb4	Green	Green	Green	Green	Green
mAb6	Green	Red	Green	Green	Green
mAb8	Green	Green	Green	Green	Orange
His (NaCl)					
mAb1	Green	Orange	Orange	Green	Green
mAb3	Green	Green	Green	Green	Green
mAb4	Green	Green	Green	Green	Green
mAb6	Green	Red	Red	Green	Orange
mAb8	Green	Green	Green	Green	Green

Score	Color Code
2	Green
3	Light Green
4	Yellow
5	Light Orange
6	Orange
7	Red-Orange
8	Red

10 mg/mL

His (w/o)	T=0	1 Month 25°C	3 Months 25°C	6 Months 25°C	11 Months 25°C
mAb1	Green	Green	Green	Green	Green
mAb3	Green	Green	Green	Green	Green
mAb4	Green	Green	Green	Green	Green
mAb6	Green	Green	Orange	Red	Green
mAb8	Green	Green	Orange	Green	Green
His (NaCl)					
mAb1	Green	Green	Green	Green	Green
mAb3	Green	Green	Green	Green	Green
mAb4	Green	Green	Green	Green	Green
mAb6	Green	Orange	Red	Orange	Green
mAb8	Green	Orange	Green	Green	Green

100 mg/mL

Figure 3.5.20. Visual inspection scores of five different mAbs at 10 mg/mL and 100 mg/mL stored at 25°C for up to 11 months. mAbs were formulated in 20 mM His/His-HCl (pH 6.0) ± 150 mM NaCl. Data are shown as mean of n=2 ± absolute deviation. The higher the score the more particles were observed.

At 25 °C the storage stability could show first differences. It was confirmed that the two least repulsive mAbs in the His (w/o) formulation (mAb6 and mAb8) have increased aggregate levels after 11 months. The addition of NaCl caused the soluble aggregate content of mAb6 to increase whereas mAb8 soluble aggregate formation was slowed down. Looking at the A_2 values in this condition shows that only mAb6 is very attractive whereas the others are rather comparable. This might support a first conclusion that a minimum threshold of A_2 is necessary in order to start aggregation.

3.5.2.3. mAbs Stability at 40 °C

The expectation was that at 40 °C storage protein aggregation would be faster because the probability of partially unfolded states in the mAb's structure and therefore aggregation is even higher.^{92,96} Already at 10 mg/mL %HMW levels did change after only three months (Figure 3.5.21). Similar to 25 °C storage mAb3 has lower aggregate levels after storage than at T=0. A reason for this could not be found. mAb1 and mAb4 showed no change. The two mAbs that increased in aggregate levels were mAb6 and mAb8. Depending on the formulation the aggregation levels were different. In this His(w/o) formulation mAb6 increased by 0.5 %HMW and mAb8 by 3.3 %HMW. At increased ionic strength mAb6 increased by 1 %HMW and mAb8 by 2.5 %HMW. A comparison to the A_2 values at both low ionic strength revealed that the least repulsive mAb (mAb8) had the most dominant increase in %HMW followed by the second least repulsive one (mAb6). As ionic strength is increased mAb6 gets attractive and therefore aggregation is increased. mAb8 at high ionic strength is now the second least repulsive mAb and aggregation is reduced. This reduction can also be explained by the fact that (as shown in chapter 3.3) an increased ionic strength tends to reduce the attractive interaction of the tested IgG4 molecules. It is valuable information to the formulation scientist that IgG4 mAbs are special in this regard. A_2 does not give the full picture for aggregate increase of mAbs however still in both formulation conditions these two mAbs are the two with the least repulsive A_2 and still to some extent the increase in aggregates can be explained by protein-protein interactions.

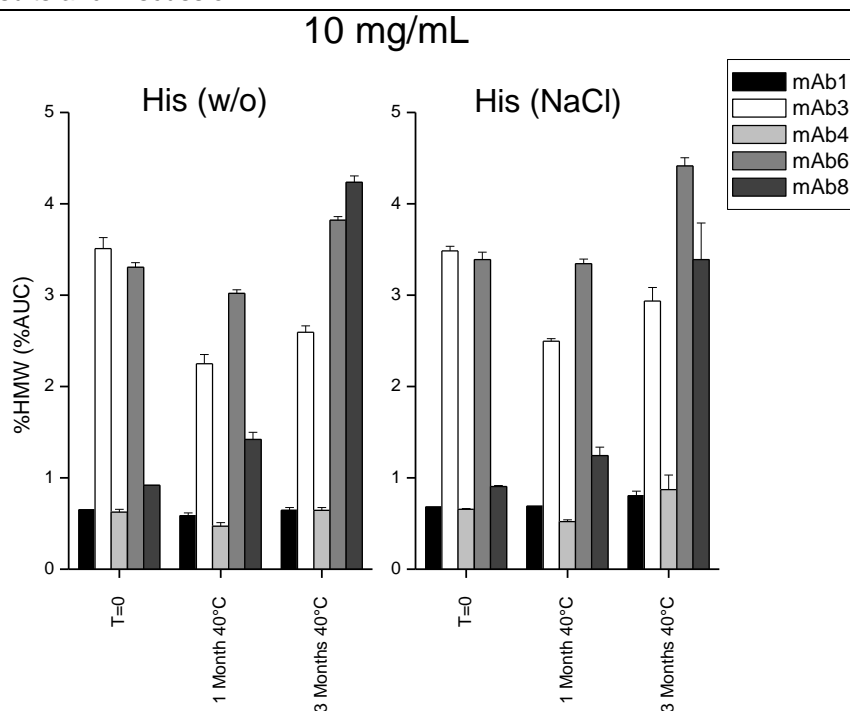


Figure 3.5.21. %HMW of five different mAbs at 10 mg/mL stored at 40 °C for 3 months. mAbs were formulated in 20 mM His/His-HCl (pH 6.0) ± 150 mM NaCl. Data are shown as mean of $n=2 \pm$ absolute deviation.

At 100 mg/mL (Figure 3.5.22) aggregation is increased for all mAbs as compared to 10 mg/mL. The increase for mAb1, 3, and 4 is rather minor and independent of the formulation condition and therefore also independent of A_2 . mAb1 +1.2 %HMW, mAb3 +1.8 %HMW, and mAb4 +1.3 %HMW. What was more interesting was a high aggregation for mAb6 and mAb8 that was formulation dependent. In the His (w/o) formulation mAb6 had +7.9 %HMW and mAb8 +7.7 %HMW and at high ionic strength mAb6 had +9.2 %HMW and mAb8 only +5.6 %HMW. The changes in aggregation when increasing the ionic strength are similar to the observation at 10 mg/mL. mAb6 had higher aggregation when NaCl was added (negative A_2). On the other hand mAb8's showed less aggregation. What was different to 10 mg/mL was the overall increase of aggregation. At 10 mg/mL mAb6 had a smaller %HMW increase than mAb8. At 100 mg/mL this was the other way round. The conclusion was that aggregation is not necessarily similar at 10 mg/mL as compared to 100 mg/mL. This stresses out the importance of doing stability studies at the intended concentration. It also supports the conclusion that in more crowded solutions short range non-ionic interactions are favored. As it is shown by high ionic strength A_2 measurements, mAb6 has stronger non-ionic attractive interactions than mAb8 which would explain the increased aggregation at high protein concentration. That protein-protein interaction can change with increasing protein concentration was shown by Scherer et al.⁶⁴ Only mAb6 and mAb8 which were in both conditions the two least repulsive mAbs increased strongest in their aggregate levels. This supports the theory that a specific threshold of A_2 needs to be reached in order for aggregation to start.²⁵

100 mg/mL stability at 40 °C was comparable to 25 °C. In His (w/o) buffer aggregation for mAb6 was higher than for mAb8 and in His (NaCl) buffer aggregation for mAb6 increased whereas mAb8 aggregation decreased. This was independent of temperatures studied.

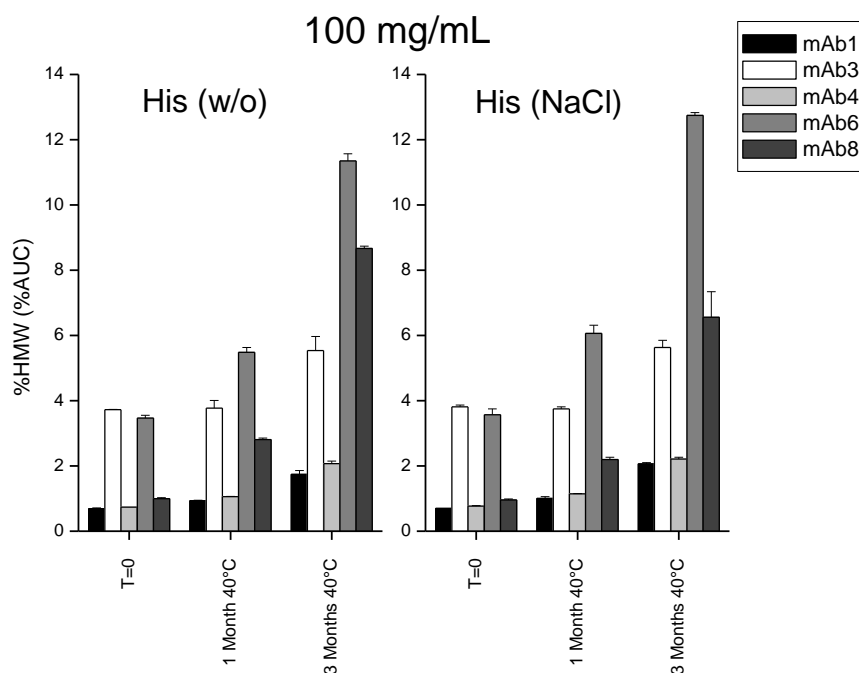


Figure 3.5.22. Soluble aggregate levels (%HMW) of five different mAbs at 100 mg/mL stored at 40 °C for 3 months. mAbs were formulated in 20 mM His/His-HCl (pH 6.0) \pm 150 mM NaCl. Data are shown as mean of $n=2 \pm$ absolute deviation.

In contrast to the %HMW levels, the turbidity values always followed the A_2 ranking in the respective formulation (Figure 3.5.23 and Figure 3.5.24). mAb6 and mAb8 which were the only two mAbs that strongly increased in turbidity showed that in the His (w/o) formulation the least repulsive mAb8 (10 mg/mL: +0.7 FTU, 100 mg/mL: +8 FTU) increased stronger than mAb6 (10 mg/mL: +0.3 FTU, 100 mg/mL: +7.6 FTU). When the ionic strength was increased the now attractive mAb6 increased strongly (10 mg/mL: +1.9 FTU, 100 mg/mL: +34.5 FTU) whereas mAb8 increased only moderately (10 mg/mL: +0.7 FTU, 100 mg/mL: +5.9 FTU). When comparing the %HMW increase to the FTU increase over time the values perfectly match especially at 10 mg/mL. So samples that increased in turbidity had also elevated soluble aggregate levels (%HMW). At 100 mg/mL this was not completely true. Even though mAb6 had the strongest increase in %HMW in the His (w/o) formulation mAb8 had a higher turbidity. Probably the FTU increase didn't outweigh the initial turbidity effect caused by different A_2 values.

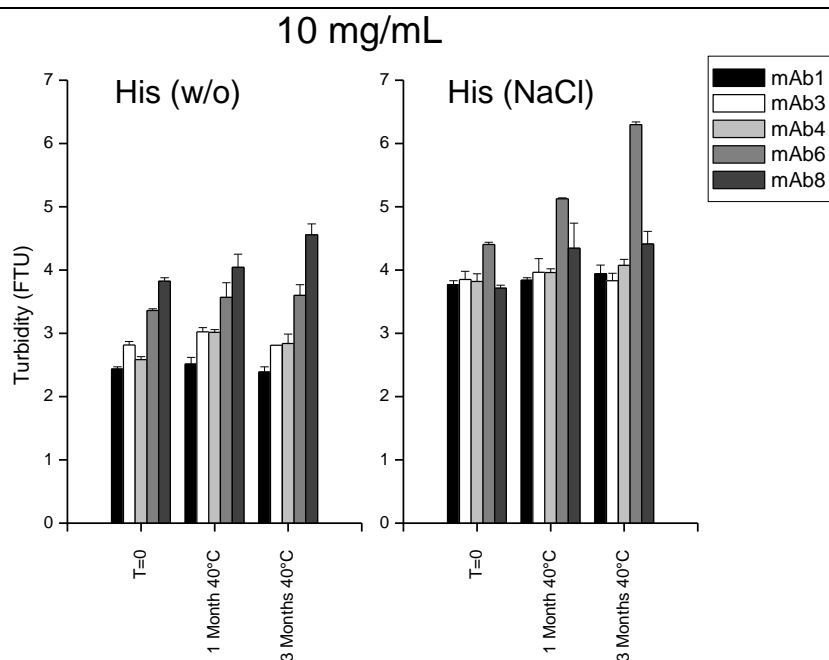


Figure 3.5.23. Turbidity of five different mAbs at 10 mg/mL stored at 40 °C for up to 3 months. mAbs were formulated in 20 mM His/His-HCl (pH 6.0) ± 150 mM NaCl. Data are shown as mean of n=2 ± absolute deviation.

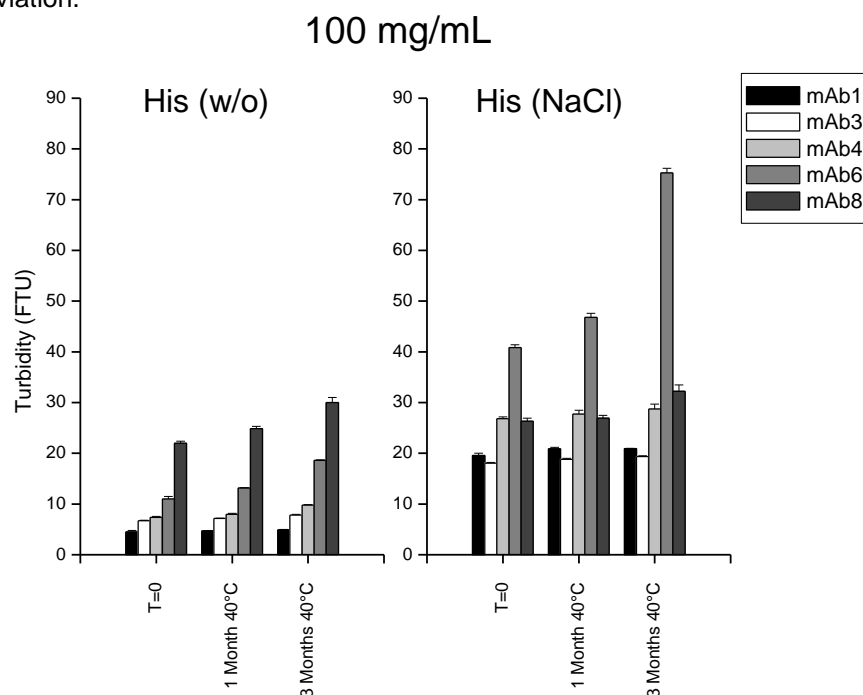


Figure 3.5.24. Turbidity of five different mAbs at 100 mg/mL stored at 40 °C for up to 3 months. mAbs were formulated in 20 mM His/His-HCl (pH 6.0) ± 150 mM NaCl. Data are shown as mean of n=2 ± absolute deviation.

Similarly to the observations made on 5 °C and 25 °C storage stability, subvisible particles were lower or at the same level as at T=0 after 3 months at 40 °C. At 10 mg/mL (Figure 3.5.25) and also at 100 mg/mL (Figure 3.5.26) counts were especially lower for mAb6. This was most pronounced for mAb8 (His(w/o)) and mAb1 and mAb6 in the His(NaCl) formulation. That subvisible particles decreased below T=0 after 3 months also at 40 °C can possibly be explained again by results published by Kiese et al.⁹⁵ It could be shown that particles generated by interfacial stress are reversible when spiked into non-

aggregated samples. After agitation of visual inspection (for T=0 analysis) samples were stored at rest.

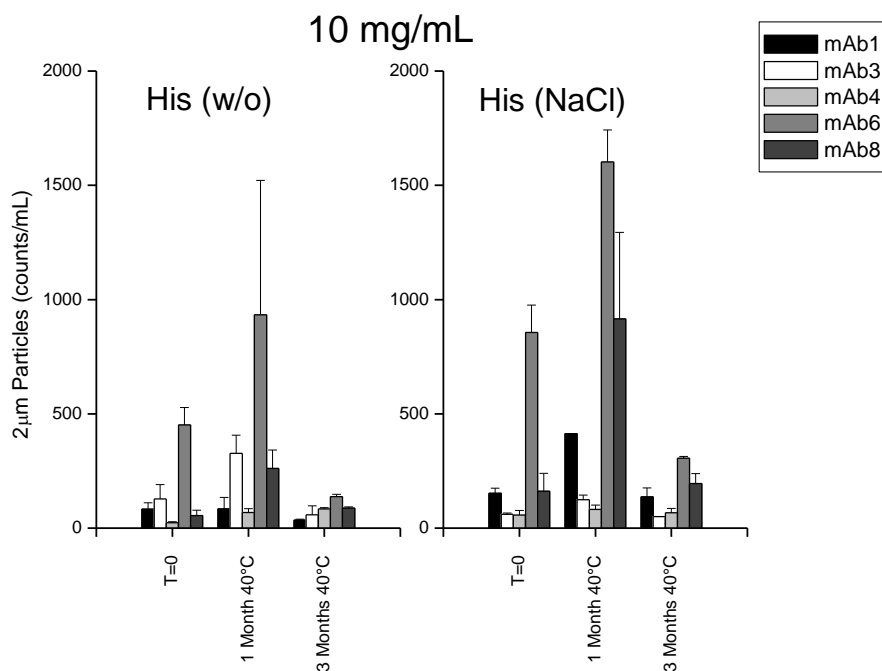


Figure 3.5.25. Cumulative subvisible particle counts $>2\ \mu\text{m}$ of five different mAbs at 10 mg/mL stored at 40 °C for up to 3 months. mAbs formulated in 20 mM His/His-HCl (pH 6.0) \pm 150 mM NaCl. Data are shown as mean of $n=2 \pm$ absolute deviation.

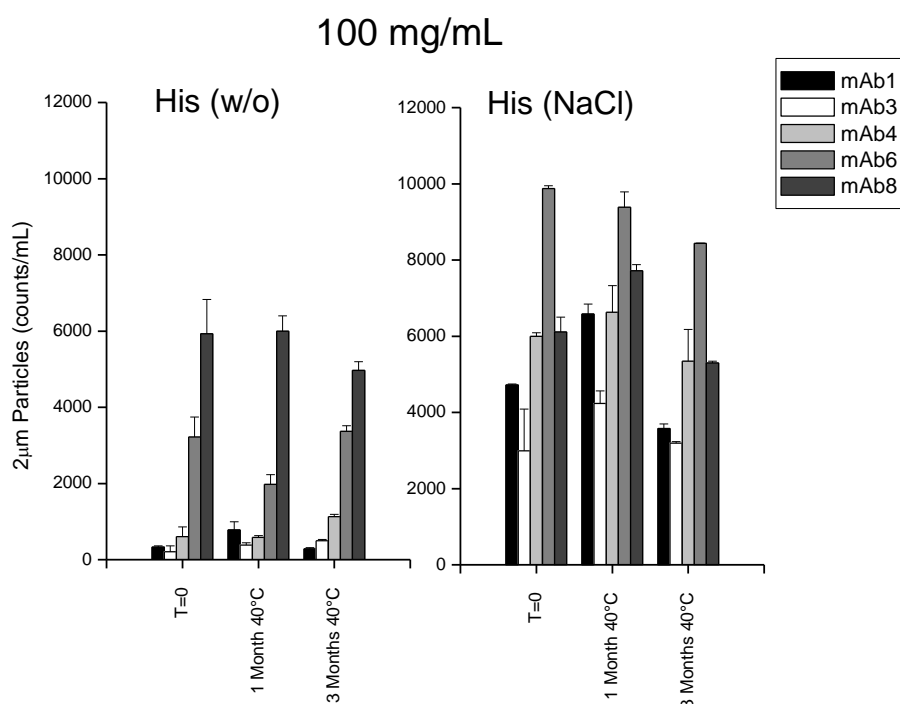


Figure 3.5.26. Cumulative subvisible particle counts of five different mAbs at 100 mg/mL stored at 40 °C for up to 3 months. mAbs formulated in 20 mM His/His-HCl (pH 6.0) \pm 150 mM NaCl. Data are shown as mean of $n=2 \pm$ absolute deviation.

The visible particle analysis (Figure 3.5.27) showed that particle levels increased after one month but tended to be lower after three months. This increase/reduction was also partially observed by subvisible particle analysis but could not be sufficiently explained.

Results and Discussion

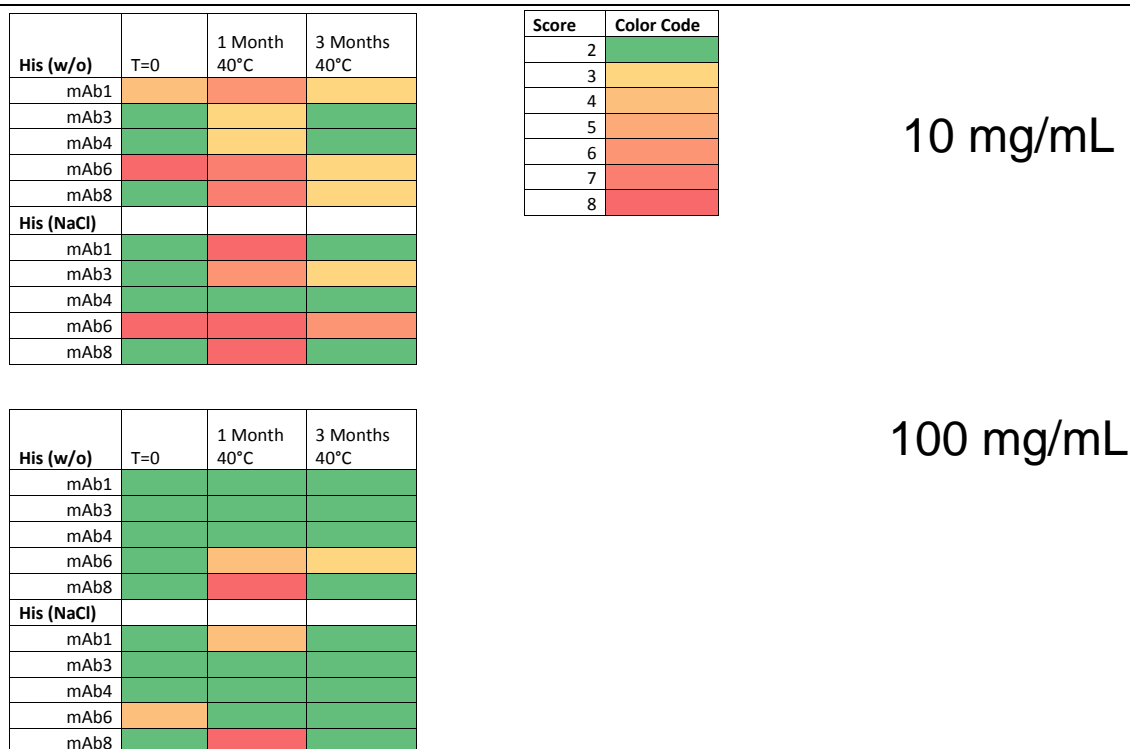


Figure 3.5.27. Visual inspection scores of five different mAbs at 10 mg/mL and 100 mg/mL stored at 40 °C for up to 3 months. mAbs were formulated in 20 mM His/His-HCl (pH 6.0) ± 150 mM NaCl. Data are shown as mean of n=2 ± absolute deviation. The higher the score the more particles were observed.

3.5.2.4. Shaking Stability

In this section the influence of interfacial stress on protein stability (i.e. shaking stability shall be discussed). In chapter 3.2.7.3 it was found out that surface activity is dependent on the mAb's A_2 . As shaking stress increases the air-liquid and air-solid interface⁹² the aim was to find out if A_2 can be used to predict shaking stability. It is important to know mAbs' susceptibility to interfacial stress as they are often shipped as a liquid to the customer. Cumulative subvisible particle counts, visible particle, turbidity and soluble aggregates by SEC after shaking are compared to the initial results. Because it was already shown that the >2 µm particle counts show the same trend as the >10 µm particle counts and to not overcrowd the section with graphs only the >2 µm particles are plotted.

Shaking stress was found very harmful to the protein with respect to cumulative subvisible particle levels (see Figure 3.5.28-Figure 3.5.31). As the particle counter is only calibrated up to 18000 counts/mL the absolute counts could only be compared up to this limit.

At 10 mg/mL in the His (w/o) formulation (Figure 3.5.28) it can be seen that already after 5 h of shaking two out of five mAbs (mAb1 and mAb6) exceed the counts/mL limit and after 24 h only mAb4 remained below. mAb1, mAb6 and mAb8 increased strongly mAb3 only moderately and mAb4 hardly changed. In section 3.5.2.1 it was concluded that the T=0 subvisible particle counts were increased because before T=0 sample analysis all samples were visually inspected which included swirling (agitating) of the samples. If this holds true then the susceptibility of the mAbs to shaking stress (formation of subvisible particles) should follow the same trend as T=0 results. At 10 mg/mL in the His (w/o) formulation (Figure 3.5.28) the only mAb that is elevated is mAb6 and indeed this mAb had

the strongest increase in subvisible particle counts on shaking followed by mAb1 and mAb8.

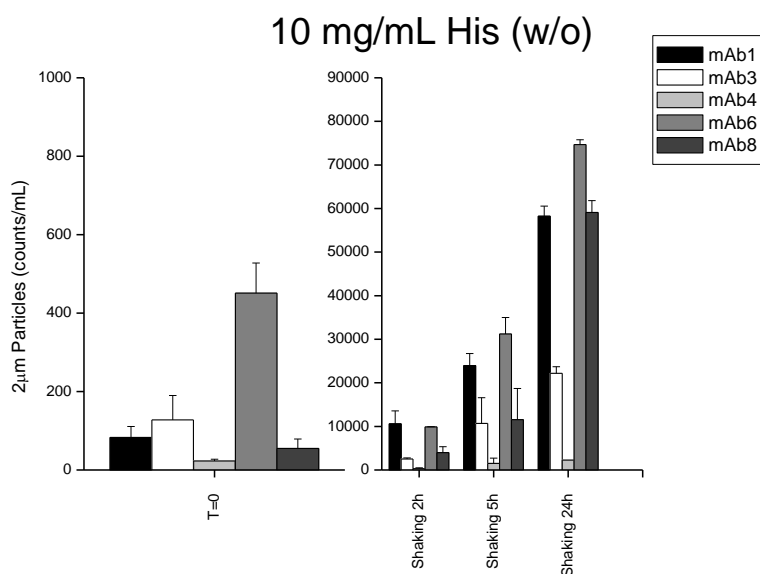


Figure 3.5.28. Cumulative subvisible particle counts $>2 \mu\text{m}$ of five different mAbs at 10 mg/mL at T=0 and on shaking for up to 24 h. mAbs formulated in 20 mM His/His-HCl (pH 6.0). Data are shown as mean of $n=2 \pm$ absolute deviation.

The particle counts in the His(NaCl) formulation at T=0 (Figure 3.5.29), given the error bars, were similar to the His(w/o) formulation (Figure 3.5.28). Only mAb6 had elevated subvisible particle counts as compared to the His(w/o) formulation. However the increase of particles over shaking time was much stronger. After 2 h of shaking, all mAbs but mAb3 and mAb4 had exceeded the maximum allowed 18,000 counts/mL and after 24 h of shaking only mAb4 stayed below this limit. Compared to His(w/o) the counts were higher. Which mAb had the strongest increase in subvisible particles cannot be said as after 2 h because already three mAbs exceeded the maximum count/mL limit.

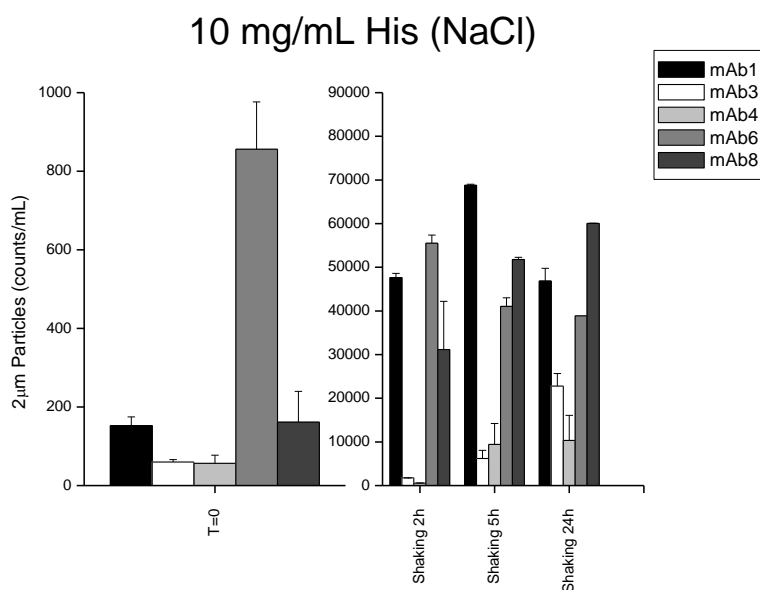


Figure 3.5.29. Cumulative subvisible particle counts $>2 \mu\text{m}$ of five different mAbs at 10 mg/mL at T=0 and on shaking for up to 24 h. mAbs formulated in 20 mM His/His-HCl (pH 6.0) + 150 mM NaCl. Data are shown as mean of $n=2 \pm$ absolute deviation.

When the protein concentration was increased from 10 mg/mL to 100 mg/mL the mAbs in the His(w/o) formulation (Figure 3.5.30) show that at T=0 subvisible were elevated. This was especially true for mAb6 and mAb8. This is different to 10 mg/mL. At this concentration the particles for mAb8 were not increased. After 2 h of shaking two out of five mAbs were above the measurement limit (mAb6 and 8) and after 24 h three out of five mAbs were above the count limit (mAb1, 3 and mAb6). Which mAb increased most can't be determined because mAb6 and mAb8 exceeded the maximum allowed counts/mL already after 2 h. mAb4 in both cases tolerated shaking stress better than the others.

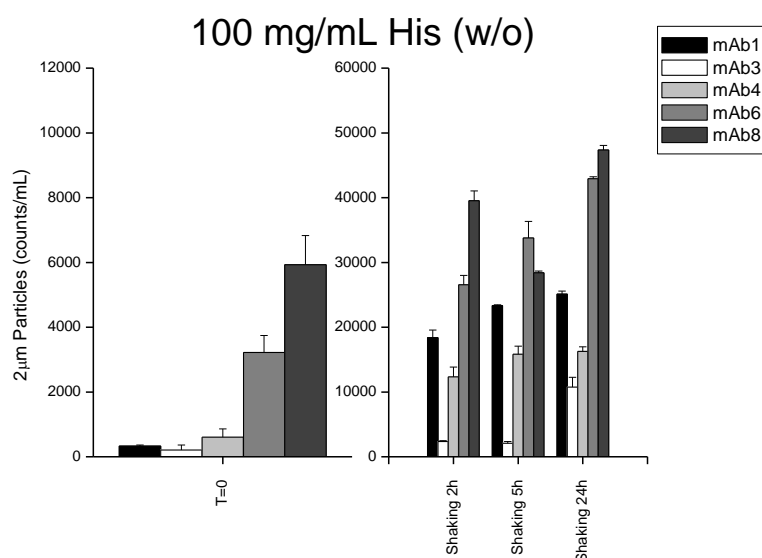


Figure 3.5.30. Cumulative subvisible particle counts >2 µm of five different mAbs at 100 mg/mL at T=0 and on shaking for up to 24 h. mAbs formulated in 20 mM His/His-HCl (pH 6.0). Data are shown as mean of n=2 ± absolute deviation.

At 100 mg/mL in the His(NaCl) formulation (Figure 3.5.31) mAb6 at T=0 had the highest counts/mL followed by mAb8 and mAb6. Which mAb had the strongest increase in subvisible particle count can't be determined as already after 2 h four out of five mAbs exceeded the maximum counts/mL. After 24 h all five exceeded the maximum counts/mL. It was concluded that formulations containing NaCl also at 100 mg/mL protein concentration have a higher susceptibility to form subvisible particles on shaking. An increased concentration (10 mg/mL to 100 mg/mL) makes proteins less stable to subvisible particle formation. This is based on the fact that more mAbs exceeded the maximum of 18,000 counts/mL >2 µm.

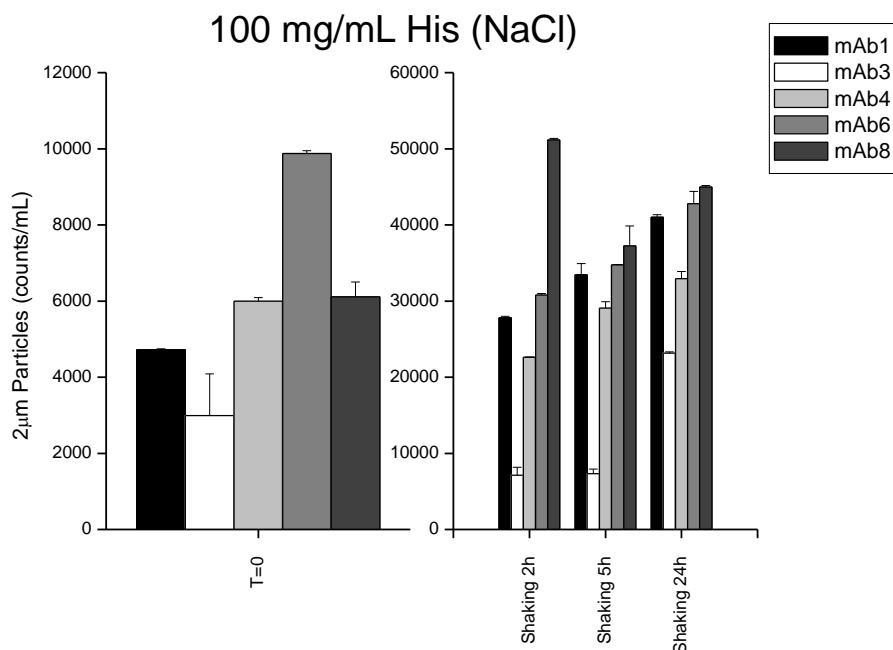


Figure 3.5.31. Cumulative subvisible particle counts $>2\ \mu\text{m}$ of five different mAbs at 100 mg/mL at T=0 and on shaking for up to 24 h. mAbs formulated in 20 mM His/His-HCl (pH 6.0) + 150 mM NaCl. Data are shown as mean of $n=2 \pm$ absolute deviation.

In contrast to subvisible particle counts, it was possible to rank the mAbs according to their increased turbidity after shaking. At 10 mg/mL in the His (w/o) formulation (Figure 3.5.32) mAb6 showed the strongest increase in turbidity followed by mAb8 and mAb1. As compared to these three mAb3 only increased moderately. mAb4 had the smallest increase in turbidity. This is in accordance to subvisible particle analysis. As bigger and higher number of particles scatter more light it was concluded, that these particles are then measured by the turbidimeter. Therefore subvisible particle counts can be compared to samples turbidity increase. Although at T=0 subvisible particles were high (especially for mAb6), this did not outweigh the A_2 effect that was causing the initial turbidity (please see 3.5.1). mAbs turbidity ranking at T=0 still followed the A_2 despite different concentrations of particles present. Probably the particle concentration was too low to scatter enough light to sufficiently contribute to turbidity. In the His (NaCl) formulation turbidity was higher (x10 as compared to His(w/o) 24 h shaking, Figure 3.5.32). As no reliable information of subvisible particles is available (limits exceeded, Figure 3.5.29) only the subvisible data at T=0 can be compared to turbidity increase on shaking. mAb6 again had the strongest increase in turbidity followed by mAb8 and 1. mAb4 was the least turbid after 24 h of shaking. If subvisible particles at T=0 were generated by swirling the sample for visual inspection then indeed turbidity increase after shaking proofed that mAb6 is most susceptible to form subvisible/visible particles.

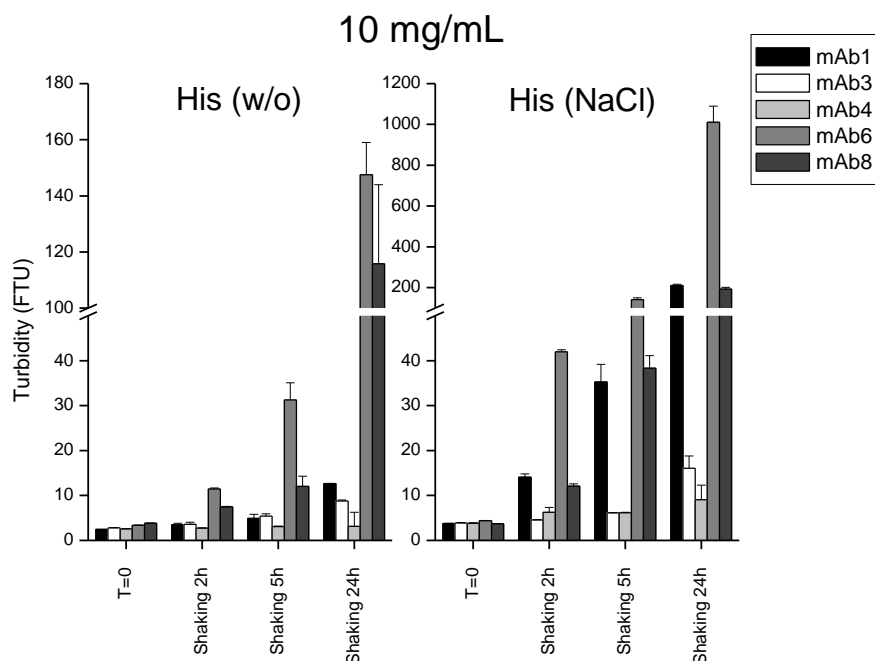


Figure 3.5.32. Turbidity of five different mAbs at 10 mg/mL upon shaking for up to 24 h. mAbs were formulated in 20 mM His/His-HCl (pH 6.0) \pm 150 mM NaCl. Data are shown as mean of $n=2 \pm$ absolute deviation.

At 100 mg/mL in the His (w/o) formulation (Figure 3.5.33) the turbidity increase followed the T=0 ranking of the subvisible particles (Figure 3.5.30). mAb8 increased strongest in its turbidity followed by mAb6. mAb1, 3, and 4 only increased moderately. In the His (NaCl) formulation turbidity increased by a factor of 4 as compared to the His (w/o) formulation upon 24 h shaking. The increase in turbidity was comparable to the amount of subvisible particles present at T=0 (Figure 3.5.31). The highest turbidity increase was found for mAb8 followed by mAb6 and mAb1. In subvisible particle counts it was mAb6 followed by mAb8 and mAb1 (at T=0). It was concluded that turbidity measurements are more reliable to see differences on shaking stress because in subvisible particle counts the limits for analysis were exceeded soon after study start.

The visual inspection data for the shaking stress is not shown because already after 2 h all formulations had the highest score (>10 visible particles per vial) and stayed at this level until 24 h shaking.

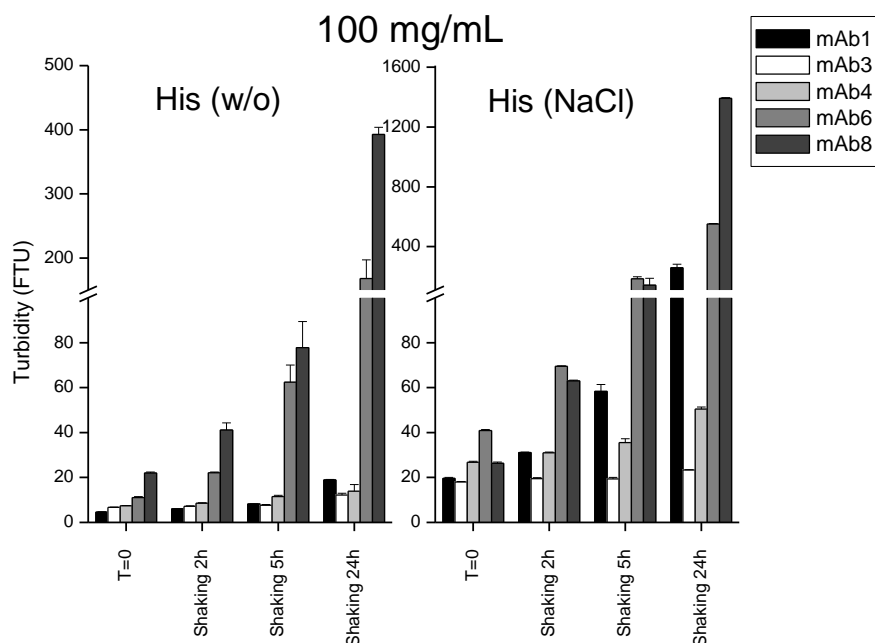


Figure 3.5.33. Turbidity of five different mAbs at 100 mg/mL upon shaking for up to 24 h. mAbs were formulated in 20 mM His/His-HCl (pH 6.0) \pm 150 mM NaCl. Data are shown as mean of $n=2 \pm$ absolute deviation.

Next the increase in protein aggregation by HPLC-SEC shall be presented. The respective %HMW levels upon shaking are shown in Figure 3.5.34 (10 mg/mL) and Figure 3.5.35 (100 mg/mL). What can be said is that changes were observed and that the three mAbs that always had the strongest increase in turbidity also increased in %HMW. Only after 24 h hours of shaking soluble aggregates formation increased to an extent that could be measured by SEC. Turbidity at the same time had increased more than tenfold. SEC was either not very sensitive to aggregates caused by surface induced stress or aggregates formed proceeded immediately to form larger particles and were therefore not detected. At 10 mg/mL (Figure 3.5.34) the strongest increase in %HMW in the His (w/o) formulation was for mAb6 followed by mAb8. In the His (NaCl) formulation it was for mAb6>mAb8>mAb1. Addition of NaCl caused more soluble aggregates to form over time. The same trend was seen in turbidity increase. Shaking at 100 mg/mL formed only with mAb1 more %HMW as compared to 10 mg/mL. mAb6 and mAb8 had lower amounts of aggregates at 100 mg/mL as compared to 10 mg/mL. No conclusions could be drawn from that.

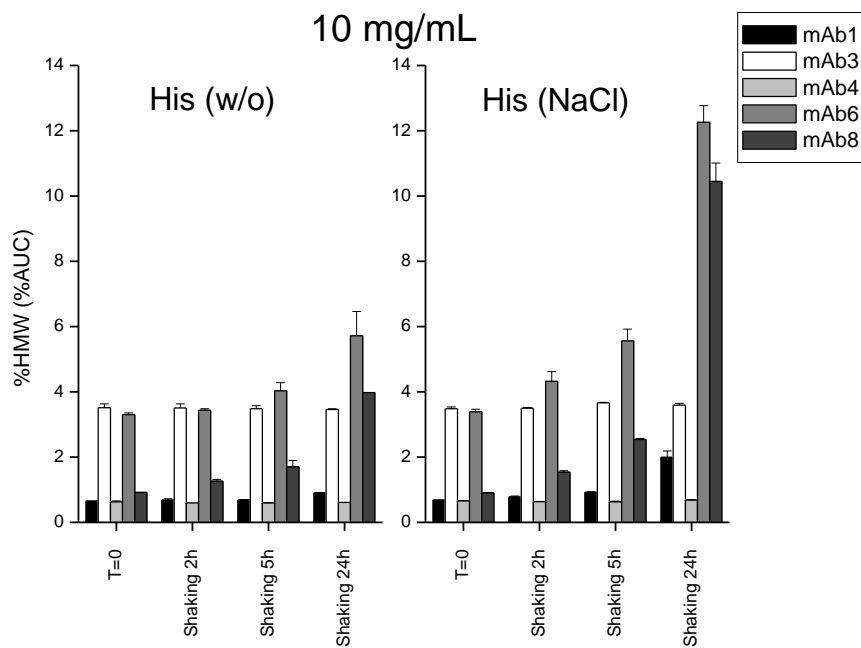


Figure 3.5.34. %HMW of five different mAbs at 10 mg/mL upon shaking for up to 24 h. mAbs were formulated in 20 mM His/His-HCl (pH 6.0) ± 150 mM NaCl. Data are shown as mean of n=2 ± absolute deviation.

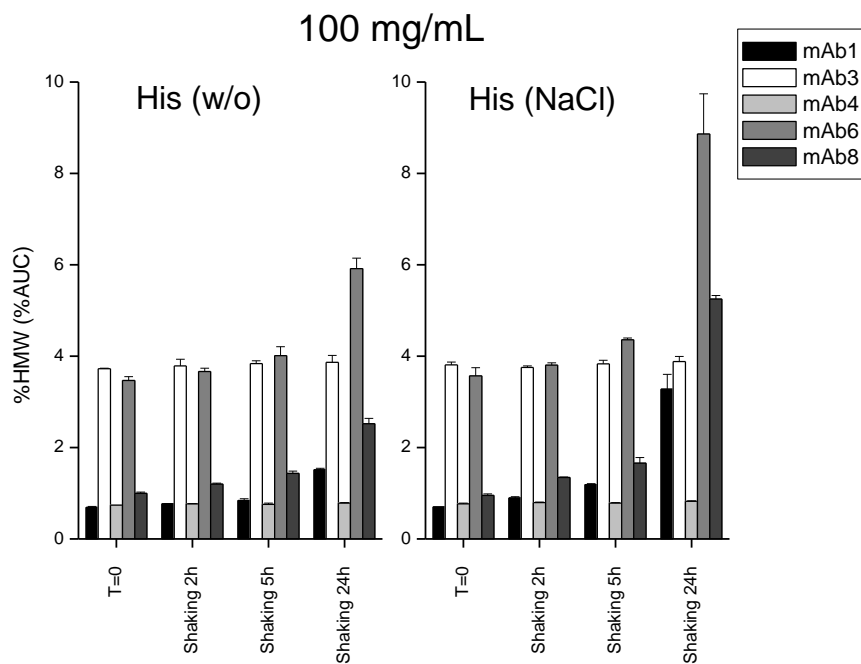


Figure 3.5.35. %HMW of five different mAbs at 100 mg/mL upon shaking for up to 24 h. mAbs were formulated in 20 mM His/His-HCl (pH 6.0) ± 150 mM NaCl. Data are shown as mean of n=2 ± absolute deviation.

Overall it was concluded that probably the shaking stress that was exerted during 100 % visual inspection of the vials has increased the T=0 subvisible particle counts. Because the formulations did not contain any surfactant, protecting the samples against surface induced stress, the samples were highly susceptible to mechanical stress. Therefore also

subvisible particle counts upon shaking stress for several hours exceeded the maximum counts/mL allowed for the light obscuration method (<18,000 counts/mL) used. It was however possible to analyze turbidity measurements and to compare them to subvisible particles at T=0. Except for 100 mg/mL His (NaCl) formulations a good relation of T=0 subvisible particle counts and the increase of turbidity during shaking could be found. The HPLC-SEC did show the same result as the turbidity assays namely that mAb6 and mAb8 are the least stable upon shaking (aggregate formation) and that mAb1 aggregation increased upon NaCl addition. However one difference was found. When increasing protein concentration from 10 to 100 mg/mL, the turbidity of mAb6 increased stronger than turbidity of mAb8. This was observed in both formulations. This was not reflected in SEC data (mAb6>mAb8).

3.5.2.5. Summary of the stability study

The overall conclusion from the stability study was that temperature stability (5 °C, 25 °C, 40 °C) showed comparable degradation patterns at all temperatures, although the aggregation at elevated temperatures was faster. This finding comforts a formulation scientist as it justifies formulation nomination on accelerated 40 °C data. The protein-protein interaction (A_2) seems to play an important role as it was shown that in low ionic strength formulations generally aggregation is lower for mAbs being more repulsive. Only the two least repulsive mAbs (mAb6 and 8) in both conditions (His \pm NaCl) tested showed a clear increase in aggregate levels. This supports the theory that a specific threshold of A_2 needs to be reached in order to start protein aggregation.²⁵ If this is true then the threshold in the His(w/o) formulation must lay specifically between $1.73 \times 10^{-4} \text{ mol mL/g}^2$ and $1.23 \times 10^{-4} \text{ mol mL/g}^2$ because these were the determined A_2 values for mAb3 (no clear aggregation) and mAb6 (clear aggregation). In the His (NaCl) formulation this threshold must lay specifically between $0.21 \times 10^{-4} \text{ mol mL/g}^2$ and $0.19 \times 10^{-4} \text{ mol mL/g}^2$ which are the determined A_2 values for mAb4 (no clear aggregation) and mAb8 (clear aggregation). The absolute values for aggregate increase, however, did not follow A_2 . At low protein concentration mAb8 always had a higher aggregate increase as compared to mAb6 (His \pm NaCl). At high protein concentration aggregation increase was generally higher but mAb6 always had a higher aggregate increase as compared to mAb8. 10 mg/mL might therefore not be comparable to 100 mg/mL data. This stresses out the importance of stability studies at the intended (final product) concentration as one might overlook specific effects not covered by A_2 . The reason for increased aggregation at higher concentrations is, that at more crowded (higher concentrated) solution conditions the likelihood of two particles colliding and aggregating is higher. This then leads to an increased aggregation.¹ Turbidity measurements (an indicator for the presence of particles), to some extent followed the %HWM trends. However because turbidity is always influenced by A_2 (Equation 25) and this is in theory also valid for dimers/aggregates formed, comparing absolute increase of turbidity is not so straightforward. The subvisible/visible particle counts in this study were not very conclusive. Although A_2 could not explain the full picture of mAbs temperature storage stability, it was found that more repulsive conditions in the respective formulation have a higher chance for success. This information, especially in combination with the toolbox of modifying A_2 based on chapter 3.4, can be very valuable in a pharmaceutical development.

In shaking stress stability it was concluded that additional NaCl had an adverse effect on shaking stability because NaCl shields the electrostatic repulsion of mAbs and therefore reduces A_2 . In respect to mAb specific protein-protein interactions it was concluded that the two least repulsive mAbs (namely mAb6 and mAb8) were the least stable in regards to shaking. However mAb1 was unstable too. This is unexpected and cannot be explained as this is one of the mAbs with the highest A_2 . mAb4 was found to be the most stable mAb with respect to shaking stress. Consistent results between turbidity and %HMW measurements were achieved. Subvisible/visible particle counts were only of limited use because due to the absence of surfactant most results exceeded the upper limits of the instrumentation. mAbs that have a low A_2 seem to have a lower stability upon shaking stress but high A_2 does not necessarily mean high stability. This is in contrast to the temperature stability study. Most likely multiple factors are influencing the shaking stability and it could not be pointed down to one single parameter.

3.5.3. Self-association of Antibodies

It is known that certain mAbs have a prominent tendency for reversible self-association. Moore et al. have shown that the recombinant humanized antibody against VEGF is predominantly present as monomer under acidic pH and low ionic strength conditions.⁴¹ At physiological conditions however the appearance of significant amounts of a non-covalent reversible dimer was observed by size-exclusion chromatography.⁴¹ In presence of high salt (1 M NaCl) the dimerization effect observed was enhanced. Interestingly, dimer formation has been observed highest at pH 7.5-8.0, i.e. close to IEP. The authors discussed that dimerization occurred primarily through hydrophobic interactions.⁴¹ Besides the effect in physiological conditions, the effect of buffer conditions on dimerization is important to understand as dimerization should be avoided for example during downstream processing where monomeric mAb material is purified.

The aim of this section is to demonstrate whether the second virial coefficient A_2 can be used to predict dimerization levels / soluble aggregate levels at different pharmaceutically used pH/buffer systems. The buffer systems and ionic strength ranges were chosen by intention, as they represent systems commonly used in protein formulations. mAb6 was chosen as a model mAb as it is known to be sensitive to pH and ionic strength and shows also self-association. After buffer exchange and final formulation (at 10 mg/mL) was done the different formulations were filtered by an 0.22 μm filter and subjected to SEC-HPLC after an equilibration time of 24 hours. By sustaining the analysis by one day it was assumed (based on data published by Moore et al.⁴¹), that an equilibrium had been established.

Figure 3.5.36 shows the comparison of A_2 values and the respective %HMW as determined by SEC. The HMW were almost exclusively found to be dimers. Samples are shown with increasing pH (pH 5.0-pH 7.0) and ionic strength (10 mM, 30 mM, and 50 mM). As expected, an increase in ionic strength reduces in general the repulsiveness of the respective formulations. At pH 5.0 e.g. all formulations were found repulsive at 10 mM ionic strength. At 30 mM ionic strength the citrate buffer system at pH 5.0 got slightly attractive and all other formulations at pH 5.0 were reduced with respect to their repulsiveness. At 50 mM ionic strength the set of formulations was further shifted to less

repulsive A_2 values. Despite the fact that the formulations differed prominently in A_2 at a given pH and ionic strength, the dimer content (%HMW) was similar for all formulations at lower pH. In addition, the decrease in A_2 with increasing ionic strength (e.g. A_2 in HisAc formulation at pH 5.0 is reduced by a factor of 5) did not cause any change in soluble aggregate/dimer levels. A discriminative effect between the formulations could only be shown starting with pH 6.0 and higher.

A possible explanation is that at low pH, the effective net charge of the protein and the degree of repulsiveness is still high enough to prevent dimerization, or in other words: the A_2 values are above a certain threshold. This might explain that – despite the vast differences in A_2 – there is barely a change in dimer content, at least in low pH. Moreover, the highest ionic strength (i.e. 50 mM) was chosen still rather low. Likely, 50 mM ionic strength is not high enough for shielding the protein net charge and to induce mid- and short-range interactions to become prominent. In the given experimental set-up the biggest influence on the %HMW present was the pH. For all formulations the degree of repulsiveness was lowered with increasing pH which resulted in higher levels of HMWs/dimers. It should be noted that – even at higher pH – the formulations' rank order with respect to A_2 did not translate into a rank order for dimerization. At 50 mM ionic strength and pH 6.0, the citrate formulation was – by far – the most attractive, however the highest HMWs/dimers were found for HisAc and His/HisHCl formulations which were the most repulsive.

It was therefore concluded that at the conditions analyzed (10-50 mM ionic strength) the surface charge (i.e. effective net charge as a function of pH) of the mAb itself plays the most important role for A_2 and dimerization. A higher pH increases the dimerization for all formulations tested. The A_2 values gave a fair trend of A_2 pH dependency and overall influence of ionic strength on A_2 . However, A_2 alone did not fully translate into dimerization tendency. Probably the dimerization is based on a specific interaction rather than on global interaction which is assessed by A_2 .

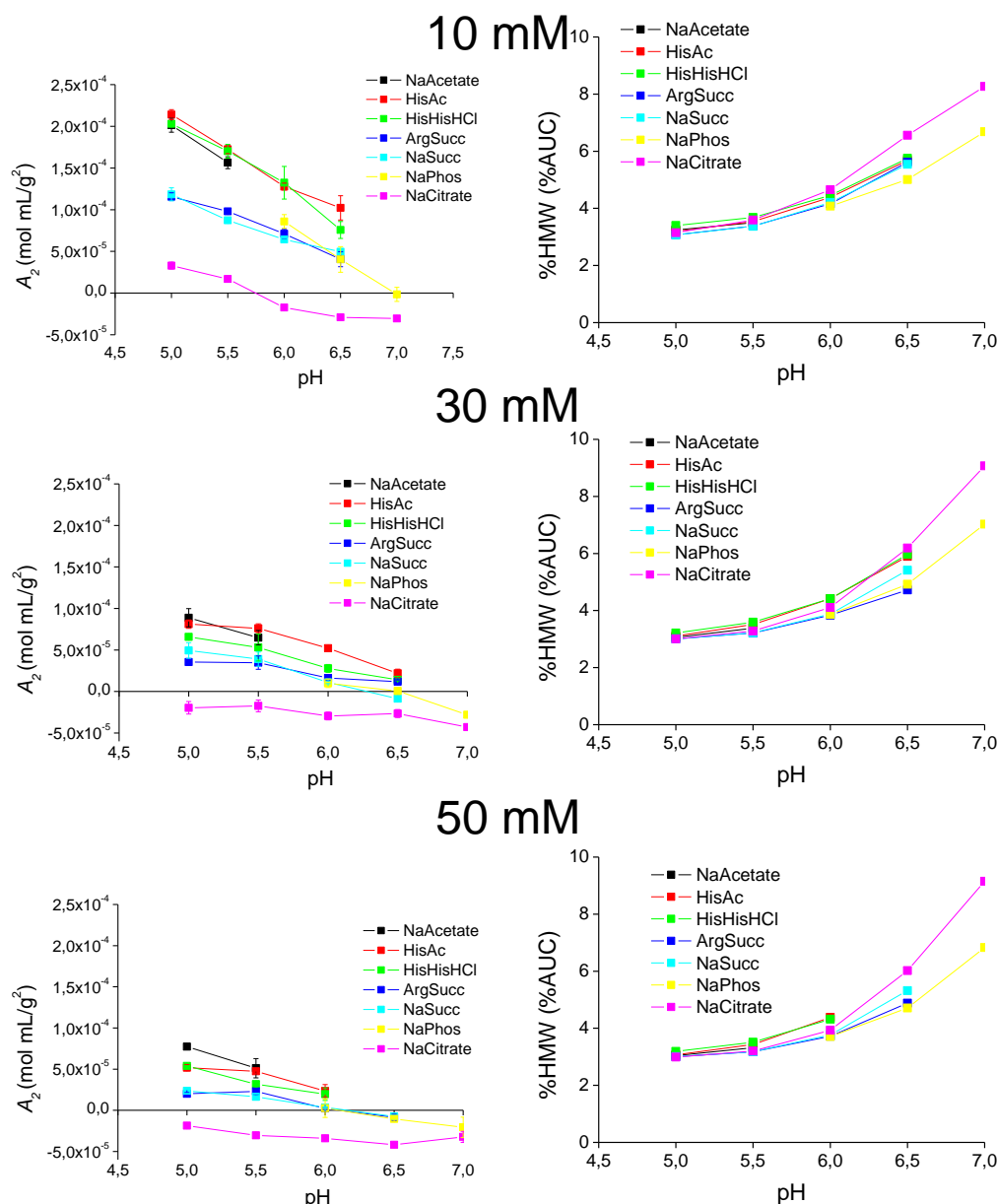


Figure 3.5.36. A_2 values of different formulations of mAb6 corresponding to the %HMW levels at pH 5.0-7.0 at various buffers (ionic strength 10, 30, and 50 mM). A_2 data are shown as mean of $n=3 \pm$ error of the linear regression.

3.5.4. A_2 and Dynamic Viscosity

Protein-protein interactions are thought to be related to mAbs' viscosity.^{2,3,5,97} This section therefore evaluates the link between A_2 and mAbs' viscosity. Several IgG1 mAbs as well as IgG4 being different repulsive/attractive regarding their A_2 were analyzed. The aim was to determine the influence of A_2 on the viscosity testing the different buffer valences as well as the influence of pH and ionic strength. The conditions were chosen based on section 3.4 data. Dynamic viscosity was measured at 150 mg/mL by a plate-cone rheometer. The working hypothesis was that the more repulsive particles are the smaller their interaction. Therefore their resistance to movement is smaller and hence the viscosity is lower.

In a first step mAbs were compared at one pH (i.e. pH 6.0). Figure 3.5.37 shows A_2 values of five different mAbs (3x IgG1 and 2x IgG4) at two ionic strengths (10 mM and 30 mM) formulated in three buffers that are mono-, di-, and tri-valent. The A_2 values were then compared to the viscosity data in the respective formulations (Figure 3.5.38).

First the influence of buffer's valence on viscosity shall be discussed. Comparison of viscosity data and A_2 at constant ionic strength and pH showed that as buffer valence is increased A_2 changes (e.g. mAb4's A_2 value in citrate buffer is about half compared to Histidine buffer). However the viscosity for all mAbs was hardly changing. The only exception is mAb8 where viscosity increased in citrate buffer. As this effect vanished when citrate concentration was increased (the effect of ionic strength is discussed shortly) it would be interesting to further investigate if citrate is able to increase a samples viscosity at very low concentrations. Maybe it was because at this citrate concentration the A_2 value for mAb8 was more attractive causing more particles to interact. What speaks against this assumption is mAb9 where this phenomenon was not observed. Although A_2 was reduced as buffer valence increased the viscosity stayed mainly at the same level. This lead to the conclusion that A_2 cannot be used to rank mAb viscosity within different buffer systems (mono-,di-,tri-valent buffers). At low ionic strength however it was nicely demonstrated that in each of the three buffer systems the viscosity indeed followed the A_2 ranking.

Next the influence of ionic strength shall be discussed. When ionic strength is increased all A_2 values move closer to zero (see Figure 3.5.37). This increase in ionic strength didn't cause hardly any change in the IgG1 formulation's viscosity (mAb4-6). What did change was the viscosity of the IgG4 mAbs (mAb8 and mAb9). Therefore a reduction in protein-protein interaction by an increase of counter ions did not affect IgG1's viscosity but only IgG4's. A possible explanation can be found in chapter 3.3. It was shown that the IgG4 mAbs tested have the tendency to interact by their dipolic charge. This is shielded as ionic strength is increased. With the exception of mAb5 all mAbs formulated in one condition followed the A_2 ranking. The observation that A_2 did change within the different buffer systems, without viscosity change, lead to the conclusion that A_2 can only be used to rank mAbs within one buffer system. An explanation why mAb5 has a higher A_2 than mAb4 at 30 mM but still mAb4 has a lower viscosity could not be found.

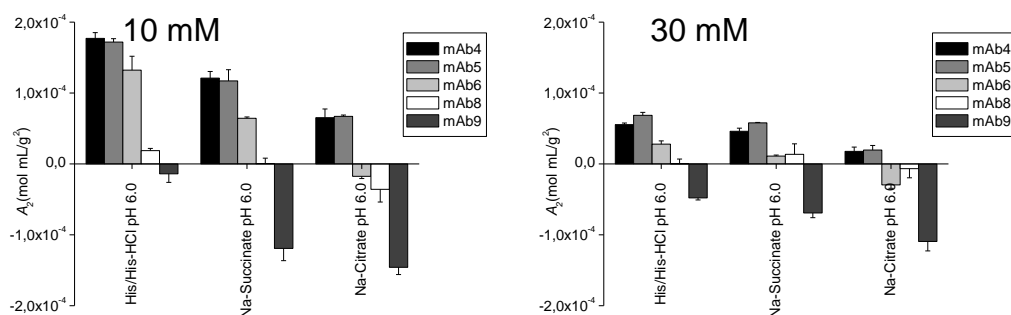


Figure 3.5.37. Second virial coefficient A_2 of five mAbs at three different formulations compared at two ionic strengths (10 and 30 mM). Data are shown as mean of $n=3 \pm$ error of the linear regression.

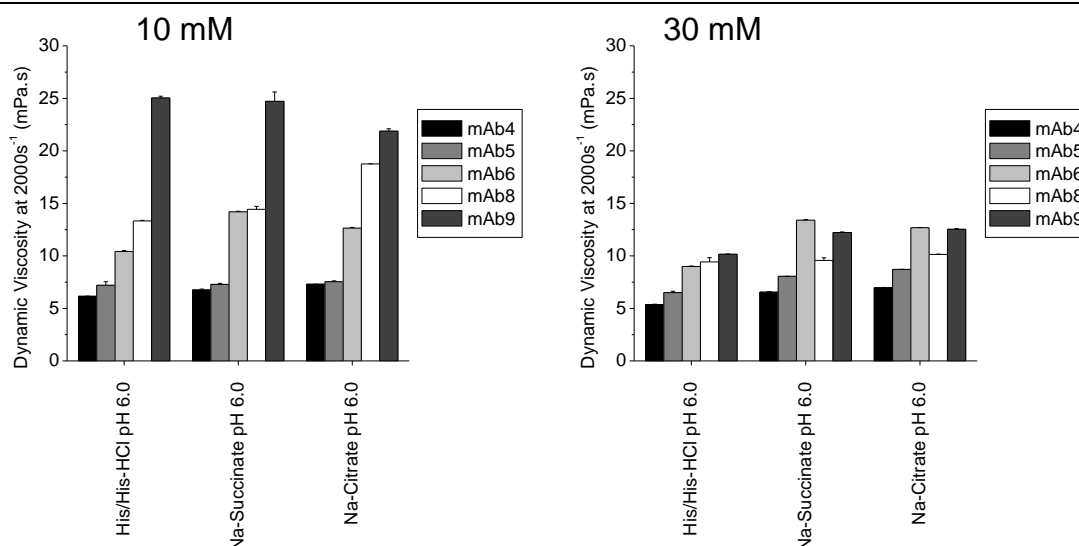


Figure 3.5.38. Dynamic viscosity of five mAbs in three different formulations compared at two ionic strengths (10 and 30 mM). Data are shown as mean of $n=2 \pm$ absolute deviation.

In a next step the influence of buffers' pH was studied. Therefore also pH 5.0 and pH 7.0 buffers were added to the set up (Figure 3.5.40 and Figure 3.5.39). As pH is lowered the A_2 values go up, which is expected. mAbs did get more repulsive due to their increased net charge. This also nicely results in a reduction of viscosity. The reverse case happens if pH is increased to pH 7.0. There the mAbs get more attractive and viscosity as compared to the same buffer at pH 6.0 increases. There is one exception, the viscosity is not changing for mAb5 at 10 mM. What is also unexpected is that mAb6 has an elevated viscosity within the pH 6.0 succinate formulation. With the present data no explanation to these phenomena could be found. More detailed experiments should be done on these effects. In this view (Figure 3.5.39 and Figure 3.5.40) it is again demonstrated that as A_2 is high, viscosity is generally lower whereas as A_2 is low or negative (attractive) viscosity is generally higher. There are however some outliers: mAb6 has the highest viscosity within the succinate formulation, mAb9 at pH 6.0 has the lowest viscosity within the citrate formulation, and although mAb9 has a higher A_2 value within the acetate formulation as compared to mAb8, mAb9 has a higher viscosity at 10 mM ionic strength. If ionic strength is increased viscosities are hardly changing for the IgG1 mAbs whereas the two IgG4 (mAb8 and mAb9) had both lower viscosity at high ionic strength.

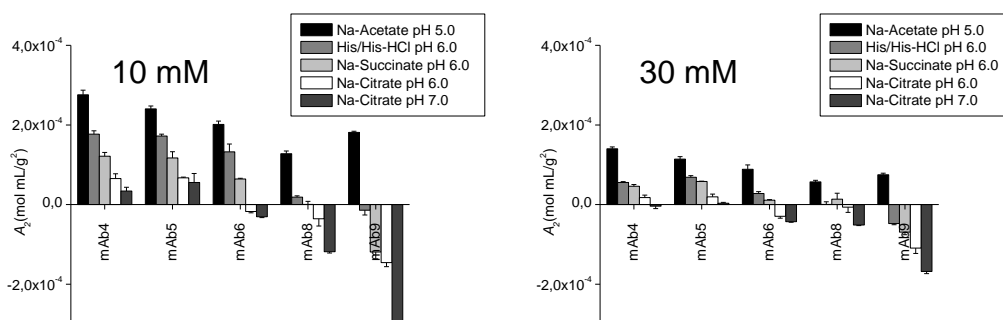


Figure 3.5.39. Second virial coefficient A_2 of five mAbs at five different formulations compared at two ionic strengths (10 and 30 mM). Data are shown as mean of $n=3 \pm$ error of the linear regression.

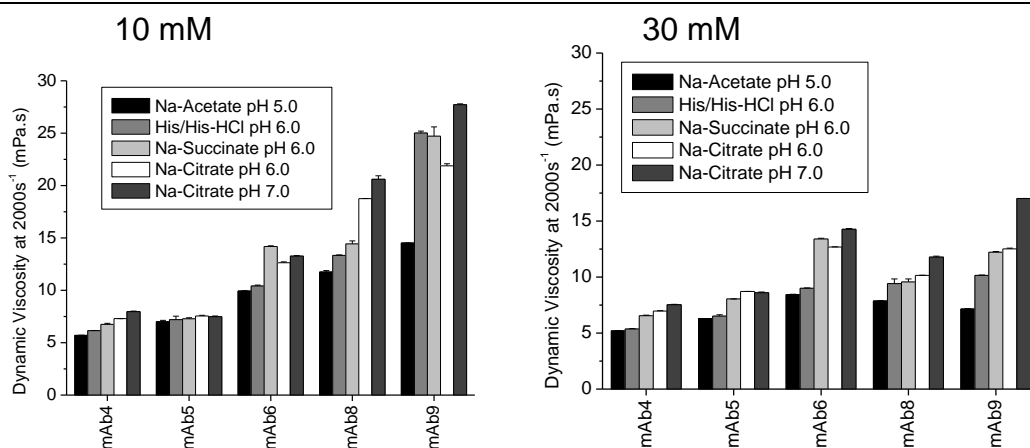


Figure 3.5.40. Dynamic viscosity of five mAbs in five different formulations compared at two ionic strengths (10 and 30 mM). Data are shown as mean of $n=2 \pm$ absolute deviation.

It was found that increasing ionic strength only helped reducing the viscosity for the two IgG4 mAbs whereas the effect on the three IgG1 mAbs was minor. On the other hand it could be shown that highly repulsive formulations (at least within one buffer system) tend to have lower viscosity. If the A_2 and the viscosity is known this knowledge can be used to modify the samples viscosity based on A_2 . Modifying A_2 has been already addressed in chapter 3.4.

Although the general trend was observed that viscosity is lower when protein-protein interactions are repulsive (positive A_2) the overall topic is more complex. This can be seen in Figure 3.5.41. Although there is a general trend, high A_2 - low viscosity and low A_2 - high viscosity, the R^2 was bad.

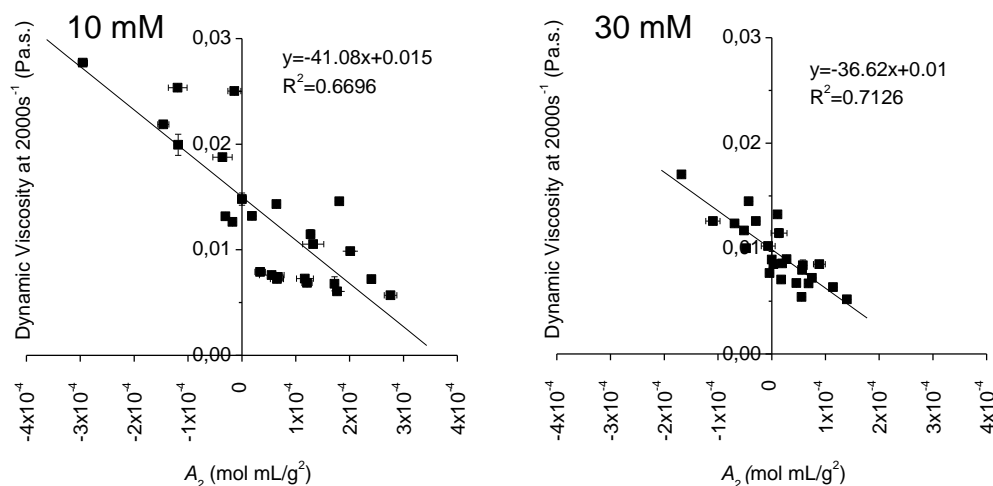


Figure 3.5.41. Dynamic viscosity (Pa.s) versus second virial coefficient A_2 (mol mL/g²) compared at two different ionic strengths (10 and 30 mM). Data shown from mAb4-6, and 8-9. Data are shown as mean of $n=3 \pm$ error of the linear regression (A_2) and as mean of $n=2 \pm$ absolute deviation (dynamic viscosity).

3.6. Assessment of D_m at High mAb Concentration

Along with other experiments the behavior of mutual diffusion coefficient (D_m) at high concentrated protein formulations was analyzed. It was already shown under 3.1.2 that D_m increases/decreases linearly with concentration up to 10 mg/mL. What was not covered so far are experimental results in the non-linear range. What happens if mAb solutions are

analyzed by DLS beyond this linear range can be seen in Figure 3.6.1. The change of D_m over concentration (up to 100 mg/mL) for five mAbs at two different formulation conditions (20 mM His/His-HCl (pH 6.0) \pm 150 mM NaCl) is shown. The figure indicates that at about 30 mg/mL the linearity of D_m over concentration is lost. Negative slopes start to get less negative whereas positive slopes get less positive or even turn negative (mAb4 and mAb6). With the exception of mAb4 and mAb3 that are maybe about to switch position the rank order of D_m at 100 mg/mL follows the rank order at 10mg/mL.

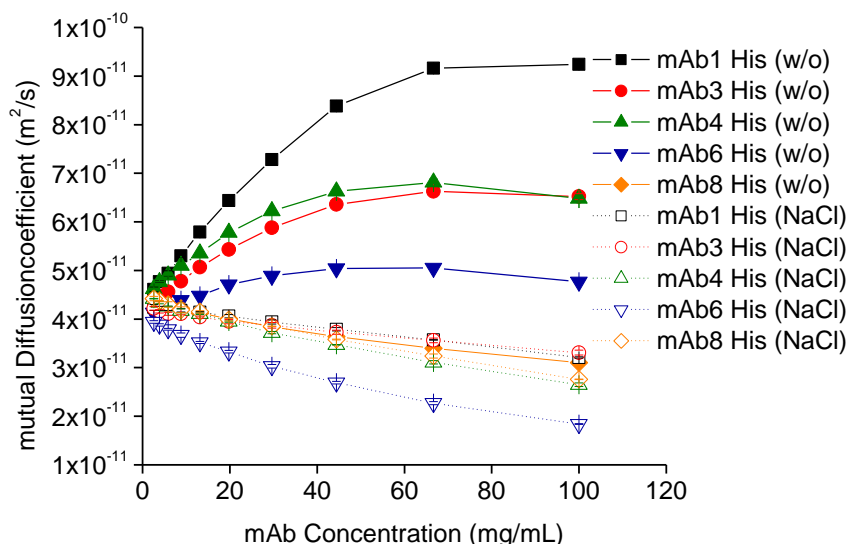


Figure 3.6.1. Change of mutual diffusion coefficient D_m with increasing mAb concentrations showing five different mAbs in two formulation conditions namely 20 mM His/His-HCl (pH 6.0) \pm 150 mM NaCl. Data are shown as mean of $n=3 \pm$ SD

In a second experiment, 5 mAbs formulated at 30 mM ionic strength in various buffer systems (Figure 3.6.2), were compared at 10 mg/mL and at 150 mg/mL. The aim was to find out what happens to the D_m at even higher concentrations as tested in the first experiment (Figure 3.6.1). At 10 mg/mL, depending on the formulation and the mAb, D_m was higher (positive A_2) or lower (negative A_2) than D_0 (i.e. $4.37 \pm 0.13 \times 10^{-11}$ m²/s). At 150 mg/mL all D_m are smaller than D_0 indicating that slopes at some point must have become negative. As already discussed in chapter 3.4 mAbs get less repulsive/more attractive as the buffer ion valence increases and the pH rises. An increase in concentration to 150 mg/mL (looking only at individual mAbs) caused all D_m to be lower than at 10 mg/mL. The overall trend is still the same regarding pH and buffer ion valence. Comparing the different mAbs one sees that on concentration increase the rankorder of mAbs within one condition changes. For example at 10 mg/mL and pH 5.0 (NaAcet) all 5 mAbs are at about the same level of of D_m . When increasing the concentration especially mAb6 and mAb8 have (compared to the others) a low D_m . It was concluded that as conditions get more crowded other short range interactions but no ionic interactions might play a stronger role causing the mAbs to be more attractive. mAb6 for example gets attractive at higher ionic strength indicating also the presence of these shorter range interactions that are not seen at 10 mg/mL. Especially mAb6 was aggregating faster in the stability study, stored at 100 mg/mL as compared to 10 mg/mL (section 3.5.2).

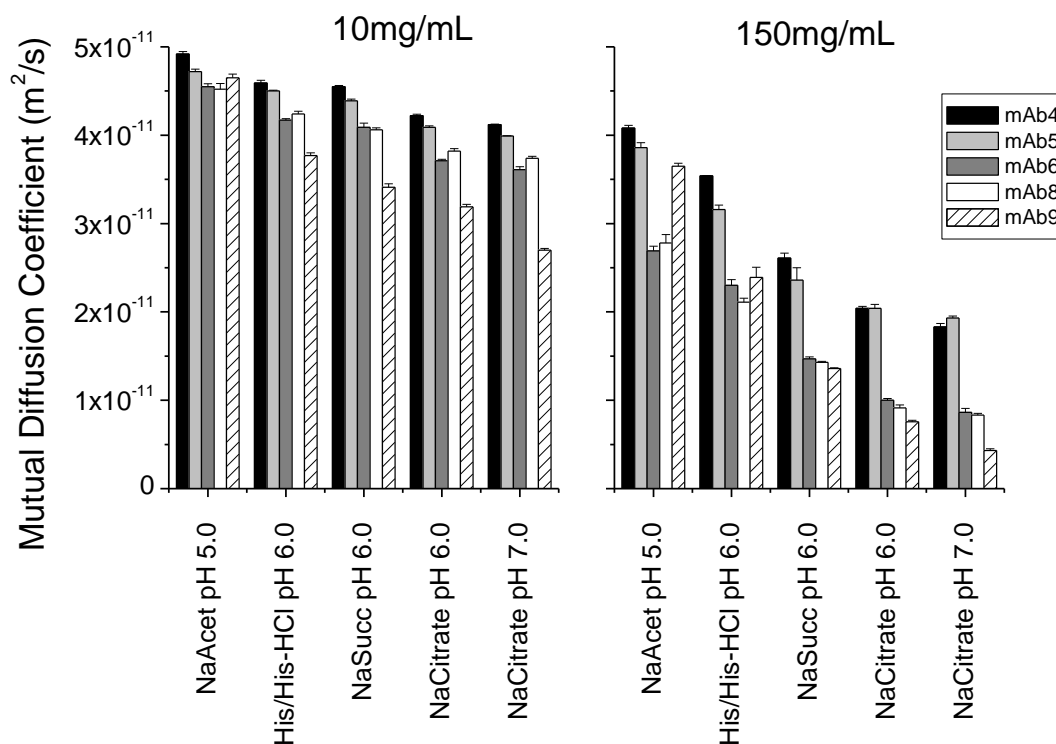


Figure 3.6.2. Mutual diffusion coefficient D_m (m^2/s) of five mAbs (mAb4, mAb5, mAb6, mAb8, and mAb9) at two different mAb concentrations (10 and 150 mg/mL) formulated in five different buffers at an ionic strength of 30 mM. Data are shown as mean of $n=3 \pm \text{SD}$

These results are in contradiction to what is described in polymer literature.²² According to theory after the linear range should be something called cooperative diffusion behavior.²² Especially at good solvent conditions (positive slope) the linear increase of D_m should be followed by a sharper increase.²² In the experiments done, this was not observed (Figure 3.6.1). Instead the slope bends towards a horizontal line (i.e. like a plateau). At higher concentration there are even hints that the curve goes down again (negative slope, Figure 3.6.2). That antibody solutions can get more repulsive as concentration is increased, as it would be expected by a sharp increase in D_m (DLS), was demonstrated by Scherer et al.⁶⁴ There the mAbs tested scattered less light as concentration was increased. As light scattering intensity is directly related to A_2 (3.5.1) this is indirect hint that the conditions switched to more repulsive. Similar to this a higher order interaction like third virial coefficient can be ruled out because it is known in polymer literature that third virial coefficient is positive.⁹⁸ This was however not observed by DLS.

The definition of D_m does not include the viscosity of the solution. It only includes the viscosity of the solvent. The solvent viscosity defines how fast a single molecule at infinite (solute) dilution can diffuse. An increase in solute viscosity would cause D_0 to decrease. Looking at Figure 3.6.3, connecting high concentration D_m data from Figure 3.6.1 to the respective viscosities, there is one important observation ruling this out. The increased ionic strength reduced only mAb8's (and mAb3's) viscosity. This phenomenon was already observed and discussed within the previous section (3.5.4). Still the mutual diffusion coefficient for mAb8 within both formulations is essentially the same. Viscosity differences can therefore be ruled out.

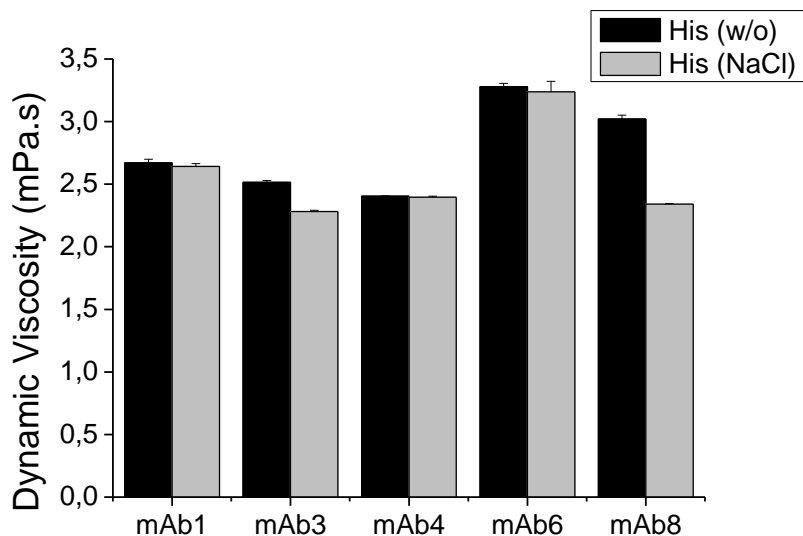


Figure 3.6.3. Dynamic viscosity of five mAbs at 100 mg/mL in two different formulations, namely His (w/o) and His (NaCl). Data are shown as mean of $n=2 \pm$ absolute deviation.

Another possible explanation would be that the DLS device used was not suitable to measure high protein concentration. One could imagine that for example protein at the glass wall interacts with the surface and is slowed down. A possibility to proof this could maybe be a special DLS device that is built differently (e.g. Nanophox by Sympatec, Clausthal-Zellerfeld, Germany). Such a device has two laser beams that enter the sample. Each scattering signal is recorded by one detector. Only the light signals that are reflected from the same particles (within the measurement cell) are analyzed whereas particles e.g. sticking to the glass surface are excluded.^{99,100}

What happens if samples are measured at high protein concentrations is very interesting and it would be worthwhile elaborating on this.

4. SUMMARY AND OUTLOOK

Self-administration of mAbs via the subcutaneous route has become increasingly important. As mAbs are typically dosed in the mg/kg range and because the maximum volume for subcutaneous injection is limited (<1.5 mL)¹ highly concentrated mAb formulations (>100 mg/mL)¹ are required. The challenges often encountered for high-concentration protein formulations are protein aggregation and solution viscosity.²⁻⁵ Self-association and protein-protein interactions, in this context, are believed to play a significant role governing both (non-covalent) aggregation and viscosity^{2-5,7-9}. This was however always based only on limited single observations. The aim of this work was to study both net charge and protein-protein interactions in a series of different mAbs/formulations in context of high concentration stability and viscosity.

First methods had to be developed to measure protein-protein interaction (i.e. the second virial coefficient, A_2). This was achieved in chapter 3.1. A method employing static light scattering (SLS) as well as a method by dynamic light scattering (DLS) could be established. The downside of DLS however was, that, prior to this work, one could not distinguish between positive or negative A_2 , i.e. repulsion or attraction. Direct comparison of SLS and DLS then resulted in a high throughput method that allowed direct assessment of A_2 by DLS. As compared to SLS the DLS method reduced the time and the sample amount needed by a factor of 10. In addition SLS/DLS results, that were published⁶⁵, were found to be comparable to A_2 values published by Connolly et al. based on an DLS/AUC approach⁶⁸.

The purpose of chapter 3.2 was first to compare biophysical properties of different monoclonal antibodies (mAbs). mAbs' theoretical isoelectric point (IEP) as well as theoretical net charge were compared to experimentally assessed values. IEP was determined by isoelectric focusing capillary electrophoresis and determination of zero electrophoretic mobility or the minimum mutual diffusion coefficient (D_m) during pH titration. Net charge was determined using electrophoretic mobility and self diffusion coefficient (D_s). Self diffusion coefficient was determined by converting mutual diffusion coefficient to self diffusion coefficient based on an approach published by Le Bon et al.⁵¹ In addition to that selected formulations were measured by NMR for their self diffusion coefficient. It was found that antibodies differ substantially in their biophysical properties, i.e. in IEP, net charge and zeta potential. Furthermore it could be shown that the self diffusion coefficient decreases as concentration increases. This is in consent with the theory published by Einstein 1905 and could demonstrate the importance of using D_s instead of D_0 (as e.g. by Chase et al¹⁷) in net charge determination. In a next step the importance of these properties was studied with respect to protein-protein interactions. This was achieved by assessing the second virial coefficient (A_2) determined by static and dynamic light scattering (SLS, DLS). It was found that at low ionic strength formulation conditions (20 mM His/His-HCl buffer pH 6.0) proteins' charge is the main driver for overall repulsive protein interaction. At high ionic strength conditions (20 mM His/His-HCl buffer pH 6.0 +150 mM NaCl), where counter-ions are shielding ionic interactions, proteins' repulsive forces were weakened, but to a different extent. It was thought that this is caused by

hydrophobic interactions. To proof this assumption several experimental set-ups were established to measure hydrophobic interactions. Methods used were theoretical calculations based on amino acid sequence, hydrophobic marker binding in electron spin resonance (ESR) and fluorescence, as well as surface tension measurements by pending drop method. The outcome was that neither the fluorescence method nor the ESR method could show a hydrophobicity ranking of the mAbs. In these methods only one mAb was positive with respect to hydrophobicity, i.e. only one mAb showed detectable hydrophobicity. This was however not related to self-interaction (unsuspicious in A_2) but rather due to its affinity to bind a hydrophobic target protein. Surface tension measurement was the only experimental method able to rank order mAbs by their hydrophobicity (surface activity). mAb3 had the highest surface activity/hydrophobicity which is in accordance with the results from fluorescence and ESR. Except for mAb3 surface activity was related to A_2 at respective formulations. This could proof that at high ionic strength, differences in hydrophobicity show up in A_2 measurements. Theoretical hydrophobicity could show which antibodies will have high surface activity in surface tension measurements. So the conclusion was that already the analysis of the full amino acid sequence can give hints on surface activity (hydrophobicity).

Chapter 3.3 focuses on difference in the two immunoglobulin subclasses analyzed. The two subclasses were IgG1 and IgG4. One of the main differences is that IgG4 antibodies have a Lysine exchanged by a Phenylalanine within their Fc region which not only causes loss of effector function but also loss of a positive charge. Next a theoretical charge analysis (based on primary sequence data) of the mAbs revealed that IgG4 mAbs as compared to IgG1 have a much more unevenly distributed charge. Especially at pH 7.0 Fc domains are negative whereas Fab fragments are positive which then might bears dipole momentum. This information was found to be very important in explaining the IgG4 behavior observed in chapters 3.4 and 3.5.

Chapter 3.4 focused on studying protein-protein interactions of mAbs in relevant pH/buffer systems and to understand effect of buffer ionic strength, pH, counter ions and IgG subtype. The A_2 high throughput method, developed in chapter 3.1, paved the way to measuring various formulation conditions. Each of the five different monoclonal antibodies (3xIgG1 and 2xIgG4) were formulated in 127 pharmaceutically applied pH/buffer systems from pH 5.0 to 7.0; in doing so the influence of ionic strength and different buffer ions as well as IgG subclass specific behavior (IgG1 vs. IgG4) was studied. The molar concentrations of the individual buffers were varied to a window of ionic strength from 10 to 50 mM. It was found that pH and especially ionic strength do have a prominent influence on protein interaction. Furthermore the antibodies tested within their subclasses (IgG1 and IgG4) showed comparable behavior at the formulation conditions tested only shifting in their absolute values depending on proteins net charge. However mAbs behavior between the two subclasses was completely different. It was found that for IgG1 protein-protein interactions always moved towards less repulsive/more attractive when increasing ionic strength, whereas IgG4 showed that at low ionic strength condition - especially at pH values close to pH 7.0 - highly attractive behavior was favored and reduced (towards zero) as ionic strength was increased. From this it was concluded that not only repulsive interactions (IgG1) but also highly attractive interactions (IgG4) are caused by ionic forces

(i.e. at low ionic strength conditions) due to unevenly distributed charges as pointed out in chapter 3.3. Finally despite equal ionic strength it was found that divalent buffer anions (succinate) as well as trivalent anions (citrate) decreased repulsion or increased attraction (IgG4) to a larger extent than monovalent (e.g. acetate) anions.

In chapter 3.5 the second virial coefficient A_2 was assessed as a predictive parameter in solutions turbidity, stressed/unstressed protein stability, self-association, and dynamic viscosity. Solutions turbidity was assessed by a turbidimeter. As samples turbidity (i.e. scattering intensity) is related to the A_2 (Debye equation), a previously unknown system constant could be determined resulting in a predictive method allowing an approximation of turbidity values at a defined mAb concentration only using A_2 at the respective formulation condition only.

In a next step a stability study evaluating the influence of A_2 on precipitation/aggregation propensity was carried out. The overall conclusion from the stability study was that temperature stability (5 °C, 25 °C, 40 °C) shows comparable degradation patterns at all temperatures, although the aggregation at elevated temperatures was faster. This finding comforts a formulation scientist as it justifies formulation nomination on accelerated 40 °C data. The protein-protein interaction (A_2) seems to play an important role as it was shown that in low ionic strength formulations generally aggregation is lower for mAbs being more repulsive. Only the two least repulsive mAbs in both conditions tested (His ± NaCl), showed a clear increase in aggregate levels. This supports the theory that a specific threshold of A_2 needs to be reached in order to start protein aggregation.²⁵ This threshold seems to be formulation dependent (±NaCl). The absolute values for aggregate increase, however, did not follow A_2 . At low protein concentration mAb8 always had a higher aggregate increase as compared to mAb6 (His ± NaCl). At high protein concentration aggregation increase was generally higher but mAb6 always had a higher aggregate increase as compared to mAb8. 10 mg/mL might not be comparable to 100 mg/mL data. This stresses out the importance of stability studies at the intended (final product) concentration not overlooking specific effects that cannot be explained by A_2 . The reason for an increased aggregation at high concentrations is, that at more crowded (higher concentrated) solution conditions the likelihood of two particles colliding and aggregating is higher. This then leads to an increased aggregation.¹ The increase in mAbs' turbidity (an indication for particles), to some extent, followed the %HWM increase. However because turbidity is always influenced by A_2 (Equation 25) and this is in theory also valid for the dimers/aggregates formed, comparing absolute increase of turbidity is not straightforward. Although A_2 could not explain the full picture of mAbs temperature storage stability, it was found that more repulsive conditions in the respective formulation have a higher chance for success. This information, especially in combination with the toolbox of modifying A_2 based on chapter 3.4, can be very valuable in a pharmaceutical development. In shaking stress stability it was concluded that additional NaCl had an adverse effect on shaking stability because NaCl shields the electrostatic repulsion of mAbs and therefore reduces A_2 . In respect to mAb specific protein-protein interactions it was concluded that the two least repulsive mAbs were the least stable in regards to shaking. Consistent results between turbidity and %HMW measurements were achieved. Subvisible/visible particle counts were only of limited use because due to the absence of surfactant most results

exceeded the upper limits of the instrumentation. mAbs that have a low A_2 seem to have a lower stability upon shaking stress but high A_2 does not necessarily mean high shaking stability as it was shown by mAb1. This is in contrast to the temperature stability study. Most likely multiple factors are influencing the shaking stability and it could not be pointed down to one single parameter.

Another potential application of A_2 has been explored. Some mAbs show a tendency to reversible self-association/dimerization. The study aimed to elaborate on the relevance of A_2 for dimerization. The study revealed that – at the given design space (i.e. buffer systems at 10-50 mM ionic strength) - likely the surface charge of the mAb (mAb6) itself plays the most important role. At low pH an influence of ionic strength on repulsiveness could be observed and measured by A_2 , however these differences did not translate into dimerization. Likely the protein charge is still high enough to prevent mAb6 from self-association. This changes with increase in pH where one can assume a lower effective net charge. Higher pH has caused higher dimerization for all formulations. Again, the differences seen in A_2 did not translate into dimerization, i.e. for some of the conditions, the most attractive formulation did not show the highest dimer rate. A possible explanation might be that the association of mAb6 is based on a very specific interaction which might be more or less pronounced in some buffer systems. Such specific interactions may not be sufficiently addressed by a global interaction parameter such as A_2 which provides information on the sum of underlying forces and not on a specific interaction. For mAb6 the influence of ionic strength or different buffer valences on dimerization was only minor given a range from 10-50 mM ionic strength at pH values from 5.0 to 7.0.

Also an application of A_2 was to predict viscosity – or at least rank mAbs or formulations in terms of expected viscosity at high concentration. The systems tested were at rather low ionic strength conditions, i.e. 10 and 30 mM ionic strength. It was found that per mAb at a given system, i.e. a given pH/buffer system, the viscosity at high concentration (150 mg/mL) was inverse to A_2 as assessed in low protein concentration. The lower A_2 , the more attractive, the higher viscosity at high concentration. In addition, it was found that di- and trivalent counter ions lower the A_2 , i.e. drive towards less repulsiveness – even at defined ionic strength. After all, the effect of counter ion valence on viscosity in high concentration was only marginal as seen e.g. at pH 6.0. Divalent counter-ions (succinate) and even more trivalent counter-ions (citrate) decrease the repulsiveness of 5 different mAbs as compared to their corresponding His/HisHCl systems. However the viscosity at 150 mg/mL was almost independent the buffer system used. Increasing the ionic strength reduced the viscosity for the two IgG4 mAbs whereas the effect on the three IgG1 mAbs was minor. This might be related to the unequal charge distribution of IgG4 mAbs as shown in chapter 3.3. A_2 is a powerful means to assess the likelihood of attraction and a resulting high viscosity at high concentration; nonetheless a good correlation of k_D (or A_2 (low concentration) with viscosity (high concentration, e.g. 150 mg/mL) cannot be expected.

The final chapter (chapter 3.6) analyzed the non-ideal behavior of mutual diffusion (D_m) as mAb concentration increases. D_m increases/decreases linearly with concentration up to 10 mg/mL. Up to 100 mg/mL this linearity is lost and D_m reached a plateau. In a different experiment it was then shown that at 150 mg/mL all D_m are smaller than D_0 indicating that

all positive slopes at some point must have become negative. It was concluded that as conditions get more crowded other short range interactions but ionic interactions might play a stronger role causing the mAbs to be more attractive. These results are in contradiction to what is described in polymer literature.²² Especially at repulsive conditions repulsion should strongly increase as the solution gets more concentrated (cooperative diffusion). Such a behavior was indicated in literature by SLS experiments where a reduced light scattering intensity at increasing concentrations might give a hint for increased repulsion.⁶⁴ What happens if samples are measured at high protein concentrations within DLS is very interesting and should be further elaborated in future.

The globally assessed parameter A_2 was found to bear valuable information regarding a formulations/mAb's behavior which is important in pharmaceutical development. However some points could not fully be solved. A_2 can be a powerful tool to predict a samples high concentration viscosity. However a good correlation of A_2 and mAb's high concentration viscosity cannot be expected (Figure 3.5.41). As A_2 was assessed at low protein concentration whereas viscosity was measured at up to 150 mg/mL this indicates that maybe in more crowded solutions interaction behavior might differ and therefore further work should elaborate on determination of protein-protein interactions at these conditions. Maybe high concentration DLS measurements can be used for that. Another method that might be interesting when looking at highly concentrated solutions is NMR self-diffusion measurements (D_s). Seeing how diffusion of a single particle changes with increasing concentrations can give information how the derived friction coefficient (ζ_1) changes. This coefficient is only constant at low protein concentrations²², which could be shown (relation k_D to A_2 via Equation 16). Because the change in D_m over concentration (k_D in DLS) is also linked to ζ_1 via Equation 16, one could possibly use this knowledge to better understand high concentration DLS/ A_2 measurements. This work could furthermore conclude that the IgG4 specific behavior as compared to IgG1 was due to an unequal charge distribution (Fab/Fc) that resulted in a possible dipole momentum. To proof this conclusion one should try to experimentally determine this dipole momentum.

5. ZUSAMMENFASSUNG UND AUSBLICK (ÜBERSETZUNG)

Die Häufigkeit mit der sich Patienten selbst therapeutische Antikörper subkutan verabreichen nimmt ständig zu. Da üblicherweise Mengen im mg/kg Bereich notwendig sind, man aber mit dem Maximalvolumen für subkutane Verabreichung limitiert ist ($<1.5 \text{ mL}$)¹, müssen Antikörper immer höher konzentriert werden ($>100 \text{ mg/mL}$). Daraus ergeben sich jedoch Herausforderungen für die Entwicklung solcher Therapeutika. Beispiele sind eine gesteigerte Proteinaggregation sowie erhöhte Viskosität.²⁻⁵ Speziell in diesem Zusammenhang werden oft Selbst-Assoziation und Protein-Protein-Interaktion als mögliche Ursachen genannt, jedoch basierte dies auf Einzelbeobachtungen.^{2-5,7-9} Es war daher das Ziel der Arbeit, sowohl die Nettoladung als auch Protein-Protein-Interaktionen verschiedener Antikörper in möglichst vielen Formulierungen zu bestimmen und zu vergleichen. Anschließend wurde getestet wie die gewonnenen Informationen die Stabilität und Viskosität vorhersagen können.

Als erstes mussten Methoden etabliert werden, die es erlaubten Protein-Protein-Interaktionen zu messen. Dies wird in Kapitel 3.1 gezeigt. Ein Faktor der diese Interaktion widerspiegelt, ist der zweite Virialkoeffizient (A_2), welcher normalerweise über statische Lichtstreuung (SLS) bestimmt wird. Diese Methode und eine weitere basierend auf dynamischer Lichtstreuung (DLS) konnten etabliert werden. Vor dieser Arbeit war es nicht möglich attraktive und abstoßende Protein-Interaktionen mit der DLS Methode zu unterscheiden, man konnte nur eine qualitative Aussage treffen. Der direkte Vergleich von SLS und DLS führte aber zu einer quantitativen DLS Hochdurchsatzmethode. Im Vergleich zur SLS Methode konnte dadurch die Probenmenge sowie die Messzeit um das Zehnfache reduziert werden. Die mit SLS/DLS generierte Ergebnisse, so wie die quantitative DLS A_2 Methode, konnten publiziert werden.⁶⁵ Connolly et al.⁶⁸ zeigten, dass diese vergleichbar waren zu A_2 Messungen basierend auf einer DLS/AUC Methode.

In Kapitel 3.2 wurden biophysikalische Eigenschaften verschiedener Antikörper verglichen. Dazu zählten sowohl der isoelektrische Punkt (IEP) als auch die Nettoladung, welche theoretisch, basierend auf der Primärsequenz und experimentell bestimmt wurden. Der IEP mittels Isoelektrische-Fokussierungs-Kapillar-Elektrophorese und über pH-Titration bestimmt. Um mittels Titration den IEP zu bestimmen, wurde sowohl der Punkt an dem die elektrophoretische Mobilität Null war, als auch der Punkt des geringsten mutualen Diffusionskoeffizienten (D_m) bestimmt. Die Nettoladung wurde mit Hilfe der elektrophoretischen Mobilität und des Selbst-Diffusionskoeffizienten (D_s) gemessen. D_s konnte bestimmt werden indem man eine publizierte Formel (Le Bon et al.⁵¹) anwandte und D_m , gemessen über DLS, in D_s umwandelte. Zusätzlich wurde noch für ausgewählte Proben der Selbst-Diffusionskoeffizient mit NMR bestimmt. Die Schlussfolgerung war, dass Antikörper sich wesentlich in ihren biophysikalischen Eigenschaften unterscheiden (z.B. IEP und Nettoladung). Außerdem konnte gezeigt werden, dass der D_s , wie schon von Einstein 1905 theoretisch beschrieben,⁷¹ abnimmt, wenn die innere Reibung des Systems (die Proteinkonzentration) zunimmt. Es ist daher wichtig D_s anstatt D_0 (wie z.B. bei Chase et al.¹⁷) bei der Nettoladungsbestimmung zu benutzen. Im nächsten Schritt, wurde der Zusammenhang der oben genannten biophysikalischen Eigenschaften in Hinblick auf

Protein-Protein-Interaktion analysiert. Hierfür wurde der zweite Virialkoeffizient (A_2) über SLS und DLS gemessen. Das Ergebnis war, dass Antikörper, welche bei niedriger Ionenstärke formuliert wurden (20 mM His/His-HCl Puffer pH 6.0), in ihrem Abstoßungsverhalten der Nettoladung folgten. Je höher also die Nettoladung, umso abstoßender die Antikörper. Wurden Antikörper hingegen in hoher Ionenstärke formuliert (20 mM His/His-HCl Puffer pH 6.0 + 150 mM NaCl), reduzierte sich die Stärke der Abstoßung in unterschiedlichem Ausmaß und folgte anschließend nicht mehr der Nettoladung. Die Schlussfolgerung daraus war, dass bei niedriger Ionenstärke ionische Wechselwirkungen primär für die Abstoßung verantwortlich sind. Nach Ladungsabschirmung, in hoher Ionenstärke, treten andere, nicht-ionische Wechselwirkungen, stärker in den Vordergrund. Es wurde vermutet, dass hydrophobe Wechselwirkungen dafür verantwortlich sind. Diese nachzuweisen war die Aufgabe im letzten Teil dieses Kapitels. Verschiedene Methoden um speziell Hydrophobizität zu messen, waren: theoretische Berechnungen, das Binden von Hydrophoben Proben basierend auf Fluoreszenz oder Elektronen-Spin-Resonanz (ESR) und die Bestimmung der Oberflächenaktivität mit Hilfe eines Tropfentensimeters. Weder Fluoreszenz- noch ESR konnten eine Rangordnung in Bezug auf Hydrophobizität zeigen. Nur ein Antikörper reagierte positiv auf den hydrophoben Marker/Spinsonde (mAb3). Dies konnte jedoch nicht in Verbindung mit dem A_2 gebracht werden. Das Binden des hydrophoben Markers/Spinsonde wurde vielmehr darauf zurückgeführt, dass der Antikörper gegen ein hydrophobes Ziel gerichtet ist. Versuche mit dem Tropfentensimeter zeigten als einzige experimentelle Methode eine Rangordnung der verschiedenen Antikörper in Bezug auf Hydrophobizität (Oberflächenaktivität). Bis auf mAb3 folgte die Oberflächenaktivität, in der jeweiligen Formulierung, dem A_2 . Dadurch konnte bewiesen werden, dass bei hohen Ionenstärken Unterschiede in der Hydrophobizität sich im A_2 zeigen. Die theoretische Berechnung, basierend auf der Aminosäuresequenz, konnte zeigen, dass theoretisch hoch hydrophobe Antikörper auch experimentell eine höhere Oberflächenaktivität (Hydrophobizität) aufweisen.

Kapitel 3.3 beschäftigt sich mit den Unterschieden der beiden in dieser Arbeit verwendeten Immunglobulin G Klassen (IgG). Diese waren IgG1 und IgG4. Ein Hauptunterschied ist, dass bei IgG4 Antikörpern im Fc Teil ein Lysin durch ein Phenylalanin ersetzt ist. Dies bewirkt nicht nur den Verlust der Immuneffektor-Funktion, sondern bringt auch den Verlust einer positiven Ladung mit sich. Als nächstes wurde die theoretische Ladung (auf der Primärsequenz basierend) analysiert. Es wurde festgestellt, dass IgG4 Antikörper im Vergleich zu IgG1 Antikörpern eine viel ungleichmäßiger verteilte Ladung aufweisen. Speziell bei pH 7.0 zeigte sich, dass der Fc Teil negativ geladen war und der Fab Teil positiv. Es besteht daher die Möglichkeit, dass der Antikörper ein Dipolmoment aufweist. Diese wichtige Information konnte zur Klärung von Effekten beitragen, die in den Kapiteln 3.4 und 3.5 beobachtet wurden.

Es war das Ziel von Kapitel 3.4 Protein-Protein-Interaktionen von Antikörpern in pharmazeutisch relevanten pH/Puffersystemen zu analysieren und zu verstehen. Die Effekte verschiedener Pufferionenstärken, pH-Werten, Ionen-Wertigkeiten und IgG Unterklassen (IgG1 und IgG4) wurden dabei untersucht. Dies war nur möglich durch Anwendung der hochdurchsatz A_2 Methode welche in Kapitel 3.1 entwickelt wurde. Fünf

Antikörper, darunter 3xIgG1 und 2xIgG4, wurden in jeweils 127 pharmazeutisch relevanten pH/Puffersystemen zwischen pH 5.0 und pH 7.0 formuliert. Die Ionenstärke der Puffer wurde dabei zwischen 10 und 50 mM variiert. Es wurde festgestellt, dass der pH und besonders die Ionenstärke die Protein-Protein-Interaktionen stark beeinflussen, es aber Unterschiede zwischen den beiden IgG Unterklassen gibt. IgG1 Antikörper wurden mit höherer Ionenstärke immer weniger abstoßend/stärker anziehend, weil repulsive ionische-Wechselwirkungen abgeschirmt wurden. Eine pH Änderung in Richtung IEP (=Verringerung der Nettoladung) bewirkte dasselbe. Hingegen zeigten IgG4 Antikörper speziell bei niedriger Ionenstärke entweder repulsive oder attraktive Wechselwirkungen. Dies konnte auf Effekte, die in Kapitel 3.3. beschrieben sind, zurückgeführt werden. Bei niedrigem pH sind sowohl Fc als auch Fab positiv geladen, was eine Abstoßung bei geringer Pufferionenstärke bewirkt. Bei hohem pH entstehen jedoch durch das Dipolmoment ionisch attraktive Wechselwirkungen. Sowohl attraktive als auch abstoßende Wechselwirkungen konnten bei IgG4 Antikörpern durch eine Erhöhung der Ionenstärke in Richtung Null-Wechselwirkung verändert werden. Unterschiede von Antikörpern in Bezug auf ihre maximalen attraktiven/anziehenden Wechselwirkungen konnten auf die Nettoladung zurückgeführt werden. Je höher geladen umso stärker diese Wechselwirkungen. Es konnte außerdem festgestellt werden, dass mehrwertige Pufferionen (Sukzinat und Zitrat) im Vergleich zu einwertigen (z.B. Azetat) die Abstoßung stärker verringern bzw. die Anziehung (IgG4) erhöhen.

Kapitel 3.5 beschäftigte sich mit der Relevanz von A_2 als prädiktiver Parameter. Es wurde untersucht wie Protein-Protein-Interaktionen die Trübung, die Stabilität und die dynamische Viskosität einer Proteinlösung beeinflussen. Außerdem wurde untersucht wie sich A_2 auf die Selbstassoziation auswirkt. Die Trübung (=Lichtstreuintensität) verschiedener Lösungen wurde mittels Trübungsmessgeräts untersucht. Da die Lichtstreuintensität und der A_2 über die Debye-Gleichung zusammenhängen, konnte diese benutzt werden, um die Systemkonstante der Gleichung für das Trübungsmessgerät zu bestimmen. Dies machte es möglich mittels des gemessenen A_2 -Wertes und der Konzentration der Formulierung die Trübung abzuschätzen.

Um den Einfluss von A_2 auf die Proteinstabilität zu untersuchen, wurde eine Stabilitätsstudie durchgeführt. Generell konnte festgestellt werden, dass bei der Lagerung bei verschiedenen Temperaturen (5 °C, 25 °C und 40 °C) vergleichbare Abbaumuster auftraten, diese waren bei höheren Temperaturen stärker. Dieses Ergebnis ist für die Formulierungsentwicklung sehr wichtig, weil hauptsächlich Formulierungs-Entscheidungen auf 40 °C Daten beruhen. Protein-Protein-Interaktionen (A_2) spielen eine wichtige Rolle. Es konnte gezeigt werden, dass generell die Proteinaggregation in Formulierungen/bei Antikörpern mit höherem A_2 geringer ist. Nur die zwei Antikörper mit dem geringsten A_2 in der jeweiligen Bedingung (His \pm NaCl) zeigten einen deutlichen Anstieg in ihrem Aggregationsverhalten. Dies unterstützt die Theorie, dass ein bestimmter Schwellenwert notwendig ist, damit Aggregation stattfindet.²⁵ Dieser Schwellenwert schien abhängig von der jeweiligen Formulierung zu sein (\pm NaCl). Der Anstieg der Aggregationswerte folgte jedoch nicht dem A_2 . Zwar hatte bei geringer Proteinkonzentration mAb8 immer einen höheren Aggregatzuwachs im Vergleich zu mAb6, jedoch bei hoher Proteinkonzentration war dies genau umgekehrt. 10 mg/mL Stabilitätsdaten sind daher nicht immer vergleichbar

zu 100 mg/mL Daten. Dies zeigte, wie wichtig es ist in der Formulierungsentwicklung Stabilitätsstudien bei der finalen Konzentration durchzuführen, um spezifische Unterschiede zu sehen, welche nicht über den reinen A_2 erklärt werden können. Die Erklärung für die Konzentrationsabhängigkeit der Aggregation ist, dass bei höher konzentrierten Lösungen die Wahrscheinlichkeit, dass zwei Partikel zusammenstoßen und aggregieren, größer ist.¹ Der Anstieg in der Trübung der Formulierungen folgte teilweise den Aggregationswerten. Da aber die Trübung immer vom A_2 beeinflusst wird (Gleichung 25) und dies theoretisch auch für Dimere/Aggregate gilt, ist ein direkter Vergleich über die Änderung der Trübung nicht einfach. Obwohl A_2 nicht komplett das Stabilitätsverhalten von Antikörpern bei Temperaturlagerstabilität erklären konnte, wurde gezeigt, dass Antikörper, welche in der jeweiligen Formulierung höheren A_2 aufweisen, mit höherer Wahrscheinlichkeit stabiler sind. Diese Information im Zusammenhang mit den Möglichkeiten, welche in Kapitel 3.4 aufgezeigt wurden A_2 zu modifizieren, kann für eine pharmazeutische Entwicklung sehr wertvoll sein. Schüttelstresstudies konnten zeigen, dass generell die Zugabe von NaCl, welches repulsive ionische Wechselwirkungen abschirmt, die Schüttelstabilität verringert. Wiederum wiesen die zwei Antikörper mit dem geringsten A_2 in beiden Formulierungen (His \pm NaCl) die geringste Stabilität auf. Es wurden vergleichbare Ergebnisse bei der Änderung der Trübung (als Anzeichen von Partikeln) und der %HMW erzielt. Subvisuelle/Visuelle Partikelmethode waren nur von geringer Aussagekraft. Weil die Formulierungen kein Tensid beinhalten, überstiegen die Ergebnisse meistens das maximale Limit der jeweiligen Methode. Nicht nur die zwei Antikörper mit dem geringsten, sondern auch der Antikörper mit dem höchsten A_2 wiesen eine verringerte Schüttelstabilität auf. Dies bildet einen Kontrast zur Temperaturlagerstabilität. Vermutlich spielen mehrere Faktoren als nur der reine A_2 eine Rolle in der Schüttelstabilität.

Der nächste Zusammenhang, der in Verbindung mit A_2 erforscht wurde, war reversible Selbstassoziation/Dimerisation. Die Studie kam zu dem Schluss, dass – begrenzt durch die Versuchsbedingungen (verschiedene Puffer bei 10-50 mM Ionenstärke) – die Oberflächenladung des Antikörpers (mAb6) die wichtigste Rolle spielt. Bei niedrigem pH-Wert konnte zwar ein Einfluss auf A_2 festgestellt werden, jedoch hatte dies keinen Einfluss auf die Dimerisation. Es ist möglich, dass die Proteinladung noch hoch genug war, um Selbstassoziation von mAb6 zu verhindern. Dies ändert sich wenn man den pH-Wert erhöht. Durch die verringerte Nettoladung, erhöht sich die Dimerisation. Dies konnte wieder nicht mit dem A_2 in Verbindung gebracht werden, weil speziell die negativsten A_2 Werte nicht mit der höchsten Dimerisation zusammenhängen. Eine mögliche Erklärung könnte sein, dass die Selbstassoziation von mAb6 auf einem sehr speziellen Mechanismus basiert, welcher in verschiedenen Puffersystemen mehr oder weniger hervorgehoben wird. Dies kann über den globalen Interaktionsparameter A_2 nicht wiedergegeben werden. Der Einfluss von Ionenstärke (10-50 mM) und Formulierungspuffer im getesteten pH-Bereich (5.0-7.0) auf die Dimerisation war daher vernachlässigbar.

Eine weitere Anwendung von A_2 war die Vorhersage von Viskosität bzw. das Erstellen einer Rangordnung von Antikörpern oder Formulierungen in Bezug auf ihre zu erwartende Viskosität bei Proteinkonzentrationen. Dabei wurden Systeme mit relativ geringer

Ionenstärke getestet (10-30 mM). Das Ergebnis war, dass für die getesteten Antikörper, in einem gegebenen System (pH/Puffer), die Viskosität bei 150 mg/mL sich invers zum A_2 , gemessen bei geringer Proteinkonzentration, verhält. Je geringer der A_2 umso höher die Viskosität. Obwohl der A_2 stark von den gewählten Pufferionen (einwertig, zweiwertig oder dreiwertig) beeinflusst wurde, war der Einfluss auf die Viskosität marginal. Wie bei pH 6.0 gezeigt wurde, verringerten zweiwertige Pufferionen (Sukzinat) und dreiwertige Pufferionen (Zitrat) den A_2 für alle fünf Antikörper stark. Auf die Viskosität hatte dies aber nur geringen Einfluss. Eine Erhöhung der Ionenstärke half die Viskosität der beiden getesteten IgG4 mAbs zu verringern. Dieser Effekt konnte bei den drei getesteten IgG1 mAbs vernachlässigt werden. Dies könnte mit der ungleichen Ladungsverteilung von IgG4 mAbs zusammenhängen (siehe Kapitel 3.3). A_2 ist ein mächtiges Werkzeug, um die Viskosität bei hohen Proteinkonzentrationen vorherzusehen, jedoch eine gute Korrelation von A_2 und der Viskosität (bei 150 mg/mL) ist nicht zu erwarten.

Im letzten Kapitel (Kapitel 3.6) wird das nicht-ideale Verhalten des mutualen Diffusionskoeffizienten (D_m) bei steigenden Antikörperkonzentrationen untersucht. In Kapitel 3.1.2 wurde gezeigt, dass sich D_m gegenüber der Konzentration bis 10 mg/mL linear verhält. Bei höherer Konzentration geht dieser lineare Zusammenhang verloren. Es wurde gezeigt, dass bis 100 mg/mL die Steigung abflacht und sich der D_m gegenüber der Konzentration kaum noch verändert. Ein weiteres Experiment zeigte dann, dass bei 150 mg/mL alle gemessenen D_m niedriger sind als D_0 . Dies bedeutet, dass speziell alle positive Steigungen sich ins Negative verändert haben müssen. Daraus wurde geschlossen, dass in konzentrierteren Lösungen Kurzstanz-Wechselwirkungen eine stärkere Rolle spielen müssen. Diese verursachen eine erhöhte Anziehung der Antikörper. Dieses Ergebnis widerspricht der Polymerliteratur.²² Speziell bei repulsiven Bedingungen sollte die Abstoßung stark erhöht werden, wenn die Proteinkonzentration steigt. Dieser Effekt nennt sich kooperative Diffusion. Hinweise auf eine solche stärkere Abstoßung mit erhöhter Konzentration kann man aus einer Publikation von Scherer et al ziehen, da dort die Lichtstreuung (die mit der Protein-Interaktion zusammenhängt) mit erhöhter Konzentration abnahm.⁶⁴ Die Ergebnisse, welche in hohen Proteinkonzentrationen in DLS erzielt wurden, sind interessant und sollten auf jeden Fall weiter untersucht werden.

Es stellte sich in dieser Arbeit heraus, dass der bei geringen Konzentrationen analysierte durchschnittliche Interaktionskoeffizient A_2 wertvolle Auskünfte über das Verhalten von Formulierungen/Antikörpern geben kann. Dies ist wichtig in der pharmazeutischen Entwicklung, insbesondere Formulierungsentwicklung. Obwohl jedoch über A_2 ein genereller Trend zur Viskosität einer hochkonzentrierten Antikörperlösung gezeigt werden konnte, war die direkte Korrelation, dieser beiden Faktoren nicht besonders stark. Nachdem A_2 bei geringen Proteinkonzentrationen bestimmt wurde, die Viskosität aber bei 150 mg/mL gemessen wurde, gibt dies womöglich Hinweise darauf, dass in stärker konzentrierten Lösungen sich das Interaktionsverhalten verändert. Weiterführende Experimente sollten daher versuchen dieses Interaktionsverhalten auch in höher konzentrierten Lösungen zu analysieren. Vielleicht können hierfür DLS Messungen in hohen Proteinkonzentrationen herangezogen werden. Eine weitere Methode, um das Verhalten hochkonzentrierter Lösungen zu analysieren, könnte die NMR Selbst-Diffusionsmessung (D_s) sein. Das Studium des Verhaltens von D_s könnte zeigen, wie sich

bei hohen Konzentrationen der abgeleitete Reibungskoeffizient (ζ_1) verändert. Dieser ist nämlich nur bei geringen Antikörperkonzentrationen konstant,²² was auch gezeigt werden konnte (Verhältnis A_2 zu k_D über Gleichung 16). Da also die Änderung von D_m über die Konzentration (k_D in DLS) mit dem Reibungskoeffizienten zusammenhängt (Gleichung 16), könnte dieser vielleicht verwendet werden, um DLS/ A_2 Messungen bei hohen Konzentrationen besser zu verstehen. Eine weitere Schlussfolgerung dieser Arbeit war, dass das unterschiedliche Verhalten von IgG4 zu IgG1 Antikörpern auf die verschiedene Ladungsverteilung (Fab/Fc) zurückzuführen war, was vermutlich ein Dipolmoment zur Folge hatte. Um diese Schlussfolgerung beweisen zu können, sollte versucht werden, das Dipolmoment von Antikörpern zu messen.

6. REFERENCES

Parts of the thesis have already been published: Lehermayr C, Mahler H-C, Mäder K, Fischer S 2011. Assessment of net charge and protein–protein interactions of different monoclonal antibodies. *Journal of pharmaceutical sciences* 100(7):2551-2562.

1. Shire SJ, Shahrokh Z, Liu J 2004. Challenges in the development of high protein concentration formulations. *J Pharm Sci* 93(6):1390-1402.
2. Kanai S, Liu J, Patapoff TW, Shire SJ 2008. Reversible self-association of a concentrated monoclonal antibody solution mediated by Fab-Fab interaction that impacts solution viscosity. *J Pharm Sci* 97(10):4219-4227.
3. Liu J, Nguyen MDH, Andya JD, Shire SJ 2005. Reversible self-association increases the viscosity of a concentrated monoclonal antibody in aqueous solution. *J Pharm Sci* 94(9):1928-1940.
4. Sukumar M, Doyle BL, Combs JL, Pekar AH 2004. Opalescent appearance of an IgG1 antibody at high concentrations and its relationship to noncovalent association. *Pharmaceut Res* 21(7):1087-1093.
5. Yadav S, Liu J, Shire SJ, Kalonia DS 2009. Specific interactions in high concentration antibody solutions resulting in high viscosity. *J Pharm Sci* 99(3):1152-1168.
6. Saluja A, Fesinmeyer RM, Hogan S, Brems DN, Gokarn YR 2010. Diffusion and Sedimentation Interaction Parameters for Measuring the Second Virial Coefficient and Their Utility as Predictors of Protein Aggregation. *Biophys J* 99(8):2657-2665.
7. Alford JR, Kendrick BS, Carpenter JF, Randolph TW 2008. High concentration formulations of recombinant human interleukin-1 receptor antagonist: II. Aggregation kinetics. *J Pharm Sci* 97(8):3005-3021.
8. Bajaj H, Sharma VK, Badkar A, Zeng D, Nema S, Kalonia DS 2006. Protein structural conformation and not second virial coefficient relates to long-term irreversible aggregation of a monoclonal antibody and ovalbumin in solution. *Pharmaceut Res* 23(6):1382-1394.
9. Lawrence MS, Phillips KJ, Liu DR 2007. Supercharging Proteins Can Impart Unusual Resilience. *J Am Chem Soc* 129(33):10110-10112.
10. Jachimska B, Wasilewska M, Adamczyk Z 2008. Characterization of Globular Protein Solutions by Dynamic Light Scattering, Electrophoretic Mobility, and Viscosity Measurements. *Langmuir* 24(13):6866-6872.
11. Cleland JL, Powell MF, Shire SJ 1993. The development of stable protein formulations: a close look at protein aggregation, deamidation, and oxidation. *Crit Rev Ther Drug Carrier Syst* 10(4):307-377.
12. Rice P, Longden I, Bleasby A 2000. EMBOSS: The European molecular biology open software suite. *Trends in Genetics* 16(6):276-277.

13. He XPZ, Que AH, Mo JJ 2009. Analysis of charge heterogeneities in mAbs using imaged CE. *Electrophoresis* 30(5):714-722.
14. Winzor DJ 2004. Determination of the net charge (valence) of a protein: a fundamental but elusive parameter. *Anal Biochem* 325(1):1-20.
15. Tanford C. 1961. *Physical Chemistry of Macromolecules*. ed., New York: John Wiley & Sons, Inc. p 710.
16. Henry DC 1931. The Cataphoresis of Suspended Particles. Part I. The Equation of Cataphoresis. *Proc R Soc Lond A* (133):106-129.
17. Chase S, Laue T 2008. The Determination of Protein Valence by Capillary Electrophoresis. *P/ACE Setter* 12(03.11.2009):1-5.
18. Moody TP, Kingsbury JS, Durant JA, Wilson TJ, Chase SF, Laue TM 2005. Valence and anion binding of bovine ribonuclease A between pH 6 and 8. *Anal Biochem* 336(2):243-252.
19. Durant JA, Chen C, Laue TM, Moody TP, Allison SA 2002. Use of T4 lysozyme charge mutants to examine electrophoretic models. *Biophys Chem* 101:593-609.
20. Chi EY, Krishnan S, Kendrick BS, Chang BS, Carpenter JF, Randolph TW 2003. Roles of conformational stability and colloidal stability in the aggregation of recombinant human granulocyte colony-stimulating factor. *Protein Sci* 12(5):903-913.
21. Atkins P, De Paula J. 2006. *Atkins' Physical Chemistry*. 8 ed., Oxford, United Kingdom: Oxford University Press. p 1064.
22. Teraoka I. 2002. *Polymer Solutions*. 1 ed., New York: John Wiley & Sons, Inc. p 338.
23. Ho JG, Middelberg AP, Ramage P, Kocher HP 2003. The likelihood of aggregation during protein renaturation can be assessed using the second virial coefficient. *Protein Sci* 12(4):708-716.
24. Crisman RI, Randolph TW 2009. Refolding of Proteins From Inclusion Bodies Is Favored by a Diminished Hydrophobic Effect at Elevated Pressures. *Biotechnol Bioeng* 102(2):483-492.
25. George A, Chiang Y, Guo B, Arabshahi A, Cai Z, Wilson WW 1997. Second virial coefficient as predictor in protein crystal growth. *Method Enzymol* 276:100-110.
26. Valente JJ, Verma KS, Manning MC, Wilson WW, Henry CS 2005. Second virial coefficient studies of cosolvent-induced protein self-interaction. *Biophys J* 89(6):4211-4218.
27. Deszczynski M, Harding SE, Winzor DJ 2006. Negative second virial coefficients as predictors of protein crystal growth: Evidence from sedimentation equilibrium studies that refutes the designation of those light scattering parameters as osmotic virial coefficients. *Biophys Chem* 120(2):106-113.
28. Wilson WW 2003. Light scattering as a diagnostic for protein crystal growth - A practical approach. *J Struct Biol* 142(1):56-65.
29. Liu W, Cellmer T, Keerl D, Prausnitz JM, Blanch HW 2005. Interactions of lysozyme in guanidinium chloride solutions from static and dynamic light-scattering measurements. *Biotechnol Bioeng* 90(4):482-490.

30. Bajaj H, Sharma VK, Kalonia DS 2004. Determination of second virial coefficient of proteins using a dual-detector cell for simultaneous measurement of scattered light intensity and concentration in SEC-HPLC. *Biophys J* 87(6):4048-4055.
31. Winzor DJ, Deszczynski M, Harding SE, Wills PR 2007. Nonequivalence of second virial coefficients from sedimentation equilibrium and static light scattering studies of protein solutions. *Biophys Chem* 128(1):46-55.
32. Moon YU, Anderson CO, Blanch HW, Prausnitz JM 2000. Osmotic pressures and second virial coefficients for aqueous saline solutions of lysozyme. *Fluid Phase Equilib* 168(2):229-239.
33. Bajaj H, Sharma VK, Kalonia DS 2007. A high-throughput method for detection of protein self-association and second virial coefficient using size-exclusion chromatography through simultaneous measurement of concentration and scattered light intensity. *Pharm Res-Dordr* 24(11):2071-2083.
34. Monera OD, Sereda TJ, Zhou NE, Kay CM, Hodges RS 1995. Relationship of sidechain hydrophobicity and α -helical propensity on the stability of the single-stranded amphipathic α -helix. *J Pept Sci* 1(5):319-329.
35. Sereda TJ, Mant CT, Sönnichsen FD, Hodges RS 1994. Reversed-phase chromatography of synthetic amphipathic α -helical peptides as a model for ligand/receptor interactions Effect of changing hydrophobic environment on the relative hydrophilicity/hydrophobicity of amino acid side-chains. *J Chromatogr A* 676(1):139-153.
36. Togashi DM, Ryder AG 2008. A fluorescence analysis of ANS bound to bovine serum albumin: Binding properties revisited by using energy transfer. *J Fluoresc* 18(2):519-526.
37. Hawe A, Sutter M, Jiskoot W 2008. Extrinsic fluorescent dyes as tools for protein characterization. *Pharm Res* 25(7):1487-1499.
38. Saitoh T, Taguchi K, Hiraide M 2002. Evaluation of hydrophobic properties of sodium dodecylsulfate/gamma-alumina admicelles based on fluorescence spectra of N-phenyl-1-naphthylamine. *Anal Chim Acta* 454(2):203-208.
39. Ofori P, Firth B, O'Brien G, McNally C, Nguyen AV 2010. Assessing the Hydrophobicity of Petrographically Heterogeneous Coal Surfaces. *Energ Fuel* 24(11):5965-5971.
40. Chari R, Jerath K, Badkar AV, Kalonia DS 2009. Long- and short-range electrostatic interactions affect the rheology of highly concentrated antibody solutions. *Pharmaceut Res* 26(12):2607-2618.
41. Moore JMR, Patapoff TW, Cromwell MEM 1999. Kinetics and thermodynamics of dimer formation and dissociation for a recombinant humanized monoclonal antibody to vascular endothelial growth factor. *Biochem* 38(42):13960-13967.
42. Dean JA. 1999. *Lange's Handbook of Chemistry*. 15th ed., Columbus, OH: McGraw-Hill. p 1521.
43. Petrucci RH, Harwood WS, Herring FG. 1997. *General Chemistry*. 8th ed., New Jersey: Prentice Hall. p 1160.
44. Reginald HG, Charles MG. 2008. *Biochemistry*. 4 ed.: Brooks Cole Pub Co. p 1059

45. Beynon RJ 1988. A Macintosh Hypercard stack for calculation of thermodynamically-corrected buffer recipes. *Cabios* 4(4):487-490.
46. Kolhe P, Amend E, Singh SK 2010. Impact of Freezing on pH of Buffered Solutions and Consequences for Monoclonal Antibody Aggregation. *Biotechnol Progr* 26(3):727-733.
47. Day RA, Underwood AL. 1980. *Quantitative Analysis*. 4th ed., New Jersey: Prentice-Hall: Englewood Cliffs.
48. Angal S, King DJ, Bodmer MW, Turner A, Lawson ADG, Roberts G, Pedley B, Adair JR 1993. A single amino acid substitution abolishes the heterogeneity of chimeric mouse/human (IgG4) antibody. *Mol Immunol* 30(1):105-108.
49. Knappik A, Ge L, Honegger A, Pack P, Fischer M, Wellenhofer G, Hoess A, Wölle J, Plückthun A, Virnekäs B 2000. Fully synthetic human combinatorial antibody libraries (HuCAL) based on modular consensus frameworks and CDRs randomized with trinucleotides. *J Mol Biol* 296(1):57-86.
50. Scalettar BA, Abney JR, Owicki JC 1988. Theoretical comparison of the self diffusion and mutual diffusion of interacting membrane proteins. *Proc Natl Acad Sci USA* 85(18):6726-6730.
51. Le Bon C, Nicolai T, Kuil ME, Hollander JG 1999. Self-diffusion and cooperative diffusion of globular proteins in solution. *J Phys Chem B* 103(46):10294-10299.
52. Duda JL, Ni YC, Vrentas JS 1979. Equation Relating Self-Diffusion and Mutual Diffusion-Coefficients in Polymer-Solvent Systems. *Macromolecules* 12(3):459-462.
53. Jossang T, Feder J, Rosenqvist E 1988. Photon-Correlation Spectroscopy of Human-IgG. *J Protein Chem* 7(2):165-171.
54. Stoner MR, Fischer N, Nixon L, Buckel S, Benke M, Austin F, Randolph TW, Kendrick BS 2004. Protein-solute interactions affect the outcome of ultrafiltration/diafiltration operations. *J Pharm Sci* 93(9):2332-2342.
55. Demeule B, Lawrence MJ, Drake AF, Gurny R, Arvinte T 2007. Characterization of protein aggregation: The case of a therapeutic immunoglobulin. *Biochim Biophys Acta* 1774(1):146-153.
56. Hartmann WK, Saptharishi N, Yang XY, Mitra G, Soman G 2004. Characterization and analysis of thermal denaturation of antibodies by size exclusion high-performance liquid chromatography with quadruple detection. *Anal Biochem* 325(2):227-239.
57. Lucas LH, Larive CK 2004. Measuring ligand-protein binding using NMR diffusion experiments. *Concept Magnetic Res A* 20A(1):24-41.
58. Germann MW, Turner T, Allison SA 2007. Translational diffusion constants of the amino acids: Measurement by NMR and their use in modeling the transport of peptides. *J Phys Chem A* 111(8):1452-1455.
59. Yeow YL, Pepperell CJ, Sabturani FM, Leong YK 2008. Obtaining surface tension from pendant drop volume and radius of curvature at the apex. *Colloid Surface A* 315(1-3):136-146.
60. Kiese S, Pappenberger A, Friess W, Mahler HC 2008. Shaken, not stirred: Mechanical stress testing of an IgG1 antibody. *J Pharm Sci* 97(10):4347-4366.

61. Kishore RSK, Kiese S, Fischer S, Pappenberger A, Grauschopf U, Mahler HC 2011. The Degradation of Polysorbates 20 and 80 and its Potential Impact on the Stability of Biotherapeutics. *Pharm Res* 28(5):1194-1210.
62. Bartsch HJ. 1994. Taschenbuch mathematischer Formeln. 16 ed., Leipzig, Germany: Hanser Verlag. p 832.
63. George A, Wilson WW 1994. Predicting protein crystallization from a dilute solution property. *Acta Crystallogr D* 50(4):361-365.
64. Scherer TM, Liu J, Shire SJ, Minton AP 2010. Intermolecular Interactions of IgG1 Monoclonal Antibodies at High Concentrations Characterized by Light Scattering. *J Phys Chem B* 114(40):12948-12957.
65. Lehermayr C, Mahler H-C, Mäder K, Fischer S 2011. Assessment of net charge and protein-protein interactions of different monoclonal antibodies. *J Pharm Sci* 100(7):2551-2562.
66. Yamakawa H 1962. Concentration Dependence of the Frictional Coefficient of Polymers in Solution. *J Chem Phys* 36(11):2995-3001.
67. Frost RA, Caroline D 1977. Diffusion of Polystyrene in a Theta Mixed Solvent (Benzene-2-Propanol) by Photon-Correlation Spectroscopy. *Macromolecules* 10(3):616-618.
68. Connolly BD, Petry C, Yadav S, Demeule B, Ciaccio N, Moore JMR, Shire SJ, Gokarn YR 2012. Weak Interactions Govern the Viscosity of Concentrated Antibody Solutions: High-Throughput Analysis Using the Diffusion Interaction Parameter. *Biophys J* 103(1):69-78.
69. Lawson EQ, Hedlund BOE, Ericson ME, Mood DA, Litman GW, Middaugh R 1983. Effect of carbohydrate on protein solubility. *Arch Biochem Biophys* 220(2):572-575.
70. Reis RA, Nobrega R, Oliveira JV, Tavares FW 2005. Self- and mutual diffusion coefficient equation for pure fluids, liquid mixtures and polymeric solutions. *Chem Eng Sci* 60(16):4581-4592.
71. Einstein A. 1905. Eine neue Bestimmung der Moleküldimensionen. *Mathematisch-Naturwissenschaftliche Sektion*, ed., Zürich: Universität Zürich. p 21.
72. Piaggio MV, Peirotti MB, Deiber JA 2005. Effect of background electrolyte on the estimation of protein hydrodynamic radius and net charge through capillary zone electrophoresis. *Electrophoresis* 26(17):3232-3246.
73. Grimsley GR, Scholtz JM, Pace CN. 2009. A summary of the measured pK values of the ionizable groups in folded proteins. ed.: Wiley Online Library. p 247-251.
74. Gokarn YR, Fesinmeyer RM, Saluja A, Cao S, Dankberg J, Goetze A, Remmele RL, Narhi LO, Brems DN 2009. Ion-specific modulation of protein interactions: Anion-induced, reversible oligomerization of a fusion protein. *Protein Sci* 18(1):169-179.
75. Loh B, Grant C, Hancock RE 1984. Use of the fluorescent probe 1-N-phenylnaphthylamine to study the interactions of aminoglycoside antibiotics with the outer membrane of *Pseudomonas aeruginosa*. *Antimicrob Agents Ch* 26(4):546-551.
76. Smith EL, Coy NH 1946. The absorption spectra of immune proteins. *J Biol Chem* 164(1):367.

77. Orner BP, Liu L, Murphy RM, Kiessling LL 2006. Phage Display Affords Peptides that Modulate β -Amyloid Aggregation. *J Am Chem Soc* 128(36):11882-11889.
78. Mahler H-C, Senner F, Maeder K, Mueller R 2009. Surface activity of a monoclonal antibody. *J Pharm Sci* 98(12):4525-4533.
79. Führling C. 2004. Interactions between Proteins, Sugars and Surfactants - Dynamic Studies on Adsorption at Interfaces. *Naturwissenschaftliche Fakultät, ed., Nürnberg: Friedrich-Alexander-Universität Erlangen.* p 161.
80. Lau H, Pace D, Yan B, McGrath T, Smallwood S, Patel K, Park J, Park SS, Latypov RF 2010. Investigation of degradation processes in IgG1 monoclonal antibodies by limited proteolysis coupled with weak cation-exchange HPLC. *J Chromatogr B* 878(11-12):868-876.
81. Zhang W, Marzilli LA, Rouse JC, Czupryn MJ 2002. Complete disulfide bond assignment of a recombinant immunoglobulin G4 monoclonal antibody. *Anal Biochem* 311(1):1-9.
82. Jiang X-R, Song A, Bergelson S, Arroll T, Parekh B, May K, Chung S, Strouse R, Mire-Sluis A, Schenerman M 2011. Advances in the assessment and control of the effector functions of therapeutic antibodies. *Nat Rev Drug Discov* 10(2):101-111.
83. Lund J, Winter G, Jones PT, Pound JD, Tanaka T, Walker MR, Artymiuk PJ, Arata Y, Burton DR, Jefferis R, Woof JM 1991. Human Fc gamma RI and Fc gamma RII interact with distinct but overlapping sites on human IgG. *J Immunol* 147(8):2657-2662.
84. Stubenrauch K, Wessels U, Regula JT, Kettenberger H, Schleypen J, Kohnert U 2010. Impact of Molecular Processing in the Hinge Region of Therapeutic IgG4 Antibodies on Disposition Profiles in Cynomolgus Monkeys. *Drug Metab Dispos* 38(1):84-91.
85. Zhou J, Tsao H-K, Sheng Y-J, Jiang S 2004. Monte Carlo simulations of antibody adsorption and orientation on charged surfaces. *J Chem Phys* 121(2):1050-1057.
86. Salinas BA, Sathish HA, Shah AU, Carpenter JF, Randolph TW 2009. Buffer-dependent fragmentation of a humanized full-length monoclonal antibody. *J Pharm Sci* 99(7):2962-2974.
87. Guggenheim EA, Schindler TD 1934. Salt Effects on Sulfonphthalein Indicators. *J Phys Chem* 38(4):543-556.
88. Esue O, Kanai S, Liu J, Patapoff T, Shire S 2009. Carboxylate-Dependent Gelation of a Monoclonal Antibody. *Pharm Res* 26(11):2478-2485.
89. Bin Omar A, Bin MatJafri M 2009. Turbidimeter Design and Analysis: A Review on Optical Fiber Sensors for the Measurement of Water Turbidity. *Sensors* 9(10):8311-8335.
90. *PharmEur.* 2012. Monoclonal antibodies for human use. 01/2012:2031, ed. p 3815-3818.
91. Yadav S, Scherer TM, Shire SJ, Kalonia DS 2011. Use of dynamic light scattering to determine second virial coefficient in a semidilute concentration regime. *Anal Biochem* 411(2):292-296.
92. Mahler HC, Borchard G, Luessen HL. 2010. *Protein Pharmaceuticals Chapter 4.* 1 ed.: Editio Cantor Verlag Aulendorf (Germany). p 464.

93. Carpenter JF, Randolph TW, Jiskoot W, Crommelin DJA, Middaugh CR, Winter G, Fan Y-X, Kirshner S, Verthelyi D, Kozlowski S, Clouse KA, Swann PG, Rosenberg A, Cherney B 2009. Overlooking subvisible particles in therapeutic protein products: Gaps that may compromise product quality. *J Pharm Sci* 98(4):1201-1205.
94. Chi EY, Krishnan S, Randolph TW, Carpenter JF 2003. Physical Stability of Proteins in Aqueous Solution: Mechanism and Driving Forces in Nonnative Protein Aggregation. *Pharm Res-Dordr* 20(9):1325-1336.
95. Kiese S, Pappenberger A, Friess W, Mahler HC 2010. Equilibrium Studies of Protein Aggregates and Homogeneous Nucleation in Protein Formulation. *J Pharm Sci* 99(2):632-644.
96. Roberts CJ, Das TK, Sahin E 2011. Predicting solution aggregation rates for therapeutic proteins: Approaches and challenges. *Int J Pharm* 418(2):318-333.
97. Yadav S, Shire S, Kalonia D 2011. Viscosity Analysis of High Concentration Bovine Serum Albumin Aqueous Solutions. *Pharm Res-Dordr* 28(8):1973-1983.
98. Yamakawa H. 1971. Modern theory of polymer solutions. Electronic Edition ed.: Harper & Row. p 434.
99. Aberle LB, Staude W, Hennemann OD 1999. Three-dimensional cross correlation technique: influence of multiply scattered light in the Rayleigh-Gans regime. *Phys Chem Chem Phys* 1(17):3917-3921.
100. Witt W, Aberle LB, Geers H. 2003. Measurement of Particle Size and Stability of nanoparticles in Opaque Suspensions and Emulsions with Photon Cross Correlation Spectroscopy (PCCS). ed.: Sympatec 29.07.2011, http://www.sympatec.com/docs/PCCS/publications/PCCS_2003_NANOPHOX.pdf. p 5.

7. CURRICULUM VITAE

Christian Lehermayr

Address:	Klammstraße 1a 6330 Kufstein, Austria	E-Mail:	c.lehermayr@imc-krems.ac.at
Place of Birth:	Austria	Cell:	+43 (0) 664 2138344
Date of Birth:	1984-09-21	Family Status:	single
		Nationality:	Austria

Education

2008 University of Applied Sciences IMC Krems GmbH, Austria
Degree Program: Medical and Pharmaceutical Biotechnology
Degree: Dipl.Ing. (FH), passed with distinction

Experience

Lab Scientist in Biopharmaceutical Development

Sandoz GmbH, Kundl, Austria, since 2011-10

Development of biosimilars

PhD Thesis

F. Hoffmann-La Roche Ltd., Basel, Switzerland in collaboration with the Institute of Pharmacy, Martin-Luther-University Halle-Wittenberg, Halle, Germany, 3 years (2008-2011)

„ Net charge and protein-protein interactions of monoclonal antibodies: analytical assessment and application in protein formulation development “

Diploma Thesis

MorphoSys AG, Munich, Germany, 8 months (2007-2008)

„Optimisation of Purification and Formulation of Therapeutic Antibodies“

Publications

Lehermayr C, Mahler HC, Mäder K, Fischer S. 2011. Assessment of net charge and protein–protein interactions of different monoclonal antibodies. *J Pharm Sci* 10.1002/jps.22506

Lehermayr C, 2008. Optimisation of Purification and Formulation of Therapeutic Antibodies, Diplomathesis, Morphosys AG, Munich, Germany (Confidentiality Agreement till Aug. 2013)

Conference Poster: High Throughput Assessment of Second Virial Coefficient and Comparison to Net Charge of different MAbs, PSWC, New Orleans, USA, November 2010

Conference Poster: Assessment of protein-protein interactions and charge of different monoclonal antibodies, AAPS NBC, San Francisco, USA, May 2010

Conference Poster: Second virial coefficients (A_2) and valence of eight different therapeutic monoclonal antibodies, PharmSciFair, Nice, France, June 2009

Date, Signature

8. EIDESSTATTLICHE ERKLÄRUNG

Hiermit erkläre ich gemäß §5 der Promotionsordnung der
Naturwissenschaftlichen Fakultäten I - III
der Martin-Luther-Universität Halle-Wittenberg, dass ich die vorgelegte Arbeit,

“Net charge and protein-protein interactions of monoclonal antibodies: analytical assessment and application in protein formulation development”

selbstständig und ohne fremde Hilfe verfasst habe. Die Ergebnisse der vorliegenden Arbeit habe ich, unter Anleitung von Herrn Prof. Dr. Karsten Mäder, selbstständig erarbeitet bzw. im Rahmen der angegebenen Kooperationen erhalten. Weiterhin habe ich keine anderen als die angegebenen Quellen und Hilfsmittel verwendet und die den benutzten Werken wörtlich oder inhaltlich entnommenen Stellen als solche kenntlich gemacht.
Die vorliegende Arbeit wurde noch keiner anderen Prüfungsbehörde vorgelegt.

Kufstein, den _____

Christian Lehermayr